



Theory and Method to Enhance Computer-Integrated Surgical Systems

**Számítógéppel integrált sebészeti rendszerek funkcionális,
alkalmazhatósági és pontossági kiterjesztésének elmélete
és módszertana**

Tamás Haidegger

Department of Control Engineering and Information Technology
Laboratory of Biomedical Engineering
Budapest University of Technology and Economics

Ph.D. Thesis

Supervisor: Prof. Zoltán Benyó (BME – IIT)
Advisors: Prof. József Sándor (Semmelweis University)
Prof. Imre Rudas (Óbuda University)

Budapest, 2010

ABSTRACT

Image-guided surgical systems and surgical robots are primarily developed to provide patient benefits through increased precision and minimal invasiveness. Furthermore, robotic devices may allow for refined surgical treatment that is not feasible by other means. The goal of my research was to develop new methods and algorithms to support image-guided systems, increase their accuracy and safety with intra-operative tracking, error reduction and advanced control. Three specific areas have been targeted for improvement, each addressed within a research project.

One of the major challenges with integrated surgical robot systems is to maintain the accuracy of the pre-operative registration procedures, and to ensure that all motions of the hardware setup or drift of the patient are promptly noticed. By applying my approach, it becomes possible to rely on the navigation system as an additional reference base to identify events of motion (named surgical cases). It is feasible to accurately monitor and compensate for any spatial changes with a selective algorithm. The concept I have developed was tested on a neurosurgical prototype system built at the Johns Hopkins University (Baltimore, USA), incorporating a navigation system and an interventional robot. The new technique can be used with various image-guided systems, offering new ways to enhance their capabilities.

In certain critical surgical procedures, physicians extensively rely on the help of navigation systems, with accuracy metrics provided by the manufacturers. Depending on the setup, inherent system errors can accumulate and lead to significant deviation in position. It is crucial to improve the precision of integrated setups, and to determine the overall task execution error—the registration and tracking errors enlarged by multiplying imperfect homogeneous transformations. The stochastic approach I developed offers an easy and straightforward solution to map and scale the error propagation. Applying pre-operative and on-site simulations, the optimal positioning of the navigation system can be achieved. This results in faster task execution and reduction of the probability of surgical errors.

Error compensation and guidance of surgical devices are gaining importance in the evolving field of long distance telesurgery. Effective control requires the appropriate handling of the latency in the communication, while ensuring the stability of the devices. I developed a framework for robotic telesurgical support of human space missions and for other long distance procedures. This incorporates the model of the interventional site with a remote controlled slave robot, the communication channel and the model of the human operator. A control structure was designed for telesurgery, relying on empirical controller design methods. It was successfully tested for robot control over a time-delay network.

It is strongly believed that robotics will have the same impact on health care in the next few decades as it had on manufacturing in the past 40 years. The methods developed within the frames of the research should contribute to the field for the benefit of future projects and systems.

KIVONAT

Az orvostechnika folyamatos fejlődésével a robotikának a következő 20 évben minden bizonnyal hasonló hatása lesz az invazív medicina egyes ágira, mint a gyártástechnikára volt az elmúlt évtizedekben. A nemrégiben megjelent kép által vezetett sebészeti rendszereket és sebészrobotokat elsősorban pontosságuk és megbízhatóságuk miatt alkalmazzák, mivel segítségükkel kisebb szöveti sérülés mellett gyorsabban és biztonságosabban végezhetőek el a beavatkozások. Így ma már korábban kivitelezhetetlennek tartott műtétek is végrehajthatók. Kutatásom célja, hogy új módszereket, modelleket és irányítási algoritmusokat dolgozzak ki kép által vezetett sebészeti rendszerek támogatása, pontosságuk és alkalmazhatóságuk növelése érdekében. Téziseimben a betegmozgás-követés, a regisztrációs hibapropagáció és a távsebészet területeken elért eredményeimet foglaltam össze.

Integrált sebészrobot rendszerek esetében az egyik legnagyobb kihívást a műtét előtti regisztrációs és kalibrációs eljárások érvényességének megtartása jelenti. Nagyon fontos annak biztosítása, hogy a kezdeti beállítások változatlanok maradjanak a beavatkozás során, az integrált eszközök és a beteg ne mozduljanak el egymáshoz képest. Az egyre inkább elterjedő műtéti navigációs rendszerek belső koordinátarendszerét kihasználva új eljárást dolgoztam ki a műtét közbeni betegmozgások követésére és kompenzálására. Az algoritmus segítségével egyértelműen azonosíthatók a nem szándékos mozgási események, és ezáltal az adott pillanatban megfelelő irányítás és szabályozás alkalmazható. A módszert először szimulációs környezetben próbáltam ki, majd a Johns Hopkins Egyetemen (Baltimore, USA) fejlesztett koponyaalapi sebészeti robotrendszeren is sikeresen teszteltem.

Bizonyos műtéti beavatkozások esetében (különösen az ortopéd- és idegsebészetben) az orvosok elsősorban a navigációs rendszer adataira támaszkodnak, ezért azok térbeli pontossága létfontosságú. Integrált rendszerek esetében tipikusan előfordulhat, hogy az eredeti mérési hiba a koordináta-transzformációk által eltorzítva, felnagyítva jelentkezik, és így akár több milliméter eltérés is lehet a valóság és a számított értékek között. Robotizált beavatkozásnál ennek nagyon súlyos következményei lehetnek. Az általam kidolgozott valószínűségi módszer megoldást jelent erre a problémára, mivel modellezéssel és a hibák leképezésével a kritikus területek a beavatkozás előtt feltérképezhetővé válnak, és javaslat adható az eszközök optimális elrendezésére. Ennek eredményeképpen gyorsabban és biztonságosabban hajtható végre az operáció.

A hibakompenzáció és eseménybecslés egyre nagyobb jelentőséget kap a távsebészeti alkalmazások esetén is. Megfelelő algoritmusok szükségesek a kommunikáció során fellépő késleltetés és egyéb zavarjelek kezeléséhez. Munkám során azonosítottam egy általános teleoperációs sebészrobot kritikus tényezőit, felállítottam egy kritériumrendszert a távvezérlés megvalósításához, és meghatároztam a technikai adottságok függvényében elérhető egészségügyi szolgáltatások körét. Egy jövőbeli, ember részvételével zajló misszió távsebészeti támogatásához kidolgoztam egy szimulációs rendszert, amely tartalmazza a beteg, a robot, a kommunikációs csatorna és a kezelő modelljét. Egy

általános szabályozási struktúrát adtam teleoperációra, amely empirikus szabályozótervezési módszerek kiterjesztésével hatékony szabályozási feltételeket teremt a rendszer hatékony működtetéséhez.

A kutatásom során kifejlesztett technikák és algoritmusok új megoldásokat nyújtanak, több oldalról közelítve meg a jelenlegi pontossági elvárásokat és hatékonysági problémákat. Eredményeim remélhetőleg a jövő orvosi robotrendszereiben alkalmazásra kerülnek.

NYILATKOZAT

Alulírott Haidegger Tamás kijelentem, hogy ezt a doktori értekezést magam készítettem, és abban csak a listában szereplő forrásokat használtam fel. Minden olyan részt, amelyet szó szerint, vagy azonos tartalomban, de átfogalmazva más forrásból átvettem, egyértelműen, a forrás megadásával megjelöltem.

DECLARATION

Undersigned, Tamás Haidegger, hereby state that this Ph.D. Thesis is my own work wherein I only used the sources listed in the bibliography. All parts taken from other works, either as word for word citation or rewritten keeping the original meaning, have been unambiguously marked, and reference to the source was included.

Budapest, December, 2010

.....
Tamás Haidegger

Contents

1	Introduction	16
1.1	Computer-Integrated Surgery: an Emerging Field	16
1.1.1	Telemedicine and telesurgery	18
1.1.2	Brief history of surgical robotics	20
1.1.3	Advantages of robotic surgery	22
1.1.4	Surgical robotic concepts	23
1.1.5	Limitations of CIS technology	23
1.1.6	Additional challenges of telemedicine	24
1.2	Surgical Robot Systems	25
1.2.1	The da Vinci surgical system	25
1.2.2	The early bird NeuroMate	26
1.2.3	Light-weight prototypes for teleoperation	27
1.3	Significant Robot Teleoperation Experiments	29
1.3.1	Long distance telesurgery	29
1.3.2	Underwater trials	30
1.4	Control Frames for Robotics	32
1.5	Accuracy Measures in CIS	32
1.5.1	Different accuracies	34
1.5.2	Current accuracy standards	37
1.5.3	Examples of accuracy measurements	39
1.6	The JHU Image-Guided Neurosurgical System	40
1.6.1	JHU System components	41
1.6.2	The modified NeuroMate robot	41
1.6.3	StealthStation intra-operative navigation system	42
1.6.4	Other system components	42
1.6.5	Operation in cooperative control mode	44
1.6.6	Applying Virtual Fixtures	45
1.6.7	Virtual fixture computation	46
1.6.8	Applying Kálmán filters to the system	48
1.6.9	Phantom and cadaver experiments	48
1.6.10	Challenges with the JHU system	49
2	Research Problem Statement	53

3	Algorithm for patient motion compensation	55
3.1	Control Structure for Image-Guided Robotic Systems	55
3.1.1	Background of patient motion tracking	55
3.2	General Concept for Patient Motion Compensation	56
3.2.1	New Surgical Case identification concept	60
3.2.2	Specific issues with motion compensation	62
3.2.3	Verification of the concept	64
3.3	Evaluation Study	66
3.3.1	Test data for evaluation	68
3.3.2	Results and discussion	69
3.3.3	Limitations	70
3.4	Summary of the Thesis	70
4	Probabilistic Method to Improve Accuracy in CIS	71
4.1	System Error Estimation Concepts	71
4.1.1	Accuracy assessment of integrated systems	71
4.2	Stochastic Modeling of Complex System Noise	74
4.2.1	Theory of complex errors	74
4.2.2	Deployment of the concept	76
4.2.3	Simulation results	76
4.2.4	Error modeling for faster surgical execution	76
4.2.5	Application to a physical system	78
4.2.6	Future deployment of the concept	79
4.3	Summary of the Thesis	79
5	Control Method for Long Distance Telesurgery	80
5.1	Telemedicine and Telesurgery for Space Applications	80
5.2	Human Model for Teleoperation Scenarios	82
5.2.1	Human operator models	82
5.2.2	The crossover model	83
5.3	Robot Model for Teleoperation Scenarios	85
5.4	Application Oriented Controller Design	86
5.4.1	Cascade controller for a telesurgical robot	86
5.4.2	Empirical design approach	87
5.5	Controller Design Solutions for Long Distance Telesurgical Applications	89
5.6	Controller Structure for a Telesurgery System	90
5.6.1	Realization of control methods	92
5.6.2	Slave side—inner loop	92
5.6.3	Master side—outer loop	96
5.6.4	Solutions to handle time delay in telesurgery	97
5.7	Summary of the Thesis	105
6	Conclusion	106
6.1	Summary of Contributions	106
6.2	Future Work	107

Appendix	109
A Regulations and Standards	109
A.1 International regulations for CIS	109
A.2 Accuracy measurement standards relevant to the field	110
A.3 Safety standards and methods for CIS	111
B Space Communication, Teleoperation and Telesurgery	113
B.1 Latency in teleoperation and human adaptation	113
B.2 Operations in weightlessness	115
C International organizations and literature of CIS	116
C.1 International organizations and literature of CIS	116
D Detailed List of Neurosurgical Robots	118
E New Surgical Robot Concepts	120
F Supplementary DVD	122
REFERENCES	123
PUBLICATIONS RELATED TO THE THESIS	145

Acknowledgment

Primarily, I am grateful to my supervisor, Prof. Zoltán Benyó (BME – IIT) for his continuous support throughout my studies. Prof. József Sándor (Semmelweis University) and Prof. Imre Rudas (Óbuda University) have guided me along the long way to graduation, and opened the door to the international community. I am also grateful to my informal supervisors and project leaders, primarily to Dr. Peter Kazanzides (Johns Hopkins University) for his tireless efforts invested and for his valuable comments and contributions. Prof. Radu-Emil Precup (“Politehnica” University of Timisoara) and Dr. Levente Kovács (BME – IIT) were tremendously helpful developing controllers for teleoperation.

I would like to acknowledge the role of my personal mentor and friend, Dr. Sándor Győri, his perspectives and ideas founded the work, and without whom, I would not have been able to get this far.

Dr. Alexandre Gattiker from Renishaw mayfield SA contributed to my work with insightful comments.

Further, I would like to thank the support and cooperation of all my laboratory mates, colleagues at the department and beyond.

I am grateful for the support of my family, their care and patience gave me significant motivation.

The research was partially supported by the National Office for Research and Technology (NKTH), Hungarian National Scientific Research Foundation grant OTKA T69055, OTKA CK80316 and the U.S. NSF EEC 9731748 grants. I am thankful for the generous scholarship of the Hungarian–American Enterprise Scholarship Fund (HAESF) that made it possible to spend two semesters in the United States and join the CISST ERC research center at the Johns Hopkins University.

*“The future of surgery is not about blood and guts;
the future of surgery is about bits and bytes.”
/Dr. Richard Satava/*

Preface

The technological development of the last decades resulted in the rise of entirely new paradigms in health care. Within interventional medicine, first laparoscopic and later robot-assisted surgery redefined the standards of clinical care. The field of Computer-Integrated Surgery (CIS) is rapidly developing, providing innovative and minimally invasive solutions to heal complex injuries and diseases. By now, over a million successful operations have been accomplished, primarily in urology, neurosurgery, orthopedics, ear and nose surgery, pediatrics and interventional radiology. In the near future, newly developed robotic systems may even conquer the most challenging fields to support patient care and to provide better medical outcome. Surgeons started to extensively rely on medical images and intra-operative navigation that allow the visualization of patient anatomy, and can be used to improve free-hand targeting, accurate positioning of equipment or guidance of robotic devices.

The first surgical robot applications appeared 25 years ago, and since then, hundreds of different prototypes have been developed. A handful of them have been approved by medical authorities and brought to the market. The commercially available da Vinci surgical system made robotic surgery widespread and acknowledged throughout the world, and the results delivered convinced most of the former critics of the technology. As the world is not ready yet to embrace automated invasive robots in health care, the best approach for the industry may be to provide incremental enhancement to existing medical practice. In the mean time, the main focus of the research community remains to significantly extend the capabilities of the human surgeon through innovative and radically new solutions.

Technology can give adequate answers to classical medical challenges, such as the real-time visualization of the procedure, the corrections of human errors, or treating patients in distant locations. In teleoperation, innovation has increasing importance in solving problems and challenges of communication, noise and latencies. Among the many technical issues affecting integrated systems, three major sources of inaccuracy can be identified: inherent error of hardware components, residual error of registration procedures and communication delay in the network. (Physiological tissue motion is not considered to be a technical issue here.) These can interfere with the procedure, and cause serious decline in spatial and temporal resolution of a system. The thesis intends to advance on these three areas, providing generalized engineering solutions and applicable tools to solve issues in CIS.

The continuation of current trends will surely lead us to a new era of technology supported medicine. As the concept of image-guided control is becoming more apparent, the engineering solutions can be applied to many other devices, suitable for a wider range of surgical procedures. The path of future development is the integration of surgical navigation, telemedicine, nanotechnology and microelectromechanical systems in a common framework supported by powerful computing and decision making.

Structure of the Thesis

The thesis consists of six chapters. Chapter 1 is an overview of Computer-Integrated Surgery and surgical robotics, enumerating core technologies, basic definitions and classification principles of the field. The most important systems are introduced in details to properly define the context in which the research was performed. The second part of the chapter thoroughly describes the JHU robotic neurosurgery system I have been working on. It gives the theoretical and practical background of the experiments and measurements conducted with the robot. The numerous engineering challenges solved during the development of the robot are documented.

Chapter 2 is a brief summary of the most urging problems of the field that my work is focusing on, and presents the specific issues in CIS that required adequate solutions. The major results of my work are organized into three thesis groups, separated into chapters.

Chapter 3–4–5 present the three thesis groups developed within the frames of my Ph.D. research. In each chapter, a brief description of the specific area is given, the proposed new solutions are introduced and experimental results are presented to support the results.

Chapter 6 is a summary and an outlook to the future of the research, followed by an extensive Appendix providing further details and background materials about advanced medical technology.

The equations, figures and tables are numbered through every chapter. The thesis was written following U.S. English grammar rules.

Notations and Symbols

TABLE 1
COMMON ABBREVIATIONS AND NOTATIONS

ASTM	American Society for Testing and Materials
CA	Commercially Available
CAD/CAM	(Surgical) Computer-Aided Design and Manufacturing
CAMI	Computer-Assisted Medical Interventions
CAOS	Computer-Assisted Orthopaedic Surgical Systems
CE	Conformité Européenne (mark)
CIS	Computer-Integrated Surgery
CT	Computer Tomography
DOF	Degree(s) of Freedom
CISST ERC	NSF Engineering Research Center for Computer-Integrated Surgical Systems and Technology
DARPA	Defense Advanced Research Projects Agency
EMT	Electromagnetic Tracking
(E)SO	(Extended) Symmetrical Optimum (method)
FDA	U.S. Food and Drug Administration
FLE	Fiducial Localization Error
FRE	Fiducial Registration Error
GUI	Graphical User Interface
HD	High Definition (image)
IG(S)	Image-Guided (Surgery)
ISO	International Organization for Standardization
IRCAD	Institut de Recherche contre les Cancers de l'Appareil Digestif
JHMI	The Johns Hopkins Medical Institute
JHU	The Johns Hopkins University
JPL	NASA Jet Propulsion Laboratory
LCSR	Laboratory for Computational Sensing and Robotics
MDD	Medical Device Directive
MIRA	Minimally Invasive Robotic Association
MIS	Minimally Invasive Surgery
MR(I)	Magnetic Resonance (Imaging)
\mathbf{n}_i	Virtual Fixture plane normal
NASA	National Aeronautics and Space Administration
NEEMO	NASA Extreme Environment Mission Operations
NSF	U.S. National Science Foundation
OR	Operating Room
PM	Phase Margin
POI	Point of Interest
RMS(E)	Root Mean Square (Error)
SC	Surgical Case
SS	(Medtronic) StealthStation intra-operative navigation system
STD	Standard Deviation
TF	Transfer Function
TQM	Total Quality Management
TRE	Target Registration Error
VF	Virtual Fixture
VPN	Virtual Private Network
Z-N	Ziegler-Nichols (method)

TABLE 2
COMMON VARIABLES AND SYMBOLS

B_S	Inertia coefficient of a slave robot
β ($\beta_{\text{Inner}}, \beta_{\text{Outer}}$)	Scaling parameter of the ESO method
CAM	Localizer's (camera's) coordinate frame (CAM)
CamMot	6 DOF motion of the Camera
d_i	Distance from the i^{th} plane during Virtual Fixture computation
D_i	Safety threshold (distance) during Virtual Fixture computation
DRB	Dynamic Reference Base (coordinate frame)
$\phi(x)$	Standard normal density function
$\Phi(x)$	Distribution function of $\phi(x)$
$f(\mathbf{t})$	Density function
$\mathbf{f}_M, \mathbf{f}_S, \mathbf{f}_T$	Forces applied to the master, the slave robot and to the tissue, respectively
$G(s)$	Model of soft tissue
η	Probability that the Point of Interest is in the forbidden zone
\mathbf{I}	Identity matrix
$\mathbf{J}(\cdot)$	Jacobian matrix
$\mathbf{K}(d)$	Scaling matrix for Virtual Fixture implementation
k_{Op}	Human operator's static gain
k_{proc}	Proportional (DC) gain of a process
λ	Controller design parameter of the ESO method
M_S	Damping coefficient of a slave robot
p, q	Tissue specific constants
\mathbf{p}_i	3D fiducial point in the patient space
PAT	Patient Anatomy (coordinate frame)
PatMot	6 DOF motion of the Patient (PAT)
\mathbf{q}_i	3D fiducial point in the robot space
REP	Robot End Point (coordinate frame)
ROB	Robot Base (coordinate frame)
RobMot	6 DOF motion of the Robot (ROB)
σ	Overshoot
\mathbf{t}	Vector of positions and Euler angles $[x, y, z, \phi, \theta, \psi]$
T_1, T_2, \dots	Time constants of a process, in decreasing order
$T_{C,1}, T_{C,2}, \dots$	Time constants of the controller, in decreasing order
T_Σ	Remnant, aggregated time constants of a process
${}^{\text{From}}_{\text{To}}\mathbf{T}$	Homogeneous transformation matrix between frames "From" and "To"
$\theta_{\mathbf{n}}$	Degree of rotation around a given \mathbf{n} axis
τ_D, d	Time delay
τ_{It}	Effect of human adaptation in teleoperation
τ_{Op}	Time for learning a teleoperation task
τ_r	Settling time
TCP	Tool Center Point (coordinate frame)
TRB	Tool Rigid Body (coordinate frame)
\mathbf{v}	Cartesian velocity of the Point of Interest
\mathbf{w}	Weighting factors for safer Virtual Fixture application
W_{sys}	Transfer Function of a system
W_0, W_c	Open loop and closed loop Transfer Function of a system, respectively
\mathbf{x}_i	Point of Interest or measurement point in the 3D space
$\mathbf{x}_M, \mathbf{x}_S$	Cartesian positions of the master and the slave robot, respectively

List of Figures

1.1	Core concept of Computer-Integrated Surgery	17
1.2	Commercially available optical surgical navigation systems	18
1.3	The NDI Polaris intra-operative navigation system	19
1.4	Different categories of telemedicine	20
1.5	Information integration in telesurgery	21
1.6	Different categories of interventional CIS systems	24
1.7	The da Vinci surgical system	26
1.8	The NeuroMate surgical robot	27
1.9	The RAMS robot and the M7 robots	28
1.10	The Zeus during transcontinental surgery	29
1.11	The Raven robot in underwater experiments	31
1.12	Definition of accuracy and repeatability	33
1.13	Definition of FRE and TRE	36
1.14	ASTM and NIST accuracy phantoms	38
1.15	The NeuroMate-based IGS system at JHU	40
1.16	Hardware and software elements of the integrated neurosurgical system	41
1.17	The drilling tool of the JHU robot	42
1.18	Slicer 3D program with phantom CT and defined Virtual Fixture	43
1.19	Admittance control of the NeuroMate	44
1.20	The control frames of the JHU system	45
1.21	Experimental setup for phantom trials	49
1.22	Experimental setup for cadaver tests	49
1.23	Timeline of information processing in the JHU system	51
1.24	Measurement noise due to latency	52
3.1	Control concept of image-guided robotic systems	57
3.2	Control frames at the end of the robot	58
3.3	Definitions of the different motions occurring in IGS systems	59
3.4	Decision-making flowchart for the evaluation of different Surgical Cases	61
3.5	Scheme of averaging for patient motion events	63
3.6	Sample motions of simulation	64
3.7	Ideal Surgical Case identification	65
3.8	The effect of noise on estimation	66
3.9	The effect of latency on estimation	67
3.10	Closing the control loop through registration	68
3.11	Novel patient motion and re-registration concept	69

4.1	Basic setup of IGS procedures	75
4.2	Distribution of the POI with a simulated IGS system	77
4.3	The POI transformed to the coordinate space of the patient	77
4.4	Anisotropic distribution of the error at the POI	78
4.5	The tooltip transformed to the coordinate space of the patient	78
5.1	Concept of telehealth support	81
5.2	Simplified model of a human from the control aspect	83
5.3	Model of a teleoperated slave robot	86
5.4	The concept of virtual reality extended control of surgical robots	90
5.5	Cascade control of the telesurgery system	91
5.6	The control structure modeled in Simulink environment	92
5.7	Step response of the closed loop system	94
5.8	Step response of the filtered, closed loop W_{Inner} system	95
5.9	Block diagram of the classical Smith predictor	99
5.10	Step response of the whole closed loop system	100
5.11	Controller designed with stretched Kessler method	101
5.12	The robustness of Kessler's method	102
5.13	Block diagram of the classical Smith predictor	103
5.14	Kessler's method employed with Smith predictor	105
A.1	The ISO 10360-1:2001 standard for coordinate measuring machines	111

List of Tables

1	Common abbreviations and notations	11
2	Common variables and symbols	12
1.1	Comparison of human and robot performance in medical applications . .	22
1.2	Different accuracies of surgical robots	39
1.3	Measurement noise due to latency within the JHU system	52
3.1	Surgical motion scenarios	58
3.2	Confusion matrix for reference SC identification	65
3.3	Confusion matrix for SC identification with noise	66
3.4	Confusion matrix for SC identification with latency	67
5.1	Controller performance parameters for the inner loop	95
5.2	Maximum latency manageable with different β_{Inner} settings	99
5.3	Controller performance parameters with different β_{Outer} settings	103
5.4	Effect of order of approximation on control parameters.	104
5.5	Effect of β_{Outer} on control parameters for Case 3 system design	104
D.I	Neurosurgical robot projects and systems	119

Chapter 1

INTRODUCTION

1.1 Computer-Integrated Surgery: an Emerging Field

Computer-Integrated Surgery (CIS) is the most commonly used term to cover the entire field of interventional technology, from medical image processing and augmented reality applications to automated tissue ablation. A subfield of it, *Computer-Aided Surgery* (CAS), usually means that the digital system employed does not take part in the physical part of the operation, it improves the quality of surgery by better visualization or guidance. CIS is also referred to as *Computer-Assisted Medical Interventions* (CAMI) or *Computer-Integrated Interventional Medicine* (CIIM). The core concept of CIS is presented in Fig. 1.1. CIS incorporates surgical CAD/CAM (*Computer Aided Design and Manufacturing*)—analogous to industrial CAD/CAM—where digital information is used to create accurate patient models and surgical plans, while technology also helps treatment delivery. Patient specific evaluation should lead to better medical outcome, while statistical evaluation may lead to the overall improvement of the operating technique (similarly to the concept of *Total Quality Management* (TQM) in industrial manufacturing).

Robotic surgery is defined by the SAGES–MIRA Robotic Consensus Group (*Society of American Gastrointestinal and Endoscopic Surgeons* and *Minimally Invasive Robotic Association*) as “a surgical procedure or technology that adds a computer-technology-enhanced device to the interaction between the surgeon and the patient during a surgical operation, and assumes some degree of freedom of control heretofore completely reserved for the surgeon. This definition encompasses micromanipulators, remotely controlled endoscopes and console-manipulator devices. The key elements are enhancement of the surgeon’s abilities—by the vision, tissue manipulation or tissue sensing—and alteration of the traditional direct local contact between surgeon and patient.”[2] Beyond remote teleoperated systems, such as the *da Vinci*, the field incorporates other smart tools and intelligent devices as well.

Minimally Invasive Surgery (MIS) once solely referred to laparoscopic procedures (keyhole surgery), where the abdominal cavity is accessed through 3–5 small incisions (0.5–3 cm in size). This procedure was first reported on humans in 1910, performed by Jacobaeus in Sweden [3]. Since then, different methods have been developed to access other parts of the body as well. Today, it is a popular alternative to open procedures in many cases to reduce patient trauma and operation risk. On the other hand, it requires a highly skilled surgeon with a significant amount of practice [4].

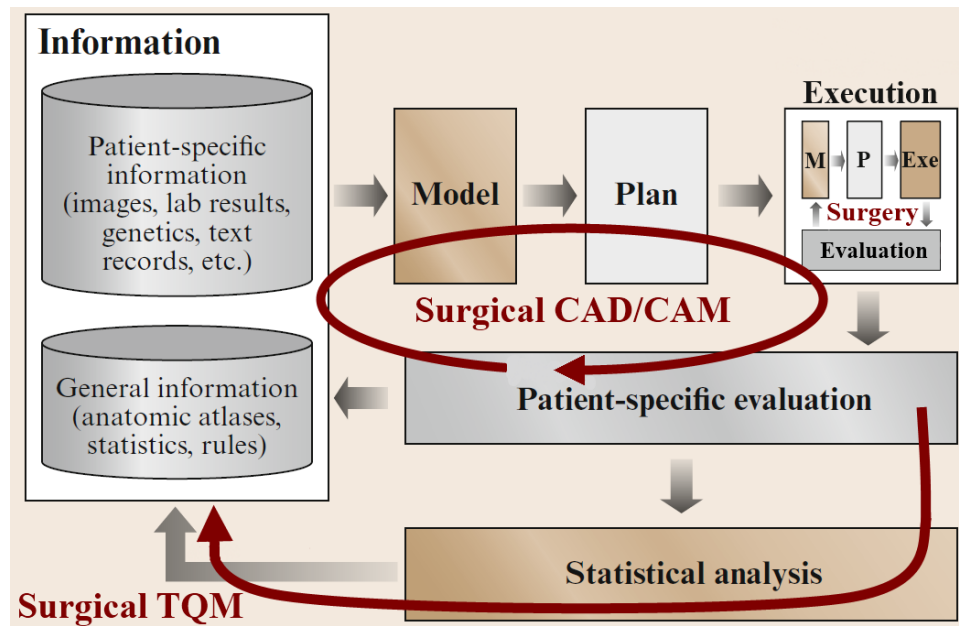


Fig. 1.1. Core concept of Computer-Integrated Surgery: integrating advanced technology supported planning (CAD), execution (CAM) and evaluation (TQM) of surgical tasks [1].

Robot-assisted MIS is often used to characterize the complete teleoperated systems, where the robot basically serves as a replacement of the human operator's hand by manipulating endoscopic tools.

Image-Guided Surgery (IGS), or *IG Treatment, Therapy* mean the accurate correlation and mapping of the operative field to a pre-operative image or intra-operative (e.g., ultrasound, fluoroscopy) data set of the patient, providing freehand navigation, positioning accuracy of equipment or guidance for mechatronic systems [5]. IGS has been primarily used in neurosurgery, pediatrics, orthopedics and also had a major impact in ear, nose and throat (ENT) and maxio-facillary reconstruction surgery. IGS had existed even before robotic innovation appeared in medicine: the idea of *stereotaxis* dates back to the 19th century, the term *stereotaxic procedure* was coined in 1908, and the first human device was built around 1918 [6]; however, the first human sub-cortical procedure was only performed in 1947 [7]. The technique was originally aimed at improving the performance of brain tumor surgeries, and became popular from the '80s due to the emergence of less expensive computational power and advanced intra-operative imaging.

A key element of medical imaging and robotics is registration (also called fusion). This means the spatial alignment of different modalities to determine the position and orientation of the patient in the operating field relative to a virtual data set of the anatomy, e.g., a pre-operative image. The registration should provide a homogeneous transformation matrix that allows the conversion of locations and control signals between different devices [8].

There are two common ways to perform the registration [9]. For the classical, *frame-based stereotaxis*, a stereotactic frame is mounted to the patient's head prior to the computer tomography (CT) or magnetic resonance (MR) imaging and serves as an fixed coordinate system by which any point of the brain can be referenced.

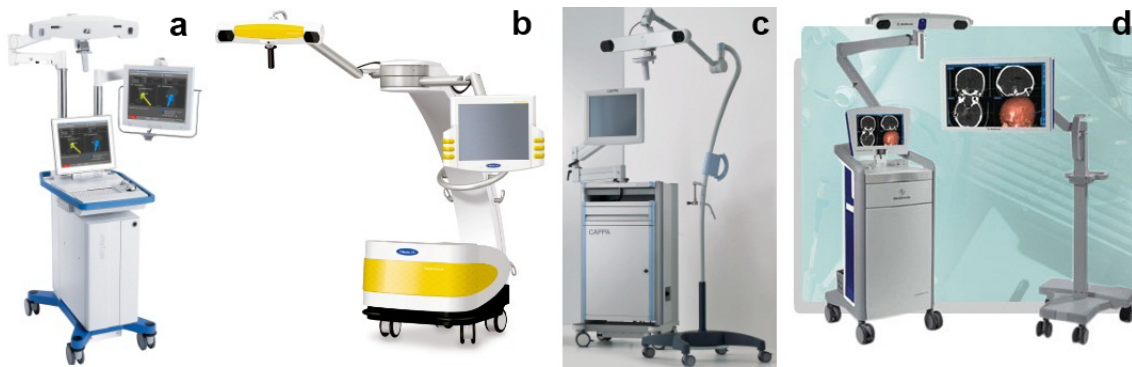


Fig. 1.2. Commercially available optical intra-operative navigation systems. (a) Stryker Navigation System II. (b) BrainLAB VectorVision2. (c) CAPP from Siemens Medical. (d) Medtronic StealthStation S7. (Courtesy of the manufacturers.)

The more recent technique—*frameless stereotaxis*—involves a hand-held surgical probe, and it does not require the rigid head-frame. The probe may be tracked by mechanical, optical, ultrasonic or electromagnetic techniques while touching designated points with it. The transformation between the image space and the tracker coordinates can be computed through fiducial-based or anatomical landmark-based registration, relying on paired-point, surface matching (point-cloud) methods or some kind of hybrid transformation [10]. *Fiducials* are artificial markers, screws or other potential reference points. Natural anatomic features such as point landmarks, ridge curves or surfaces can also be used. Surgical navigation systems match the two frames and provide the tool coordinates in image space, through the spatial tracking of a *Tool Rigid Body* (TRB). The patient's body must be fixed relative to the mounted reference frame (*Dynamic Reference Base*—DRB), otherwise the registration loses its validity.

Intra-operative navigation is commonly achieved with a camera system that is able to track rigid bodies within its workspace. Commercially available systems are shown in Fig. 1.2. These are based on infrared (IR) stereotactic cameras and active (flashing LED) or passive (reflective paint-covered) markers. The most commonly used *NDI Polaris* in Fig. 1.3a is developed by Northern Digital Inc. (Waterloo, ON, Canada). Fig. 1.3b shows the effective workspace of the Polaris system.

More recently, electromagnetic tracking (EMT) has also become popular as it offers the advantage of not requiring a line of sight for operation. However, optical systems tend to be more accurate, and not susceptible to magnetic distortions and to the proximity of metallic materials [11].

1.1.1 Telemedicine and telesurgery

Virtual presence and remote delivery of services have great scientific and commercial potential in health care. The term *telehealth* usually refers to clinical and non-clinical services such as education, administration or research. *Telemedicine* generally means only the provision and delivery of clinical services. It is defined as “*The use of medical information exchanged from one site to another via electronic communications for the health and education of the patient or health care provider and for the purpose of improving patient care.*”

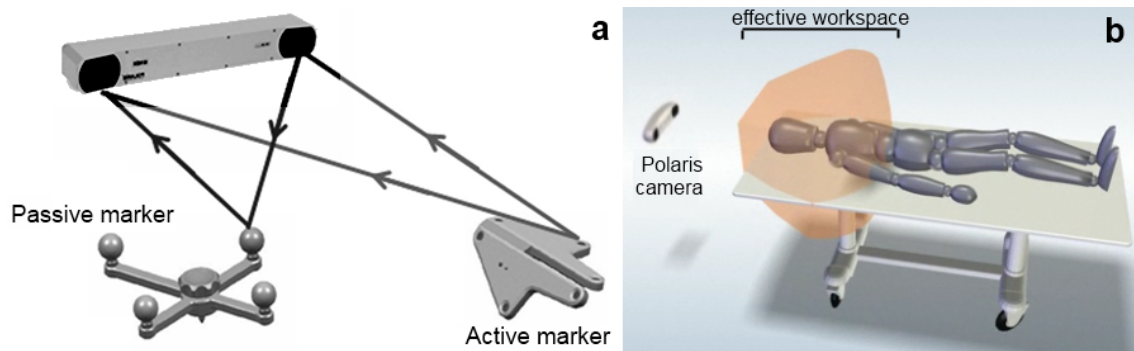


Fig. 1.3. (a) The NDI Polaris intra-operative navigation system is able to track two or more rigid bodies (sets of markers) at a time, providing the position and orientation of the two frames relative to each other. (b) Effective workspace of the Polaris Vicra camera. (Courtesy of NDI.)

Telemedicine includes consultative, diagnostic and treatment services” [12]. Similarly, the SAGES group defines it as “*The practice of medicine and/or teaching of the medical art, without direct physical physician–patient or physician–student interaction, via an interactive audio-video communication system employing tele-electronic devices*” [13].

The advantages of telemedicine are various: in the case of short distance operations, the technology involved can mean great added value, such as the control of a tool holder or a surgical robot [14]. In long distance telerobotics, the time/cost effectiveness and the provided higher level of medical care are the most important benefits, while in extreme telemedicine, such as space exploration, telepresence may be the only available form of adequate medical aid.

Telemedicine can be online (real-time) or offline (asynchronous), depending on the technical quality of the communication link. Further, it can be broken down to three main categories based on the timing and synchrony of the connection (Fig. 1.4). *Store-and-forward telemedicine* means there is only one way communication at a time, the remote physician evaluates medical information offline, and sends it back to the original site at another time. Next, *remote monitoring* services enable medical professionals to collect information about patients with different modality sensors from a distance. Finally, *interactive telepresence* provides real-time communication between the two sites, which might be extended with various forms of interactions, allowing for a set of telemedicine services.

From the application point of view, *telesurgery* (also referred to as *remote surgery* or *telepresence surgery*) enables physicians to invasively treat patients spatially separated from themselves. Unconstrained bandwidth and real-time remote access to the medical site means that the surgeon is actually capable of performing operations through robots and other teleoperated devices.

When the network connection is not reliable enough or the technical tools are not given, a remote surgeon can direct the local one based on semi-real-time (slightly delayed) video and voice feed from the Operating Room (OR). This technique is called *telerobotics* (also referred to as *teleproctoring*), practically the spatial extension of classical mentoring and professional guiding—the monitoring and evaluation of surgical trainees from a distance. Telerobotics may not only be useful for surgical education, but it has also

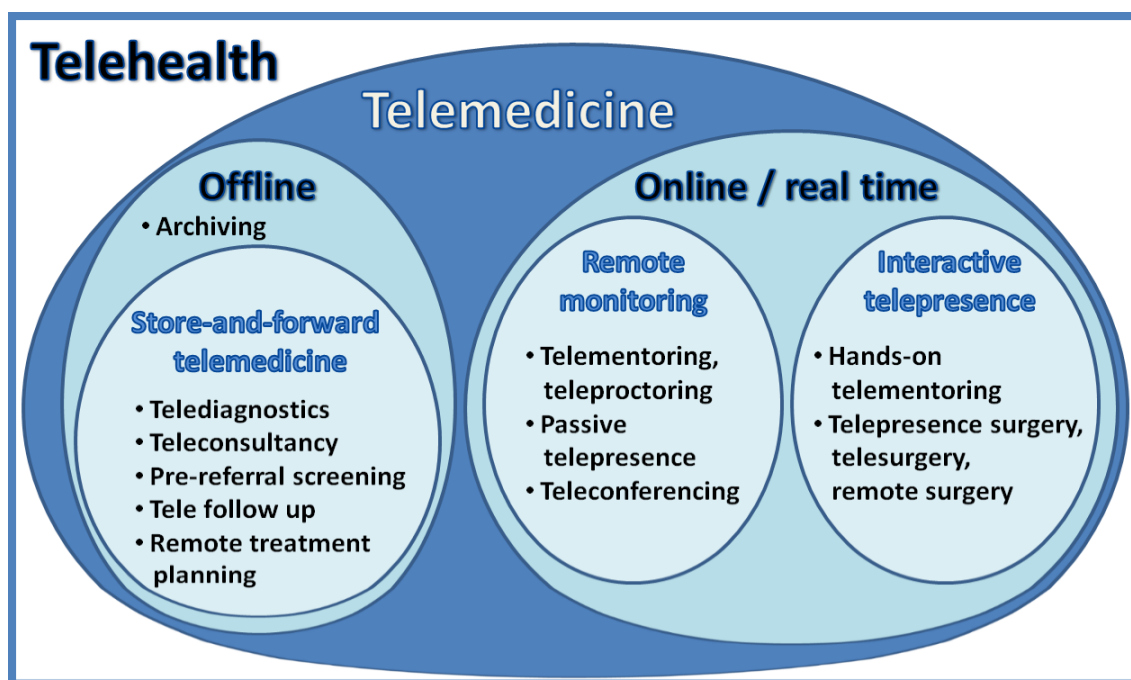


Fig. 1.4. The different categories of remote technologies servicing telemedicine.

been proved that surgically unqualified people can satisfyingly perform complex medical procedures with it [15].

When low communication quality or latency does not even allow semi-real-time connection, *consultancy telemedicine* (or telehealth consultancy) may still be used. It only requires a limited bandwidth access to the remote site, and as a consequence, the distant group cannot use real-time services or information updates.

Fig. 1.5 shows the integration of sensory inputs to the control diagram of telesurgery concept [16]. Currently, the dominant form of feedback is visual, as that provides the highest density of information.

Due to the fact that surgeons navigate mostly based on a camera image, telemedicine techniques are very applicable to laparoscopy. MIS is considered to be one of the most important breakthroughs in medicine in the past decades, and the technology keeps developing in many new fields.

1.1.2 Brief history of surgical robotics

Since the 1980s, many medical robotic research projects have been initiated, creating a set of instruments for remote and local robotic surgery. CIS and telemedicine have become widely used around the world, surgeons and engineers created systems and networks for advanced patient care, demonstrated over a hundred different procedures, transcontinental surgery and performed procedures in weightlessness [17, 18].

It was first proven twenty-five years ago that robotics can extend human surgeons' capabilities. The first robot used on a human patient was a *Puma 200* (Programmable Universal Machine for Assembly), manipulating a biopsy cannulae using a *Brown-Roberts-*

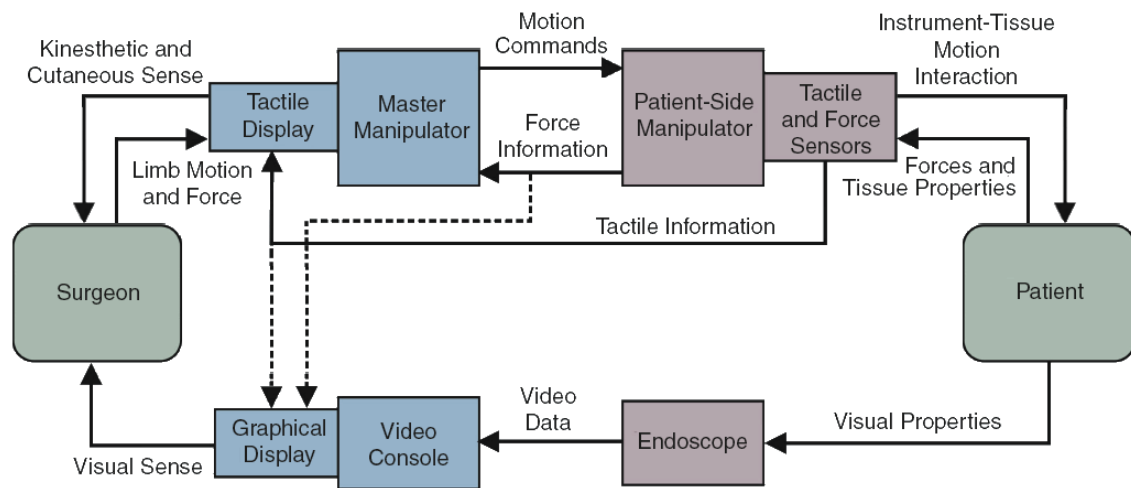


Fig. 1.5. High level integration of different modality feedback information in telesurgery. Interaction is only possible through a system of sensors and human-machine interfaces. (Based on [16].)

Wells stereotactic frame (mounted on the robot's base). The operation took place in the Memorial Medical Center (Long Beach, CA, USA) in 1985 [19]. In later experiments, the Puma performed complete stereotactic neurosurgical operations based on CT scan, processing the scanned images, positioning the arm and manipulating different probes.

The U.S. Army has long been interested in robotic surgery for the battlefield, and currently, the *Telemedicine & Advanced Technology Research Center* (TATRC) supports research to test and extend the reach of remote health care. With the help of mechatronic devices physicians were first able to affect distant patients with the *Green telepresence system* in 1991 [20], and the first long distance telerobotic experiment was in 1993 between JPL in Pasadena and Milan [21]. The U.S. Department of Defense (DoD) aims to develop a system—*Trauma Pod*—by 2025 that allows combat surgeons to perform life saving operations from a safe distance [22, 23]. The general idea of telerobotic health care in space was born in the early '70s, proposed in a study for NASA to provide surgical care for astronauts with remote controlled robots [24]. In the late '80s, the idea of commercial surgical robotics was born on the principle to extend the surgeon's dexterity.

The first telehealth projects begin to use audio/video links between medical sites for information sharing [25]. Successful human telesurgery consultation was reported in 1996, and in 2000 the first completely remote telesurgical animal trials were conducted [26]. Research projects are focusing on space applications, to support flight surgeons to achieve the high level medical education and continuous training, and projects are also focusing on alternative approaches, to replace the humans. Simulated surgical experiments in weightlessness showed that endoscopic procedures provide a real option to perform surgery in a confined body cavity, handling body fluids and organs [27].

Nowadays, the U.S. Robotics roadmap points to robotic telesurgery as a major focus of research in order to improve quality of health care [28]. It calls for engineering solutions to ensure natural interaction between the human operator and the remote robot through specific patient models, from whole-body level to tissue characteristics. This would allow for advanced surgical planning, automated guidance and also for realistic training opportunity.

1.1.3 Advantages of robotic surgery

Medical robots are mostly employed for the accuracy and reliability of their mechanics; however, it may still be hard to fully exploit their features, as surgical tasks are typically unique, involving the semi-autonomous manipulation of deformable objects in an organic, limited environment. Table 1.1 compares relevant features of a robot versus a human operator.

Robot-assisted procedures offer remarkable advantages both for the patient and the surgeon. The ability to perform operations on a smaller scale makes microsurgery more accessible, and the use of mechatronic devices can increase the stability of the system. Medical imaging gives the capability to navigate and position the surgical tool at the target point. Furthermore, there is the option to introduce advanced digital signal processing to control or record the spatial Point of Interest (POI) and motions. This can be useful for surgical simulation and risk-free training. Finally, robotized equipment can greatly add to the ergonomics of the procedures. The main advantages of robotic surgery systems are the following (based on [30, 31]):

- superior 3D spatial accuracy provided by the robot,
- specific design for maximum performance (including miniature robots),
- stabilization of the instruments within the surgical field,
- improvement of manual dexterity, motion scaling,
- physiological tremor filtering,
- integrated 3D vision system with high definition (HD) resolution,
- advanced ergonomics supporting long procedures,
- stable performance,
- high fidelity information integration,
- invulnerability to environmental hazards,
- patient advantages (reduced blood loss, less trauma, shorter recovery time),
- decreased costs (per treatment) due to shorter hospitalization,
- possibility to provide better and more realistic training to physicians.

TABLE 1.1

COMPARISON OF HUMAN AND ROBOT PERFORMANCE IN MEDICAL APPLICATIONS, BASED ON [29].

Feature	Human		Robot	
Coordination	Limited hand–eye coordination	–	Great precision	+
Dexterity	High within sensory range	+	Limited by the actual sensors, range can exceed human perception	+
Information integration	High capacity on high level	+	Limited by AI on high level	–
	Easy to overload on low level	–	High capacity on low level	+
Adaptivity	High	+	Depends on design, but limited	–
Stable performance	Degrades rapidly by time	–	No degradation	+
Scalability	Biologically limited	–	Depends on design, can be high	+
Sterilization	Acceptable	+	Acceptable	+
Accuracy	Biologically limited	–	Designed to exceed human scales	+
Space occupation	Generally given (human body)	+/-	Depends on design, can be small	+
Exposure	Susceptible to radiation and infection	–	Unsusceptible to environmental hazards	+
Specialty	Generic (depending on training)	+	Specialized	–

Current research projects are trying to increase the utility of the surgical equipment along different strategies. They are mainly focusing on three areas for improvement:

- augmenting the overall accuracy and/or efficacy of the classic stereotactic systems,
- increasing the added-value of the equipment,
- further enhancing the capabilities of the human surgeon, providing smarter tools.

1.1.4 Surgical robotic concepts

Robots can be involved in medical procedures with various level of autonomy [32]. Some of them serve as a robust tool holding equipment having been directed to the desired position. Systems that are able to perform fully automated procedures—such as CT-based biopsy or cutting—are called *autonomous* or *supervisory controlled* devices (Fig. 1.6a). A human supervisor would always be present to intervene if deviations from the surgical plan are noticed. When the planning is completed, the physicians have to register the robot's coordinates with the patient's anatomical points, mapping the physical space to the robot's working frame. Once the registration is completed, the robot can autonomously perform the desired task by strictly following the pre-programmed plan.

On the other hand, if the robot is entirely *teleoperated* or *remote-controlled* (robotic telesurgery system) the surgeon is absolutely in charge of its motion (Fig. 1.6b). These complex systems (such as the da Vinci) consist of three parts: one or more slave manipulators, a master controller and a vision system providing feedback to the user. Based on the gathered visual (and sometimes haptic) information, the surgeon guides the arm by moving the controller and closely watching its effect. In most of the cases, mechatronic systems and cameras are the remote hands and eyes of the surgeon, and therefore key elements of the operation.

Modifying the teleoperation control paradigm we can introduce *cooperative control* (also called *shared control* or *hands-on surgery*). It means that the surgeon is directly giving the control signals to the machine through a force sensor. It is possible to read and process these signals in real-time to create the robot's motion (Fig. 1.6c). The human is always in contact with the robot, as the master and the slave devices are physically identical. In this case, the robot is the extension of the doctor's hand, equipped with special features and effectors. This approach keeps the human in the loop, and still allows the surgeons to use all their senses. It is often used in the case of micro-manipulation operations, such as micro-vascular, urologic, eye or brain procedures. Cooperative control is a promising way to provide highly integrated robotic support for procedures while applying all the necessary safety standards. For more details on safety measures applied to CIS, see Appendix A. It is believed that currently this method provides the highest effectiveness according to the criteria hierarchy for surgical robots [33].

1.1.5 Limitations of CIS technology

Despite their success in various applications, there are some concerns that prevent CIS technologies from becoming dominant in most of the areas. While there is a clear need for accuracy and robust operation for many procedures, the associated high expenses are not welcomed. Several projects turned out to be financial failures, as the high development and

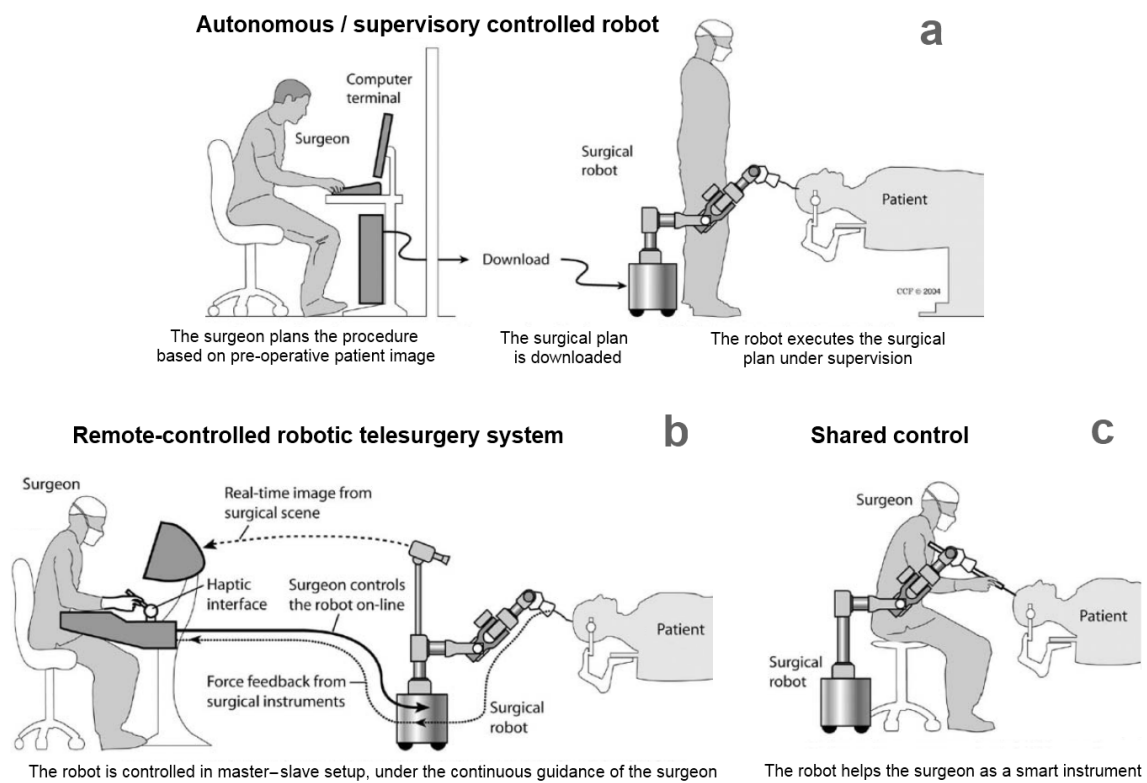


Fig. 1.6. Different categories of interventional CIS systems, based on their control concept [32].

production costs can only pay back, when significant market penetration is achieved. In many countries, the state-run health care system cannot support costly robot investments, forming a barrier to their deployment [34].

The working environment of a surgical robot is not entirely predictable and cannot be modeled completely, therefore complete automation of procedures is extremely hard. Some specific tasks, such as bone milling for implants has been successfully realized with semi-automated robotic support (e.g., the ROBODOC system [35] or the RONAF project [36]). Safety concerns delayed or prevented the approval of many automated interventional systems, and led the research community towards human-integrated control solutions, such as telesurgery and hands-on surgery.

Regulatory and legislative bodies are not prepared to legally handle the extensive use of CIS technology, as it is rapidly spreading [37]. Certain moral and ethical questions associated with automated health-care must be dealt with to handle complex situations from surgical error to cross-border teleoperation. (See Appendix A for more details about regulations affecting the field.)

1.1.6 Additional challenges of telemedicine

Effectiveness of surgical care heavily relies on the prompt delivery of treatment, and extreme long distance teleoperation serves this principle. Reduced access to medical equipment, constrained resources and limited experience of the on-site staff are significant factors already; however, further technical difficulties arise with extreme telesurgery. The

primary difficulty with teleoperation over large distances (especially beyond Earth orbit) is the communication lag time. Even in the case of intercontinental teleoperation—assuming the usage of commercial communication links—latency can be hundreds of milliseconds. While military satellite networks show better performance, these are not accessible for regular use. Surgery robot control communication protocols must be robust and fault-tolerant, while advanced visualization and augmented reality techniques should help the human operators to better adapt to the special challenges.

Significant delay in the sensor feedback can distract the surgeon and cause serious safety hazards, as examined by different research groups [38, 39]. Engineering methods have been developed to overcome the difficulties originating from insufficient quality of communication, unpredictable propagation conditions and hardware failures.

The continuous development of the internet backbone infrastructure has resulted in a significant reduction of typical latencies. Using commercial services, delay may be around 85 ms across the United States, and the lag time might be up to 400 ms world-wide. A recent telerobotic experiment, *Plugfest 2009* showed 21–112 ms latency for various connections within the U.S. and 115–305 ms for intercontinental connections [40]. Due to the Transmission Control Protocol over Internet Protocol (TCP/IP) and the routing algorithms latency can vary over trials, and can further degrade user performance. (Description on the existing space and ground communication infrastructure and the human ability to compensate for latency can be found in Appendix B.)

1.2 Surgical Robot Systems

In the past decades, several different robotic surgery devices have been created, and a few reached the market. The *Medical Robotic Database* [41] lists almost 400 international surgical robotic projects, several dozens are with the capability of teleoperation. Parallel, the number of surgical robotics related publications has been steadily rising in the past years [33]. Many books, tutorials and articles have been published on surgical robotics in the past 25 years, a subjective selection of the most notable ones include [1, 42, 43, 44, 45, 46, 47, 48, 49, 50]. The more generic field of surgical robotics is well covered by conferences, journals and periodicals. (Detailed introduction to these is given in Appendix C.) In this section, only the most commonly used systems are introduced briefly, along with the prototypes created for extreme environment telesurgery. The primary application in the focus of the thesis work is neurosurgery, therefore a complete and up-to-date list of all major neurosurgical robot projects (44 items) can be found in Appendix D.

1.2.1 The da Vinci surgical system

The market leader *da Vinci* from Intuitive Surgical Inc. (Sunnyvale, CA), is a complete teleoperated robot, created with roughly 500M USD investment [51]. The company was founded in 1995, licensing many promising technologies, and by 1997 the first prototype (Lenny) was ready for animal trials. Prototype Mona performed the first human trials in Belgium in 1997, and the first da Vinci unit was created within a year [52]. The *U.S. Food and Drug Administration* (FDA) cleared the system for *general laparoscopic surgery* (July 2000), *thorascopic surgery* (March 2001) and *laparoscopic radical prostatectomy* (May

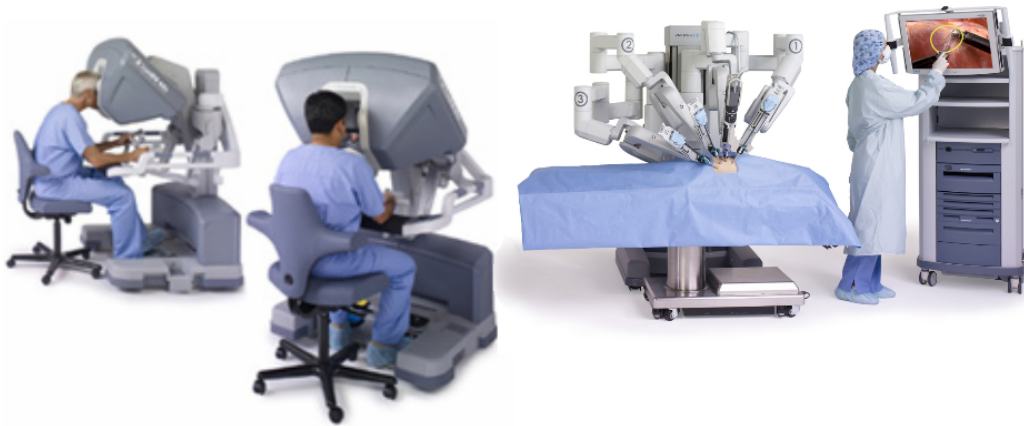


Fig. 1.7. Master controllers and the patient side manipulators of the newest da Vinci Si HD surgical system. (Courtesy of Intuitive Surgical Inc.)

2001), followed by many other approvals; most recently for *transoral otolaryngologic procedures*.

The da Vinci is basically a smart tool interface between the hands of the surgeon and the laparoscopic instruments in use. The patient side consists of two (or optionally three) tendon-driven, 6+1 *Degrees of Freedom* (DOF) slave manipulators. These are designed with a *Remote Center of Motion* (RCM) kinematics, resulting in an inherent safety regarding the spatial stability of the entry port. The camera holder arm navigates along 3 DOF, controlled with the same master interface. The system provides high quality 3D vision with stereo-endoscopes, adjustable tremor filtering (6 Hz) and motion scaling (1:1–1:5). The total weight of the system is 850 kg, and the setup takes up significant floor space in the OR.

Intuitive Surgical continued perfecting the system, and the second generation, the *da Vinci S*, was introduced in 2006 (Fig. 1.7). The latest version—the *da Vinci Si*—became available in 2009 with improved full HD camera system, advanced ergonomic features, and most importantly, the possibility to use two consoles for assisted surgery. Currently, there are more than 1600 da Vinci units around the world, $\frac{2}{3}$ of them in the U.S. The number of procedures performed is over 600,000, the most successful application being prostatectomy. According to Intuitive, around 90% of all *radical prostate removal* procedures were performed robotically in the U.S. in 2009.

1.2.2 The early bird NeuroMate

The *NeuroMate* was the first neurosurgical robotic device to get CE (Conformité Européenne) mark in Europe, and then the FDA approval in 1997 for stereotactic neurosurgical procedures [53]. It also has an approval for neuro-endoscopic applications and for frameless stereotactic surgery. Originally developed at the Grenoble University and produced by *Innovative Medical Machines International* (IMMI—Lyon, France), the 5 DOF NeuroMate provides accurate and trusted assistance for supervised needle positioning for

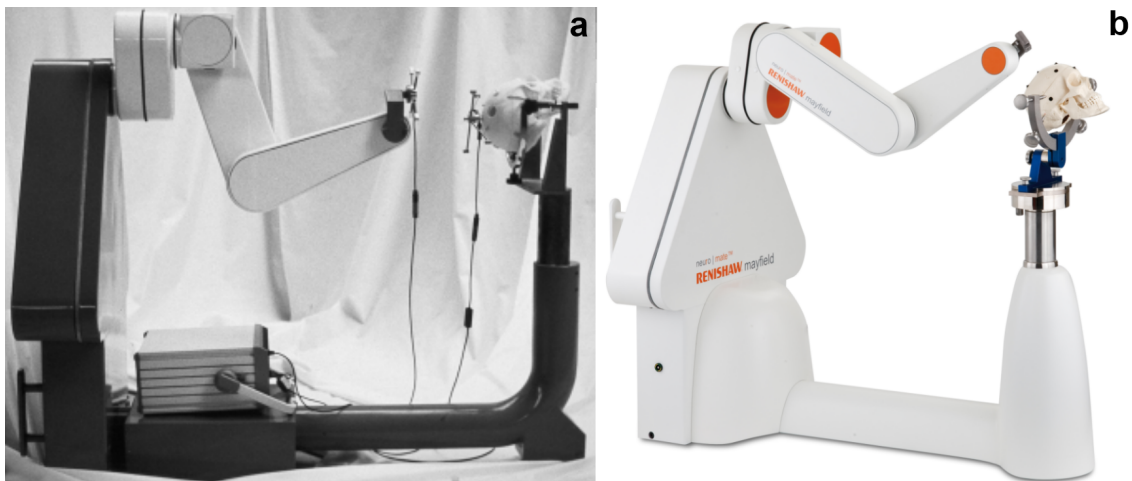


Fig. 1.8. The NeuroMate surgical robot for stereotaxis. (a) The ISS Inc. version. (b) The new design of the robot by Renishaw plc. (Courtesy of the manufacturers.)

brain biopsy (Fig. 1.8a). Combined with pre-operative images, it offers real-time visualization to give the surgeon precise location of a tumor [54]. The technology was bought by *Integrated Surgical Systems Inc.* (ISS—Sacramento, CA) in 1997. In the first couple of years of operation, the company has installed around 25 NeuroMate systems in the United States, Europe and Japan. The NeuroMate technology was acquired by *Schaerer Mayfield NeuroMate AG* (Lyon, France) in 2007, and reappeared on the market in *Renishaw plc's* (Wotton-under-Edge, UK) product line. It received a facelift, and ran under the trademark *neuro|mate* (Fig. 1.8b). More recently, the robot has been used for thousands of electrode implantation procedures for *Deep Brain Stimulation (DBS)*, *Stereotactic Electroencephalography (SEEG)* and *Transcranial Magnetic Stimulation (TMS)*.

The NeuroMate's reported intrinsic accuracy (i.e., the precision of the individual hardware and software components) is 0.75 mm, with a repeatability of 0.15 mm [55]. In a human stereotactic surgical experiment conducted in 2002, the application accuracy (the overall precision in performing the desired task) was measured to be 0.86 ± 0.32 mm (mean \pm standard deviation—STD) in frame-based configuration and 1.95 ± 0.44 mm in frameless mode [54]. The average application accuracy of 10 different robots was measured to be 0.6 mm.

1.2.3 Light-weight prototypes for teleoperation

Some systems never got commercialized, although they were created with the aim to significantly improve telesurgery. The *National Aeronautics and Space Administration's Jet Propulsion Laboratory* (NASA JPL, Pasadena, CA) and *MicroDexterity Systems Inc.* (Albuquerque, NM) developed the *Robot-Assisted Micro-Surgery (RAMS)* system in the mid '90s [56]. The RAMS consists of two 6 DOF arms, equipped with 6 DOF tip-force sensors, providing haptic feedback to the operator (Fig. 1.9a). It uses a kinematically identical master controller; however, the operator sits right next to the slave arms. The robot was originally aimed for ophthalmic procedures, especially for laser retina surgery. It is capa-

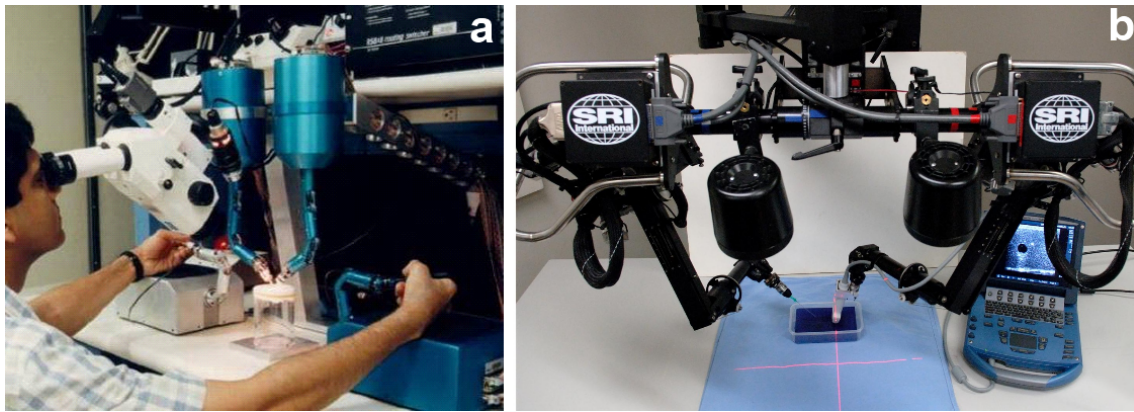


Fig. 1.9. (a) The RAMS robot developed at NASA JPL in 1998. (Courtesy of NASA.) (b) The M7 robot demonstrating autonomous ultrasound-guided tissue biopsy on a phantom. The procedure was live broadcasted at the American Telemedicine Conference 2007. (Courtesy of SRI International.)

ble of 1:100 scaling (achieving 10 micron accuracy), tremor filtering (8–14 Hz) and eye tracking. Currently, the prototype rests idle at JPL, as the project was discontinued.

Medical doctors and scientists at the BioRobotics Lab., University of Washington (Seattle, WA) have developed a portable surgical robot that can be a compromise solution to install even on spacecrafts with its 22 kg overall mass [57]. The U.S. Army's *Defense Advanced Research Projects Agency* (DARPA) supported *Raven* works along the same principle as the da Vinci. It has two articulated, tendon-driven arms, each holding a stainless steel shaft for different surgical tools. It can easily be assembled even by non-engineers, and its communication links have been designed for long distance remote-control. The system participated in multiple field tests, and now several units are being built for large scale clinical trials [58].

Realizing the importance of a light, but stiff structure, *Stanford Research International* (SRI, Menlo Park, CA) started to develop the *M7* robot in 1998 (Fig. 1.9b). The system weighs only 15 kg, and it is equipped with two 7 DOF arms, motion scaling (max. 1:10), tremor filtering and haptic feedback [59]. The end-effectors can be changed very rapidly, and even a laser tissue welding tool can be mounted on it. The controller has been designed to operate under extremely different atmospheric conditions, therefore it only contains solid-state memory drives. The software of the *M7* was updated later to better suit the requirements of teleoperation and communication via Ethernet link. The *M7* performed the world's first automated ultrasound guided tumor biopsy in 2007.

The *German Aerospace Center* (DLR) Institute of Robotics and Mechatronics (Wessling, Germany) has already built several generations of light-weight robotic arms for ground and space applications [60]. They have also taken part in many telerobotic space experiments in the past decades. The *KineMedic* and the most recent *MIROsurge* system—consisting of three 7 DOF MIRO robots—are considered for teleoperation even in extreme locations, as one arm is only 10 kg and capable of handling 30 N payload with high accuracy [61, 62]. (Further concepts are introduced in Appendix E.)

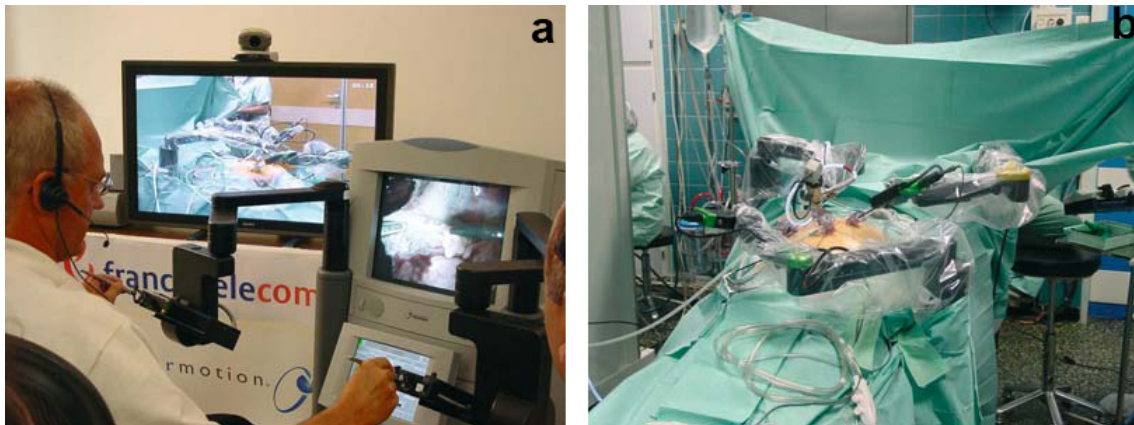


Fig. 1.10. The Zeus robot during the first intercontinental surgery; colectomy was performed on the patient in Strasbourg (b) from New York (a). (Courtesy of IRCAD.)

1.3 Significant Robot Teleoperation Experiments

1.3.1 Long distance telesurgery

To push the limits of remote surgery, several experiments have been conducted in the past two decades. The most important ones are briefly introduced here to outline the tendencies in the field and to support the scientific relevance of the thesis project.

The former *Zeus robot* (Computer Motion Inc., Goleta, CA) was controlled in master–slave setup, and received FDA clearance in 2001. In 2003, the whole company was bought by Intuitive Surgical, and the product line was stalled.

The Zeus used UDP/IP (User Datagram Protocol over Internet Protocol) for communication, facilitating various telesurgery experiments [63, 64]. It proved to be a solid platform to test and experiment different telesurgical scenarios. Between 1994 and 2003, the French *Institut de Recherche contre les Cancers de l'Appareil Digestif* (IRCAD) (Strasbourg, France) and Computer Motion worked together in several experiments to learn about the feasibility of long distance telesurgery and effects of latency, signal quality degradation. After six porcine surgeries, the first transatlantic human procedure—the Lindbergh operation—was performed with a Zeus in 2001 [65]. The surgeons were controlling the robot from New York (NY), while the patient laid 7,000 km away in Strasbourg (France) (Fig. 1.10). A high quality, dedicated 10 Mbps *Asynchronous Transfer Mode* (ATM) optical fibre link was provided by France Telecom, transmitting not just the control signals and video feedback, but also servicing the video conferencing facilities. Based on previous research [66], it was estimated that the time delay between the master console and the robot should be less than 330 ms to perform the operation safely, while above 700 ms, the operator may have real difficulties controlling the Zeus. An average of 155 ms communication lag time was experienced, out of which roughly 85 ms was the delay through the transmission, and 70 ms the coding and decoding of the video signals.

In Canada, the world's first regular telerobotic surgical service network was built and managed routinely between the *Centre for Minimal Access Surgery* (CMAS) at McMaster University Centre (Hamilton, ON, Canada) and a community hospital in North Bay (ON,

Canada) some 400 km away, using the Zeus robot [38]. The group also conducted various experiments on human performance degradation applying simulated signal latency [67]. The average latency recorded was about 150 ms using *Virtual Private Network* (VPN) on a commercial high-speed internet link. CMAS performed 22 telerobotic cases with *North Bay General Hospital* and over 35 telementoring cases with the *Complexe Hospitalier La Sagamie* (Québec, QC). The network was later extended to include more centers in Canada. While in the USA, the FDA only permitted the single case of telesurgery of the Lindbergh operation, Canadian health authorities cleared the method for routine procedures. Other groups found lower tolerance margin for latency while performing various robotic tasks [68].

The concept of the da Vinci (Fig. 1.7) theoretically allows remote teleoperation, but the previous versions of the robot used a proprietary short distance communication protocol through fibre optic to connect the master and the slave, and only the da Vinci Si system facilitates further displacement of the two units. However, in 2005, the U.S. TATRC presented collaborative telerobotic surgery (four nephrectomies on porcine) with modified da Vinci consoles, being able to overtake a master controller with a remote one through public internet connection [69]. During the experiment, the average roundtrip latency was 450 ms from Denver (CO) to Sunnyvale (CA) and 900 ms from Cincinnati (OH) to Sunnyvale, which degraded the performance of the physicians [70]. The *Canadian Surgical Technologies and Advanced Robotics* (CSTAR) in London (ON, Canada) used Bell Canada's *surgical grade VPN* to test the telesurgery-enabled version of the da Vinci. They performed six successful telesurgical porcine pyeloplasty procedures in Halifax (Nova Scotia, Canada), 1700 km away. The average network latency was 66 ms, the overall delay was over five times higher, originating from video signal processing, synchronization and projection [71].

More recently, an international research collaboration demonstrated the feasibility of intercontinental telesurgery through connecting 14 heterogeneous devices in 28 different configurations around the globe within 24 hours [40]. The Plugfest 2009 event showed how different robotic systems can communicate and share control. Basic surgical tasks (*Telerobotic Fundamentals of Laparoscopic Surgery* [72]) were practiced by surgeons to test the quality of the communication link.

1.3.2 Underwater trials

NASA has conducted several experiments to examine the effect of latency on human performance in the case of telesurgery and telementoring. The *NASA Extreme Environment Mission Operations* (NEEMO) take place on the world's only permanent undersea laboratory, Aquarius, a training and experiment facility for astronauts. It operates a few kilometers away from Key Largo in the Florida Keys National Marine Sanctuary, 19 meters below the sea surface. A special buoy provides connections for electricity, life support and communication, and a shore-based control center supports the habitat and the crew. Fourteen NEEMO projects have been organized since 2001, and three were focusing on teleoperation.

The 7th NEEMO project took place in October 2004. The mission objectives included a series of simulated medical procedures with an Automated Endoscopic System for Optimal Positioning robot (AESOP from Computer Motion), using teleoperation and tele-

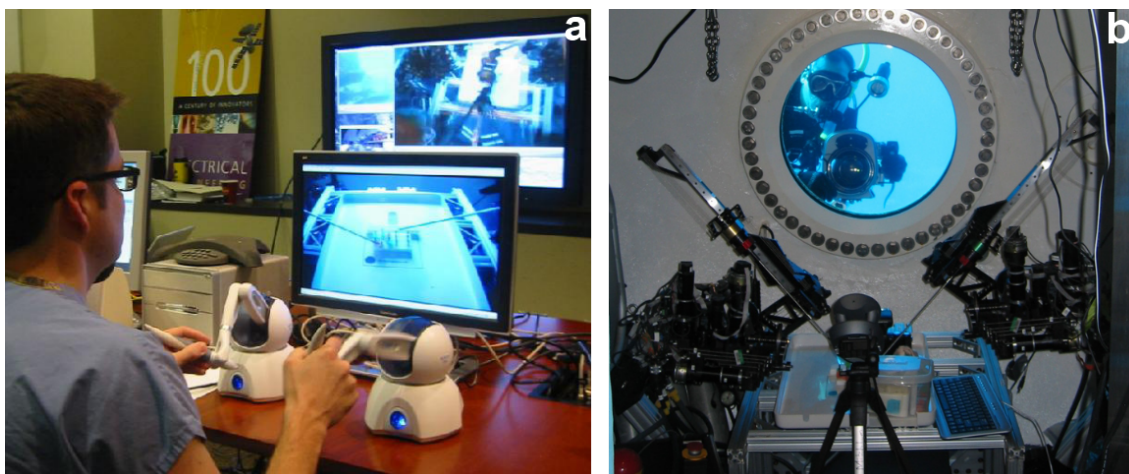


Fig. 1.11. The Raven robot performing the Fundamentals of Laparoscopic Surgery tasks on board of NASA Aquarius in Florida (b) while guided by a surgeon from Seattle (a). (Courtesy of University of Washington and NASA.)

mentoring [15]. The four crew members (one with surgical experience, one physician without significant experience and two aquanauts without any medical background) had to perform five test conditions: ultrasonic examination of abdominal organs and structures, ultrasonic-guided abscess drainage, repair of vascular injury, cystoscopy, renal stone removal and laparoscopic cholecystectomy. The AESOP was controlled from the CMAS (Ontario, Canada) 2,500 km away. A *Multi-Protocol Label Switching* (MPLS) VPN was established, with a minimum bandwidth of 5 Mbps. The signal delay was tuned between 100 ms and 2 s to observe the effects of latency. High latency resulted in extreme degradation of performance: a single knot tying took 10 minutes to accomplish. The results showed that the non-trained crew members were also able to perform satisfyingly by exactly following the guidance of the skilled telementor. They outperformed the non-surgeon physician, but fell behind the trained surgeon. Scientists also compared effectiveness of the telementoring and the quality of teleoperated robotic procedures. Even though the teleoperation got slightly higher grades, it took a lot more time to complete [73].

During the 9th NEEMO in April 2006, the crew had to assemble and install an M7 robot, and perform real-time abdominal surgery on a patient simulator. Microwave satellite connection was used for the procedure, and time delay was 3 s to mimic the Moon–Earth communication links. Each of the four astronauts had to train at least 2 hours with the wheeled in-vivo robots designed at the University of Nebraska. In another experiment, pre-established two-way telecom links were used for telementoring. The crew had to prove the effectiveness of telemedicine through the assessment and diagnosis of extremity injuries and surgical management of fractures. The influence of fatigue and different stressors on the human crew’s performance in extreme environments were also measured. Latency was set up to 750 ms in these experiments. The significant performance degradation of the microwave connection was noticed during stormy weather, causing a jitter in latency up to 1 s [73].

The 12th NEEMO project ran in May 2007, and one of its primary goals was to measure the feasibility of telesurgery with the Raven and the M7 robots (Fig. 1.11). NASA sent

a flight surgeon, two astronauts and a physician into the ocean. Suturing operations were performed on a phantom in simulated zero gravity environment to measure the capabilities of surgeons controlling the robots from Seattle. This time, the Aquarius was connected to the mainland through a Spectra 5.4 GHz Wireless Bridge, allowing for a minimum of 30 Mbps bandwidth, with an average latency of 70 ms. The HaiVision CODEC was used for video compression providing very good quality, but also introduced significant latency, up to 1 sec.

A group of three professionals guided the robot using commercial internet connection, while the communication lag time was increased till up to 1 s. Several simple tasks were performed, selected from the Fundamentals of Laparoscopic Surgery (FLS) [74] training set. The M7 demonstrated the first IG autonomous surgery (using a portable ultra sound system). It was live broadcasted at the American Telemedicine Conference 2007 (Nashville, TN), when the M7 precisely inserted a needle into a tissue phantom by itself.

1.4 Control Frames for Robotics

Similarly to classical robotics, homogeneous transformations are used in CIS to express coordinate frames (bases) and their manipulations. To facilitate the understanding of the equations, the commonly employed notations are defined in accordance with [75]. In general, a *homogeneous coordinate transformation* between coordinate frames A and B is constructed from a *translational* and *rotational* part, and described in the form:

$$\mathbf{x}_B = {}^A_B\mathbf{T}\mathbf{x}_A = {}^A_B\mathbf{T}_{\text{Rot}}\mathbf{x}_A + {}^A_B\mathbf{T}_{\text{Trans}}, \quad (1.1)$$

where \mathbf{x}_A and \mathbf{x}_B are 3D points (e.g. origins) in homogeneous form $[x, y, z, 1]^T$ and

$${}^A_B\mathbf{T} = \begin{bmatrix} {}^A_B\mathbf{T}_{\text{Rot}}^{3 \times 3} & {}^A_B\mathbf{T}_{\text{Trans}}^{3 \times 1} \\ \mathbf{0}^{1 \times 3} & 1 \end{bmatrix}. \quad (1.2)$$

Out of the many possible forms, rotations are most often given in *Euler angles* (ϕ, θ, ψ around three defined axes, respectively—e.g. x, y, z or more commonly in robotics, around z, y, z), therefore:

$${}^A_B\mathbf{T} \xrightarrow{\text{Rot2Euler}} \mathbf{t} = [x, y, z, \phi, \theta, \psi]. \quad (1.3)$$

Rot2Euler and *Euler2Rot* transformations are performed based on [75]. Alternatively, rotation can also be expressed with an angle (θ) around a given axis $\mathbf{n} = [n_x, n_y, n_z]$:

$${}^A_B\mathbf{T}_{\text{Rot}}(\mathbf{n}, \theta) = e^{\theta\mathbf{N}}, \text{ where } \mathbf{N} = \begin{bmatrix} 0 & -n_z & n_y \\ n_z & 0 & -n_x \\ -n_y & n_x & 0 \end{bmatrix}. \quad (1.4)$$

1.5 Accuracy Measures in CIS

Beyond introducing the different robotic devices and remarkable experiments, it is also important to enumerate the performance metrics applied to these systems. Probably the most important characteristic of interventional CIS systems is spatial accuracy, inherently determining their applicability, functionality and safety [1, 76, 77]. Errors and imperfections may originate in:

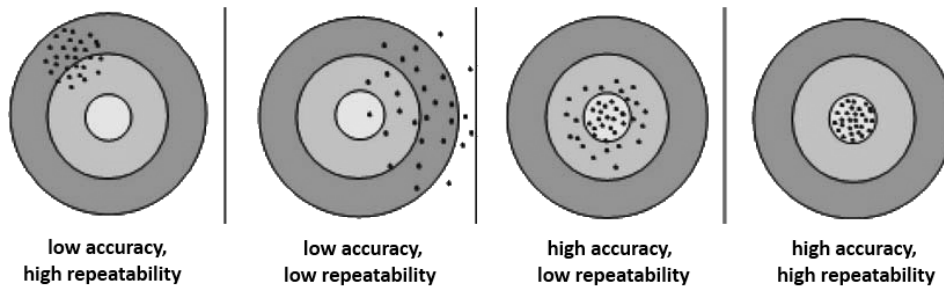


Fig. 1.12. Difference between accuracy and repeatability. (Based on [79].)

- imaging errors,
- volume model generation errors,
- treatment planning errors,
- errors introduced by hardware fixturing,
- intra-operative data noise,
- registration errors,
- inherent inaccuracies of surgical tools and actions.

Precision of robotic systems can be represented by the *accuracy* and *repeatability* of the device to characterize the overall effect of the encoders' fineness, rigidity of the structure and the compliance of the hardware elements (the servo motors, the gears or the links). Both terms are defined for industrial robots in the ISO 9283 standard (ISO TC-184/SC2/WG2). Accuracy refers to a robot's ability to position its end at a desired target point within the work volume. Generally, the absolute positioning accuracy shows the error of the robot when moving to a prescribed joint angle or Cartesian position. This expresses the mean difference between the actual pose (position and orientation) and the pose calculated from the mathematical model of the robot. "*Repeatability is the ability of the robot to reposition itself to a position to which it was previously commanded or trained*" [78]. It is the standard deviation of the positioning error acquired through multiple trials to reach the same joint values (Fig. 1.12). Repeatability is typically smaller for manipulators than accuracy, while both numbers are largely depending on speed, payload and the range of motion [76, 79].

From the clinical point of view, the accuracy of treatment delivery is important, knowledge of the task specific uncertainty. However, this may be difficult to measure routinely; requires mock operations, cadavers or the use of pre- and post-operative imaging combined. Some manufacturers have tried to construct advanced measurement tools to facilitate system assessment [80]. Alternatively, phantoms (artifacts) can also be used to replicate clinical conditions as much as possible.

In the case of IG therapies, the same metrics could be applied; however the effect of imperfect registrations and coordinate transformations have major contribution to the overall error. Performance estimation focuses on precision, noise, static/dynamic accuracy or latency. Medical device manufacturers typically provide maximum spatial error values with standard deviations, and publish limited experimental results on the distribution of

errors. According to [81], two conditions are necessary to correctly assess a positioning system's performance:

- characteristic statistics (defining trueness and precision),
- a specifically defined assessment protocol (on which the measurement is based).

1.5.1 Different accuracies

It is crucial to properly document the experiments evaluating the usability of a system. There are three different types of accuracies (in terms of spatial errors) that can be specified with different error numbers (determined in general) according to [9, 82]:

- intrinsic (technical) accuracy (0.1–0.6 mm),
- registration accuracy (0.2–3 mm),
- application accuracy (0.6–10 mm).

Intrinsic accuracy applies to certain elements, such as the robot or the navigation system. It describes the average error of the given component in operational use. Random errors (e.g., mechanical compliance, friction, loose hardware), resolution of the imaging device, inadequate control and noise can all result in low intrinsic accuracy. On the user interface side, discretized input and modeling errors may further decrease precision.

Registration errors are also present, as computational methods involve some kind of residual errors. It is only possible to find a normalized (e.g., least squares optimized) solution for a mathematical fitting problem. In IGS, a major source of error can be the markers (different types, forms and materials), displacement of the fiducials and determination of the center of the fiducials. Even though the distribution of error for one fiducial in a particular set of measurements is usually Gaussian, the aggregated error for many fiducials can only be approximated to comply with it.

Application accuracy refers to the overall targeting error of the integrated system while used in a clinical procedure or a mock setup. It realistically measures the task specific effectiveness of a system and is commonly used for validation. The application accuracy depends on all other sources of errors in a complex, non-linear way, therefore typically phantom, cadaver or clinical trials are required to determine it.

Further problems arise with the simple, ergonomic expression of spatial errors. Physicians may need a single number showing the precision of the system. In many applications, only the absolute distance from a desired location matters, therefore the *root mean square error* (RMSE) is given for the system:

$$E_{\text{RMS}} = \sqrt{\frac{1}{N} \sum_{i=1}^N (\mathbf{x}_i - \mathbf{x})^2}, \quad (1.5)$$

where N is the number of measurements, \mathbf{x} is the desired point and \mathbf{x}_i is the i^{th} measured point. RMSE incorporates both mean and standard deviation values [83]:

$$E_{\text{RMS}}^2 = E_{\text{mean}}^2 + E_{\text{STD}}^2. \quad (1.6)$$

The RMSE is only an unbiased representation of isotropic and independent errors in the 3D space. For other cases, the covariance matrix of the distribution should be used.

Equation (1.5) does not incorporate the angular errors of the system, even though any 3D registration or tracking component with a rotational error will affect the translational accuracy. Even worse, the factor of degradation is dependent on the value of the translational vector, due to the nature of the homogeneous transformation matrix multiplication. This is especially bothersome in the case of intra-operative navigation systems that are supposed to be used with a Dynamic Reference Base, therefore the rotational inaccuracy's effect on the linear accuracy will depend on the distance between the camera and the patient, and will have anisotropic distribution. This model is valid for zero-mean Gaussian distributions, and RMSE gives a single value even to multi-dimensional distributions. Chapter 4 addresses this issue in more details.

Evaluating robotic systems usually involves not only mathematical modeling and simulation, but also extensive accuracy tests. One of the difficulties in evaluating an IG robot is to acquire the ground truth—the gold standard. This is feasible through the use of a significantly more precise device (e.g., laser scanner, accurate camera system), the use of a measurement phantom or other trusted method (providing the ground truth).

In industrial robotics, accuracy measures and tests have been widely used, and some got straight applied to CIS [77]. Most commonly, the medical device is guided (directed) to different positions and orientations along a precisely known set of landmarks (fiducials) or an accuracy board. The positions can also be recorded with an independent localizer.

To evaluate the different point-based tests, certain measures have been developed and used. Let us assume that there are $N + M$ points in total used during the experiment. These can either be artificial fiducials or anatomical landmarks; $\mathbf{p}_1, \mathbf{p}_2, \dots, \mathbf{p}_N$ points are used during the registration, and $\mathbf{p}_1^*, \mathbf{p}_2^*, \dots, \mathbf{p}_M^*$ points are used during the procedure (and to derive the error at the target).

Specific to the tracker and the setup, the *Fiducial Localization Error* (FLE) includes the intrinsic and extrinsic sources of error, representing the accuracy of a position tracker to localize a \mathbf{p}_i ($i = 1, \dots, N$) point, consequently the centroid of the cluster of measured points [84]. FLE can be defined as the mean value of the error of all samples:

$$E_{\text{FLE}} = \frac{1}{N_{\text{Fiducial}} M_{\text{Trial}}} \sum_{i=1}^{N_{\text{Fiducial}}} \sum_{j=1}^{M_{\text{Trial}}} \varepsilon(i, j), \quad (1.7)$$

where ε is the error of a single measurement at a given fiducial. One of the most precise optical trackers available on the market is the *Optotrak Certus* from NDI. It has a 0.1–0.15 mm (RMSE) FLE according to the specifications. Typical surgical navigation systems provide less accurate measurements, a 0.2–1 mm RMSE error.

Fiducial Registration Error (FRE) is the mean square distance between homologous fiducial points; the residual error of the paired-point registration between the given subset of the known and recorded fiducial coordinates ($\mathbf{p}_i, i = 1, \dots, N$) during an accuracy test [85]:

$$E_{\text{FRE}} = \sqrt{\frac{1}{N} \sum_{i=1}^N \|\mathbf{T}\mathbf{p}_i - \mathbf{q}_i\|^2}, \quad (1.8)$$

where N is the number of fiducials used during the registration, \mathbf{q}_i is the position of the i^{th} fiducial in one space (may be the robot), \mathbf{p}_i is the same point in the other (patient space) and \mathbf{T} is the computed homogeneous transformation as defined in (1.1). FRE is connected

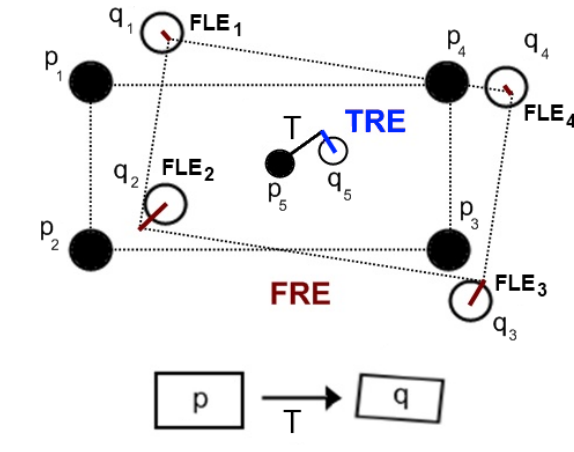


Fig. 1.13. Definition of FRE and TRE to assess point-based registration methods. The black and white circles represent corresponding point pairs in the two different spaces. FLE is the spatial deviation between the true and the recorded position of the landmark points that the registration is built on. FRE is the residual error of the applied transformation calculated over the points used to derive the T transformation. TRE is the error of mapping (a set of) independent points from the original space to the registered space.

to FLE [85] through:

$$E_{FRE}^2 = \left(1 - \frac{1}{2N}\right) E_{FLE}^2. \quad (1.9)$$

Target Registration Error (TRE) is the deviation between points (\mathbf{p}_i^* , $i = 1, \dots, M$) in the reference and the other (registered) coordinate system. FLE, FRE and TRE are presented in Fig. 1.13. TRE is typically used for the characterization of schematic point-based registrations. Ideally, FRE and TRE both equal zero.

$$E_{TRE} = \sqrt{\frac{1}{M} \sum_{i=1}^M \|\mathbf{T}\mathbf{p}_i^* - \mathbf{q}_i\|^2}, \quad (1.10)$$

where M is the number of fiducials used to compute TRE (that are not identical to any of the points used during registration). In medical cases, TRE might be computed based on distinguished anatomical points. Mean TRE is related to mean FLE through [86]:

$$E_{TRE}^2(\mathbf{r}) \approx \frac{E_{FLE}^2}{N} \left(1 + \frac{1}{3} \sum_{i=1}^3 \frac{d_i^2(\mathbf{r})}{f_i^2}\right), \quad (1.11)$$

where \mathbf{r} is the target point, N the number of fiducials, $d_i(\cdot)$ the distance of the target from the axis i of the fiducial points and f_i is the RMSE distance of all the fiducial points from that same axis. Novel research publications show that TRE and FRE are independent for point-based registrations, therefore (1.11) can only be used to estimate TRE for a given fiducial configuration and a defined target position [86, 87]. The FRE in a particular case does not correlate with TRE for any arbitrary chosen configuration. Many commercially available surgical navigation systems use (incorrectly) FRE as a metric for the precision of the system, while others use proprietary algorithms to define an accuracy number to display to the surgeon.

Different research groups defined further types of errors to better describe their models or procedures [88, 89, 90, 91]:

- *Image Plane Error* (IPE) is the measurement error of the camera sensor. It contains the focus, distortions and other imperfections of the lens through the extrinsic and intrinsic camera parameters,
- *Calculated Registration Error* (CRE) is the correlation of pre-operative image and intra-operative anatomical data,
- *Mean Fiducial Error* (MFE) is similar to CRE, using fiducials for registration,
- *Mean Target Error* (MTE) represents the 6 DOF error of a rigid tracking target in the centroid of the fiducials. Its value depends on the FLE of each fiducial and the spatial arrangement of the tracking target,
- *Target Positioning Error* (TPE) is the spatial mismatch between the position of the device and the surgical target that incorporates TRE plus confounders in clinical use.
- *Target Localization Error* (TLE) is the spatial mismatch between the reported position of the device versus its ideal location.
- *Total Targeting Error* (TTE) is the overall error. For the RMSE values, $E_{\text{TTE}}^2 = E_{\text{TRE}}^2 + E_{\text{TLE}}^2$.

More recently, iterative solutions have been developed to solve the *absolute position/orientation problem* in registration [92] under the assumption of anisotropic FLE [93, 94]. Other methods are focusing on the real-time approximation of FLE to improve registration accuracy [95]. The need to define better accuracy metrics has gained more attention in the international research community [90, 77].

1.5.2 Current accuracy standards

International bodies are making efforts to standardize medical robotics similarly to industrial robotics, but currently, there are no widely accepted regulations. Some of the existing robotic and medical device development standards are applicable to CIS. (See Appendix A for further details.)

In 2004, the *American Society for Testing and Materials* (ASTM) initiated a new standards committee (ASTM F04.05) under the title *Standard Practice for Measurement of Positional Accuracy of Computer Assisted Orthopaedic Surgical Systems (CAOS)*. The goal was to develop an international standard for metrology, validation and performance of CAOS systems [79]. The first draft (from 2007) deals with the localizer functions of navigation systems (optical, mechanical or electromagnetic). The defined generic measurement board—nicknamed *Nebraska phantom*—was machined from aluminum-alloy, and was tested with three different CIS systems [96]. Practically, it is a multi-surface object with 47 identical fiducial points (0.75 mm deep cone-shape holes) distributed on its surfaces (Fig. 1.14a).

ASTM F04.05 plans to develop a set of standard for specific tasks (cutting, drilling, milling, reaming), distinct surgical applications (joint replacement, implant nailing, plating, osteotomy) and imaging modalities (fluoroscopy, CT, MR, ultrasound).

Supporting the ASTM group, a multi-institution technical committee presented a white paper, calling for standardization in many areas of CIS [98, 99]. Based on technological

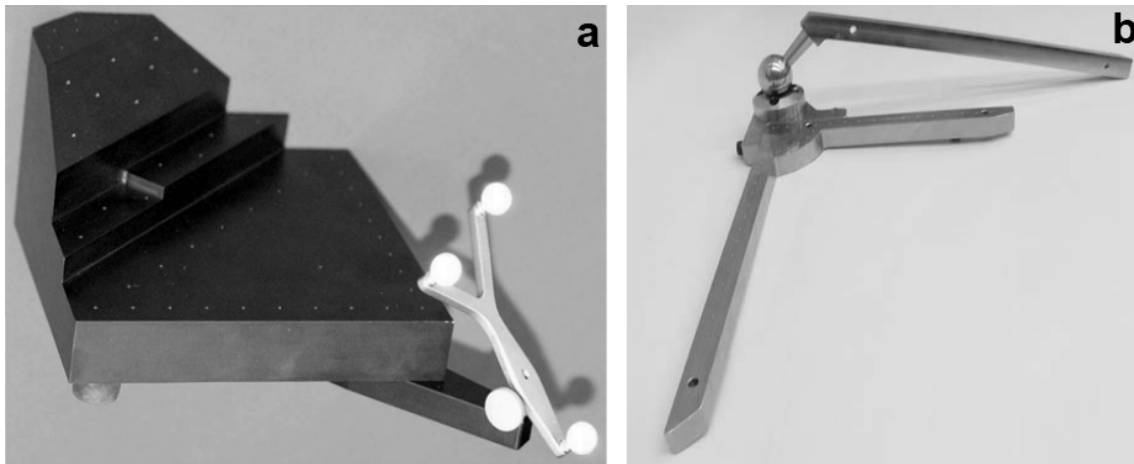


Fig. 1.14. (a) ASTM CAOS draft standard accuracy phantom [96]. (b) NIST CAOHS Artifact for the verification of hip replacement surgery [97].

and economic analysis, metrology and standards should be applied especially to the following categories of medical devices:

- computer-assisted navigation and surgery,
- surgical robots (mostly in manual control mode),
- surgical robots and phantom (artifact) devices,
- stimulation devices,
- drug-delivery and physiologic monitoring devices.

Another clinical phantom (*the Computer-Assisted Orthopaedic Hip Surgery—CAOHS Artifact*) was built at the *National Institute of Standards and Technology* (NIST) to quantify task specific measurement uncertainty [97]. It was designed to mimic hip joint using magnetic ball-and-socket to be able to simulate hip replacement procedures (Fig. 1.14b).

More recently, a workgroup has been created to prepare an extension to the existing ANSI/AAMI ES60601-1:2005 standard on Medical Electrical Equipment, focusing on medical robotics and personal care robots. The first meeting was held in early 2010, and the new amendment is due August 2013. Working together with the subcommittee of the *International Organization for Standardization* (ISO TC 184) dealing with robotic devices, the priorities of the new standard are:

- defining medical software systems and associated technical requirements,
- streamlining the application of risk management,
- clarifying the definition of essential performance,
- identifying essential performance and mitigating risk.

TABLE 1.2

DIFFERENT ACCURACIES PUBLISHED FOR MAJOR SURGICAL ROBOT SYSTEMS. DETAILS OF THE EXPERIMENTS ARE NOT PUBLISHED IN MANY CASES. VALUES ARE GIVEN WITH MEAN \pm STANDARD DEVIATION. ^ATARGET REGISTRATION ERROR ^BREGISTRATION PERFORMED WITH A STEREOTACTIC FRAME (HEAD FIXATOR) ^CREGISTRATION IN FRAMELESS MODE ^DFIDUCIAL LOCALIZATION ERROR

Robot	Company	Intrinsic accuracy	Repeatability	Application accuracy
Puma 200 [19]	Memorial Medical Center		0.05 mm	2 mm
ROBODOC [100, 101, 102]	Integrated Surgical Systems Inc. Curexo Technology Corporation	0.5–1.0 mm		1.0–2.0 mm 1.05 mm
NeuroMate [55, 54, 103]	Innovative Medical Machines Int. Integrated Surgical Systems Inc. Renishaw plc	0.75 mm 0.6 mm 0.36 ± 0.17 mm ^a	0.15 mm	0.86 ± 0.32 mm ^b 1.95 ± 0.44 mm ^c
da Vinci [104]	Intuitive Surgical Inc.	1.35 mm ^a 1.02 ± 0.58 mm ^d		
da Vinci S [105]	Intuitive Surgical Inc.	1.05 ± 0.24 mm ^d		
CyberKnife [106, 107]	Accuray Inc.			0.42 ± 0.4 mm 0.93 ± 0.29 mm
B-Rob I [108] B-Rob II [108]	ARC Seibersdorf Research ARC Seibersdorf Research		1.48 ± 0.62 mm 0.66 ± 0.27 mm	1.1 ± 0.8 mm
SpineAssist [109]	Mazor Surgical Technologies			0.87 ± 0.63 mm

1.5.3 Examples of accuracy measurements

In indirect IGS 3–5 mm RMSE accuracy is considered acceptable, whereas 2 mm is recommended for IG neurosurgery. However, sub-millimeter precision is recommended for robot assisted procedure (direct IGS) [9]. When CIS system accuracies are reported in research papers most often none of the generic standards is followed. Instead, custom metrics, protocols and measurement boards are used. As a consequence, it is extremely hard to effectively evaluate and compare the results, and in many cases, the experiments are not described in details (e.g., application accuracy refers only to a single component of a system). While these protocols are better regulated in the industry, the assessment techniques are various both in the case of medical robots and surgical navigation systems. (For more details, consult Appendix A.)

Table 1.2 summarizes the published accuracy measures of the most important surgical robots. These were mostly conducted in engineering laboratories, using different methods.

Understandably, the control mode of the robot can greatly influence the overall accuracy of the system. It should be noted that for many systems—like the da Vinci—safety originates from keeping the human in the control loop at all times through real-time sensory feedback. This means the intrinsic positioning accuracy of the robot is not crucial anymore; the surgeon uses the provided visual information to compensate for any positioning errors. However, this approach introduces the generic limitations of a human operator (such as physiological latency), and even in this case, the intrinsic accuracy of the components has significant effect on the performance.

1.6 The JHU Image-Guided Neurosurgical System

I was given the unique chance to be involved in a neurosurgical project as a visiting scholar at the *Center for Computer-Integrated Surgical Systems and Technology* (CISST ERC) incorporated in the *Laboratory for Computational Sensing and Robotics* (LCSR) at the Johns Hopkins University (JHU, Baltimore, MD) in 2007/08. Later, I continued working on the system as an international collaborator. Due to this, I could gain first-hand experience in surgical robot development, and the first two thesis groups were prototyped for and tested on the JHU skull base surgery system (Fig. 1.15). This chapter is an introduction to the fundamentals of the robot, presenting my collateral work in understanding the specialties and identifying the parameters of the system, along with the results of preliminary phantom and cadaver studies.

We have developed the integrated surgical robotic system at JHU to support skull base drilling. The system consists of a modified *NeuroMate* robot (see Section 1.2.2), a *Stealth-Station* (SS) surgical navigation device from Medtronic Navigation Inc. (Louisville, CO) and adequate network and control equipment (Fig. 1.16). The goal was to improve the safety and quality of neurosurgery while reducing the operating time. The robotized solution is only used for the removal of the bone tissue, to gain access to the anatomical region affected by a tumor or other lesions. Our technical approach was to use pre-operative imaging to identify the region of the skull base that could be safely drilled. We chose a cooperative control implementation (also called shared or compliant control), in which the surgeon applies forces to move the robot and the robot enforces the safety boundaries. Other example for robots with similar *hands-on* control concept include the Steady-Hand Robot at JHU [110, 111] and the Acrobot, developed at Imperial College (London, UK) for total knee replacement [112]. Other groups targeted skull base procedures with different approaches [113, 114, 115, 116, 36, 117], and similar setups have been used for cochlear implant placement as well [36, 118, 119, 120], which supports the validity of our approach.

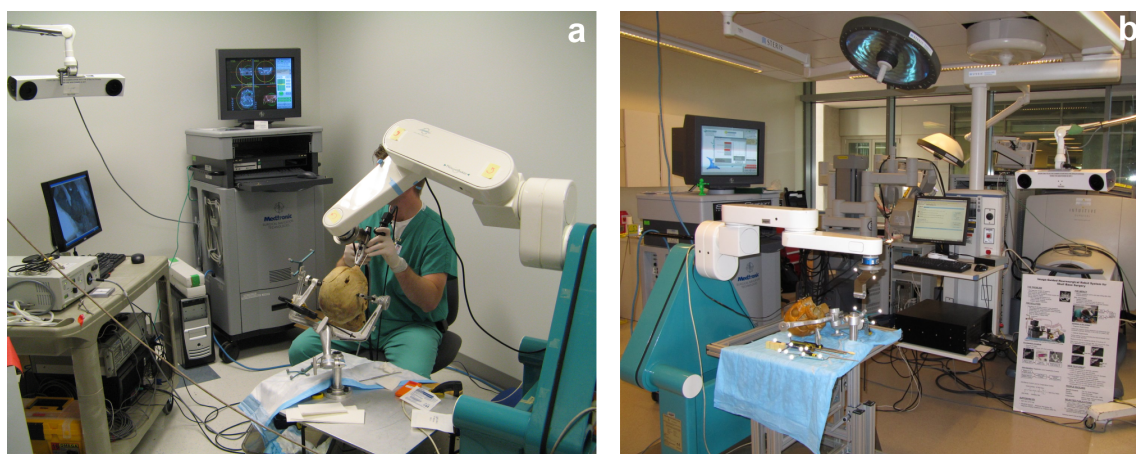


Fig. 1.15. The NeuroMate-based IGS system at JHU. (a) The NeuroMate in action: bone cutting on the skull base in a cadaver experiment at JHMI. (b) The integrated robotic system moved to the R. A. Swirnow Mock Operating Room at JHU Homewood campus.

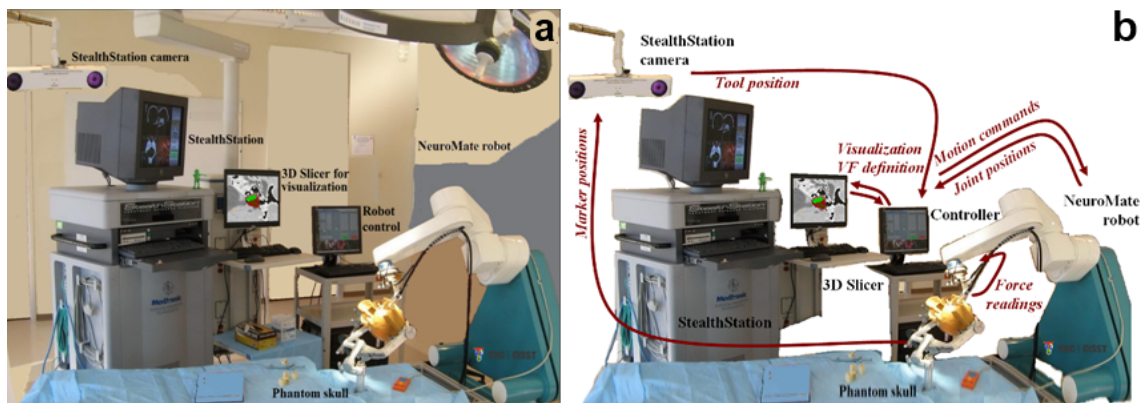


Fig. 1.16. Hardware and software elements of the integrated neurosurgical system. (a) Physical arrangement of the devices. (b) Major flow of information between the system components.

The JHU system has three major advantages. First, it offers advanced visualization features typical used in stereotactic surgery; the tool's position can be followed on the 3D model of the patient, acquired from pre-operative CT scans. Second, the surgical tool is mounted on the rigid robot, thereby improving its stability. The surgeons still hold the classic drill tool and directs its movement, but they can release the tool any time. Finally, the most important advantage—and the novelty of the application—is that the physician can define virtual boundaries on the CT scan prior to the operation. This is called *Virtual Fixture* (VF), and once registered to the robot, it is strictly enforced, thus preventing the tip of the tool from going beyond the defined safe area. These features together can greatly increase the safety and the reliability of the procedure, ease the surgeon's task and potentially reduce operating time.

1.6.1 JHU System components

1.6.2 The modified NeuroMate robot

The FDA-cleared NeuroMate consists of 5 revolute joints, each mobilized by a separate, high precision servo motor. The robot contains embedded joint controller boards that are integrated into the links, significantly reducing the required cabling. The JHU version has slightly different controller architecture (provided by Integrated Surgical Systems Inc.) than the commercial version. Each joint controller board contains a microprocessor and is responsible for two axes of the robot, also dealing with power amplification.

The power supplies are placed in the triangle shaped base, eliminating the need for a separate controller rack. The JHU system communicates with the main PC through a *Controller Area Network* (CAN) bus, which is a broadcasting based differential serial bus protocol for connecting electrical control units. It allows each node to send and receive messages in one direction at a time. In every communication cycle (18.2 ms), the joint encoders are read, and new commands are sent to the motors. On the lowest level, the joints are given velocity commands. The highest linear velocity of the robot is approximately 50 mm/sec.

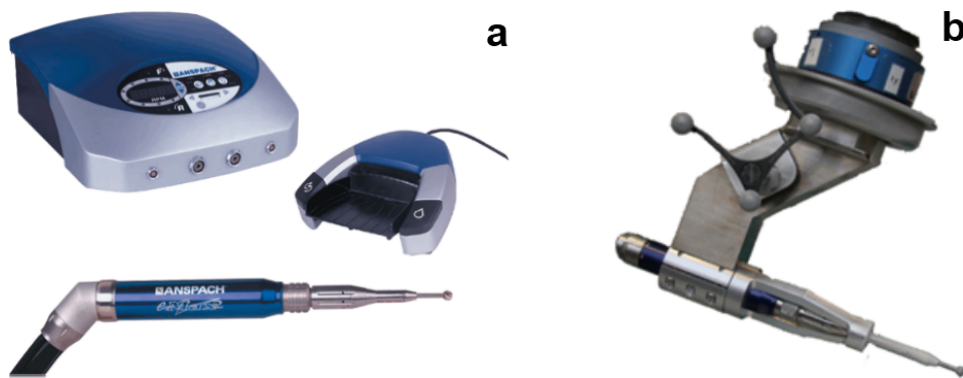


Fig. 1.17. (a) The Anspach eMax 2 surgical drill's base unit, foot pedal and hand-held tool. (Courtesy of The Anspach Effort Inc.) (b) The JR3 force sensor, optical markers and the eMax 2 drilling tool attached to the NeuroMate robot.

1.6.3 StealthStation intra-operative navigation system

The system uses an FDA-approved *Medtronic StealthStation* for navigation. The SS has an infrared LED array to illuminate the target area (in the range of approximately 1.5–2 meters and 15–20 degrees), whereupon the reflections are monitored by a pair of Polaris cameras (NDI Inc.), with a base distance of 0.5 m. The images are segmented and processed by cameras and transferred to the SS rack for further handling. Each rigid body used with the SS has four or five marker balls mounted in different arrangements. If all markers are visible, the system computes the base point relevant to the rigid body (by fitting the pre-defined geometric parameters). The SS is only capable of tracking two rigid bodies at a time (one reference frame—DRB and one tool—TRB), and there is an option to manually switch between different reference frames and tools.

It is possible to access the raw data from the SS through the *StealthLink* research interface [121]. The homogeneous transformation matrices connecting the inner base (camera) coordinate frame to the two tracked rigid bodies can be acquired along with a geometry error number that gives information about the accuracy of segmentation and model fitting.

We use three different rigid bodies in our setup (two at a time):

- a *Tool Rigid Body* is fixed on the robot's end-effector (therefore specifically we may call it *Robot Rigid Body*—RRB),
- one is connected to the patient (e.g., at a *Mayfield head clamp*).

These two rigid bodies allow us to determine the robot's position with respect to the skull. A third tool, a hand-held pointing probe is used to register the CT image coordinates (the patient anatomy) to the Patient Image (PAT).

1.6.4 Other system components

The tool serving as the end-effector is an *Anspach eMax 2* high-speed instrument (The Anspach Effort Inc., Palm Beach Gardens, FL). This is a classical, air-driven, hand-held surgical device, controlled by a foot-pedal (Fig. 1.17a). It provides torque compensation,

bi-directional rotation, operates at a maximum velocity of 80,000 rpm and comes with interchangeable tool-heads. There are various 3–5 mm diamond coated milling and drilling heads available. The tool-holder (with reinforced bracket) is attached to the end of the NeuroMate through a force sensor (Fig. 1.17b). A 6 DOF sensor (JR3 Inc., Woodland, CA) measures the forces and torques applied on the end-effector, hence enabling cooperative control. It is useable up to 100 N force in x , y directions and 200 N in z direction, with a sensitivity of $[0.1, 0.1, 0.2]$ N in x , y , z directions, respectively and a time resolution of 400 Hz. Sensor output is acquired from the vendor’s custom adapter board installed in the PC.

The system further integrates the *3D Slicer* (www.slicer.org) software [122] for pre-operative planning and intra-operative visualization (Fig. 1.18). 3D Slicer is an open source, cross-platform application for visualizing and analyzing medical image data, developed within the frames of an international cooperation, coordinated from the *Brigham & Women’s Hospital* (Boston, MA).

3D Slicer is used as our planning system because it enables us to create complex VFs and export them in an open file format (VTK polydata). Prior to the operation, the image editing and model creation features of *Visualization Toolkit* (VTK) is used to define the VF (www.vtk.org). The open platform allows implementation of various tools and features. During the procedure, Slicer displays the cutting tool with respect to the VF and pre-operative image (the SS can only display the image, since we have no means to download the VF to it).

The high-level controller of the robot runs on a separate PC workstation containing the *Real-Time Application Interface* (RTAI) for Linux [123]. RTAI is an open-source, real-time extension for Linux kernel that applies strict timing constraints. The robot control software was written in C++ language and contains approximately 10,000 lines. It uses the *cisst* open source CISST ERC Software library package (<https://trac.lcsr.jhu.edu/cisst>). This is a set of libraries developed at JHU for CIS applications [124, 125]. It facilitates the use of basic linear algebra operations, matrix manipulations and numerical methods.

The control software consists of *mainTask*, *controlTask*, *devStealthLink* and *neuromateTask* threads. The *neuromateTask* communicates with the robot through the CAN bus

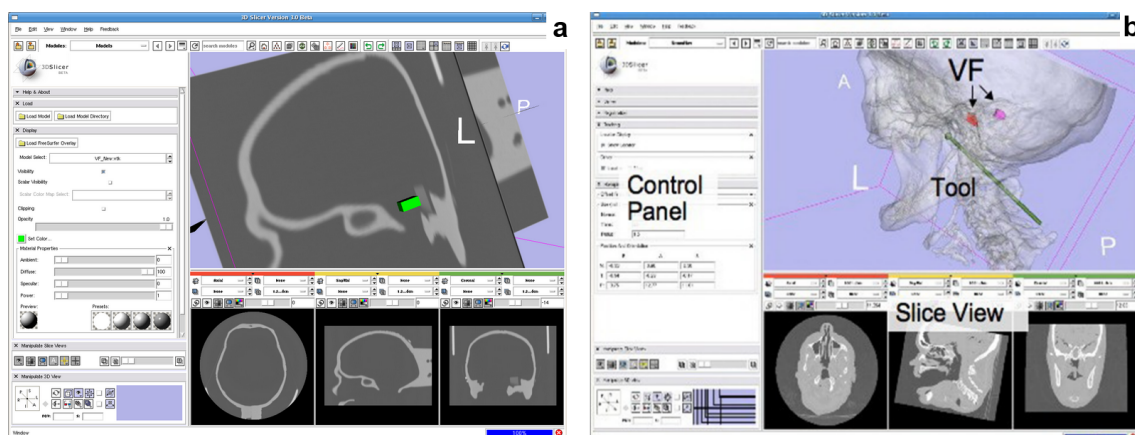


Fig. 1.18. Screenshot of the Slicer 3D program with loaded phantom CT and defined Virtual Fixture.

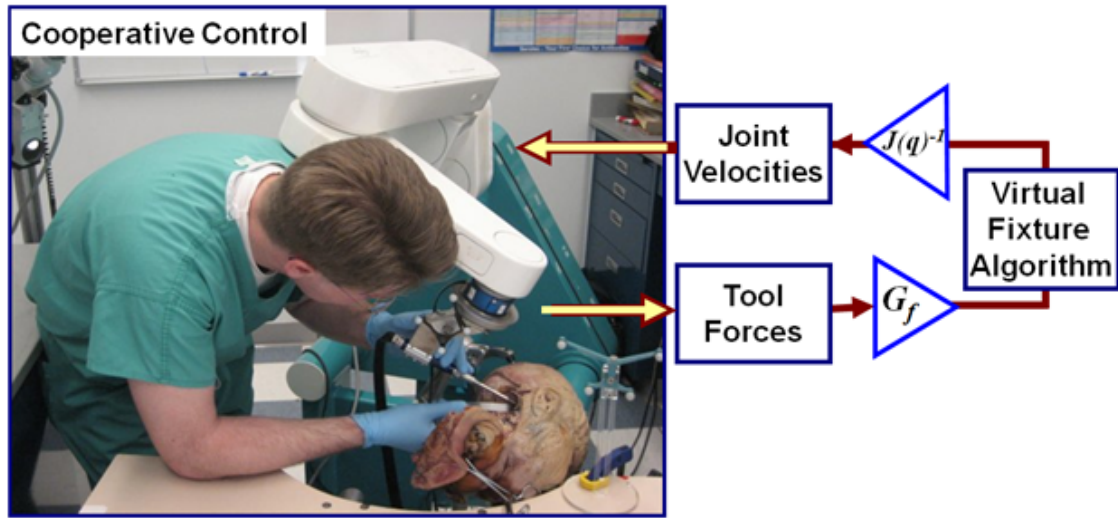


Fig. 1.19. Admittance control of the JHU skull base surgery robot (during a cadaver experiment) [126].

to gather the joint feedbacks and establish target joint positions. Joint velocity commands are created on this level. The `devStealthLink` handles the `StealthLink` to access the research interface of the SS. The `controlTask` implements the supervisory control layer and is responsible for the realization of the cooperative force control and VF computation during drilling. It also communicates with the SS and reads the force sensor. The `neuromateTask` and `controlTask` require periodic, real-time execution, which is provided by RTAI. On the highest level, the *Graphical User Interface* (GUI) is managed by the main thread, and it was created using the *Fast Light ToolKit* (FLTK—www.fltk.org).

1.6.5 Operation in cooperative control mode

In our setup, the NeuroMate robot is able to run in cooperative control mode, where the readings of the force sensor are used to control its motion. Depending on the orientation of the force exerted by the surgeon, the robot moves in the prescribed direction with a velocity proportional to the force. For convenience, it is possible to choose translational or rotational motion of the tooltip separately. The lower level controller program on the PC (`neuromateTask`) communicates with the embedded processors in the robot over the CAN bus in every 18.2 ms (55 Hz). While in compliance mode, the robot uses the following admittance control law:

$$\dot{\mathbf{q}} = \mathbf{J}^{-1}(\mathbf{q})\mathbf{f}(d)\mathbf{G}_f \begin{bmatrix} \mathbf{F}_w \\ \mathbf{T}_w \end{bmatrix}, \quad (1.12)$$

where \mathbf{q} is the joint vector, $\mathbf{J}(\mathbf{q})$ is the Jacobian matrix resolved at the tooltip, $\mathbf{f}(d)$ is a location-dependent diagonal matrix of scale factors (see more details in Section 1.6.7), \mathbf{G}_f is a diagonal matrix of admittance gains, \mathbf{F}_w is the measured force and \mathbf{T}_w is the vector of the torques (Fig. 1.19). The 5 DOF kinematics does not constrain the application as surgeons would seldom need rotation around the drill shaft.

The GUI serves as the ultimate control panel for the robot. In addition to displaying basic information, it offers the possibility of switching between different guidance modes,

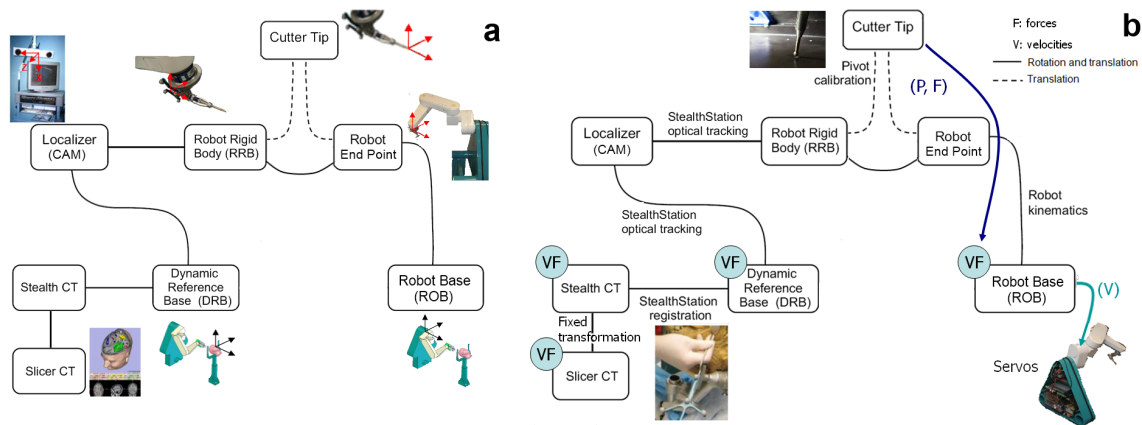


Fig. 1.20. (a) The control frames of the JHU system. (b) The calibration/registration procedures connecting the frames, allowing the control of the whole system. Blue VF circles means that the Virtual Fixture is valid in that frame.

force/position control, performing calibration/registration or saving the motion sequences of the robot.

Before operation, a series of setup and registration procedures have to be performed. The system uses several different coordinate systems, as every device has its own frame (Fig. 1.20a). Homogeneous coordinate transformations allow us to compute the position and orientation of an arbitrary point in any of the frames once the intermediate transformations are known. The purpose of the setup is to determine all the transformation of the system through the following steps:

1. Calibration procedures
 - calibration of robot parameters (once per installation),
 - calibration of the navigation system (once per setup to determine camera noise),
 - calibration of the surgical tool (pivot calibration after every toolchange).
2. Registration procedures
 - register pre-operative image to patient (through regular fiducial-based method),
 - register pre-operative image to 3D Slicer (DICOM's *Left Posterior Superior to Right Anterior Superior*),
 - robot to patient registration (through arbitrary chosen spatial points).

Transformation connecting the *Robot End Point* (REP) and the *Robot Base* (ROB)— \mathbf{T}_{REP}^{ROB} —is obtained by computing the forward kinematics. Eventually, all the coordinate frames are connected as shown on Fig. 1.20b, and therefore the given control sequence (e.g., a Virtual Fixture) is valid in every relevant frame.

1.6.6 Applying Virtual Fixtures

The concept of Virtual Fixtures was originally introduced more than 15 years ago [127], and successfully applied to robotic surgery at JHU, e.g., with the Steady-Hand Robot [128].

Implementing a VF involves the superposition of a pre-defined subspace on the real workspace. By applying different control rules within the VF, the effectiveness of telepresence and telemanipulation can be greatly improved [129]. VF serves as a 3D ruler guide, allowing the user to move along a certain boundary. Once the pre-operative image is registered to the robot coordinate system, it can enforce that the mounted tool remains within the safe zone. Beyond safety, the ergonomic implementation of the VF is also important, it can smoothen the robot's motion to mimic the human hand movements.

Generally, there are forbidden-region VF and guidance (guiding type) VF, its inverse. The latter divides the robot's workspace into three areas:

- *free space* (well within the VF), where the robot is free to move,
- *boundary zone* (within the proximity of the edge VF), where the robot's speed is reduced,
- *forbidden zone*, where the robot is not allowed to move beyond the VF.

In our application the Virtual Fixture is defined in 3D Slicer as an arbitrary volume, and approximated with a convex hull for further computations. The VF needs to be registered to the patient to ensure the tool to stay within the predefined anatomical area. Depending on which region the robot operates in, different control strategy is chosen. Within the proximity of any of the planes of the VF, the robot controller rescales the corresponding component of the motion through the $\mathbf{f}(d)$ vector in (1.12), resulting in a proportional reduction in velocity near the boundary. If the surgeon still pushes the robot towards the edge of the VF, the rigidity of the manipulator prevents major overcut. (Although it is still possible to force the robot's tip past the VF by approximately 1 mm due to the structural compliance of the mechanical parts.)

1.6.7 Virtual fixture computation

One of our specific tasks was to find a proper way to compute the effect of differentially shaped Virtual Fixtures. There are various ways to rescale the velocity vectors [110]. Assuming that the robot tooltip is at point \mathbf{p} , with a desired velocity vector of \mathbf{v} (based on the applied forces). For a given infinite plane i , defined by a point \mathbf{q}_i on the plane and a normal \mathbf{n}_i , we compute the distance d_i from the plane as:

$$d_i = (\mathbf{p} - \mathbf{q}_i) \cdot \mathbf{n}_i. \quad (1.13)$$

Our current implementation anticipates a convex VF, so we can employ this distance computation using infinite planes [130]. By convention, we define the normal \mathbf{n}_i , to point towards the safe side of the plane, so that d_i is positive when the robot tooltip is inside the Virtual Fixture. Let us consider the robot being in the boundary zone whenever $d_i < D$, where D is the width of the zone. The robot is slowed down whenever it is in the boundary zone and heading towards one or more of the VF planes. In other words, the i^{th} boundary plane is defined by a point $\mathbf{q}_i + D\mathbf{n}_i$ and normal \mathbf{n}_i .

Specifically, we slow down the robot (using an f scaling factor) for any plane i where $d_i < D$ and $\mathbf{v}\mathbf{n}_i < 0$ via the following equation:

$$\mathbf{v}_i = \mathbf{v} - f_i \cdot \mathbf{v} \mathbf{n}_i \cdot \mathbf{n}_i, \quad (1.14)$$

$$f_i = \begin{cases} 1 - \frac{d_i}{D}, & \text{for } d_i > 0 \\ 1, & \text{for } d_i \leq 0 \end{cases}. \quad (1.15)$$

If the point \mathbf{p} is within D of more than one plane and moving in the direction of both planes, we just perform the computations sequentially. For example, if this occurs for the planes defined by \mathbf{n}_1 and \mathbf{n}_2 , we can compute the velocities as follows:

$$\mathbf{v}_1 = \mathbf{v} - f_1 \cdot \mathbf{v} \mathbf{n}_1 \cdot \mathbf{n}_1 \quad (1.16)$$

$$\mathbf{v}_2 = \mathbf{v}_1 - f_2 \cdot \mathbf{v}_1 \mathbf{n}_2 \cdot \mathbf{n}_2 \quad (1.17)$$

$$= \mathbf{v} - f_1 \cdot \mathbf{v} \mathbf{n}_1 \cdot \mathbf{n}_1 - f_2 \cdot (\mathbf{v} - f_1 \cdot \mathbf{v} \mathbf{n}_1 \cdot \mathbf{n}_1) \mathbf{n}_2 \cdot \mathbf{n}_2 \quad (1.18)$$

$$= \mathbf{v} - f_1 \cdot \mathbf{v} \mathbf{n}_1 \cdot \mathbf{n}_1 - f_2 \cdot \mathbf{v} \mathbf{n}_2 \cdot \mathbf{n}_2 + f_1 f_2 \cdot \mathbf{v} \mathbf{n}_1 \cdot \mathbf{n}_1 \mathbf{n}_2 \cdot \mathbf{n}_2. \quad (1.19)$$

For the two-plane case, the final velocity, \mathbf{v}_f is given by the above equation for \mathbf{v}_2 :

$$\mathbf{v}_f = \mathbf{v} - f_1 \cdot \mathbf{v} \mathbf{n}_1 \cdot \mathbf{n}_1 - f_2 \cdot \mathbf{v} \mathbf{n}_2 \cdot \mathbf{n}_2 + f_1 f_2 \cdot \mathbf{v} \mathbf{n}_1 \cdot \mathbf{n}_1 \mathbf{n}_2 \cdot \mathbf{n}_2. \quad (1.20)$$

We note that the order of performing the computations has a small effect on the result. In particular, if we perform the first velocity reduction for plane 2 instead of (1.20), we get a different final velocity, \mathbf{v}'_f :

$$\mathbf{v}'_f = \mathbf{v} - f_1 \cdot \mathbf{v} \mathbf{n}_1 \cdot \mathbf{n}_1 - f_2 \cdot \mathbf{v} \mathbf{n}_2 \cdot \mathbf{n}_2 + f_1 f_2 \cdot \mathbf{v} \mathbf{n}_2 \cdot \mathbf{n}_2 \mathbf{n}_1 \cdot \mathbf{n}_1. \quad (1.21)$$

The only difference is due to the $\mathbf{v} \mathbf{n}_1 \cdot \mathbf{n}_2$ term in (1.20) and the $\mathbf{v} \mathbf{n}_2 \cdot \mathbf{n}_1$ term in (1.21). It is straightforward to verify that $\mathbf{v} \mathbf{v}_f = \mathbf{v} \mathbf{v}'_f$, so the difference between these equations represents a tradeoff between the magnitude and direction of the final velocity. If we assume that $\mathbf{v} \mathbf{n}_1$ has a larger magnitude than $\mathbf{v} \mathbf{n}_2$, then the net effect is that (1.20) produces a higher final velocity that diverges a little more from the direction of the user-specified velocity \mathbf{v} . Conversely, (1.21) produces a lower velocity, but is better at preserving the original direction of motion. Therefore, if we wish to optimize for the highest final velocity, the sequential computation should be started by considering the boundary plane i for which $\mathbf{v} \mathbf{n}_i$ has the largest magnitude. In practice, the difference between these two equations is negligible, thus we do not impose any particular ordering on the sequential computation.

Our implementation of the Virtual Fixture computation can therefore be summarized by the following pseudo-code:

```

 $\mathbf{v}$  = initial velocity (calculated based on the applied force)
 $f = 0$ 
for each plane  $i$  do
   $d = (\mathbf{p} - \mathbf{q}_i) \cdot \mathbf{n}_i$  (distance to plane)
  if  $d < D$  then
     $v_i = \mathbf{v} \cdot \mathbf{n}_i$  (velocity along normal)
    if  $v_i < 0$  then

```

```

    f = 1
    if d > 0 then
        f = 1 - d/D
    end if
    v- = f v_i n_i
end if
end if
end for

```

1.6.8 Applying Kálmán filters to the system

To improve the tracking capabilities of the StealthStation, different types of *Kálmán filters* (KF) have been tested with the system. Kálmán filtering is used to smoothen the StealthStation measurements [131]. The navigation system's measurements are pre-filtered to reduce the inherent measurement noise described in Section 1.6.10. Optionally, *Unscented KF* [132] might be used to compensate for small or gradual changes of the robot to patient transformation [133]. The state vector of the KF is:

$$\mathbf{x}_{\text{est}} = [p_x, p_y, p_z, \phi, \theta, \psi, \dot{p}_x, \dot{p}_y, \dot{p}_z, \dot{\phi}, \dot{\theta}, \dot{\psi}], \quad (1.22)$$

where \mathbf{x}_{est} is constructed from the Cartesian positions ($\mathbf{p}_{x,y,z}$), the Euler representation of the orientation (ϕ, θ, ψ) and the velocities of the aforementioned variables. The position and orientation parameters determine the dynamically changing robot to patient transformation. The discrete input of the filter derives from the measurement of the navigation system. Similar approach has been lately applied by other groups as well [134, 135].

1.6.9 Phantom and cadaver experiments

We performed phantom and cadaver experiments to measure the efficacy and performance of the system. A box-like VF was defined, corresponding to an interchangeable foam block installed inside a plastic skull, as described in [136]. Prior to the tests, 2 mm slice width CT scans were taken of the skull with mounted adhesive fiducials (Fig. 1.21a). We performed the registrations required, and set up the system for mock operations (Fig. 1.21b).

After cutting 12 foam blocks in cooperative control mode, I used calipers to measure the actual size of the cavity and compared it to the desired shape (size of the VF). Errors were separated into a placement error (the difference in centroid locations between desired and actual cavities) and a dimensional error (the deviation in dimensions), which were 0.6 ± 0.8 mm (mean \pm STD) and 0.6 ± 0.3 mm, respectively. An example of cavities milled in the foam blocks are shown on Fig. 1.21c.

Cadaver tests were performed at the *Johns Hopkins Medical Institute* (JHMI) to verify the system with a more complex VF, and to gain insight to the emerging difficulties of a more realistic setup. A neurosurgery resident performed the cuttings and provided valuable feedback on the system for further development. An appropriate VF was created for the resection of bone to treat a hypothetical acoustic neuroma via a sub-occipital approach. This is a typical skull base operation that involves the cutting of around $0.2\text{--}1$ cm³ of bone tissue. We used a surgical endoscope camera and lights to aid the surgeon during the

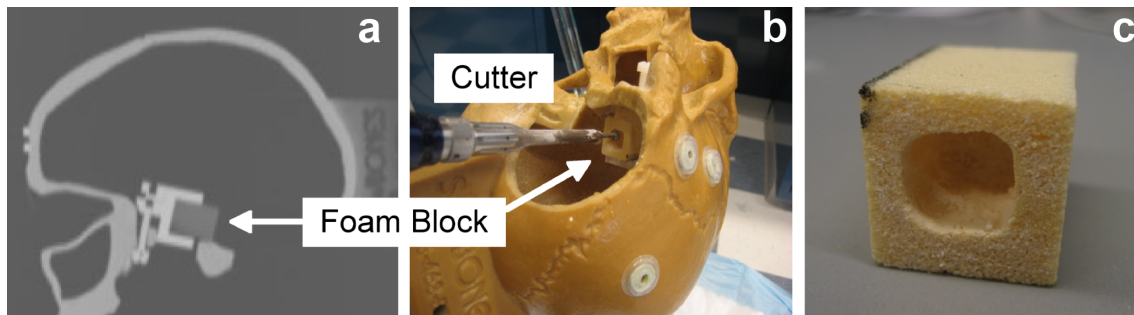


Fig. 1.21. Experimental setup for phantom tests. (a) The CT scan of the plastic skull. (b) Fixation of the skull with a foam block, simulating a skull base procedure. (c) Results of the foam block trials, a typical example for the rectangular cavity drilled. [126].

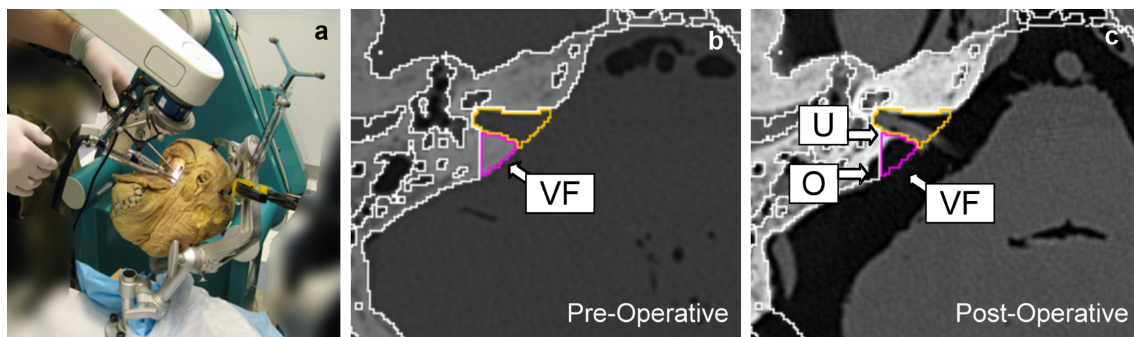


Fig. 1.22. (a) Experimental setup for cadaver tests. (b) Pre- and (c) post-operative CT scans of the cadaver, showing the Virtual Fixture and the error of the cut [137].

procedure (Fig. 1.22a). Clinical accuracy of the experiment was determined by manually aligning the pre- and post-operative CT scans (Fig. 1.22b,c). By overlaying the VF on the post-operative images we saw typical overcuts of about 1 mm, with a maximum of 2.5 mm. It should be noted that the treatment of live patients requires significantly higher accuracy thresholds, as cadavers do not move or breathe, and the tissue deforms very little due to the formalin fixation.

Phantom and cadaver tests are essentials in the process of validating any surgical system for further studies and finally for clinical use, as discussed in Section 1.5. However, many times, the accuracy numbers do not solely represent the theoretical performance of the devices, but also certain effects of the operating environment. My thesis is focusing on reducing these disturbing effects, and improving the quality of the procedures.

1.6.10 Challenges with the JHU system

There are two major performance metrics regarding any navigation system or mechatronic device delivering a treatment: accuracy and speed. The accuracy of CIS systems have been thoroughly discussed in Section 1.5, and extensive measurements have been performed to determine the relevant parameters of the JHU system [103]. Speed is referred to as the update rate of the system and the overall time taken to process the given information or

to execute a command. Communication link and network issues are also examined and discussed below.

Accuracy and speed of the robot

The NeuroMate is a steady platform for various procedures. The joint values are read by encoders with a resolution of $\frac{1}{26825}$ degree due to the high gearing, resulting in an insignificant 0.001 mm STD noise. In our experiments, the intrinsic accuracy of the robot was 0.36 ± 0.17 mm [103]. Repeatability was not measured, as the robot is only used in cooperative control. Multiple sets of complete measurements with the Nebraska phantom (Fig. 1.14a) derived 0.36 mm FRE based on 23 points, and 0.34 ± 0.17 mm (TRE) for the rest of the target points on the board. Most of the error comes from the bending of the tool used for the procedure. The same phantom was used for pivot calibration of the drills, where the position of the TRB relative to the tip can be determined with an average translational residual error of 0.73 mm, and the position of the REP with an average residual error of 0.57 mm.

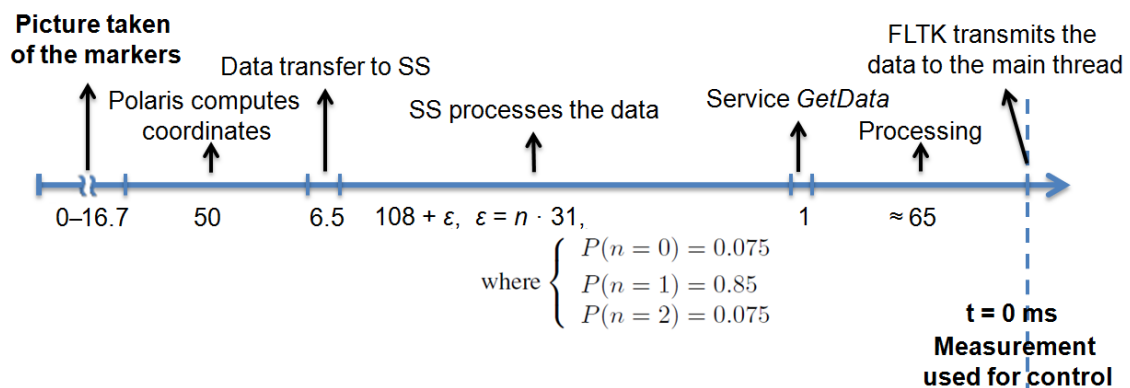
It is possible to communicate with the joint controller board at 55 Hz through the CAN bus. The serial port of the PC is used for communication, providing minimum latency (a few ms). During our measurements, we synchronized our timing to the robot measurements, and focused on determining the latency of the navigation system relative to the NeuroMate.

Accuracy and speed of the navigation system

The reported intrinsic accuracy of the StealthStation is 0.04–0.29 mm in different arrangements [136], with an application accuracy of 1.6 ± 0.68 mm [138], though it was seen to be susceptible to the lighting conditions. The position of the probes and line of sight for the infrared CCD cameras are critical issues throughout the procedure, as covering of any of the optical markers can result in significant error. Experiments on the Nebraska phantom with the Medtronic hand-held probe resulted in 0.51 ± 0.42 mm TRE (with 0.52 mm FRE), averaged over 3 trials. With the Robot Rigid Body, the accuracy numbers were 0.49 ± 0.22 mm TRE (FRE: 0.49 mm), based on 5 trials. The accuracy of the navigation system is fairly isotropic throughout the manufacturer-defined workspace. The system only provides valid measurements if the geometry error parameter is below 0.5 mm. This value tends to rise at the edges of the workspace, and also depends on the cleanliness of the markers and their proper fixation.

Initial experiments concluded that the SS provides position information updates at every 131 ± 19.7 ms [103]. More sophisticated tests showed that the variance is smaller, and basically caused by the discrete (unknown) sampling frequency of the SS cart towards the Polaris. On average, the SS updates its interior position information in every 108 ms, and the distribution of the update rate suggests that the internal frequency of polling the Polaris is 31 ms. In approximately 2% of the time, the SS does not update its buffer, therefore additional safety measures have to be taken for those periods. Further experiments could be conducted based on the techniques described in [139] for even more precise approximation; however, that would not change the chosen control approach.

StealthStation (total delay: ~275 ms)



Robot System (total delay: ~15 ms)

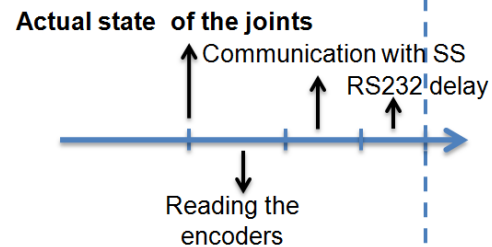


Fig. 1.23. Detailed timeline of information processing in the JHU system based on thorough measurements.

Latencies in the system

I performed extensive measurements to better understand the timing issues with the integrated system. With network communication analysis tools (*tcpdump* and *WireShark* from CASE Technologies), it was possible to roughly reconstruct the pathway of the signals; Fig. 1.23 shows the relative timing of the information propagation and processing within the system. Based on synchronized robot and camera experiments, post-processing and smoothing the data, I could determine that the average generalized latency of the SS is 259.89 ± 9.02 ms relative to the robot. This can be broken down to several components. First, the Polaris cameras integrated to the StealthStation run at 60 Hz, and it takes 3 cycles (50 ms) to process an image. (As our setup uses passive markers, evaluation of a frame is based on a single pair of stereo images.) However, the SS only allows to fire the LEDs and get a new image at 20 Hz. The result of the image processing (the transformations connecting the rigid bodies) is polled by the SS in a discrete mode. NDI claims a 6.5 ms transition time at 115,200 bps for the Polaris data.

The communication between the SS and the controller PC is Ethernet based. After sending the *GetData* command, the packets are transmitted in the following pattern (one polling takes 0.55 ms on average):

```
client — GetData → SS
client ← ACK — SS
client ← XXX — SS
client — ACK → SS
```

TABLE 1.3

INCREASE OF MEASUREMENT NOISE DUE TO THE UNCOMPENSATED LATENCY CAUSED BY THE STEALTHSTATION. THE SPEED OF THE THIRD JOINT WAS GRADUALLY INCREASED, WHILE THE FOURTH JOINT OF THE NEUROMATE WAS AT 0° . MEAN, STANDARD DEVIATION AND MAXIMUM ERROR VALUES MEASURED ARE INDICATED. ALL VALUES ARE IN MM.

Joint speed	Mean error	STD	Max error
0	-0.01	0.45	1.14
1°/sec	-0.06	0.46	1.14
2°/sec	-0.06	0.51	1.36
3°/sec	-0.1	0.59	1.91
4°/sec	-0.14	0.65	2.41
5°/sec	-0.15	0.75	2.09

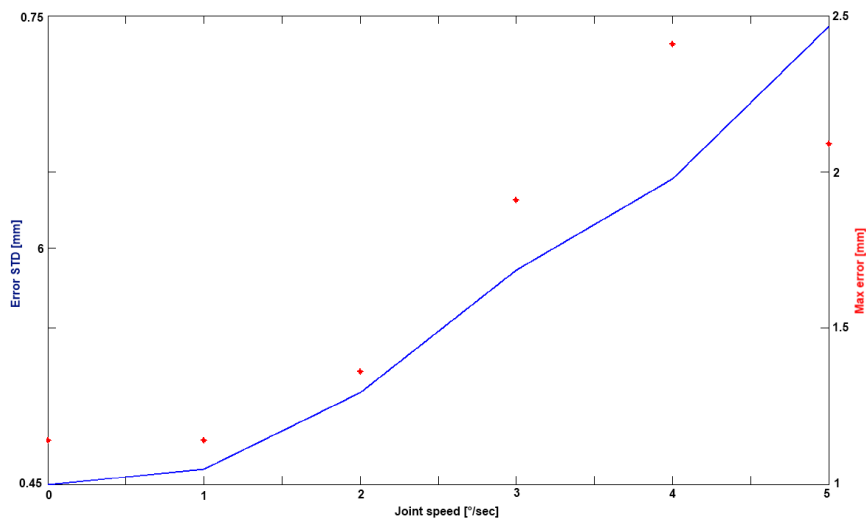


Fig. 1.24. Standard deviation and maximum of the measurement noise caused by latency.

client \leftarrow *CoordTraj* \rightarrow SS

client \rightarrow *ACK* \leftarrow SS.

The FLTK toolbox deals with the processing of the incoming data, and provides the transformation values to our code with some additional delay.

The uncompensated latency in the system has a definite degrading effect on the Stealth-Station's accuracy, proportional to the speed of the robot. Experiments were conducted to exactly measure it. The NeuroMate was set into a configuration close to 0° (most stretched), and only the third joint was moved with different speeds. This gives a fairly large linear velocity to the end effector. Table 1.3 and Fig. 1.24 show the numeric results, verifying the theory described above.

Chapter 2

RESEARCH PROBLEM STATEMENT

There is a clear trend in medicine to shift towards less invasive treatment solutions. Technology can only conquer the Operating Room gradually, as it takes a long time and a significant amount of training to change the general way procedures are performed. Many surgeons are reluctant to use novel devices or protocols that they do not completely understand or control. Image guidance in surgery at the same time is a steadily emerging field, representing a more than \$2 billion annual market. Physicians recognize the value of better imaging, more precise tools and smarter devices, as long as they stay in absolute control. Currently, the leading direction of development is to provide incremental updates to existing protocols and instruments. This means the enhancements of already deployed navigation devices, better simulation, accurate modeling, information coupling and error-resistant control.

In the case of robot-assisted image-guided surgery or radiation therapy, accuracy is paramount, therefore precise positioning of the surgical tools is required. Typical practice is the rigid and invasive fixation of the patient, and the employment of additional hardware to ensure safety. Accuracy of treatment delivery can also be affected by the many changing factors in the OR. There are several people in the room moving around the numerous medical devices surrounding the patient. IGS is based on the principle that the real-world setup does not change unpredictably over time and its registration to the still patient image space remains valid. IGS is sensitive to spatial changes, when the patient is unintentionally moved relative to the marker that tracks their motion. These events should be monitored and compensated separately.

- *Problem 1:* There is an urgent clinical need to reduce invasiveness through relying on the existing hardware in the OR. In the mean time, further costs and consuming too much space should be avoided. Integrated IGS systems must provide increased safety and accuracy features.

On the way towards having more robotic technology involved, a major problem is the proper modeling of system noises and their propagation. Even a semi-autonomously guided machine with a misaligned image overlay can be the source of malpractice. Effective mapping of spatial error based on a priori information is necessary to support the operation of integrated medical tools. Generalized error values and the experience of the medical staff determines the use of a system under different conditions. This means, worst

case safety margins have to be applied all along the procedure, while more thorough analysis of the distribution of spatial error would allow for optimized approach, leading to better treatment.

- *Problem 2:* Surgical procedures and integrated medical devices relying on patient imaging should provide a clear indication of the system's expectable error distribution at the Point of Interest. Generally accepted metrics should be applied to make existing devices comparable.

While pilot experiments have been conducted for distant telesurgery around the globe and between continents, regularly performed remote operations have many practical obstacles and limitations. Primarily, these systems need robust and stable controllers to deal with technological issues in the communication, and also to incorporate an adequate model of human-machine teleoperation.

- *Problem 3:* Long distance telesurgical applications require adequate control algorithms to support the operator and to handle latency. Effective emergency medical care in space requires innovative considerations and solutions.

Beyond these areas, there are many other challenges within the field of CIS attracting researchers. The ongoing efforts of the scientific community result in the continuous flow of technical breakthroughs and theoretical achievements. The problems identified above summarize three areas covering an important set of interconnected issues, and addresses scientific problems relevant to the clinical practice.

Chapter 3

ALGORITHM FOR PATIENT MOTION COMPENSATION

3.1 Control Structure for Image-Guided Robotic Systems

3.1.1 Background of patient motion tracking

Image-guided surgery requires trackable markers used as references (or perfect immobilization of the patient). The event of patient motion occurs when the body's position moves relative to the base frame of the device executing the surgical plan. The fundamental problem with patient motion is that without proper identification and compensation, the whole surgical plan may become obsolete, and the treatment potentially becomes harmful. From the clinical point of view, a few millimeters of error could be tolerated at the most (see Section 1.5.3), and depending on the speed of the tool this translates to 0.5–2 s delay. If it is noticed in time, re-registration is demanded to avoid damaging the patient. However, re-registration is usually time consuming (and might be cumbersome), therefore it should be avoided, whenever possible [140]. From the technical point of view, many forms of errors can be handled as patient motion. The main sources of external (i.e., excluding physiological) patient motion during surgery include:

- large forces applied by surgeon (e.g., bone milling, leaning against the patient),
- bumping into the operating table,
- inadequate fixation,
- equipment failure.

Physiological organ motion is not addressed within the frames of this research, as generally it requires different tracking techniques. Instead of surgical navigation systems, optical imaging devices and image processing algorithms are applied to extract non-rigid surface motion. This remains a distinct and important area of research [141, 142].

Dynamic correction for unforeseen events with the use of typically deployed intra-operative navigation systems remains a major challenge. While significant effort has been invested to describe the surgical workflow with mathematical models [143, 144], few projects have dealt with the modeling of the OR setup and environment in general. (Modeling for surgical robot systems has been more commonly addressed [145, 146].)

The robot's position information and the tracking data must be kept consistent throughout the operation, especially in the case of neurosurgical or orthopedic procedures, where high precision is absolutely crucial. Practically, this can be achieved with a rigid mechanical fixation between the device and the patient. Smaller robots, such as the SmartAssist (Mazor Surgical Technologies Inc., Caesarea, Israel) [147] or the Mini Bone-Attached Robotic System (MBARS, ICAOS and Carnegie Mellon University, PA, U.S.) [148] may be bone-mounted. This requires more invasive fixation on the patient side (bone screws), and large forces may still cause relative motion between the patient and the tool. In orthopedics, there are significant contact forces, making it necessary to use stronger screws. Employing a large, powerful robot may lead to serious tissue damage. The ROBODOC system (Curexo Technology Corporation, Fremont, CA) [149] was the first FDA-cleared automated bone milling robot for hip replacement, and it employs bone screws and a bone motion sensor to detect fixation failures. If the bone moves more than 2 mm despite the fixation, the system halts, and calls for re-registration.

One option to reduce tissue trauma is to use multiple dynamic reference bases to follow the motion of the robot base and the patient separately. Unfortunately, not every tracking system supports this, and it may cause difficulties to maintain the line-of-sight without disturbing the physician. Extending the active workspace of a tracking system may result in higher inherent accuracies due to the inhomogeneity of its field. Some commercially available systems combine surface-mounted and in-body fiducials to track external and physiological organ motion, though this requires a separate operation placing the markers. A successful example is the CyberKnife radiation therapy system (Accuray Inc., Sunnyvale, CA) that can track skin motion through a special suit and organ motion by taking bi-plane x-ray images and locating fiducials (gold beads) that were implanted pre-operatively [150]. Other groups tried different filtering approaches with limited effectiveness [120], and the same problem was observed with different experimental robotic setups [151, 152].

Robotic setups could incorporate accelerometers and gyroscopes, primarily to detect sudden changes; however these require electrical coupling and their resolution might not be sufficient for proper compensation. Besides, these would increase the costs and complexity of the system. *Charge-coupled device* (CCD) cameras can survey the OR, and image processing techniques could solve the localization problem, but the resolution may not be high enough, and it might have significant hardware requirements.

Dynamic registration and correction for patient motion has been implemented with PET/SPECT scanners to improve image quality through compensated reconstruction [153, 154, 155]. However, these setups only considered rigid environment, where neither the camera, nor the PET gantry move.

3.2 General Concept for Patient Motion Compensation

I proposed a tracking-based minimally invasive concept for patient motion compensation to support systems with less rigid fixation setup or limited surgical navigation capabilities. A general framework has been developed that may fit various setups. It is based on the principle that during regular operation, the position of the surgical tool mounted on an IG robot can be controlled precisely, once its location relative to the base coordinate system is known. The base frame can be chosen arbitrarily as long as it is mapped to the robot frame

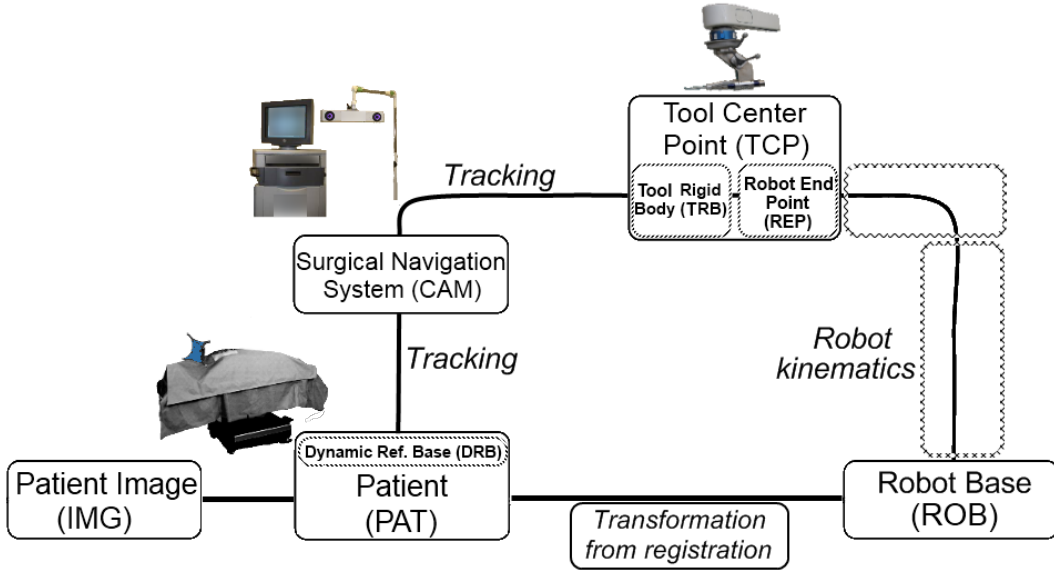


Fig. 3.1. General control concept of image-guided robotic systems. Solid line represents the typical route of control, while dashed lines is the proposed closed loop approach.

(and possible other control frames, such as the navigation systems) through known homogeneous transformations. A generic robot-integrated IGS system's schematic diagram is shown in Fig. 3.1. The nodes represent control frames and the lines are homogeneous transformations. The camera system is able to track both the motion of the Dynamic Reference Base (anchored to the patient) and another Tool Rigid Body. The navigation system is used to register the pre-operative image of the patient to the DRB with the help of e.g., a hand-held probe and skin fiducials. The TRB is typically attached to the robot, and the origin of the trackable TRB's frame and the Robot End Point is different. As illustrated in Fig. 3.2, this allows for the tracking of the tooltip (Tool Center Point—TCP) in 6 DOF, provided, the fixed transformation ${}_{TCP}^{TRB}\mathbf{T}$ and ${}_{TCP}^{REP}\mathbf{T}$ are obtained from calibration (or known a priori). The TCP is in the focus of interest regarding the application. The CAM and the ROB frames can be connected through ${}_{ROB}^{REP}\mathbf{T} = {}_{TCP}^{TRB}\mathbf{T}^{-1} \cdot {}_{TCP}^{REP}\mathbf{T}$. Hereafter, for simplicity, TCP will be used to address the frame of the robot tip, without explicitly mentioning the additional transformations.

The control signals to move the robot are practically computed in the patient's coordinate system (PAT) based on the treatment plan, and are transformed to the robot base frame (ROB) executing the transformations through the camera's coordinate frame (CAM):

$$\text{Control}|_{\text{IMG}} = {}_{ROB}^{TCP}\mathbf{T} \cdot {}_{TCP}^{CAM}\mathbf{T} \cdot {}_{CAM}^{PAT}\mathbf{T} \cdot \text{Control}|_{\text{PAT}}, \quad (3.1)$$

where $\text{Control}|_{\text{ROB}}$ and $\text{Control}|_{\text{PAT}}$ stand for the control signals expressed in the robot's and the patient's frame, respectively. It is possible to close the entire control loop in Fig. 3.1 performing another registration, acquiring the transformation between the ROB and the PAT frames. This can be computed under stationary conditions (during the setup phase) by calculating:

$${}_{ROB}^{PAT}\mathbf{T} = {}_{ROB}^{TCP}\mathbf{T} \cdot {}_{TCP}^{CAM}\mathbf{T} \cdot {}_{CAM}^{PAT}\mathbf{T}. \quad (3.2)$$

Throughout the surgical procedure, when unintentional motions of the patient with

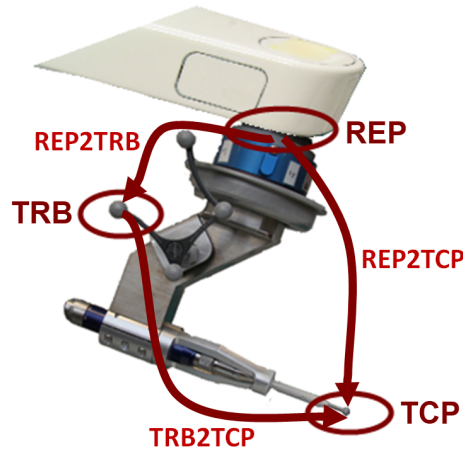


Fig. 3.2. The different control frames of the robot's end. The kinematics provide the Robot End Point, optical tracking determines the position of the Tool Rigid Body, and a priori calibration leads to the Tool Center Point.

TABLE 3.1

DIFFERENT SURGICAL MOTION SCENARIOS TOGETHER WITH THE REQUIRED ACTION TO TAKE IN THAT DISTINCT SURGICAL CASE.

Event (Yes/No)	SC1	SC2	SC3	SC4	SC5	SC6	SC7	SC8
Camera Moving	Y	Y	Y	Y	N	N	N	N
Patient Moving	Y	Y	N	N	Y	Y	N	N
Robot Moving	Y	N	Y	N	Y	N	Y	N
Desired action	Re-register	Wait for reg. update	Slow down the robot	Wait for reg. update	Slow down the robot	Wait for reg. update	Regular operation	Regular operation

respect to the robot are detected—i.e., deviations from the original PAT to ROB transformation—it is possible to compensate for the change by recomputing (3.2). This ensures that the original surgical plan stays valid.

The effectiveness of the concept depends on the inherent accuracy of the different components (the robot and the navigation system) and the registration. Importantly, the spatial localization can be corrupted by noise. In the case of the most typically used optical trackers, noise varies with the used marker type, the lighting conditions and the position and angle of the rigid bodies in the cameras' field of view. In the case of EMT, susceptibility to ferromagnetic materials in the proximity of the sensor can cause significant distortion. Beyond measurement noise, latency is also a major problem, making it harder to close the control loop for compensation through (3.2). Furthermore, robotic systems typically run in 20–100 Hz cycles at the highest control level, while commercially available tracking systems are not capable of more than 5–60 Hz data acquisition. Slower sampling rate only allows less frequent and therefore less accurate localization [156].

In an integrated surgical robotic setup (Fig. 3.1), changes in the OR means that the different elements move. My concept assumes that alterations can be modeled as distinct events of camera motion (*CamMot*), patient motion (*PatMot*), the regular motion of the

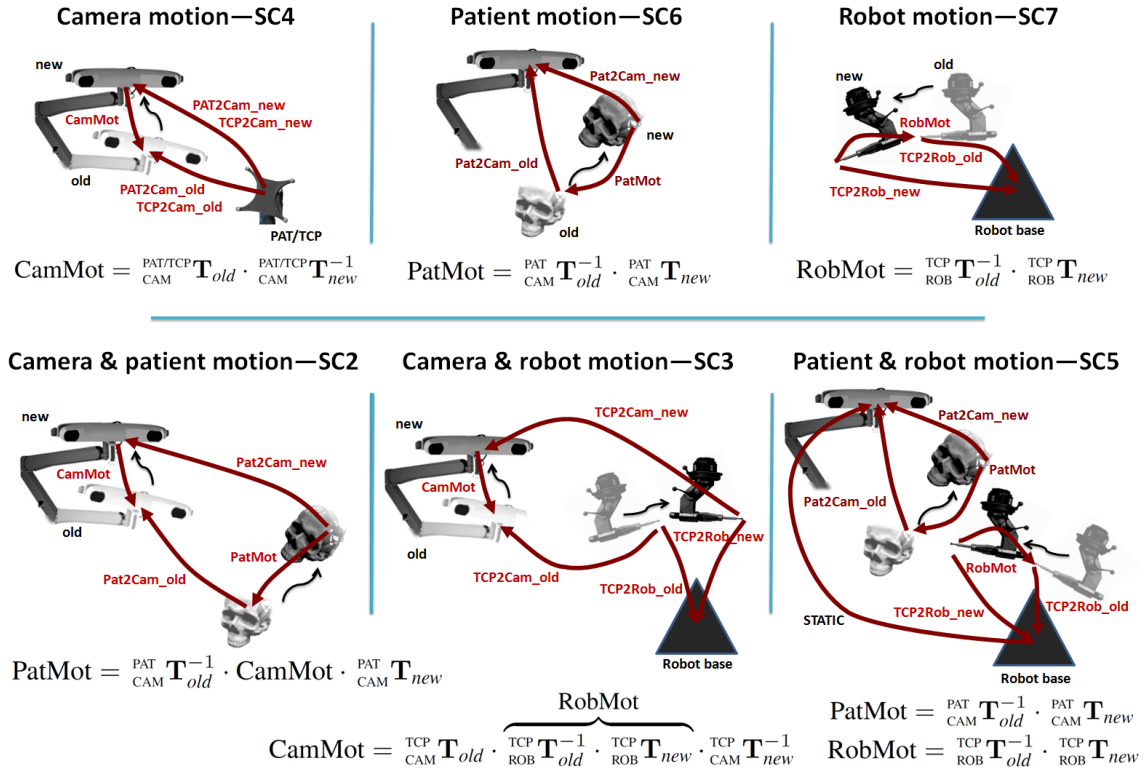


Fig. 3.3. Definitions of the different motions—Surgical Cases—occurring in an IGS system.

robot (*RobMot*) or the arbitrary combination of these. These are 6 DOF motions, without any general constraints. It is assumed that the robot is rigidly anchored to the ground, therefore its base cannot move during the procedure. From the control point of view, eight categories can be derived—referred to as *Surgical Cases* (SC)—listed in Table 3.1.

Fig. 3.3 shows the systematically defined motion vectors. Assuming that only one motion is happening at a time, the three possibilities are defined as:

$$\begin{aligned}
 \text{CamMot} &= \begin{matrix} \text{PAT} \\ \text{CAM}_{\text{old}} \end{matrix} \mathbf{T}^{-1} \cdot \begin{matrix} \text{PAT} \\ \text{CAM}_{\text{new}} \end{matrix} \mathbf{T} = \begin{matrix} \text{TCP} \\ \text{CAM}_{\text{old}} \end{matrix} \mathbf{T}^{-1} \cdot \begin{matrix} \text{TCP} \\ \text{CAM}_{\text{new}} \end{matrix} \mathbf{T} \quad (\text{SC4}), \\
 \text{PatMot} &= \begin{matrix} \text{PAT}_{\text{old}} \\ \text{CAM} \end{matrix} \mathbf{T}^{-1} \cdot \begin{matrix} \text{PAT}_{\text{new}} \\ \text{CAM} \end{matrix} \mathbf{T} \quad (\text{SC6}), \\
 \text{RobMot} &= \begin{matrix} \text{TCP} \\ \text{ROB}_{\text{old}} \end{matrix} \mathbf{T}^{-1} \cdot \begin{matrix} \text{TCP} \\ \text{ROB}_{\text{new}} \end{matrix} \mathbf{T} \quad (\text{SC7}).
 \end{aligned} \tag{3.3}$$

From the application point of view, these surgical events can be categorized either as *free motion* (regular safe operation), *potentially dangerous situation* (when something is moving, but it is still possible to compensate for it) or *forbidden event*, when re-registration is necessary to regain accuracy in control. During potentially dangerous events, it is necessary to slow down the robot proportionally to the factor of the risk, to allow for the collection of new sensor measurements to reduce the probability of damage due to spatial misalignment. If the robot is not moving, but motion has been detected, the robot must be halted until the update of the registration is completed (relying on the robot's stable position).

3.2.1 New Surgical Case identification concept

A robust method is required to identify the different SCs, and then an optimal position estimation technique for each can be derived separately [157]. In industrial robotics, *Behavior-based Control* and *Situation Recognition Techniques* have been developed before. I propose a similar solution for surgical applications. According to Table 3.1, SC8 refers to the completely stationary state, which is required for registration at the setup. During regular operations, only the robot is moving and performing the desired tasks (SC7). To support flexibility and line of sight, the camera might be moved or relocated (quite rarely). General practice allows for the free adjustment of the camera position, as only ${}_{\text{CAM}}^{\text{PAT}}\mathbf{T}^{-1} \cdot {}_{\text{CAM}}^{\text{TCP}}\mathbf{T}$ is used to generate control signals. It is crucial to reliably distinguish SC1, SC2, SC5 and SC6 from the others, as patient motion is the critical event we wish to compensate for.

To apply the concept described above, the changes of PAT (i.e., the amount of patient motion) must be known. The novelty of the concept is that it also incorporates the navigation system's inner coordinate base frame in the calculations—with certain constraints. To be able to rely on the camera's internal frame, it must be assured that the camera itself does not move during the evaluation period. In a general OR setup, this may be inconvenient to achieve through the rigid fixation of the camera system, therefore dynamic event recognition is required. Let us emphasize that camera repositioning occurs infrequently during a procedure, although it must be monitored and compensated accurately. SC5, SC6, SC7 and SC8 can be best handled by using the camera frame as an individual reference for patient motion (basically equivalent to having an additional DRB frame). This allows for the easy handling of SC5, as long as we have an accurate recording of the robot's motion:

$$\begin{aligned} \text{PatMot} &= {}_{\text{CAM}}^{\text{PAT}_{\text{old}}}\mathbf{T}^{-1} \cdot {}_{\text{CAM}}^{\text{PAT}_{\text{new}}}\mathbf{T} \\ \text{RobMot} &= {}_{\text{ROB}_{\text{old}}}^{\text{TCP}}\mathbf{T}^{-1} \cdot {}_{\text{ROB}_{\text{new}}}^{\text{TCP}}\mathbf{T} \end{aligned} \quad (\text{SC5}). \quad (3.4)$$

When the robot is static, we can use its position as a temporary reference frame to determine possible CamMot (SC2 and SC4) by subtracting the camera motion from the recorded difference in the PAT's position. PatMot can be identified and numerically determined through $\Delta({}_{\text{PAT}}^{\text{CAM}}\mathbf{T}^{-1} \cdot {}_{\text{TCP}}^{\text{CAM}}\mathbf{T}) = 0 + \text{PatMot}$, where Δ means the increment between two control cycles, therefore:

$$\begin{aligned} \text{CamMot} &= {}_{\text{CAM}}^{\text{TCP}}\mathbf{T}_{\text{avg}_{\text{old}}}\mathbf{T} \cdot {}_{\text{CAM}}^{\text{TCP}}\mathbf{T}_{\text{avg}_{\text{new}}}^{-1} \\ \text{PatMot} &= {}_{\text{CAM}}^{\text{PAT}}\mathbf{T}_{\text{avg}_{\text{old}}}^{-1} \cdot \text{CamMot} \cdot {}_{\text{CAM}}^{\text{PAT}}\mathbf{T}_{\text{avg}_{\text{new}}} \end{aligned} \quad (\text{SC2}), \quad (3.5)$$

where *avg_old* and *avg_new* refer to the fact that the values might be derived from multiple measurements with averaging (as described in the next section). If PatMot = 0, (3.5) leads to SC4, otherwise, it is considered to be SC2. Either way, the relevant motions can be numerically determined using the definitions in Fig. 3.3 and (3.3).

When the robot is moving, equation (3.3) is extended with the precisely known displacement of the robot's tip in the last cycle (RobMot), transformed to the camera's coordinate frame (SC3). It can be broken down to:

$$\text{CamMot} = \underbrace{{}_{\text{CAM}}^{\text{TCP}}\mathbf{T}_{\text{avg}_{\text{old}}}}_{\text{old measurement}} \cdot \underbrace{\left({}_{\text{REP}}^{\text{TCP}}\mathbf{T}^{-1} \cdot \text{RobMot} \cdot {}_{\text{REP}}^{\text{TCP}}\mathbf{T} \right)}_{\text{RobMot propagated to CAM frame}} \cdot \underbrace{{}_{\text{CAM}}^{\text{TCP}}\mathbf{T}_{\text{avg}_{\text{new}}}^{-1}}_{\text{new measurement}} \quad (\text{SC3}). \quad (3.6)$$

3.2.2 Specific issues with motion compensation

In practice, different kinds of errors complicate the process of SC identification (see Section 1.6.10). Each decision point becomes less reliable due to the distribution of random errors. Fig. 3.4 summarizes the new surgical event decision concept, including the error margins. Every time the camera measurement is involved in the decision, an error tolerance zone should be considered—proportional to the noise parameters (Fig. 3.5). Based on the literature, anisotropic Gaussian noise distribution is considered [94]. The navigation system’s noise parameter ($Noise_{Cam}$) should be determined for every device based on manufacturer’s specification or experiments. Typically, intra-operative tracking systems provide sub-millimeter accuracy through the consistent calculation of ${}_{CAM}^{PAT} \mathbf{T}^{-1} \cdot {}_{CAM}^{TCP} \mathbf{T}$. If the sum of two independent measurements are used from the camera (e.g., to distinguish SC2 and SC4), the resulting noise distribution is the convolution of the component noise distributions. If X_i has Gaussian distribution with parameters $\mathcal{N}(0, \sigma^2)$, then $\sum_{i=1}^n X_i$ also has Gaussian distribution with parameters $\mathcal{N}(0, n\sigma^2)$.

Let us make the following assumptions in order to treat different systems and setups in a unified way:

- information about the state of the robot is available,
- the robot is more precise than the navigation system,
- the noise parameters of the components are known,
- the latencies between the system components are known.

In general, all relevant information given at a point of measurement should be used to make optimal decision on what surgical conditions apply to the current OR setup. First, average latencies occurring in the system must be compensated. Next, we need to distinguish whether the robot is moving or not. Usually, this information is directly available through the servo feedback. Averaging over time may help to reduce the error; however, the safe control of the system during patient motion events must also be addressed. Alteration might either be a sudden or a gradual event (drift or shift), and the patient with the reference frame (PAT) can take seconds to settle. It must be ensured that in the meantime the robot does not move beyond a user-defined safety margin—typically 1 mm—thus its motion is scaled down accordingly (see Section 1.6.6). To dampen the effect of noise (primarily in the camera system), filtering can be applied to the signal. Due to the sudden changes (relative to the time resolution of a navigation system), average filtering is only employed when the system is static. Based on the average noise distribution of a camera system, we defined the window size for averaging. Position and orientation values of the rigid bodies are averaged through a maximum of 50 cycles. If patient motion occurs, these values (averaged over avg_old cycles) will be stored, and motion event will be computed relative to these. When the system stabilizes, a new average is cumulated in every cycle (avg_new). When $avg_new = avg_old$, we update the older value with the new one. Fig. 3.5 illustrates a single patient motion event to support this concept (in 1D for clarity). While performing PatMot and CamMot computations based on Fig. 3.4, the following values are stored:

$$\Delta TCP = \Delta {}_{CAM}^{TCP} \mathbf{T} = {}_{CAM}^{TCP} \mathbf{T}_{avg_new} - {}_{CAM}^{TCP} \mathbf{T}_{avg_old}, \quad (3.7)$$

$$\Delta PAT = \Delta {}_{CAM}^{PAT} \mathbf{T} = {}_{CAM}^{PAT} \mathbf{T}_{avg_new} - {}_{CAM}^{PAT} \mathbf{T}_{avg_old}. \quad (3.8)$$

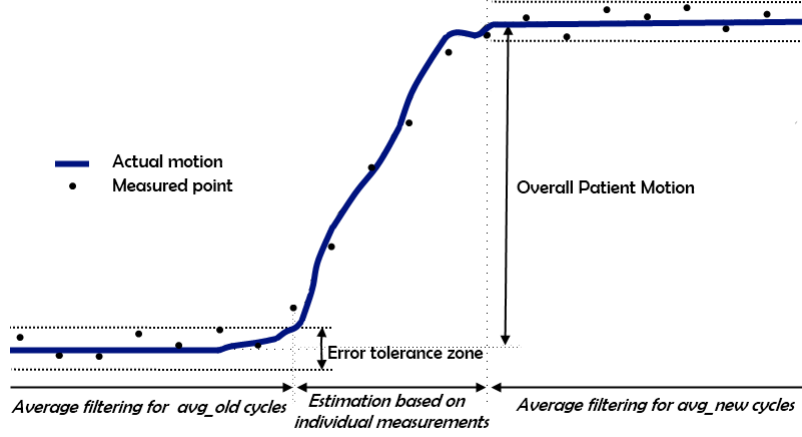


Fig. 3.5. Scheme of averaging for patient motion events.

Based on these, it is possible to update $\mathbf{T}_{\text{ROB}}^{\text{PAT}}$ and $\mathbf{T}_{\text{ROB}}^{\text{CAM}}$ transformations, originally determined at the initial robot registration phase.

The number of samples required for averaging is defined based on the a priori known noise of the camera system. If the samples arrive according to an $\mathcal{N}(0, \sigma^2)$ Gaussian distribution, then the distribution of the average of k samples is $\mathcal{N}(0, \sigma^2/k)$. The density function of the average distribution is:

$$f_k(x) = \frac{\sqrt{k}}{\sigma} \phi\left(\frac{\sqrt{k}}{\sigma}x\right), \quad (3.9)$$

where $\phi(x)$ is the standard normal density function. There is a tradeoff between the accuracy achievable through the averaging and the possible deviation of the measurement introduced through the latency. It is proposed therefore to average enough samples to fit into a 95% confidence interval. The probability that a sample falls into the $\pm t$ interval is [83]:

$$F_k^t = \int_{-t}^t f_k(x) dx, \quad (3.10)$$

or alternatively:

$$F_k^t = \Phi\left(\frac{\sqrt{k}}{\sigma}x\right) - \Phi\left(-\frac{\sqrt{k}}{\sigma}x\right), \quad (3.11)$$

where $\Phi(x)$ is the distribution function of $\phi(x)$. This allows for the calculation of the required number of samples for any given σ .

In the unlikely event when everything is moving at the same time (CamMot, PatMot, RobMot), the algorithm should still be able to determine the individual positions, but the overall uncertainty of the estimation would be too large, therefore it is recommended to re-register the system. In currently deployed robots (such as the ROBODOC), it is a common practice to require re-registration if deviation from the original registration is noticed.

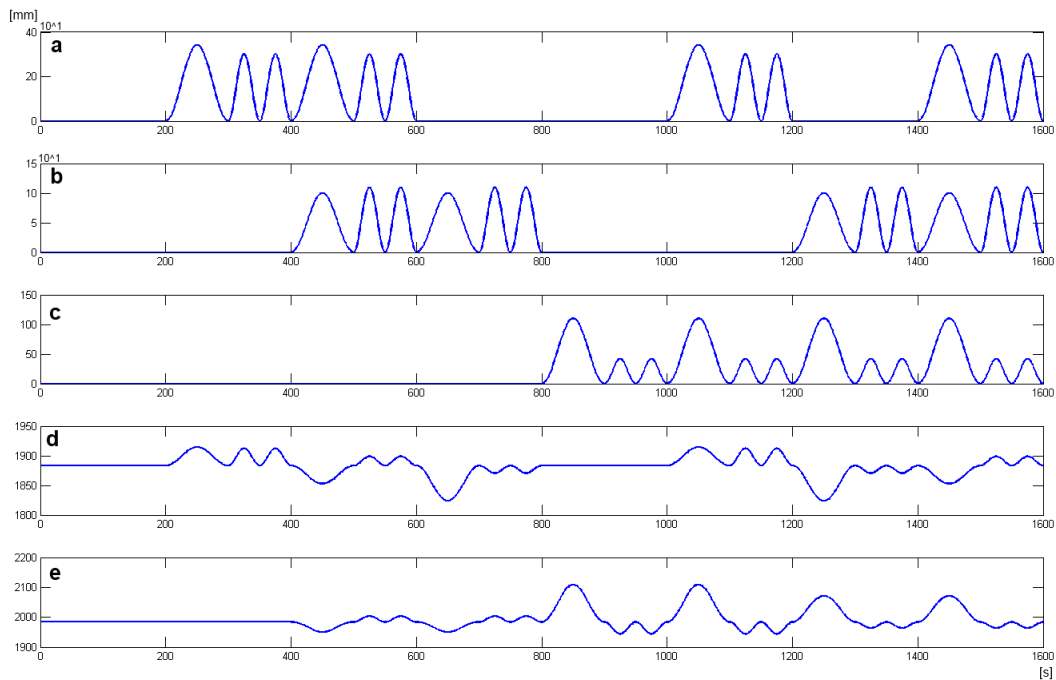


Fig. 3.6. Sample motions used for simulations to test the concept. (a–c) Time-distance graphs show the distance traveled from origin for the Robot, Camera and Patient, respectively. (d–e) The motion of the TCP and the PAT relative to CAM.

In addition, if patient motion and camera motion occur within k updates, re-registration is required, due to the decreased accuracy of the shorter averaging period. To increase safety, further semaphores can easily be implemented in the higher level controller, e.g., to require re-registration if a PatMot happened too soon after a CamMot, and the proper new transformations could not be acquired yet. This may depend on the clinical application, accuracy and safety requirements.

Through the adjustment of the decision-parameters, the algorithm can be tuned to lower or higher error tolerance. This is an important feature, as the consequences of *false-positive* or *false-negative* decisions are not equal. Leaving a patient motion event unnoticed and uncompensated could mean serious danger to the patient, while miss-categorizing any event to SC1 (requiring re-registration) would rather mean prolongation of the procedure.

3.2.3 Verification of the concept

A simulation environment was developed under MATLAB R2008b (Mathworks Inc., Natick, MA) to verify the new concept. A setup similar to Fig. 3.1 was defined, where a robot and the patient are both tracked. Simulation parameters were chosen to mimic a generic surgical robot regarding both range and speed of motion. Patient and camera motion events were determined based on previous observations during experiments [158]. Fig. 3.6 shows the simulation signals in time domain, with the distance traveled from the origin, for clarity. The total length of the simulation was 160 s, assuming 10 Hz control cycle. RobMot, CamMot and PatMot events were repeated, leading to the following SC

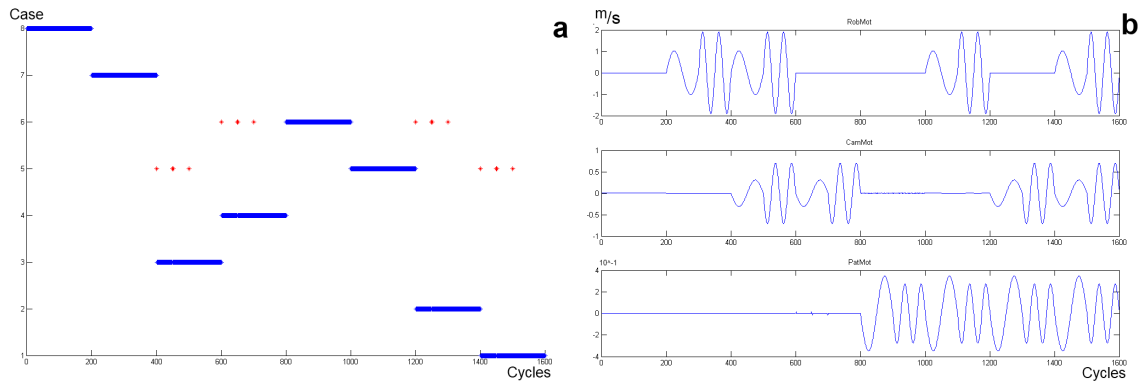


Fig. 3.7. (a) SC identification for noiseless data. (b) Reconstruction of the original TCP speed profile from the sensor data using the new concept.

TABLE 3.2
CONFUSION MATRIX FOR REFERENCE SC IDENTIFICATION

	Real Case							
	1	2	3	4	5	6	7	8
1	191	0	0	0	0	0	0	0
2	0	192	0	0	0	0	0	0
3	0	0	192	0	0	0	0	0
4	0	0	0	192	0	0	0	0
5	8	0	8	0	200	0	0	0
6	0	8	0	8	0	200	0	0
7	0	0	0	0	0	0	200	0
8	0	0	0	0	0	0	0	200

series in accordance with Table 3.1: 8–7–3–4–6–5–2–1, each lasting for 20 s, and consisting of a larger scale motion and two smaller, but faster motions. The two other plots in Fig 3.6 show the norm of the TRB and PAT measurements of the simulated camera, respectively.

Simulations were first performed under idealized conditions, with no noise and zero latency. The results showed the perfect identification of the SC (Fig 3.7a). The few outlier points—marked with red stars—are realistic, as the differential motion becomes temporarily zero at the transition between the two patterns. Averaging was not necessary in this simulation. The overall effectiveness was 99.5%, expressed with the percentage of correct SC identifications. A confusion matrix is given for the classification, showing the reference SC numbers versus the identified ones (Table 3.2.3).

As described above, it is absolutely possible to extract and reconstruct the different events, and get an understanding of the device positions in the OR. The incremental position changes for the whole simulation are shown in Fig. 3.7b.

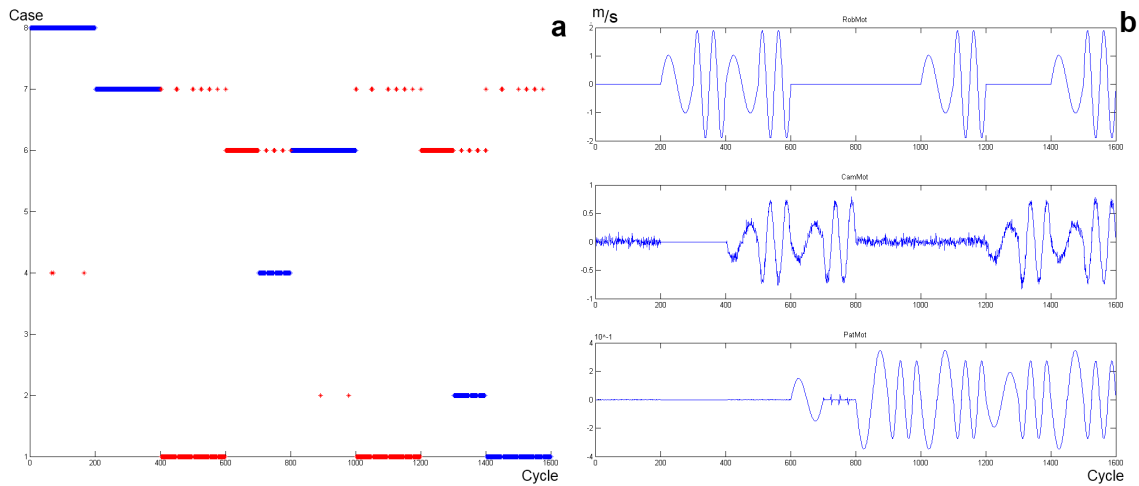


Fig. 3.8. Inherent noise in the navigation system can significantly reduce the performance of an image-guided robot. (a) SC identification for a noisy input. Misclassified SCs are marked with red stars. (b) Estimated robot tool speed for the same trial.

TABLE 3.3
CONFUSION MATRIX FOR SC IDENTIFICATION WITH NOISE

Identified Case	Real Case							
	1	2	3	4	5	6	7	8
1	188	0	184	0	188	0	0	0
2	0	136	0	0	0	0	0	0
3	0	0	0	0	0	0	0	0
4	0	0	0	138	0	0	0	0
5	0	0	0	0	0	0	0	0
6	0	64	0	62	0	200	0	0
7	11	0	16	0	12	0	200	0
8	0	0	0	0	0	0	0	200

3.3 Evaluation Study

Simulations were conducted with additional noise in the system in accordance with the literature. Adding $[0.02, 0.02, 0.02]$ mm and $[0.002, 0.002, 0.002]$ rad STD Gaussian noise to x, y, z and ϕ, θ, ψ , respectively yielded to the decrease of the performance to 66.4% as shown on Fig. 3.8a. Misclassified SCs are marked with red stars. The algorithm has most difficulties to distinguish CamMot from PatMot, when the measurements are imprecise, as shown on Fig. 3.8b. A confusion matrix is also given for clarity (Table 3.3).

Registration procedures may also have significant effect on the overall system, as they connect the different frames (see Section 1.6). A 1 mm STD registration error can further decrease the identification accuracy by 11%. Eventually, the effect of latency should also be incorporated. The problem with latency is that it makes significantly harder to accurately transform the RobMot to the valid CAM coordinate system. Introducing only a

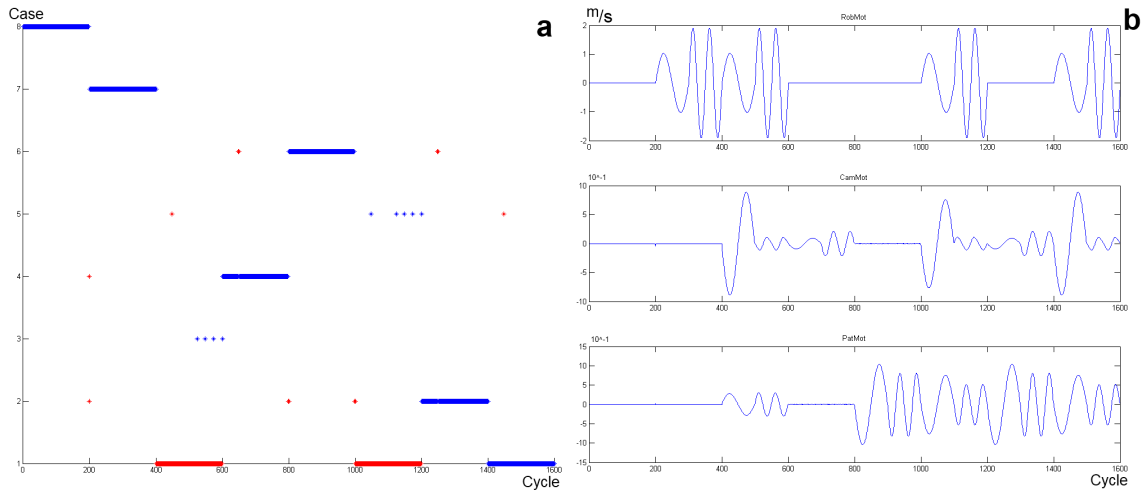


Fig. 3.9. Latency (with no additional noise) can distort measurements, and result in frequent call for re-registration. Misclassified SCs are marked with red stars.

TABLE 3.4
CONFUSION MATRIX FOR SC IDENTIFICATION WITH LATENCY

Identified Case	Real Case							
	1	2	3	4	5	6	7	8
1	196	0	195	0	195	0	0	0
2	0	198	0	2	0	2	0	1
3	0	0	4	0	0	0	0	0
4	0	0	0	196	0	0	0	1
5	1	0	1	0	5	0	0	0
6	0	2	0	2	0	198	0	0
7	0	0	0	0	0	0	200	0
8	0	0	0	0	0	0	0	198

small delay in the model (2 cycles \approx 260 ms), when the robot can move more within one cycle than CAM noise, it will automatically lead to the misclassification of SC3 and SC5 to SC1, as shown in Fig. 3.9. Note that regular operation (SC7 and SC8) are not affected; however, the reaction time of the algorithm to unforeseen events will be larger, as shown in the confusion matrix (Table 3.3). Altogether, this shows the importance to identify and compensate for average latency in a system (as shown in Fig. 1.23).

My concept introduced in this chapter was also tested on the neurosurgical robot system developed at the Johns Hopkins University, and described in Section 1.6. The robot is guided in cooperative control mode for the removal of cranial bone on the skull base, while Virtual Fixtures are applied to protect critical anatomical structures. To run the setup, we employed a paired-point registration method [159] that directly estimated ${}^{\text{ROB}}_{\text{PAT}}\mathbf{T}$, then computed ${}^{\text{REP}}_{\text{TRB}}\mathbf{T}$. Alternatively, it is possible to use a *hand-eye calibration* method [160] to directly estimate ${}^{\text{REP}}_{\text{TRB}}\mathbf{T}$; while ${}^{\text{REP}}_{\text{TCP}}\mathbf{T}$ and ${}^{\text{TRB}}_{\text{TCP}}\mathbf{T}$ can be acquired from pivot calibration. Once ${}^{\text{REP}}_{\text{TRB}}\mathbf{T}$ is known, it can be used to compensate for patient motion via (3.2). Specifically for

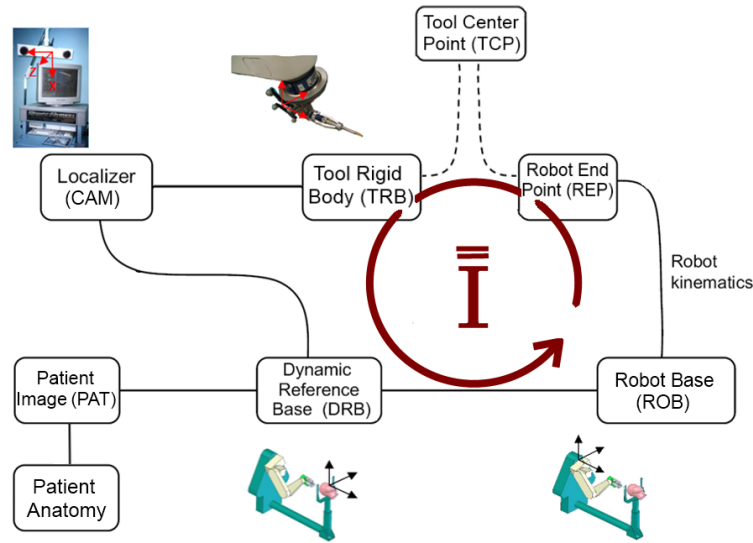


Fig. 3.10. Closing the control loop for an integrated IGS system via registration.

the JHU system, the control-frame-diagram presented in Section 1.6.5 allows to close the control loop as shown in Fig. 3.10:

$$\mathbf{I} = \begin{matrix} \text{PAT} \\ \text{CAM} \end{matrix} \mathbf{T} \cdot \begin{matrix} \text{CAM} \\ \text{TRB} \end{matrix} \mathbf{T} \cdot \begin{matrix} \text{TRB} \\ \text{TCP} \end{matrix} \mathbf{T} \cdot \begin{matrix} \text{TCP} \\ \text{REP} \end{matrix} \mathbf{T} \cdot \begin{matrix} \text{REP} \\ \text{ROB} \end{matrix} \mathbf{T} \cdot \begin{matrix} \text{ROB} \\ \text{PAT} \end{matrix} \mathbf{T}, \quad (3.12)$$

where \mathbf{I} is the identity matrix.

This means that even when the patient was moved relative to the robot ($\begin{matrix} \text{PAT} \\ \text{ROB} \end{matrix} \mathbf{T}$ changed) as shown in Fig. 3.11a, I was able to compensate for that motion real-time through the preserved $\begin{matrix} \text{TRB} \\ \text{REP} \end{matrix} \mathbf{T}$ transformation, applying (3.2) as illustrated in Fig. 3.11b.

3.3.1 Test data for evaluation

Unfortunately, there is very limited published data on patient motion [161, 162]. For consistency, I examined several motion patterns correlating to the different events within the OR, described in Section 3.1.1. For evaluation purposes, I generated the following motion patterns:

- arbitrary forces on the cranial frame,
- arbitrary forces on the robot,
- arbitrary forces on the patient cart,
- crisp motion of the PAT (bumping into it),
- drifting motion of the PAT (primarily rotation).

The initial experiments showed that the compliance of the cranial frame (*Mayfield Infinity Skull Clamp*) and the NeuroMate arm can already result in 0.85 mm and 1.55 mm RMSE errors, respectively, therefore reducing the effectiveness of the treatment without proper compensation.

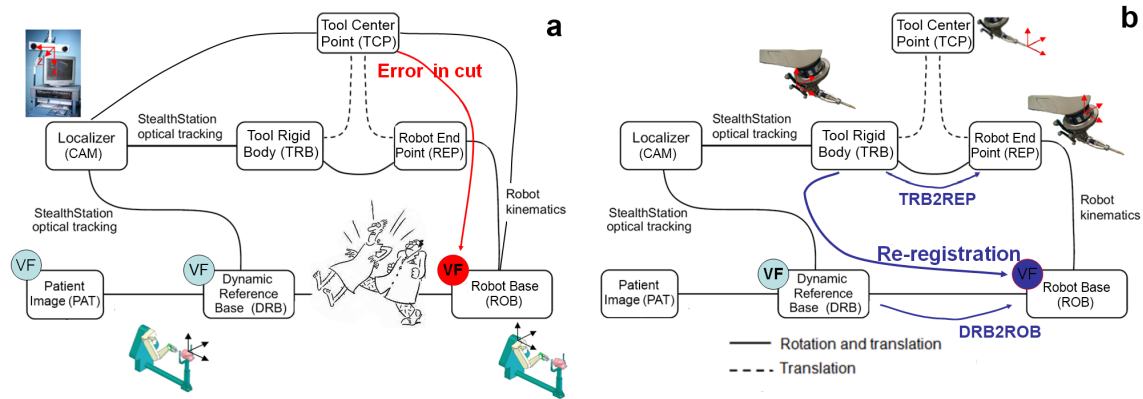


Fig. 3.11. (a) Patient motion corrupts the original registration, therefore a Virtual Fixture (or any other control constraints) will not be projected correctly to the target frame. (b) The proposed method gives the possibility to update the registration without starting over the setup procedure.

I performed test sequences about the eight surgically relevant scenarios presented in Table 3.1. These recordings were used for comparable evaluation of the new method. In order to apply event based compensation, the specific parameters of the JHU system had been identified. I found that the inherent noise (Standard Deviation) of the StealthStation is $[0.019, 0.013, 0.047]$ along x, y, z axes (in mm) and $[0.003, 0.001, 0.003]$ in rotation along the same axes (in degrees), respectively. Spatial location within the workspace of the camera showed little deviation from these averaged values. The STD of the tooltip calibration—the computation of the 3D transformations ${}_{\text{TRB}}^{\text{REP}}\mathbf{T}$ and ${}_{\text{TCP}}^{\text{REP}}\mathbf{T}$ defined in Fig. 3.2 are $[0.537, 1.146, 0.99]$ and $[0.228, 0.512, 0.519]$, respectively. The 6 DOF registration procedure we employed (described in Section 1.15) has zero mean error with an STD $[3.836, 3.573, 1.337, 0.022, 0.004, 0.006]$ along \mathbf{t} defined in (1.3). Based on the camera parameters and (3.10) it is derived that 3 consecutive measurements (0.4 s) are required for averaging to be within the 0.005 mm radius of the actual point with a 90% probability.

3.3.2 Results and discussion

Experimental results proved that my method managed to identify SC1 and SC8 with 100% accuracy, and the more complex events with approximately 80% on average. SC6 and SC7 can be identified with a higher success rate, while SC2 and SC4 (and also SC3 and SC5) are harder. Unfortunately, there is no perfect benchmark, as in the case of a real system, there is no feedback on the registration and calibration procedures' accuracy, and the motions were generated manually. The algorithm had to be tuned to find the appropriate values. The proposed gradually extending window averaging provides position estimation as soon as the DRB (therefore the patient) stabilizes, and updates the registration transformations continuously, with increasing precision. As the data sets were acquired on a physical system, imperfections of the different devices could lead to false clustering. Naturally, these numbers are to be increased, however, any increase in the correct classification of SC2, SC5 and SC6 would mean improvement to the current procedure without patient motion compensation.

Frequency domain identification of simultaneous motion types may help to differ SC1

from SC3. It should be mentioned that these cases happen seldom during regular clinical settings (the assistant should not adjust the camera while the surgeon is operating). The overall structure of the SC identification allows for a more generic, probability-based handling of the events that may lead to a more robust classification in the future.

3.3.3 Limitations

The theoretical performance and robustness of the proposed method may be affected by many factors (e.g., latency or unknown noise characteristics). While average communication latency can be compensated accurately, the overall prediction will be delayed with the maximum latency. This must be taken into consideration when designing the safety margins for the application. Sometimes, due to timing issues, latency may have a variance or jitter. Overall safety boundaries should be built in the surgical plans to tolerate maximum localization errors caused by occasional longer delays. If one component is significantly slower than the other, it may be hard to achieve real-time compensation. Correlated motion patterns (applying large force on the patient with the tool) may further degrade accuracy. This may cause problems with actual bone milling with loose head fixation, when the robot's motion can induce patient motion, and the whole can look like a camera motion from the control point of view. There is a possibility to decrease the robot's speed to collect sufficient information; however, this may result in the unnecessary prolongation of the surgical procedure which is absolutely undesired. While false positive characterization of patient motion events may not mean inherent danger, these should be avoided.

Both the inherent inaccuracies of the components and the registration procedures may introduce localization errors. In the case of an integrated system, this error can be magnified through the computation of a chain of homogeneous transformations, where angular errors (in the estimation of rotation angles) will be multiplied by the translational parameters. This should be handled through the extension of the current method, involving probability based calculations about the location of the surgical tool instead of using deterministic models. This idea is further evaluated in the next chapter.

3.4 Summary of the Thesis

The aim of my research was to improve surgical robot navigation through identification of Surgical Cases in the Operating Room. A new approach has been proposed for integrated IGS systems, using the intra-operative navigation device's internal coordinate base frame to better estimate the possible changes in the environment. Decision-tree based event recognition was proposed, allowing to choose the best control option for the given SC. Possible events have been categorized and defined as patient motion, camera motion, robot motion and the arbitrary combination of these. A measurement-based method was given to identify the actual SC, and to perform the desired action to enhance patient safety. The advantage of the method is that it is scalable to fit many surgical setups without additional hardware requirements. It was tested on the cooperatively controlled neurosurgical robot developed at the Johns Hopkins University CISST center. Different motion scenarios were simulated and recorded. The algorithm successfully identified the most frequently occurring Surgical Cases.

Chapter 4

PROBABILISTIC METHOD TO IMPROVE ACCURACY IN CIS

4.1 System Error Estimation Concepts

Validation and assessment of image-guided robotic systems can be cumbersome, thus significant effort has been invested into metrology and standards development by the research community. Deterministic spatial accuracy analysis of image registration and surgical robot systems was performed by many research groups [91, 104, 163, 164]. Stochastic analysis has mostly been avoided due to the fact that it is computationally demanding and can lead to extremely complex solutions [165]. Without effective and easy means of assessment, it is utterly difficult to verify IG systems. Even today, the most successful surgical robot system (the da Vinci) relies on the direct control of the surgeon. The human-in-the-loop control strategy allows for more flexible (and less autonomous) hardware solutions, where the surgeon is entirely responsible for patient safety. It is believed that development is towards improved machine intelligence and automation, and as a major step, the inherent precision of the future systems has to be enforced.

As discussed in Section 1.5.1, a major challenge is to find the best homogeneous transformation that accurately registers matching point pairs in two different data sets as described in (1.1). Different metrics, such as the FLE, FRE and TRE have been defined beforehand (see Chapter 1.5.1), and this chapter describes a new, stochastic approach to deal with the imperfections of an integrated system in a practical manner.

4.1.1 Accuracy assessment of integrated systems

It is crucial to meaningfully describe a system's *application accuracy*. It may be a highly non-linear function of the intrinsic and registration accuracies of the components, therefore requiring special handling. Various error propagation techniques have been proposed in the literature—summarized and further evolved here—to determine system errors as a function of the different integrated components. One of the typical assumptions of these methods (based on the *central limit theorem*) is to use Gaussian distribution to model the noise of the original measurements. Focusing solely on registration error estimation, [94] compares the different noise models found in literature. It is concluded that all the algo-

rithms can be unified through the model presented in [166] that assumes inhomogeneous and anisotropic zero-mean Gaussian noise. For the modeling of navigational devices, identical, isotropic, zero-mean Gaussian noise is used most commonly [167, 168], although some measurements suggest that the noise may be different for all existing surgical navigation systems [169]. The manufacturers claim to improve on homogeneity continuously, therefore identical distribution will be assumed hereafter. First, let us review previously developed solutions for error estimation, to be able to present their limitations and shortfalls.

Erroneous transformation matrix calculation

The most generic form describing the geometric relation between point clouds for IGS has been derived in the early 1990s. In IG therapy, usually only the positional error is indicated, as the accuracy of the treatment delivery—in these applications—depends on the 3D spatial error [164]. Let us assume that we only have an erroneous ${}^A\tilde{\mathbf{T}}_B$ approximation of the ideal ${}^A\mathbf{T}_B$ transformation:

$${}^A\tilde{\mathbf{T}}_B = {}^A\mathbf{T}_B \cdot \Delta {}^A\mathbf{T}_B \text{ and } \Delta {}^A\mathbf{T}_{\text{Rot}} \approx \mathbf{I} + \boldsymbol{\theta}\mathbf{N}, \quad (4.1)$$

where $\mathbf{I} + \boldsymbol{\theta}\mathbf{N}$ is a first-order Taylor series approximation of (1.4).

A measured \tilde{x}_A value is the approximation of a real x_A ,

$$\tilde{\mathbf{x}}_A = \mathbf{x}_A + \Delta \mathbf{x}_A, \quad (4.2)$$

then the transformed value derives to be:

$$\tilde{\mathbf{x}}_B = {}^A\tilde{\mathbf{T}}_B \mathbf{x}_A = \mathbf{x}_B + \Delta \mathbf{x}_B, \quad (4.3)$$

with uncertainty:

$$\Delta \mathbf{x}_B = {}^A\mathbf{T}_{\text{Rot}} (\boldsymbol{\theta}\mathbf{N}\mathbf{x}_A + \Delta \mathbf{x}_A + \Delta {}^A\mathbf{T}_{\text{Trans}}). \quad (4.4)$$

The disturbance effect of small rotations on small translations is neglected:

$$\Delta {}^A\mathbf{T}_{\text{Rot}} \cdot \Delta {}^A\mathbf{T}_{\text{Trans}} \approx \Delta {}^A\mathbf{T}_{\text{Trans}}. \quad (4.5)$$

This method analytically calculates position error accumulation; however, it may be difficult to compute and not accurate enough for certain applications (due to the Taylor series approximation).

Covariance matrix based approximation

It is possible to use a computed estimate of the steady-state error covariance of a system to determine its accuracy [170]. This means that given the vector of the state variables $\mathbf{x}_1, \mathbf{x}_2, \dots, \mathbf{x}_k$, the error covariance can be determined for every measurement point:

$$\boldsymbol{\Sigma}_{\mathbf{x}_i} = E\{\Delta \mathbf{x}_i \Delta \mathbf{x}_i^T\} = E\{(\mathbf{x}_i - \tilde{\mathbf{x}}_i)(\mathbf{x}_i - \tilde{\mathbf{x}}_i)^T\}, \quad (4.6)$$

where \mathbf{x}_i and $\tilde{\mathbf{x}}_i$ represents the true and estimated states at point i , respectively. The noise distribution of each point \mathbf{x}_i is given by the covariance matrix $\boldsymbol{\Sigma}_{\mathbf{x}_i}$. There are different

methods to estimate $\Sigma_{\mathbf{x}_i}$ directly from state-space models through e.g., the closed-formed solution of the discrete algebraic Riccati equation [170]. The limitation of the method is that it requires an accurate model of the system and a larger number of a priori measurements. Let us assume that $\mathbf{x}_B = f(\mathbf{x}_A, \mathbf{t})$, where \mathbf{t} is the representation of the position and orientation, as defined in (1.3). Then a linearized solution can be given to (4.4):

$$\Delta \mathbf{x}_B = \left. \frac{\partial f(\mathbf{x}_A, \mathbf{t})}{\partial \mathbf{t}} \right|_{\mathbf{t}=\tilde{\mathbf{t}}} = \mathbf{J}_f \Delta \mathbf{t}, \quad (4.7)$$

where \mathbf{J}_f is the Jacobian matrix (first-order Taylor series approximation) of function f [171]. It is possible to acquire the least squares solution for $\Delta \mathbf{t}$ through:

$$\Delta \mathbf{t} = (\mathbf{J}_f^T \mathbf{J}_f)^{-1} \mathbf{J}_f^T \Delta \mathbf{x}_B. \quad (4.8)$$

The covariance of \mathbf{t} is given by the expected value of the outer product:

$$\begin{aligned} \Sigma_{\mathbf{t}} &= E\{\Delta \mathbf{t} \Delta \mathbf{t}^T\} \\ &= (\mathbf{J}_f^T \mathbf{J}_f)^{-1} \mathbf{J}_f^T \overbrace{\begin{bmatrix} \Sigma_{\mathbf{x}_B} & \cdots & 0 \\ \vdots & \ddots & \vdots \\ 0 & \cdots & \Sigma_{\mathbf{x}_B} \end{bmatrix}}^{\bar{\Sigma}_{\mathbf{x}_B}} ((\mathbf{J}_f^T \mathbf{J}_f)^{-1} \mathbf{J}_f^T)^T, \end{aligned} \quad (4.9)$$

where $\bar{\Sigma}_{\mathbf{x}_B}$ is constructed from the covariance matrices of \mathbf{x}_B .

Covariance propagation

Instead of measuring the covariance of the system separately, it can also be calculated with backward and forward propagation through the approximation of the non-linear, affine coordinate transformations according to [89, 172]. Given (4.7), the covariance matrix Σ_f can be determined:

$$\Sigma_f = E\{(\mathbf{J}_f \Delta \mathbf{x}_A)(\mathbf{J}_f \Delta \mathbf{x}_A)^T\} = \mathbf{J}_f \Sigma_{\mathbf{x}_A} \mathbf{J}_f^T, \quad (4.10)$$

If the covariance of \mathbf{x}_B is known, backward propagation can be used, which means employing (4.10) on the inverse f function:

$$\Sigma_{f^{-1}} = \mathbf{J}_{f^{-1}} \Sigma_{\mathbf{x}_A} \mathbf{J}_{f^{-1}}^T = (\mathbf{J}_f^T \Sigma_{\mathbf{x}_A}^{-1} \mathbf{J}_f)^{-1}. \quad (4.11)$$

Pseudo-inverse methods can be applied to get the solution for overparametrized cases. With the help of (4.11) and (4.10) it is possible to compute the covariance at a Point of Interest through the known homogeneous transformations leading to the target point from the original base frame.

This form of description allows us to analytically derive the errors in different frames and representations. An example is the computation of the following errors [89]:

- deriving the 2D covariance matrix of a single camera image of a navigation system,
- propagating the error to 3D FLE error based on a camera model,
- deriving the 6D rigid body error based on the FLE,

- propagating the rigid body error to the POI to derive the 3D TRE.

The advantage of this approach is that it allows to build up the whole computation from the lowest level of errors within the imaging system (that may originate in internal camera calibration inaccuracies, imperfect lenses, inaccurate computational algorithms or image blur). However, usually very limited information is available about a navigation system at this level of details, therefore the simplified models applied may end up contributing the similar amount of distortion in the computation than empirically derived higher-level models would.

4.2 Stochastic Modeling of Complex System Noise

A serious limitations of the above described methods is that most of them do not deal with the orientation error at a target, and do not provide any information about the error distribution. Originally, the concept of coordinate frame registration handled accuracy as a norm of the deviation in x, y, z from the target point—entirely disregarding the orientation uncertainty. In several applications, such as an IG interventional robot applying Virtual Fixtures (see Section 1.6.6), it is critical to consider rotational errors as well.

4.2.1 Theory of complex errors

Let us consider a system where the Point of Interest is tracked with an intra-operative navigation system (with any modality). The Dynamic Reference Base is rigidly attached to the patient, and registered to the pre-operative image through any registrational method, with a known angular and translational residual error. The markers (enabling tracking) on the tool are determining a certain coordinate frame—Tool Rigid Body—that is connected to the POI through another transformation acquired from e.g., a pivot calibration, again with known error statistics. The goal is to transform the spatial constraints (e.g., Virtual Fixture) defined in the registered pre-operative image space to the POI in real/time by the set of homogeneous transformations (see Section 1.6.5). Let us note that in the case of a typical robotic IGS system the POI corresponds to the Tool Center Point. Fig. 4.1 shows the general arrangement of the setup. VF defined in the PAT frame can be acquired in the POI frame using the following chain of homogeneous transformations:

$$\begin{matrix} \text{PAT} \\ \text{POI} \end{matrix} \mathbf{T} = \begin{matrix} \text{TRB} \\ \text{POI} \end{matrix} \mathbf{T} \cdot \begin{matrix} \text{CAM} \\ \text{TRB} \end{matrix} \mathbf{T} \cdot \begin{matrix} \text{DRB} \\ \text{CAM} \end{matrix} \mathbf{T} \cdot \begin{matrix} \text{PAT} \\ \text{DRB} \end{matrix} \mathbf{T}. \quad (4.12)$$

It is assumed that all terms have known Gaussian distribution in the form given in (1.3), therefore the probability distribution of the POI is anisotropic Gaussian (as described in Section 4.1.1) with density function $f(\cdot)$. The overall transformation can be expressed as the function of the ideal and noise terms:

$$\begin{matrix} \text{PAT} \\ \text{POI} \end{matrix} \mathbf{T} = f(\mathbf{t}) + f(\Delta\mathbf{t}), \quad (4.13)$$

and it is necessary to express $f(\Delta\mathbf{t})$ for the setup in a simple and effective way. The VF can be described with a convex hull [126], and the probability $\mathbf{P}(\text{POI} \notin \text{VF})$ that the POI is in the forbidden region can be analytically calculated as:

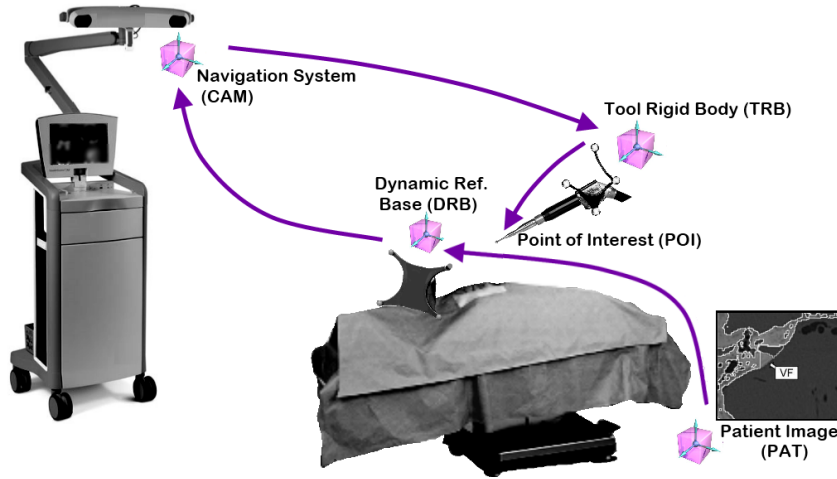


Fig. 4.1. Basic setup of IGS procedures, showing the different coordinate frames used in control to determine the tool's position relative to the pre-operative image.

$$\mathbf{P}(\text{POI} \notin \text{VF}) = \int_{\mathbf{t} \notin \text{VF}} f(\mathbf{t}) \, d\mathbf{t}. \quad (4.14)$$

It is possible to apply a stochastic approach through (4.14) to determine the location of the tooltip. This can be considered as the general extension of the approach proposed in [168]. Once we have the VF definitions transformed to the POI's coordinate system, we can derive the exact probability of the tool hitting the forbidden region. Current computational devices allow for the handling of these functions.

Similarly to $\mathbf{P}(\text{POI} \notin \text{VF}_1)$, let us denote by $\mathbf{P}(\text{POI} \notin \text{VF}_2)$ the probability that the POI is deeply in the forbidden sector (beyond a given threshold). An η penalty function—to control the device delivering the treatment—can be built by arbitrary weighting coefficients or functions (\mathbf{w}) tailored to the application. We can derive η by integrating the density function within the different VFs and scale it with \mathbf{w} . In a practical case, significant errors occurring with lower probability can be considered as:

$$\eta = w_1 \mathbf{P}(\text{POI} \notin \text{VF}_1) + w_2 \mathbf{P}(\text{POI} \notin \text{VF}_2), \quad (4.15)$$

where $w_1 > w_2$, if VF_1 is more limiting than VF_2 . The whole concept can be extended to incorporate more regions.

In addition, the angular distribution can also provide information about the probability that the POI is moving toward the VF. This is critical e.g., in automated bone drilling tasks. The exact calculation of the probability of the error gives a much stricter control over the motion of the tool, resulting in higher accuracy and safety.

An important feature of the proposed method is implicitly managing a previously challenging case: critical errors with low probability. With the help of differently chosen VF segments and \mathbf{w} factors, any complex constraint function can be built and applied to the IG system in real-time during the execution of the operation.

4.2.2 Deployment of the concept

The above presented method has several advantages. It can be applied to IGS systems during the setup phase to verify the performance of the devices in the actual OR arrangement. The manufacturer should provide the generic accuracy numbers of the tracking device and the robot system or these can be acquired pre-operatively. This is especially useful in the case when pre-operatively defined control features are applied, such as Virtual Fixtures.

At the beginning of the surgical procedure, when the devices are roughly positioned around the patient, the simple reading of the actual position information can serve as the input for the simulation. The stochastic method provides the error distribution based on the Monte Carlo simulation in a very short time, and with that knowledge, the surgeon can decide to re-arrange the setup or proceed with the operation.

The algorithm can be extended to call for re-assessment if the devices are significantly relocated compared to the original location. (E.g., the camera is pulled to the opposite side of the room.) However, this seldom happens in the case of real surgeries, where the physicians typically follow a pre-defined protocol.

4.2.3 Simulation results

I performed simulations to verify the concept. An IG bone drilling setup has been simulated (based on Fig. 4.1) with the parameters of an anthropomorphic robotic arm and a typical OR setup with an optical navigation system. A simplified VF was used to protect a certain region of the patient, while the robot operates in the proximity of it. The actual parameters were chosen to mimic the NeuroMate (see Section 1.2.2), and the registrations were defined based on multiple dry-lab tests. The distribution of the POI's error was acquired with Monte Carlo simulation using 20,000 samples (Fig. 4.2 (a–h)). Numeric results were derived for test cases, where one VF was a 0.2 mm radius sphere and another was a 0.4 mm radius sphere (Fig. 4.3), corresponding to a very delicate operation, e.g., the acoustic nerve during a hemifacial spasm treatment via suboccipital approach, pedicle screw placement or laser osteotomy on the sternum. Results showed that the method was effective by providing the probabilities, and showed great flexibility in application. The reason for the extreme-scale anisotropy of the final distribution is the further displacement of the camera base, which is absolutely necessary in a real OR arrangement.

4.2.4 Error modeling for faster surgical execution

The main collateral advantage of the new approach is to allow for the a priori estimation of the POI's distribution. Based solely on the devices' known intrinsic accuracy parameters and the registration values (acquired before the surgical procedure) thorough error distribution estimation can be performed according to Section 4.2.1. Unless the OR setup changes (which problem was addressed in Chapter 3), this simulation leads to better approximation of the surgical tool's position. With the known anisotropic Gaussian distribution, it is possible to determine which directions are more dangerous from the application point of view (where the STD is larger). The robot can be allowed to move faster towards directions with lower error distribution.

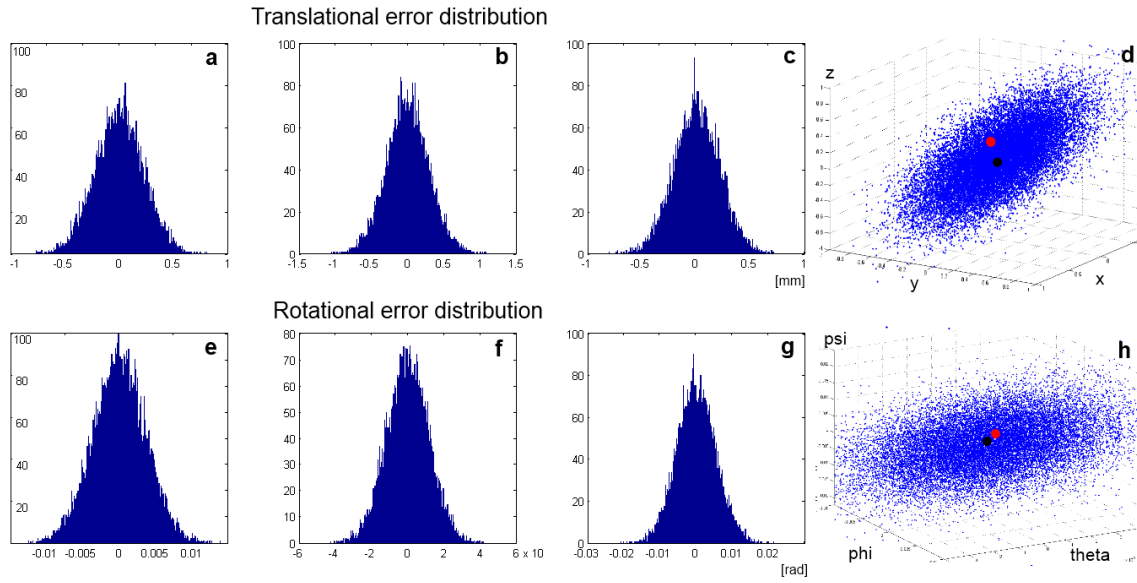


Fig. 4.2. Distribution of the Point of Interest with a simulated IGS system. (a–c) Distribution of position (compared to the deterministic approach); [0.32, 0.28, 0.30] mm STD along x, y, z , respectively. (d) 3D plot of the translational error. Red dot shows the theoretical position, black dot represents the effect of the registrational errors, i.e., the position estimation according to the classical deterministic method. (e–g) [0.0023, 0.0027, 0.0051] rad STD rotation error around x, y, z , respectively. (h) 3D plot of the angular errors along $[\phi, \theta, \psi]$

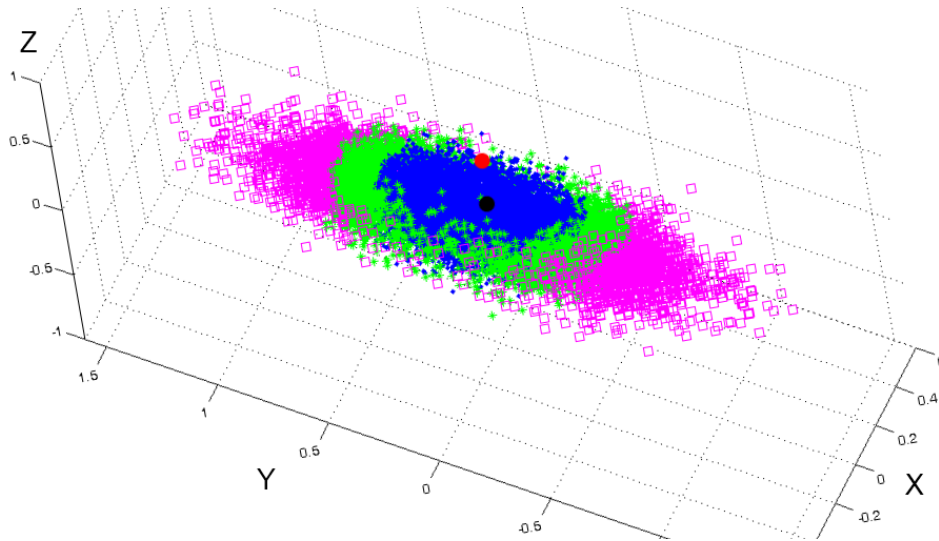


Fig. 4.3. The POI (tooltip) transformed to the coordinate space of the patient. Green stars show where the overall RMSE error is larger than 0.2 mm and magenta squares mark the region where the error is over 0.4 mm. The exact probability of the POI being beyond the VF is 0.438 and 0.214 for the 0.2 and 0.4 mm VF, respectively. Red dot shows the theoretical position, black dot represents the effect of the registration errors.

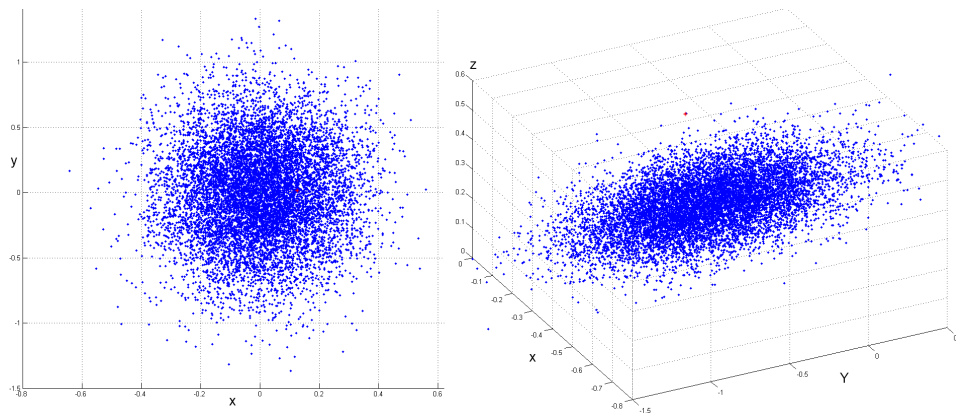


Fig. 4.4. (a) The POI's position transformed to the coordinate space along axis z . (b) The distribution of the POI shows highly anisotropic distribution along axis x .

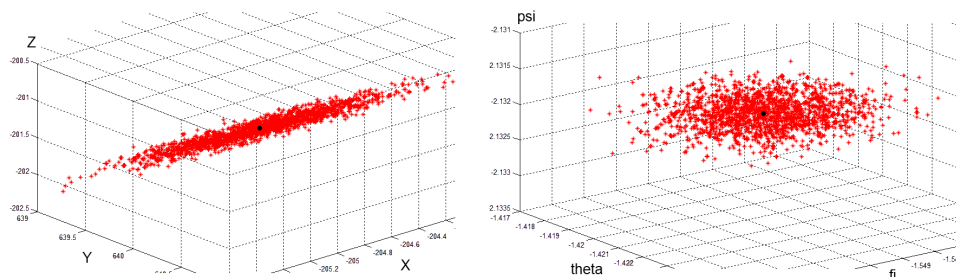


Fig. 4.5. (a) The POI (tooltip) position transformed to the coordinate space of the patient on the real JHU setup. (b) The distribution of the rotation.

Fig. 4.4 shows the differences in the distribution of the POI along different axes. The ratio of the STDs along the principal axes can be tenfold, even with the original distributions being isotropic. Principal component analysis showed that two components account for 98% of the variance. This means that if the typical motion of the tool during the surgery is towards the directions with lower error distribution, the robot can speed up due to the lower error. Consequently, the optimal arrangement of the camera system can be given for each procedure, based on a pre-operative simulation and analysis.

4.2.5 Application to a physical system

In the next step, I verified the concept on a real IG setup. The ongoing neurosurgical setup at the Johns Hopkins University presented in Section 1.6 is a valid platform, complying with the standard description provided in Section 4.2.1. While the previously presented error propagation approaches result in a moderately distorted POI distribution for a similar setup, in reality, measurements showed significant distortion of the error parameters for the actual robot tool. Fig. 4.5a shows the translational distribution, while Fig. 4.5b displays the angular distribution of the JHU system's drill. Principal component analysis showed that two components account for 99.7% of the variance in x, y, z directions and 98.6% of the rotations along x, y, z axes.

4.2.6 Future deployment of the concept

One of the future application of this concept could be the relatively new field of Natural Orifice Translumenal Endoscopic Surgery (NOTES) procedures. In the case of this surgical technique, the entire abdomen or other cavities are reached through the natural openings of the human body (the mouth, rectum or vagina), while making a small incision in the inner side of the fascias and membranes to reach the target location. This procedure requires highly dexterous tools, such as controllable flexible endoscopes and snake-like robots, therefore the kinematic modeling of these continuum robots calls for proper modeling of the associated errors. Simulation tests and phantom trials will be required to determine the proper VF parameters and weighting functions for these applications.

Another recent approach to improve the quality of IGS is to apply adaptive and online FLE statistic estimation [95], even with anisotropic distribution over the markers [93]. Most recent—combined technique—efforts promise even better results [87, 173].

4.3 Summary of the Thesis

Despite the many different approaches to estimate the absolute accuracy of treatment delivery of integrated IGS systems, there is a continuous need to provide better and more simple solutions. The proposed stochastic method combines computation and simulation to provide a general error distribution for a given setup. Simulations and computations can be performed before the operation and used for the optimization of the setup. The new method is meant to impose additional safety measures through the application of Virtual Fixtures, as it becomes feasible to accurately compute the possibility of spatial errors. This enables faster and safer task execution for any integrated systems using a pre-operative surgical plan combined with an intra-operative interventional tool. It has been shown that the neurosurgical robotic setup at the Johns Hopkins University is an appropriate platform to apply this technique.

Chapter 5

CONTROL METHOD FOR LONG DISTANCE TELESURGERY

Effective teleoperation has been a keen interest for many applications from industrial manufacturing to military campaigns. Robots have already been able to explore remote planets, hazardous sites, the depth of the oceans and many other places, relying mainly on the guidance of a distant human operator. NASA and other agencies have already performed a large number of experiments and developed various setups to push the boundaries of teleoperation [21, 57, 59]. Different control schemes have been developed and tested to facilitate and enhance telepresence and to deal with issues such as transparency, bandwidth and latency [174, 175, 176, 177]. In order to overcome the difficulties originating in signal latency, many ideas have been prototyped from predictive displays, supervisory control, passivity based control to wave variables and soft computing methods [25, 178, 179]. Understandably, this vast field of research could not be addressed completely within the frames of the thesis, however the major goal was here to delimit the problem to find a narrower focus, and to define the key areas where the results of my project can serve as the foundation of further investigations and experiments.

5.1 Telemedicine and Telesurgery for Space Applications

While advanced internet-based communication theoretically enables telesurgery, serious technological problems arise in the case of long distance operations or space exploration missions. Space application of telerobotic surgery has been a major focus of the research community since the early days of the field (see Chapter 1.1.2). Currently, it still seems inevitable to have a flight surgeon on board of the spacecraft for the proposed long term exploration missions, as robots do not have enough autonomy to adapt to unpredictable events. To cope with the difficulties of endoscopic surgery in weightlessness and generic space-system requirements, I propose a three-layered mission architecture to achieve the highest degree of performance possible by combining robotic and human surgery [180, 181]. Depending on the physical distance between the spacecraft and the ground control center, different telepresence technologies may provide the best performance (Fig. 5.1). The effectiveness of real-time control strategies and communication techniques decreases significantly with the accumulation of latency. Beyond Earth orbit, radio and microwave

frequency signals (30 kHz – 300 GHz) propagate at almost the speed of light in space, but even in the range of long distance manned space missions, several minutes of latency can be experienced. Planet Mars (currently in the focus of human exploration) orbits 56–399 million km from Earth, which means a 6.5 to 44 minutes of delay in transmission. In addition, for about two weeks every synodic period, direct communication can be blocked, as the Sun stays in between the Earth and Mars. Time-varying latency (due to the continuous change of the communication conditions) poses additional problems [182].

Mainly within the range of 380,000 km (the Earth–Moon average distance), semi-real-time telesurgery techniques can be used to provide medical support in the case of emergency. Apparently, this stage is reachable with current technology, hence my primary focus was directed towards it. Leaving Earth orbit, special control engineering algorithms have to be applied (e.g., virtual coupling of the remote environment [183], predictive displays projecting the intended motion of the tools ahead in time [184]) to extend the feasibility of telesurgery up to a maximum of 2 s of delay. This means significantly stretching human capabilities, as under regular conditions surgeons perform significantly worse above 250–300 ms latency between sensory input and actuation.

With robot assisted surgery, a shared control approach should be followed, integrating high-fidelity automated functions into the robot to extend the capabilities of the human surgeon through image processing and force sensing. This concept could be most beneficial for long duration on-orbit missions, primarily on board of the *International Space*

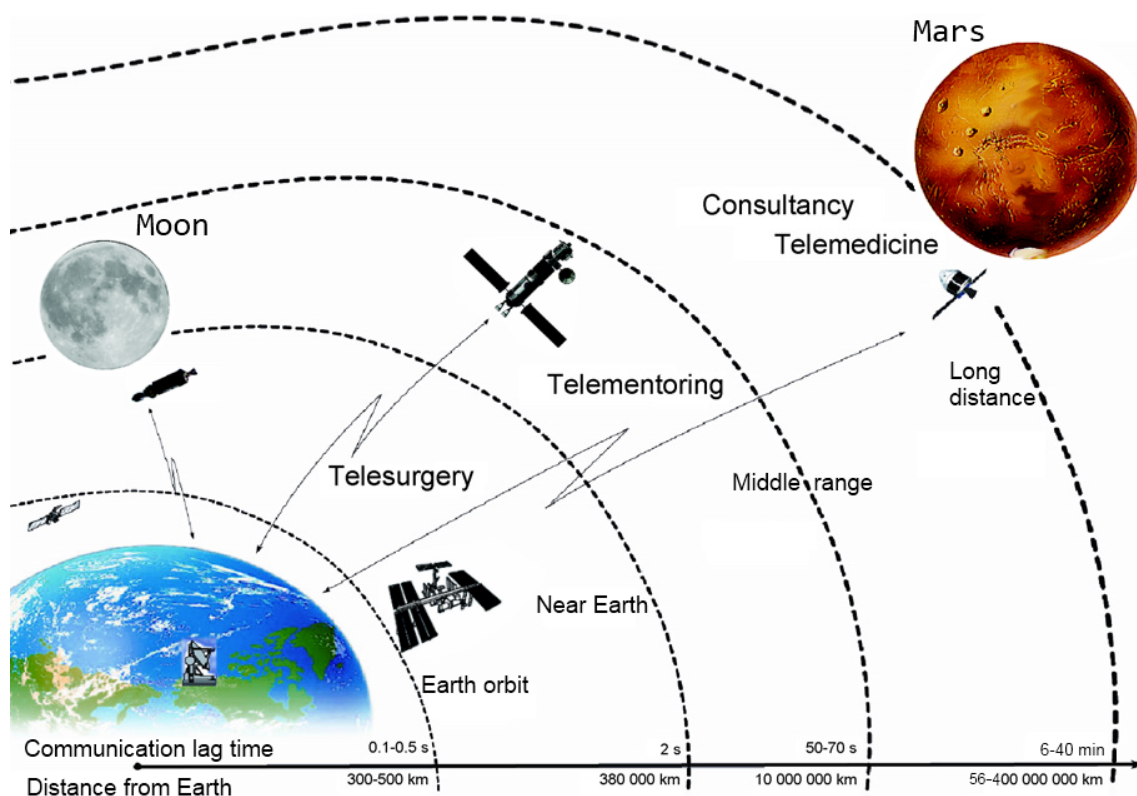


Fig. 5.1. Concept of telehealth support to provide maximum level of available medical care to astronauts during interplanetary exploration missions [181].

Station (ISS). Presently, there is no other option on the ISS than the immediate evacuation of the affected astronaut that poses significant additional health risk and huge costs. Teleoperational surgical robots would provide an alternative, where controller design has a huge role ensuring high quality control signals and sensory feedback [185]. On the other hand, this concept could also be used to perform telesurgery from one spacecraft to another, assuming we had already created human outposts on the Moon or beyond.

Flying further from the Earth, and reaching the limits of semi-real-time communication, the procedures should be performed by the flight surgeon under the *telementoring* guidance of a master surgeon on the ground (Chapter 1.1.1). Telementoring transforms into *consultancy telemedicine* above a certain signal delay. Around one minute of delay, it is inconvenient and impractical for the crew to wait for the reactions of the master side after every procedural step. For these missions, targeting extremely remote areas of space, the flight surgeon must be trained to conduct the operation and make decisions on its own. However, the ground staff can provide high value support by patient specific simulations and thorough consultancy beforehand the operation. Pre-operative surgical modeling and simulation is an emerging field not addressed in depth here [186].

5.2 Human Model for Teleoperation Scenarios

5.2.1 Human operator models

In order to design a suitable control scheme for teleoperation scenarios introduced above, it is necessary to derive the applicable model of the human operator (*master*—M) and the robot (*slave*—S). Teleoperation through a human–machine interface based on visual information has been shown to correlate to an *equalization type* or *look and move* task, where the human subject needs to reach to a prescribed point in space.

In the 1960s, several research projects were undertaken to develop accurate models of human fighter pilots [187]. The results revealed that while the human body presents a variety of non-linear and time-varying behavior, it is possible to determine a quasi-linear equivalent model [188]. These concepts have been extended later in order to better model the central nervous system's behavior responsible for voluntary movements [189, 190].

It has been shown in the '60s that people can adapt to latency (up to a certain limit) through a *move and wait strategy* [191]. This means, the operator stops the motion while waiting the round-trip delay for sensory confirmation of the performed action. It is possible to apply a small, incremental position change open loop (without feedback); however, the larger the latency, the slower the movement gets, with a bigger inherent risk of causing some damage due to the prolongation of the unmonitored periods. Experiments clearly supported prior assumptions that teleoperation task performance is a direct function of the lag time, the ratio of the movement's length/accuracy and some other minor aspects [188].

While this strategy has successfully been applied e.g., to planetary rovers, it has serious limitations in the case of telesurgery, where processes are time-critical, and prompt reaction is required. Therefore the human operator should be supported with prediction-based augmented reality, model based predictive control and similar technologies to deal with extreme (> 1 s) round-trip latency.

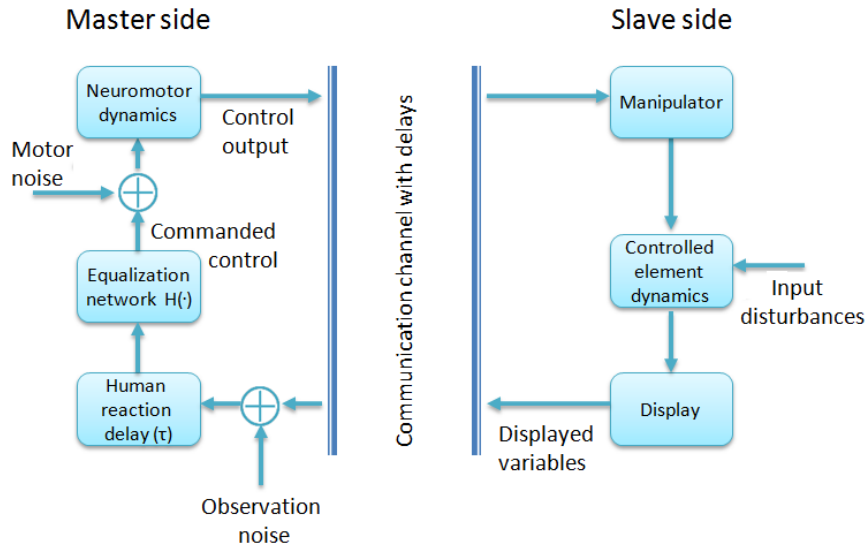


Fig. 5.2. Simplified model of a human from the control aspect in the case of a simple tracking (equalization type) task performed in teleoperation mode through a delayed channel, based on [187].

5.2.2 The crossover model

The physiology driven block scheme of the human control—originally developed for pilots—is given in Fig. 5.2. The different aspects of the human sensory system's behavior (retinal excitation, nerve conduction, processing in the central nervous system, etc.) have been aggregated to lumped equivalent perceptual time delay τ . The $H(\cdot)$ *Transfer Function* (TF) represents the human operator's attempts to optimize its control strategy. Naturally, there are other remnant terms that determine the general behavior of a human operator; however, these may be better represented in a statistical manner, and will be omitted from further considerations due to their minor effect on the overall motion. Observation and task execution (motor) noises are also neglected [192]. The generally used model of the operator (or pilot) containing simplifications (e.g., neglecting high frequency terms) with a first-order neuromuscular lag time is:

$$W_{Op} = k_{Op} \frac{(\tau_l s + 1) e^{-s\tau}}{(\tau_i s + 1)(\tau_n s + 1)}, \quad (5.1)$$

where k_{Op} is the operator's static gain, the $e^{-s\tau}$ term reflects the pure time delay caused by the human sensory system limitations, τ_l is the lead time constant (relative rate-to-displacement sensitivity), τ_i is the lag time constant, τ_n the neuromuscular and activation mechanism lag time. The remaining terms represent the human's equalization characteristics. They are adjustable according to the task requirements and are chosen such that the closed loop characteristics will invoke a good feedback control system [193].

In many cases, the amplitude ratio data is best approximated with (5.1), called the *crossover model*. The open loop TF with one pole can be derived in the form:

$$W_{Op2} = k_{Op2} \frac{\omega_c}{s} e^{-s\tau_d}, \quad (5.2)$$

where k_{Op2} is the static gain, ω_c is the crossover frequency (meaning the limitation of the human operator's reaction based on the information feedback) and τ_d is the delay between the observation and the reaction of the motor system [39]. Rule of thumbs are described in [194, 195] to properly choose ω_c and k_{Op2} .

Assuming zero physiological time delay, (5.2) yields to *Fitts' law* [196]. This is a widely accepted model that describes the time taken to acquire a visual target using some kind of manual input device. In the most generic (Shannon) form, the average time (t) taken to complete the movement is:

$$t = a + b \log_2 \left(1 + \frac{D}{w} \right), \quad (5.3)$$

where a represents the start time, $1/b$ stands for the inherent speed of the device, D is the distance from the starting point to the center of the target and w is the width of the target measured along the axis of motion (practically, the tolerable error). The crossover model leads to the following form of Fitts' law, determining the task completion time for moving an object over a given distance:

$$t_{\text{Fitts}} = \frac{1}{\omega_c} \ln \left(\frac{2D}{w} \right), \quad (5.4)$$

where D is the distance and $w/2$ is proximity of the target that should be reached.

While these are simplistic models, they have been proved to be effective in not only fighter-simulators, but also in haptic experiments and robotic teleoperation. More recent experiments explicitly showed the validity of Fitts' law in the case of da Vinci type telerobotic surgery [197].

As the delay increases, the exponential motion becomes oscillatory, therefore loses stability. This also leads to the increase of the overall completion time, hence it should be avoided. The model can be extended with additional terms representing short and long term human learning [39]. More realistically, in the case of unknown delays, human reaction is a function of:

$$\tau_{Op} = \tau_{Op,0} + \left(\tau_{Op}^* - \tau_{Op,0} \right) e^{-t/\tau_{lt}}, \quad (5.5)$$

where $\tau_{Op,0}$ represents the time it takes to the human operator to learn the amount of delay, τ_{Op}^* is the assumed delay and $\tau_{lt}(\tau_{Op}, N)$ is the effect of long term learning over N repetitions of the task. It might be possible to acquire the proper τ_{lt} parameters in a simulated experiment, while it is a complex function of personal skills and experience in the case of real-life surgery. The influence of learning has been shown to follow an exponential pattern. The human operator's k_{Op} gain is also altered by learning over time:

$$k_{Op} = k_{Op,0} + \left(k_{Op}^* - k_{Op,0} \right) e^{-t/\tau_{lt}}, \quad (5.6)$$

where $k_{Op,0}$ is the original gain and k_{Op} is the new gain acquired through learning over t time. The importance of human learning cannot be overestimated, however, the subject is too wide to be addressed in depth within the frames of my thesis.

5.3 Robot Model for Teleoperation Scenarios

It can be assumed that the robot is a series of rigid links with typical mechanical properties, and the servo motors are driven by the local robot controller according to the control commands from the master side. In telesurgery, it is desirable to minimize the load to the patient's tissue, therefore force control may be used. Commonly, the impedance characteristics of both the master and the slave devices are modeled separately (master controllers are very sophisticated and compliant nowadays). A simple dynamic model of the manipulator is:

$$\mathbf{f}_S = M_S \ddot{\mathbf{x}}_S + B_S \dot{\mathbf{x}}_S, \quad (5.7)$$

where M_S and B_S are the inertia and damping coefficients of the robot, respectively, \mathbf{f}_S is the force applied to the manipulator and \mathbf{x}_S is the position displacement on the Slave side [198]. This form is suitable to describe a force-controlled robot, where the commands to the local robot controller are given as position (velocity) commands. It may be adequate to incorporate the deviation of the tool from the master controller's position, yielding to the extension of (5.7):

$$\begin{aligned} \mathbf{f}_S = & k_S (\mathbf{x}_S(t) - \mathbf{x}_M(t - T_{\text{lat}})) \\ & + B_S (\dot{\mathbf{x}}_S(t) - \dot{\mathbf{x}}_M(t - T_{\text{lat}})) + M_S \ddot{\mathbf{x}}_S(t), \end{aligned} \quad (5.8)$$

where \mathbf{x}_S and \mathbf{x}_M are the Cartesian positions of the slave and the master, respectively, k_S is the stiffness of the slave manipulator and T_{lat} is the latency of the communication network [199].

Tissue characteristics are considered through Fung's exponential force–stretch ratio curve [200], deriving the relation between Lagrangian stress and stretch ratio:

$$\mathbf{f}_T = \alpha e^{\beta \mathbf{x}_S(t)}, \quad (5.9)$$

where α and β tissue-specific constants were determined to be 4.3^{-7} and 13, respectively for in-vivo abdominal tissue [201]. This represents the exponential resistance of soft tissue towards external forces applied on it. The model was later refined, and described in the form:

$$\mathbf{f}_T = p \left(e^{q \mathbf{x}_S(t)} - 1 \right), \quad (5.10)$$

where p and q are 0.2 and 400 for live tissue, respectively. In my application, strains are low, therefore the tissue behavior can be modeled as linear. $G(s)$ represents the linearized, frequency domain equivalent of (5.10). The slave robot can be modeled according to Fig. 5.3, together with an observer to determine \mathbf{f}_T . Deviation originating from the physical realization of the robot's mechanical structure (imperfections and friction) have been omitted from the model, resulting the TF:

$$\begin{aligned} W_{S'} &= \frac{\mathbf{f}_S}{\tilde{\mathbf{x}}_M} = \frac{k_S + B_S s}{s} \left[1 - (M_S s^2 + B_S s + k_S) \frac{1}{M_S s^2 + B_S s + k_c + G(s)} \right] \\ &= \frac{(k_S + B_S s) G(s)}{s (M_S s^2 + B_S s + k_S + G(s))}. \end{aligned} \quad (5.11)$$

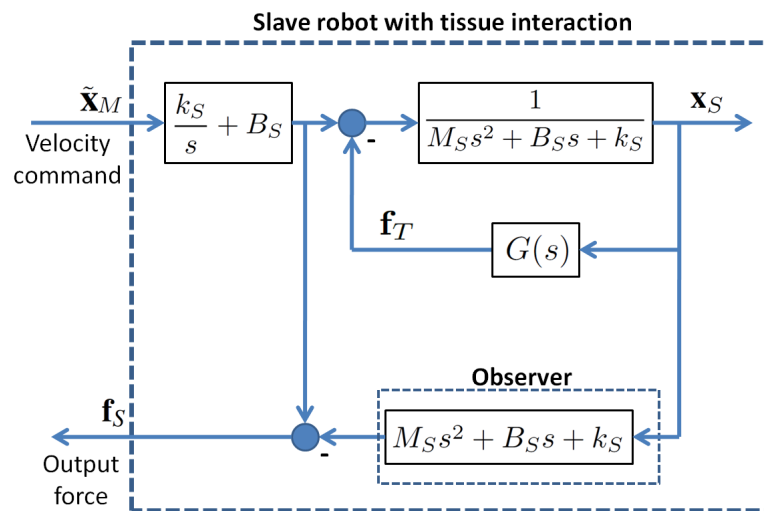


Fig. 5.3. Model of a teleoperated slave robot with an Observer to determine tissue force reactions. (Based on [199].)

5.4 Application Oriented Controller Design

5.4.1 Cascade controller for a telesurgical robot

Out of the many criteria towards telesurgical systems, stability and transparency have been considered to be the most important. Due to the fact that the robot–human–sensor triplet can be well delimited, an adequate method for control could be the design of a cascade controller.

A realistic teleoperation system—as it was presented in Section 5.2—suffers from time delays during communications between the master (controller) and slave side (effector system). Unless the process is significantly slower than the latency, the control lag time can cause the deterioration of the control quality and instability can occur due to unwanted power generation in the communications. Time-varying delay poses further difficulty to classical PID controllers.

Cascade control can improve control system performance over single-loop control whenever disturbances affect a measurable intermediate/secondary process output that directly modifies the primary process output or if the gain of the secondary process (including the actuator) is non-linear. Advantages of cascade control have been widely studied and published [75], both for telesurgical and generic space robotic applications [202]. Cascade control in general:

- allows faster secondary controller to handle disturbances in the secondary loop,
- allows secondary controller to handle complex non-linear problems,
- allows operator to directly control secondary loop during certain modes of operation (such as startup).

Requirements can be summarized as follows:

- secondary loop dynamics must be faster than primary loop dynamics,

- secondary loop must have influence on the primary loop,
- secondary loop must be observable and controllable.

5.4.2 Empirical design approach

Auto-calibration methods

Based on (5.2), the inner part of the cascade control scheme (robot) can be described in a compact form [203]. It is well known that empirical methods can provide a solution for automatic calibration, which is a promising approach in the case of many industrial processes. Method follows the mainstream approach of control theory, first performing the identification of the plant and then determining the controller parameters. In general, the following requirements stand for auto-calibration [204]:

- simple computation of the parameters,
- easy interpretation of the tuning,
- clear indications for *accelerating* and *slowing down* phases,
- large field of application (guaranteed performance),
- test the plant with small signals, no interference with the general workflow,
- good robustness margins in the (targeted) field of application,
- acceptable performance and stability beyond the theoretical field of application,
- only readily available prior knowledge should be required for the design,
- reasonable time required to be carried out.

Kessler's methods and their extensions

As first proposed by Kessler in 1958, the class of plants characterized by TF:

$$W_P(s) = \frac{k_p}{s(1+sT_1)(1+sT_\Sigma)}, \quad (5.12)$$

or

$$W_P(s) = \frac{k_p}{s(1+sT_1)(1+sT_2)(1+sT_\Sigma)}, \quad (5.13)$$

can be well controlled through empirical methods [205, 206]. In (5.12) and (5.13) T_Σ is a small time constant or aggregated time constant corresponding to the sum of parasitic time constants, $T_\Sigma < T_2 < T_1$). The use of a PI or PID controller having the TF:

$$W_C(s) = \frac{k_c}{s}(1+sT_{C1})(1+sT_{C2}) \quad (5.14)$$

can ensure acceptable performance [207]. T_Σ can also include the time constants used to approximate the time delay. In (5.12), the process pole ($p_1 = -1/T_1$) may be compensated by the controller zero ($z_1 = -1/T_{C1}$), and similarly for $p_2 = -1/T_2$ in (5.13), in order to obtain the desired open loop TF— $H_0(s)$ —in the form:

$$W_0(s) = W_C(s)W_P(s) = \frac{k_0(1+sT_{C1})}{s^2(1+sT_\Sigma)}, \quad (5.15)$$

with $k_0 = k_c k_p$. However, in certain practical applications, its performance—that can be specified a priori for a given process—is rather unacceptable [206]. The TF of the closed loop control system can be expressed as:

$$W_c(s) = \frac{W_0(s)}{1 + W_0(s)} = \frac{b_0 + b_1 s}{a_0 + a_1 s + a_2 s^2 + a_3 s^3}, \quad (5.16)$$

with $b_0 = a_0$ and $b_1 = a_1$, due to the expression of $H_0(s)$.

For the tuning of controller parameters k_c and T_{C1} , while $T_{C2} = T_1$ through compensation, the literature recommends the *Modulus/Magnitude Optimum Criteria* (MO) or the *Symmetrical Optimum* (SO) method proved to be advantageous in practice because it provides well established tuning relations.

MO can be applied for plants with TF given by (5.12) (with no integrator term). SO may be used for plant described in the form (5.13). However, the performance of Kessler's methods become unacceptable due to a large sensitivity with respect to the modification of k_p , accompanied by an alleviation of the Phase Margin (PM). It only ensures $\sigma_1 \approx 43\%$ overshoot, $t_s \approx 16.3 T_\Sigma$ settling time, $t_1 \approx 3.7 T_\Sigma$ first settling time and $PM \approx 36^\circ$ PM. This shortcoming can be more disturbing if T_Σ falls close to the sum of parasitic time constants.

To compensate for the above mentioned limitations, extensions were proposed in the literature both for the SO [208] and for the MO methods [209]. It was proven in [207] that the closed loop TF (5.16) should fulfill the condition:

$$2a_0 a_2 = a_1^2, \quad 2a_1 a_3 = a_2^2, \quad (5.17)$$

to ensure optimal performance of the SO method. In this case, the parameters of the PI or PID controllers can be given as:

$$k_c = \frac{1}{8k_p T_\Sigma^2}, \quad T_{C1} = 4T_\Sigma \quad \text{and} \quad T_{C2} = T_1. \quad (5.18)$$

Further, the generalized form of (5.17) is:

$$\sqrt{\beta} a_0 a_2 = a_1^2, \quad \sqrt{\beta} a_1 a_3 = a_2^2, \quad (5.19)$$

where $\beta > 1$ is a design parameter, set by the developer. This is called the *Extended Symmetrical Optimum* (ESO) method [208]. (5.18) can be generalized:

$$k_c = \frac{1}{k_p \beta^{\frac{3}{2}} T_\Sigma^2}, \quad T_{C1} = \beta T_\Sigma, \quad T_{C2} = T_1. \quad (5.20)$$

Tuning parameters are directly correlated to the desired control system performance indices. The value of β is typically chosen to be in the $[4, 20)$ interval [210]. It is possible to optimize β for maximum PM for any given k_p constant. (As the PM is required to reach the maximum of the open loop Bode phase plot under conditions of symmetry.) Depending on β , the closed loop systems poles (p_1, p_2, p_3) can be [211]:

- $p_{1,2}$ are complex conjugated, if $\beta < 9$,
- $p_{1,2,3}$ are real and equal, if $\beta = 9$,
- all poles are real and distinct for $\beta > 9$, but the system remains oscillatory.

On the basis of (5.19), the open loop and closed loop TF can be given as:

$$W_0(s) = \frac{1 + \beta T_\Sigma s}{\beta^{\frac{3}{2}} T_\Sigma^2 s^2 (1 + T_\Sigma s)}, \quad (5.21)$$

$$W_c(s) = \frac{1 + \beta T_\Sigma s}{\beta^{\frac{3}{2}} T_\Sigma^3 s^3 \beta^{\frac{3}{2}} T_\Sigma^2 s^2 \beta T_\Sigma s + 1}. \quad (5.22)$$

5.5 Controller Design Solutions for Long Distance Telesurgical Applications

Considering the previously discussed challenges, the pre-control context for telesurgery can be well defined, hence, different control methods can be formulated. I was focusing on classical control options to provide a simple, universal and scalable solution [212]. In the case of a cascade structure, the data of the inner loop gives feedback to the outer loop, but no a priori knowledge about the inner loop's dynamics is required to design the outer controller. On the other hand, it is possible to explicitly consider the remote dynamics in the outer controller in order to predict the inner behavior [213]. This can be based on the well-known *Smith predictor* scheme or similar predictors [75, 214].

A predictor in the outer loop helps to deal with the computation of the delayed information from the inner part, whereas a classical PID controller is implemented at the inner part. This is a crucial and effective observation, as in the case of teleoperating a robot on board of a spacecraft, significant delays can appear in the control loop. Hence, cascade control combined with predictors could be considered for the presented problem. The control commands given to the robot-simulator are sent to the remote robot using a time-delay network.

Consequently, the ground workstation contains a model of the uplink and the downlink delays as well as a model of the actual states of the real robot and its environment. Several alternatives exist to superimpose the predicted robot model as presented in [202], such as the use of predictive video displays or augmented sensory fusion solutions [215]. This structure is suitable to later include more complex models of the human (e.g., fuzzy control model [216] or optimal control model [217]) and the robot to acquire a complete representation of the whole telesurgical scenario presented in Fig. 5.4. The key of the setup is to accurately model the surgical environment (for a short time horizon matching the latency time), therefore a realistic and valid environment can be displayed to the physician. This technique may be the most advantageous for varying latency, especially when the delay rarely reaches higher values. With adaptive motion scaling of the robot and blending of the augmented reality with the continuous sensory information update, an ergonomic surgical working environment can be created. It should be noted that the setup requires advanced safety features on the slave side to prevent any injuries in the case of prolonged discontinuity in the control signal transmission.

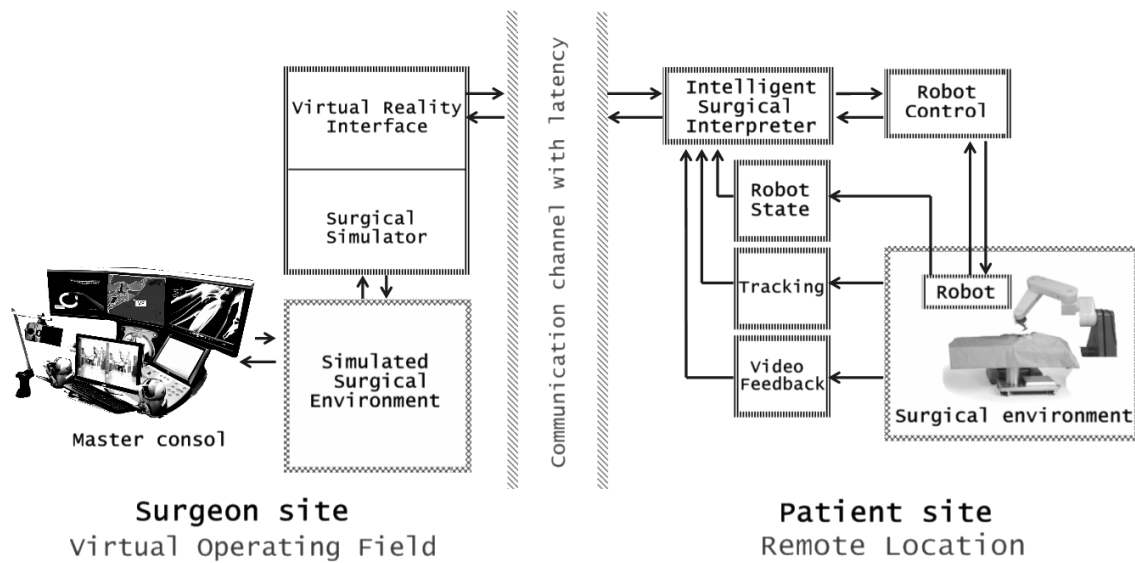


Fig. 5.4. The concept of VR augmented control of surgical robots in order to locally deal with the disturbing effects of latency.

5.6 Controller Structure for a Telesurgery System

Based on the requirements and assumptions for an effective space telesurgery system (identified in Section 5.1) I propose a cascade control structure employing empirical controller design to address the challenges of a system with large and probably varying latencies. The use of empirical design methods is justified with the need for simple and quick algorithms in cases when model predictive control may be cumbersome to apply. In fact, a human physician controls the robot, and it is extremely difficult to develop plausible model for their behavior from the control point of view. Fig. 5.5 shows the schematic block diagram of the controller structure. It is important to identify the right model of each component and to define the required parametric filtering enabling the smooth handling of the whole cascade structure. My goal was to give a scalable solution for the first phase of advanced telesurgical support (Fig. 5.1) based on classical control theory.

While state feedback control is an alternative approach to attack complex problems like creating a valid robot model (as it offers the possibility to obtain better performance using additional information from the process expressed as state variables), the design of Luenberger observers or of Kálmán filters to obtain the state-space models of the process poses additional challenges. It would be difficult to design the observers because of the variable time delay and of the fact that the process is really characterized by distributed parameter systems. It would also mean higher design and implementation costs compared to empirical methods which has been widely applied successfully in electrical drives. I focused on Kessler's Extended Symmetrical Optimum method and developed its first embedded application in the broader domain of robotics.

The proposed method for controller design relies on the adaptive and optionally repetitive computation of the following steps:

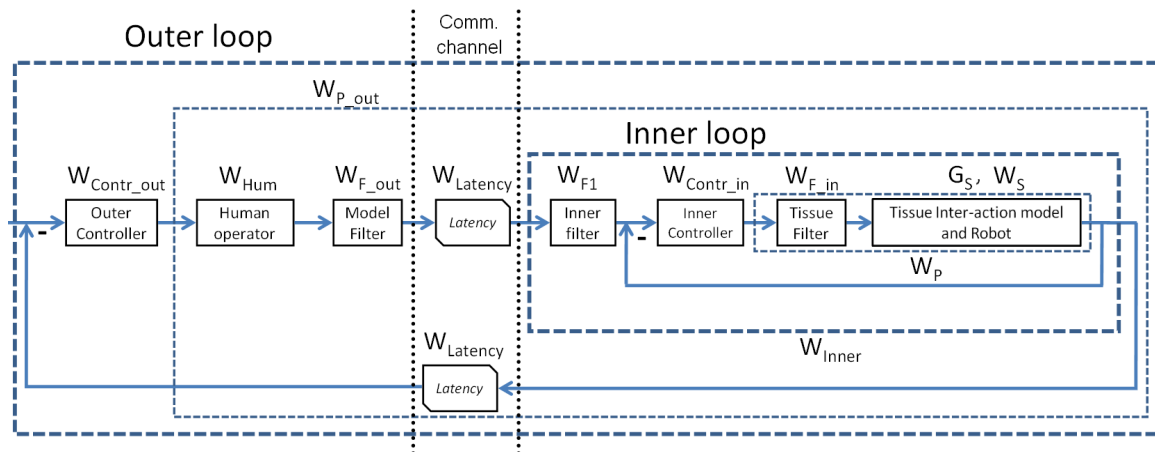


Fig. 5.5. The concept of applying cascade control to deal with extreme latencies in telesurgery.

Before the surgery

- define the model structure of the slave robot,
- define the model parameters of the slave robot,
- identify default communication lag time between the master and the slave side,
- identify the surgeon's personal settings (physiological parameters).

During the surgery

- automatically update tissue model properties based on local sensory feedback (e.g., impedance measurements),
- automatically adjust latency parameters (analyzing communication channels),
- adjust controller parameters until it reaches the limits of the structure (defined through previous simulations), then
 - apply Kessler's Extended Symmetrical Optimum method on the slave side,
 - employ complex filters before signal transmission to compact the slave model,
 - use approximated model of the system latencies,
 - apply Kessler's Extended Symmetrical Optimum method on the master side,
- advanced, automated safety features can be realized on the slave side, e.g.,
 - physiological organ motion compensation,
 - external patient motion detection and compensation (described in Section 3.1.1),
 - Virtual Fixture based proximity sensing and tissue safeguarding,
 - automated bleeding reduction with coagulation,
- redesign the controllers if the parameters change,
- rely on remote side human assistance through telementoring and consultancy telemedicine if necessary (as described in Section 5.1).

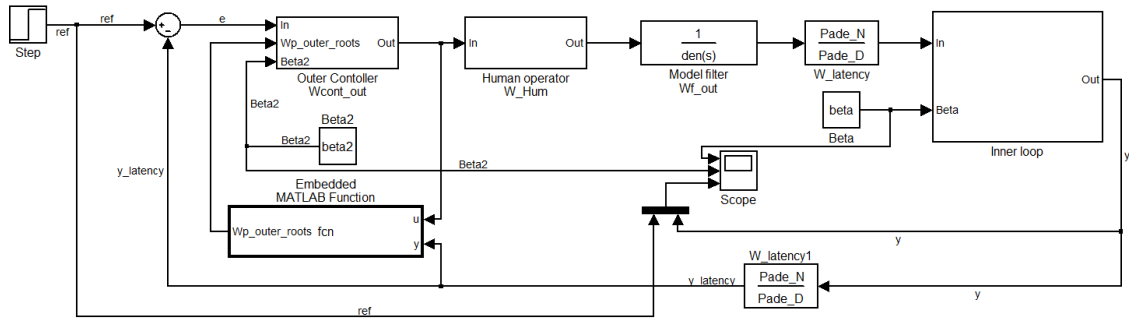


Fig. 5.6. The control structure modeled in Simulink environment.

5.6.1 Realization of control methods

The above presented telesurgery support method has been tested in simulations to show its effectiveness. The models for teleoperation have been defined (as described in the previous section) and implemented under MATLAB R2009b and Simulink 7.1 environment. The detailed results of the simulations are discussed here.

Master–slave robots are typically used in a discrete position-controlled mode, therefore the use of step function for excitation during evaluation is suitable to analyze the performance of different controllers. While robot parameters are given in SI units below, the step function’s amplitude/time diagrams scale down proportionally, as a robot would not move faster than 100 mm/s, while in the low level control, it must be regulated with 1–10 kHz control cycle. During the evaluation, a critical factor was to ensure that the PM is between 45–60°, where the system is inherently, and I also set requirements for reasonable performance in terms of overshoot (σ), the absolute maximum of the signal and settling time (τ_t), the time by the signal reaches the $\pm 2\%$ proximity of its final value.

5.6.2 Slave side—inner loop

In this section, the previously defined models are applied and used to build up a controller structure presented in Fig. 5.5. (The same notations are followed.) The entire slave robot (W_S) can be modeled in accordance with (5.11) using the transfer function:

$$W_S = \frac{(k_S + B_S s) G(s)}{s(M_S s^2 + B_S s + k_S + G(s))}. \quad (5.23)$$

The tissue model in s domain, assuming constant contact force being (integral term):

$$G(s) = p(e^{qK} - 1) = \frac{k_t}{s}. \quad (5.24)$$

However, when $K = \mathbf{x}_S(t)_{\text{const}}$, substituting $G(s)$ into (5.23) the plant’s TF (meaning the slave robot and the tissue in contact together) becomes:

$$W_P = \frac{k_t B_S s + k_t k_S}{s(M_S s^2 + B_S s + (k_S + k_t))} \quad (5.25)$$

Assuming a reasonably small slave robot that might be suitable for long duration space missions based on [199]: $M_S = 0.1$ kg, $B_S = 20$ Ns/m, $k_S = 400$ and $x_S = 0.001$ m. Tissue interaction parameters were chosen similarly: $p = 0.2$ and $q = 400$. Without specific control, this results in an unstable system with time constants $T_P = [0.0443, 0.0056]$.

First, let us employ an input filter on the plant:

$$W_{F.in} = \frac{k_S}{B_S s + k_S}, \quad (5.26)$$

which is based only on the identified model parameters, and allows the broader handling of the plant's TF (5.12): This leads to a filtered plant with TF:

$$W_{PF} = \frac{k_p}{s(1 + sT_{P1})(1 + sT_\Sigma)}, \quad \text{where} \quad (5.27)$$

$$k_p = \frac{k_S k_t}{k_S + k_t} = 0.0983, \quad (5.28)$$

$$T_{P1} = \frac{2M_S}{B_S - \sqrt{B_S^2 - 4M_S(k_S + k_t)}} = 0.0444s \quad \text{and} \quad (5.29)$$

$$T_\Sigma = \frac{2M_S}{B_S + \sqrt{B_S^2 - 4M_S(k_S + k_t)}} = 0.0056s. \quad (5.30)$$

Good control system performance indices (overshoot, settling time, control error) can be obtained with a PID controller having the TF:

$$W_{Contr.in} = \frac{k_{Contr.in}}{s}(1 + sT_{C1})(1 + sT_{C2}) \quad (5.31)$$

applied to the inner control loop.

The following tuning equations—specific to the Extended Symmetrical Optimum method [208]—lead to the tuning parameters of the PID controller in the inner loop:

$$k_{Contr.in} = \frac{1}{\beta \sqrt{\beta} k_p T_\Sigma^2}, \quad T_{C1} = T_{P1}, \quad T_{C2} = \beta T_\Sigma, \quad (5.32)$$

where $\beta = \beta_{Inner}$ is the tuning parameter of the inner control loop. The designer sets the value of this parameter to ensure an acceptable compromise in the control system performance indices.

The open loop and closed loop TFs (W_0 and W_C , respectively) derive to be:

$$\begin{aligned} W_0 &= W_{PF} W_{Contr.in} \quad \text{and} \\ W_C &= \frac{W_0}{1 + W_0} = \frac{1 + \beta T_\Sigma s}{(1 + \sqrt{\beta} T_\Sigma s) \left(1 + (\beta - \sqrt{\beta}) T_\Sigma s + \beta T_\Sigma^2 s^2 \right)}. \end{aligned} \quad (5.33)$$

The step response of W_C for $\beta_{Inner} = [4, 19]$ is shown in Fig. 5.7. It is clearly observable that with the rise of β_{Inner} , the overshoot and the settling time are also growing. For $\beta = [4, 9]$, W_0 contains a complex conjugated pole pair, with slightly decreasing absolute

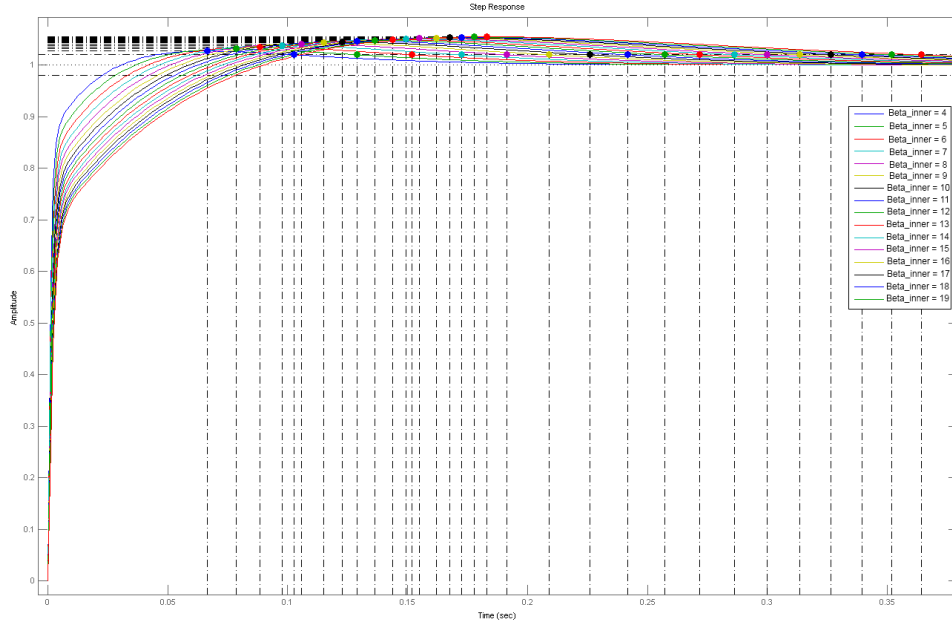


Fig. 5.7. Step response of the closed loop W_0 slave side system. β_{inner} has been tuned between [4, 19].

values. Therefore it is advisable to apply filtering in accordance with [208]. Filtering for $p_{1,2}^*$ means to compensate for the complex conjugated poles in the $\beta = [4, 9]$ domain.

$$W_{F1} = \frac{1 + (\beta - \beta^{\frac{1}{2}}) T_{\Sigma} s + \beta T_{\Sigma}^2 s^2}{(1 + \beta T_{\Sigma} s)(1 + \lambda T_{\Sigma} s)}, \quad \text{where } \lambda = \beta - \beta^{\frac{1}{2}} - 1. \quad (5.34)$$

When the W_{F1} filter is applied, the closed loop TF of the inner control loop (W_{Inner}) is:

$$W_{Inner} = W_{F1} W_C = \frac{1}{(1 + \sqrt{\beta} T_{\Sigma} s)(1 + \lambda T_{\Sigma} s)}. \quad (5.35)$$

In this case, the W_{F1} filter will not contain a complex conjugated zero pair for any $\beta_{Inner} > 9$. E.g., for $\beta_{Inner} = 10$:

$$W_{F1} = \frac{0.0003176s^2 + 0.03853s + 1}{0.001854s^2 + 0.08925s + 1}, \quad (5.36)$$

and its zero–pole–gain (ZPK) form is:

$$W_{F1} = \frac{(1 - s/z_{F1.1})(1 - s/z_{F1.2})}{(1 - s/p_{F1.1})(1 - s/p_{F1.2})}, \quad (5.37)$$

where $k_{F1} = 0.171$, $z_{F1.1} = -83.728$, $z_{F1.2} = -37.609$, $p_{F1.1} = -30.397$ and $p_{F1.2} = -17.745$. The step response of W_{Inner} for $\beta_{Inner} = [4, 19]$ is shown in Fig. 5.8.

Based on the data presented in Table 5.1, β_{Inner} must be over 5 to ensure 45° PM, resulting in inherent stability of the system. Overshoot is 0% in every case due to the fact that I employed a (5.34) type filter. Based on the experiments, it is advantageous to choose $\beta_{Inner} = 6$ for further design calculations, providing the best performance. This allows for 12 Hz control cycle (comparable to the performance of current optical tracking systems). The inner loop PID controller's parameters are for $\beta_{Inner} = [4, 16]$:

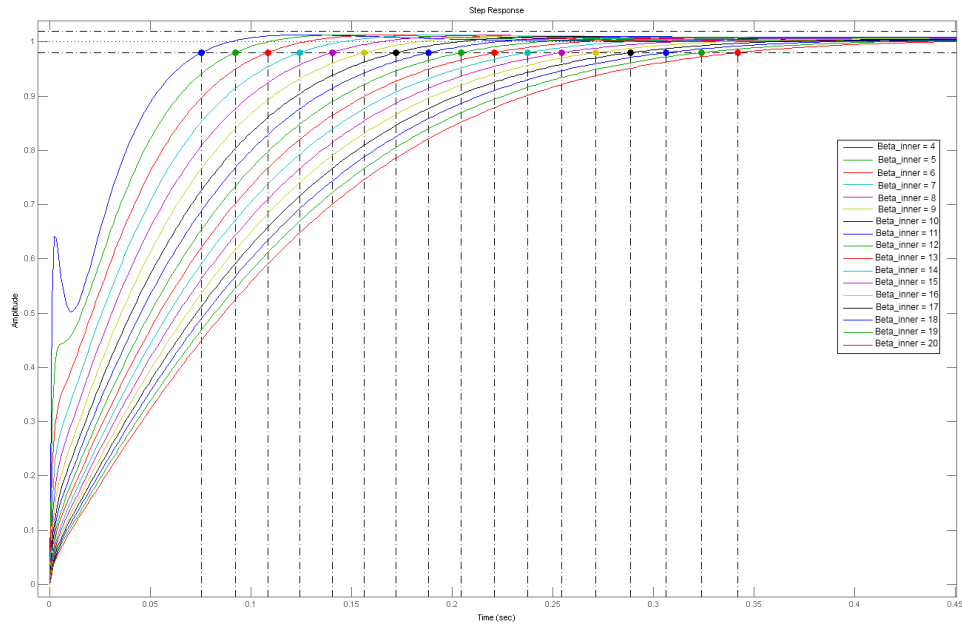


Fig. 5.8. Step response of the filtered, closed loop W_{Inner} system. The response needs to be fast in order to allow the implementation of another control layer in the outer loop.

TABLE 5.1

CONTROLLER PERFORMANCE PARAMETERS FOR THE INNER LOOP WITH DIFFERENT β_{INNER} SETTINGS

β	Phase Margin	Overshoot	Settling time
4	36.9°	0%	0.052 s
5	41.8°	0%	0.066 s
6	45.6°	0%	0.082 s
7	48.6°	0%	0.099 s
8	51.1°	0%	0.117 s
9	53.1°	0%	0.135 s
10	54.9°	0%	0.154 s
11	56.4°	0%	0.173 s
12	57.8°	0%	0.192 s
13	59°	0%	0.212 s
14	60.1°	0%	0.231 s
15	61°	0%	0.251 s
16	61.9°	0%	0.271 s

- $T_{C1} = 0.0444$ (for every β_{Inner}),
- $T_{C2} = 0.0225 \dots 0.0902$,
- $k_{\text{Contr.in}} = 40026 \dots 5003.3$.

5.6.3 Master side—outer loop

Padé approximation technique developed in 1892 is suitable to incorporate the effect of the latency within the model in TF form [75]. The method is based on matching the TF's coefficients with the Taylor series approximation coefficients of a rational function, therefore the approximant's power series agrees with the power series of the function it is approximating (up to the rank desired by the user). In general, odd order Padé approximation is applied, thus the largest time constant of the latency term will be a real number, and we can apply (5.34) to deal with the complex conjugated poles deriving from higher order approximation. The 1st order Padé approximation transforms the latency in the following TF form such that to simplify the simulation of the cascade control system structure:

$$W_{\text{Latency}} = e^{-sT_{d.0}} \approx \frac{2 - sT_{d.0}}{2 + sT_{d.0}}, \quad (5.38)$$

where a typical one-way delay is $T_{d.0} = [0.1, 1]$ s in this application.

The human operator's model (W_{Hum}) in accordance with the crossover model (5.2) can be approximated as:

$$W_{\text{Hum}} = k_{P_{\text{Hum}}} \frac{\omega_{c_{\text{Hum}}}}{s} e^{-sT_{\text{Hum}}} \approx W_{\text{Hum.Padé}} = k_{P_{\text{Hum}}} \frac{\omega_{c_{\text{Hum}}}}{s} \frac{2 - sT_{\text{Hum}}}{2 + sT_{\text{Hum}}}, \quad (5.39)$$

where T_{Hum} is the human operator's physiological latency. In accordance with the literature, $T_{\text{Hum}} = 0.1$ s and therefore:

$$k_{P_{\text{Hum}}} \omega_{c_{\text{Hum}}} = 1. \quad (5.40)$$

Filtering in the outer loop can be used to speed up the system. Let us compensate for the denominator of the inner closed loop transfer function in (5.35). Symbolically, (5.35) can be written in the form:

$$W_{\text{Inner}} = \frac{1}{(1 + T_{P1}s)(1 + T_{P2}s)}. \quad (5.41)$$

The TF of the outer loop filter being:

$$W_{\text{F.out}} = \frac{1 + sT_{\text{Comp}}}{1 + sT_{\text{F}}}, \quad (5.42)$$

where T_{F} is a *filter time constant* and T_{Comp} is chosen to compensate for the largest time constant in (5.35):

$$T_{\text{Comp}} = \max(T_{P1}, T_{P2}), \text{ therefore} \quad (5.43)$$

$$T_{\text{Comp}} = \max\left(\sqrt{\beta}T_{\Sigma}, \lambda T_{\Sigma}\right) = \begin{cases} \sqrt{\beta}T_{\Sigma} & \text{if } 1 < \beta \leq 3 + 2\sqrt{2} \\ \lambda T_{\Sigma} = \left(\beta - \sqrt{\beta} - 1\right) T_{\Sigma} & \text{if } \beta > 3 + 2\sqrt{2} \end{cases}$$

In addition, T_F is a small filter time constant fulfilling the condition:

$$0 < T_F \ll \min\left(\sqrt{\beta}T_\Sigma, \lambda T_\Sigma\right). \quad (5.44)$$

The TF of the outer loop process is derived in the following form:

$$\begin{aligned} W_{P_out} &= W_{Hum}W_{F_out}W_{Latency}W_{Inner}W_{Latency} = \frac{k_{P_out}}{s(1+sT_F)(1+sT_{P2})}e^{-sT_m}, \\ k_{P_out} &= k_{P_Hum}\omega_{c_Hum}, \\ T_m &= T_{Hum} = 2T_{d0}. \end{aligned} \quad (5.45)$$

The TF defined in (5.45) can be used in the design and tuning of the outer loop controller with TF W_{Contr_out} . The open loop and closed loop TF being:

$$\begin{aligned} W_{0_out} &= W_{Contr_out}W_{P_out} \text{ and} \\ W_{C_out} &= \frac{W_{0_out}}{1 + W_{0_out}}. \end{aligned} \quad (5.46)$$

Using (5.44), a simplified version of the TF in (5.45) can be derived:

$$W_{P_out} \approx \frac{k_{P_out}}{s(1 + T_{P_out})}e^{-sT_m}, \text{ where } T_{P_out} = T_F + T_{P2}. \quad (5.47)$$

Using Padé approximation defined in (5.38), the TF of the outer loop process is approximated as:

$$\begin{aligned} W_{P_out} \approx W_{P_out_Padé} &= W_{Hum_Padé}W_{F_out}W_{Padé}W_{Inner}W_{Padé} = \\ &= \frac{k_{P_out}(1 - sT_{Hum}/2)(1 - sT_d/2)^2}{s(1 + sT_F)(1 + sT_{P2})(1 + sT_{Hum}/2)(1 + sT_d/2)^2}. \end{aligned} \quad (5.48)$$

5.6.4 Solutions to handle time delay in telesurgery

In this Section, plausible options to deal with the outer controller design are discussed. Different approaches have been considered, simulated and evaluated to determine their usability in the given cascade structure for teleoperation. Analysis of various controller structures and design parameters were conducted to provide a higher degree of freedom to the designer in choosing the controller parameters in a simple and transparent manner. This way, it could be ensured the the finally proposed structure will be able to compensate for the process model uncertainties, and this is believed to be the first step towards combining sets of linear controllers to ensure performance improvement.

My goal was to find an appropriate empirical control method that is capable of handling the latency, and can be integrated to the cascade structure defined beforehand. The idea is to use simpler controller design techniques that allows to redesign the parameters frequently while the network parameters—and therefore the latency—are changing. The obvious failure of certain models already provides useful information as it demonstrates the limitation of their application.

Case 0: Empirical approach through extended Ziegler–Nichols method

A classical controller tuning method was described by *Ziegler and Nichols* (Z–N) [218], and was only simulated to provide the reference context of further experiments. In the case of the above described cascade system, a PID controller for the outer loop—consisting of the entire slave side and the human operator model as in Fig. 5.5—can be designed applying Z–N. It needs a practical extension to handle a generic system (W_{P_gen}) having the TF:

$$W_{P_gen} = \frac{k_P}{s(1+sT)} e^{-sT_m} \quad (5.49)$$

a stable PID controller in the form of:

$$W_{Contr_out} = \frac{k_{Contr_out}}{s} (1+sT_I)(1+sT_D) \quad (5.50)$$

can be designed using the following parameters:

$$\begin{aligned} k_{Contr_out} * k_P * \rho &\leq 1.2, \\ \rho &= \frac{T_m}{T_{pl}}, \\ T_I &= 2T_m \text{ and} \\ T_D &= T_m, \end{aligned} \quad (5.51)$$

where T_m is the aggregated latency in the system and T_{pl} is the time constant of the plant. In this case, the approximated system should have $T = T_1 + T_2$.

For the surgical teleoperation system $T_m = T_d + T_{Hum}$, where $T_d = 2T_{d,0}$ is the round-trip latency. The extension means we handle the model of the human operator with the given parameters as a latency within the system. Then, the Z–N method can be applied to (5.45).

Performing simulations for the system, the Ziegler–Nichols method results in stable controllers for different possible β_{Inner} parameters of the inner loop, but with very low PM, therefore large oscillations. From the inner loop's criteria, $\beta_{Inner} = 6$ is the optimal choice, as derived above. The method creates very slow systems for the different latencies, tuned from 0.1–1 s as shown on Fig. 5.9. Assuming a maximum communication link latency ($T_d/2$) of 1 s in accordance with (5.1), the following parameters are employed:

$$\begin{aligned} T_m &= 2.1, \\ T_{pl} &= 0.05, \\ \rho &= 21, \\ k_C &= 1.2, \\ T_I &= 4.2 \text{ and} \\ T_D &= 2.1. \end{aligned} \quad (5.52)$$

The simulation results derived $\tau = 6.76$ s, $\sigma = 0\%$ and $PM = 88.3^\circ$.

It can be stated that the Z–N method fails to provide a universal solution to the control problem of delayed teleoperation, the resulting systems are too slow for any time-critical application.

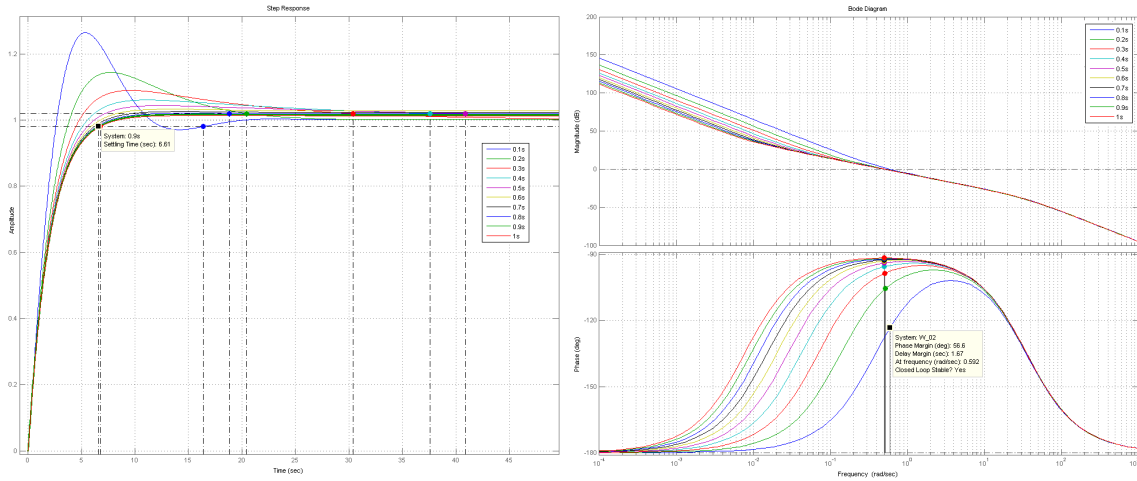


Fig. 5.9. Closed loop step response and open loop Bode diagram of the delayed system, designed with the Z–N method. T_d has been tuned between 0.1–1 s.

TABLE 5.2

MAXIMUM LATENCY MANAGEABLE WITH DIFFERENT β_{INNER} DESIGN PARAMETER SETTINGS IN THE INNER LOOP’S CONTROLLER.

β_{Inner}	4	5	6	7	8	9	10	11	12	13	14	15	16
$T_{d\text{max}} [s]$	0.0162	0.0275	0.0218	0.0162	0.0106	0.0049	0	0	0	0	0	0	0

Case 1: Straight application of Kessler’s method

Originally, the TF of a plant applicable to Kessler’s method does not include latency. Delays in the system must be approximated and handled in an aggregated manner. Without distorting the effectiveness of Kessler’s method, we can employ Padé approximation for latencies not effecting the largest time constant of the original plant:

$$T_1 \geq \overbrace{(T_d + T_2)}^{T_\Sigma}, \tag{5.53}$$

where T_1 is the largest time constant of the process, T_d is the total time delay and T_2 being the aggregation of the smaller time constants.

Depending on the β_{Inner} scaling factor applied in the inner loop, the time constants of the outer loop will vary, therefore different amount of latency can be handled this way. I could show based on Table 5.1 that to achieve maximum latency handling—while respecting (5.53)— $\beta_{\text{Inner}} = 5$ provides the highest value. However, as presented in Table 5.2, stability of the inner loop is only guaranteed with higher β_{Inner} , therefore $\beta_{\text{Inner}} = 6$ is the optimal choice.

With this assumption, latency in the system can be handled. Let us consider the previously discussed robotic teleoperational setup, where the time constants of the outer loop TF denominator are $T_{\text{Outer}} = [0.05, 0.0138, 0.0144]$ s, therefore an approximated TF with

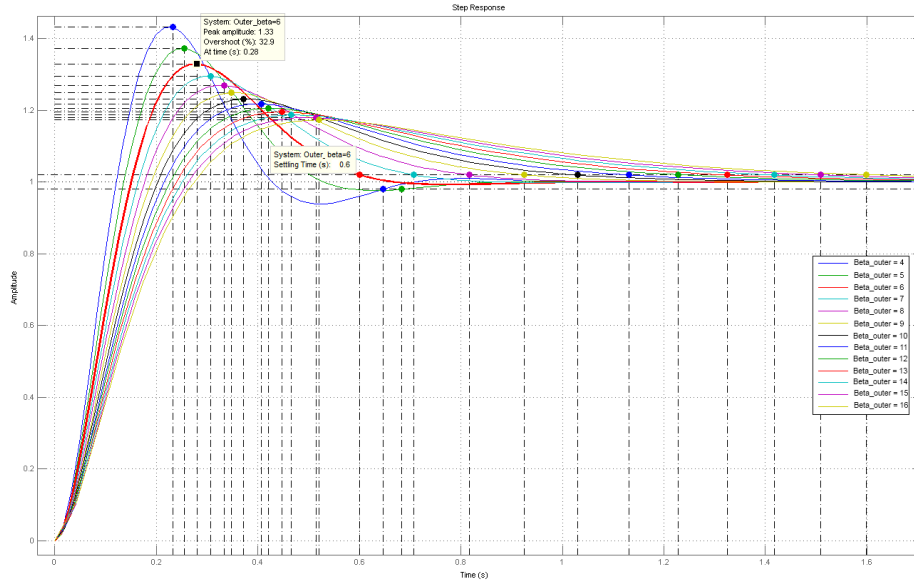


Fig. 5.10. Step response of the whole closed loop system with different β_{Outer} settings (classical ESO) and a maximum of 0.0218 s communication lag time. Kessler's classical method was employed for controller design.

time constants:

$$\begin{aligned}
 T_1 &= 0.05 \text{ and} \\
 T_\Sigma &= \overbrace{(0.0138 + 0.0144)}^{0.0282}.
 \end{aligned} \tag{5.54}$$

In terms of (5.53), a maximum of 0.0218 s latency can be tolerated by this design mode. Applying $T_d = 0.0218$ to the simulations, the derived stable controller's performance is shown in Fig. 5.10.

This results in a slow controller (with $\tau_{\text{min}} = 0.6$ s settling time) with significant ($\sigma = 33\%$) overshoot. Clearly, this method has a major limitation towards latency handling, and further design consideration are to be made to enable the tolerance of higher latencies, as discussed below.

Case 2: Stretching Kessler's robustness

It is possible to overcome the limitation of the above mentioned setup by violating condition (5.53). While the ESO method only guarantees overshoot and settling parameters if the largest time constraint is compensated, the robustness of the design method can be exploited. Understandably, this will return the same results as the previous (classical) method for $T_d \leq 0.0218$, but will also give stable solutions for larger latencies. Fig. 5.11a,b show the results for $T_d = 0.1$, the step response and Bode plot for $\beta_{\text{Outer}} = [4, 16]$ values. β_{Inner} was set to the optimal value, 6. The best outcome was achieved at $\beta_{\text{Outer}} = 6$, where

$\sigma = 33\%$ and $\tau = 1.28$ s. The PM is increasing along with β_{Outer} , as the system is getting slower and slower due to the nature of combined time constant approximation. With increasing time delay, only the settling time grows (Fig. 5.11c). For the desired maximum design constraint of 1 s latency (with $\beta_{Outer} = 6$), this method gives $\sigma = 33\%$ and $\tau = 8.11$ s, which is unacceptable for teleoperational application.

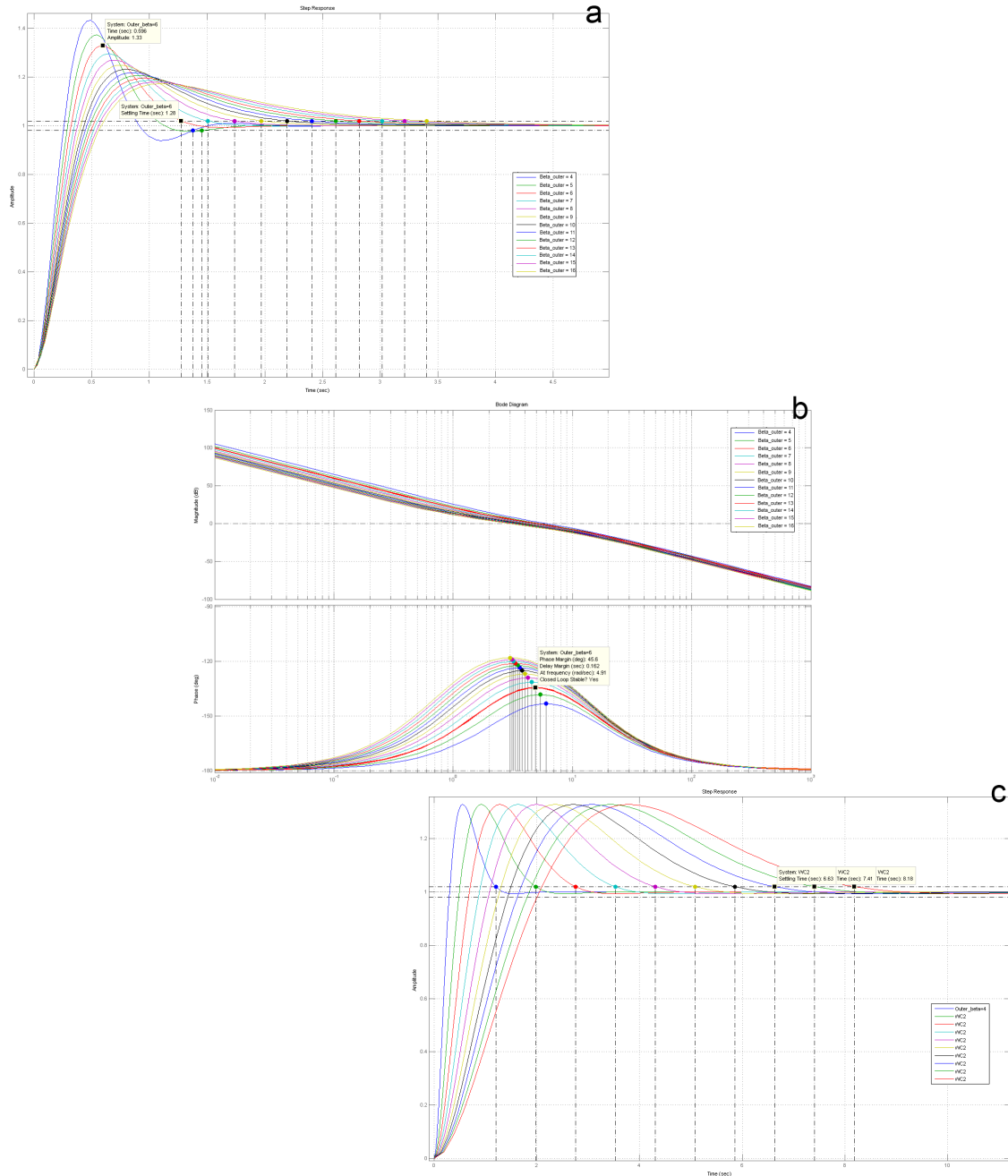


Fig. 5.11. a) Step response of the whole closed loop system with different β_{Outer} settings employing the stretched version of Kessler’s method. T_d was 0.1 s. b) Bode plot of the system with the same settings. c) Step response of the system with $\beta_{Inner} = \beta_{Outer} = 6$ and $T_d = 0.1-1$ s.

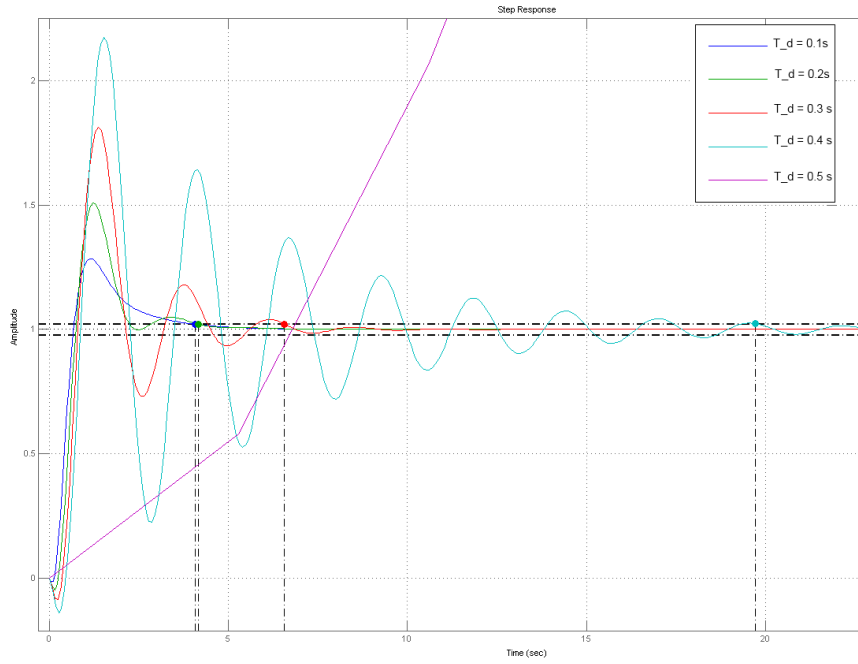


Fig. 5.12. The robustness of Kessler's method proven through its ability to compensate for latencies up to 0.5 s, originally not incorporated in the system model.

It is also possible to test the robustness of Kessler's method through not incorporating the latency in T_σ . In this case, applying the previous β settings, the controller designed will be unstable. However, the extreme choice of the parameters ($\beta_{\text{Inner}} = \beta_{\text{Outer}} = 16$) leads to a stable controller for up to 0.5 s through slowing down the system, as shown in Fig. 5.12. In fact, latency over 0.2 s results in an under-damped system.

This analysis leads to the conclusion that a different method is required to reach the 2 s round-trip latency range with a safe and effective controller design.

Case 3: Kessler's method with Smith predictor

Smith predictor [75, 214] is a model based prediction method which handles the time delay outside of the control loop and allows a feedback design based on a delay-free system as shown in Fig. 5.13. For a generic system having the TF:

$$W_{P,\text{gen}} = W_P e^{-sT_d}, \quad (5.55)$$

where T_d is the latency and the $W_P(s)$ plant TF is assumed to be open loop stable, the closed loop TF derives to be:

$$W_{C,\text{Contr}} = \frac{W_{C,\text{Contr}} W_P}{1 + W_{C,\text{Contr}} \tilde{W}_P + W_P (W_P e^{-sT_d} - \tilde{W}_P e^{-s\tilde{T}_d})} e^{-sT_d}, \quad (5.56)$$

where \tilde{W}_P is the model of the plant and \tilde{T}_d is the approximation of the time delay. When these models match perfectly, the closed loop TF becomes:

$$W_C = \frac{W_{C,\text{Contr}} W_P}{1 + W_{C,\text{Contr}} W_P} e^{-sT_d}. \quad (5.57)$$

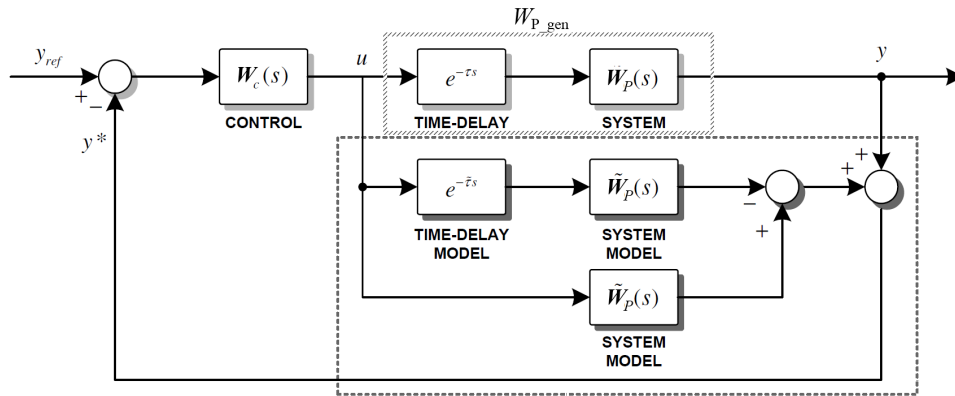


Fig. 5.13. Block diagram of the classical Smith predictor, based on [214].

TABLE 5.3

CONTROLLER PERFORMANCE PARAMETERS FOR CASE 3 WITH DIFFERENT β_{OUTER} SETTINGS

β_{Outer}	Phase Margin	Overshoot	Settling time
4	41°	43%	0.57 s
5	41.5°	37%	0.54 s
6	42.3°	33%	0.47 s
7	43.3°	30%	0.61 s
8	44.3°	27%	0.69 s
9	45.3°	25%	0.77 s
10	46.2°	23%	0.84 s
11	47.1°	22%	0.92 s
12	47.9°	21%	0.99 s
13	48.7°	20%	1.06 s
14	49.4°	19%	1.12 s
15	50.1°	18%	1.19 s
16	50.8°	17%	1.26 s

Applying this to (5.45):

$$W_{C_out} = \frac{W_{\text{Contr.out}} W_{P_out}}{1 + W_{\text{Contr.out}} W_{P_out}} e^{-sT_d}. \quad (5.58)$$

Similar conditions have been simulated than before, and in the case of $T_d = 0.1$ s, the deriving system performs better than in the previous cases. Table 5.3 summarizes the numeric results for $\beta_{\text{Inner}} = 6$, employing 5th order Padé approximation for the latency. It can be seen that $\beta_{\text{Outer}} = 9$ gives the best results along the pre-defined criteria.

With this controller structure, it is finally possible to properly address the issues with large latencies (e.g., $T_d = 1$ s, as targeted before). To ensure the smooth hold phase of the system, higher order ($> 5^{\text{th}}$) Padé approximation was used. This also increased the overshoot, therefore a rational compromise was chosen. From the application point of view, the amplitude of the oscillation (A_{max}) during the hold phase can be critical, thus it is a limiting factor regarding the choice of order and the overshoot. It has been determined to only allow a maximum of 10% overshoot during the hold phase, therefore ($> 15^{\text{th}}$) order Padé approximation should be used based on Table 5.4.

TABLE 5.4
EFFECT OF ORDER OF APPROXIMATION ON CONTROL PARAMETERS.

Order of Padé approximation	A_{\max}	Overshoot	Settling time
1	95.3%	0%	4.58 s
3	50.6%	2%	3.19 s
5	32.5%	6%	3.04 s
7	25.1%	12%	2.83 s
9	17.4%	17%	2.71 s
11	14.8%	21%	2.64 s
13	12.2%	24%	2.61 s
15	10%	25%	2.60 s
17	8.6%	27%	2.67 s
19	7.2%	27%	2.69 s
21	6.2%	28%	2.71 s

TABLE 5.5
EFFECT OF β_{Outer} ON CONTROL PARAMETERS FOR CASE 3 SYSTEM DESIGN.

β_{Outer}	A_{\max}	Overshoot	Settling time
4	18.4%	22%	2.58 s
5	15.7%	25%	2.61 s
6	13.6%	26%	2.62 s
7	12.1%	27%	2.49 s
8	11%	25%	2.54 s
9	10%	25%	2.61 s
10	9.5%	24%	2.79 s
11	8.9%	23%	2.85 s
12	8.5%	22%	2.9 s
13	8%	21%	2.95 s
14	7.7%	20%	3 s
15	7.4%	20%	3.06 s
16	7.1%	19%	3.14 s

Previous considerations for β are valid here as well, therefore $\beta_{\text{Inner}} = 6$ provides a rational compromise between rise-time and overshoot. With 15th order Padé approximation the effect of the $\beta_{\text{Outer}} = [4, 16]$ parameter on the system is shown in Fig. 5.14. The smoothing effect of higher β in return of slowing down the system is displayed numerically in Table 5.5. The optimal parametrization of the control structure (Section 5.6) for extreme teleoperation with 2 s latency has been derived: $\beta_{\text{Outer}} = 6$ and $\beta_{\text{Outer}} = 9$ result in a system with $\tau = 2.61$ s and $\sigma = 25\%$, while the initial oscillation does not exceed 10%.

In this section various controller alternatives have been investigated with the aim to provide a stable solution for a simplified model developed for a future space teleoperation applications. The results showed the serious limitations of certain more simple methods, and defined the boundary conditions under which the Extended Symmetrical Optimum method can be used in this setup.

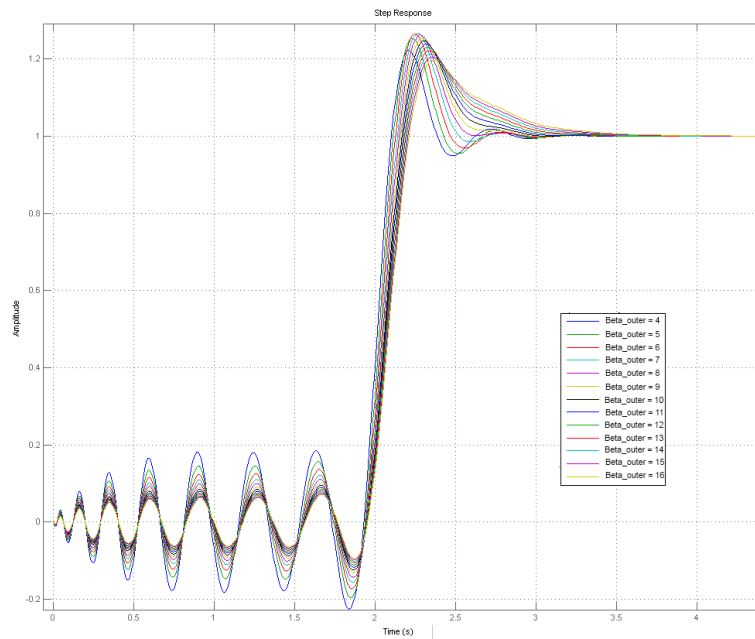


Fig. 5.14. Kessler's method employed with Smith predictor for large latencies. The β_{Outer} control parameter's effect in the oscillation in the hold phase.

5.7 Summary of the Thesis

Teleoperation of surgical devices opens an entirely new field in medicine. However, manipulation of the tools over large distance with communication latency poses significant challenge from the control point of view. I developed a unified framework for the application of different telemedicine technologies enabling the support of a future human space exploration mission. Particularly, my solution focuses on the handling of large delays during real-time teleoperation of a remote surgical robot. In addition, modeling approaches were discussed, and simplified human and machine representations were derived to accommodate long distance telesurgical applications. I have proved that a cascade control structure that relies on empirical design can be effectively used to serv a realistically modeled telesurgical system. A suitable controller was designed based on the extension of Kessler's methods in the inner loop, supported by predictive technique in the outer loop. The failure of more simple classical methods provides important information about those controller capabilities. The proposed cascade loop combining the Extended Symmetrical Optimum method with Smith predictor may be a good solution to support future teleoperational missions.

Chapter 6

CONCLUSION

6.1 Summary of Contributions

During my Ph.D. research, probably the most important aspects of Computer-Integrated Surgery were studied. I have been working on major challenges of surgical robotics, converging towards unified solutions facilitating real-life application of the technology. I presented a pioneering effort in Hungary to develop new methods and algorithms to improve existing systems, and to foster the creation of future medical devices.

Motivated by *Problem 1* (described in Chapter 2), I developed a new method for patient motion tracking and compensation. As described in Chapter 3, different approaches have been experimented to robustly identify surgical events—such as patient motion—that may endanger the success of an operation or could cause harm to the patient. My algorithm relies on the robust identification of different Surgical Cases in the Operating Room. I incorporated in the computations the internal coordinate frame of the navigation system, allowing for the reduction of hardware requirements. The algorithm was tested on simulated data and on the neurosurgical robot setup at the Johns Hopkins University. Numeric results gained proved that the method managed to reconstruct generic cases with 100% accuracy, and the more complex events with approximately 80% on average. Data collection of actual patient motion events in the Operating Room during surgeries will help the development of valid statistical models for different procedures, allowing to customize the algorithm.

Related publications: [HT-1, HT-2, HT-3, HT-4, HT-5, HT-6, HT-7, HT-8, HT-9, HT-10, HT-11, HT-12, HT-13].

The other major focus of my research was to improve the theoretical tools and practical means available for accuracy assessment of interventional devices. The classical approach to simple 3D error theory is not sophisticated enough to ensure the highest level of safety for many advanced surgical robotic systems. In order to answer *Problem 2*, I proposed a new concept—stochastic approach to determine the 6 DOF error distribution of a generic Image-Guided Surgical system. The method is based on the direct handling of the error distribution function and forbidden regions defined as a Virtual Fixture, and can provide the actual distribution of errors at the tool right before the intervention begins. This allows for the optimal placement of the devices in order to reduce the overall effect of navigation and registration errors. Simulation results showed the applicability of the theory, and computations have also been performed for the JHU robot system, where the inhomogeneity

of the distribution along different axes was shown to be over a hundred fold, therefore seriously limiting the performance of the system.

Related publications: [HT-14, HT-15, HT-16].

Furthermore, I developed a new control framework to support long distance telesurgery, aiming for future space applications. I have shown that the extension of Kessler's empirical design method is applicable to robotics, and in a cascade setup it could serve a complex master–slave teleoperation system, giving adequate solution to *Problem 3*. I incorporated the valid model of the robot, the operator and the communication channel. A controller design structure was developed and simulated successfully under various conditions and in different cases. I derived the first successful application of Kessler's Extended Symmetrical Optimum method in the field of robotics to control the modeled system, and determined the optimal parameters for the β tuning parameters of the algorithm.

Related publications: [HT-17, HT-18, HT-19, HT-20, HT-21, HT-22, HT-23, HT-24, HT-25, HT-26, HT-27].

Through advanced technological solutions, it is possible to improve the quality of future health care and justify the higher investment costs of robotic interventions. Systems currently under development will soon deliver great clinical advantages and improved safety features providing benefits both to the patient and the surgeon. Nowadays, it is particularly relevant and desirable to advance in the field of medical technology, to meet the needs of complex surgical procedures and to provide modern health care support even in remote areas.

6.2 Future Work

I am dedicated to the broader extension of my thesis work and to conduct further research in the field. For the next 2 years, the National Office for Research and Technology (NKTH), Hungarian National Scientific Research Foundation grant OTKA CK80316 is supporting my ongoing research efforts. Numerous B.Sc. and M.Sc. students are involved with these projects, and we are looking for new results along each research topic.

The thesis research initiatives have become the foundation of new international collaborations. Beyond the cooperation with the Johns Hopkins University (*cisst.org*), our laboratory at BME started a joint project with the newly founded Austrian Center for Medical Innovation and Technology (ACMIT, *www.acmit.at*) in 2010 on patient motion tracking and radiation treatment plan compensation for gynecological brachytherapy. Further, some parts of my project is affiliated with the Department of Automation and Applied Informatics of "Politehnica" University of Timisoara, Romania (*www.aut.upt.ro*), focusing on the extension of classical control paradigms for telesurgical scenarios.

Concerning the first thesis group, data collection is scheduled in the near future to record patient motions during actual surgical procedures. This will result in the more refined tuning of the motion compensation algorithm, while soft-computing methods, such as micro–macro neural networks [219] may also boost its performance. The customizable algorithm will be useful for various research groups.

The error propagation simulation can provide important data on the accuracy of any surgical setup; next, I plan to develop an interface to the JHU robot system to incorporate

the algorithm in the current program framework. The method may help manufacturers giving recommendations for OR setups.

There is an increasing demand to include haptic feedback to the teleoperation as well, therefore the concept should be investigated. There are two major issues that need to be addressed in the case of delayed teleoperation with haptics: passivity and transparency. The reflection of physical load on the master side may have a significant effect on human performance, therefore should be investigated.

In the past years, many different solutions have been developed for bilateral teleoperation scenarios [220, 221, 222]. My next step is to investigate the effectiveness of the *network disturbance concept with a communication disturbance observer* to replace the Smith predictor [223]. Also, a more complex tissue model could be incorporated, based on [141]. Other algorithms, like soft-computing or modern control paradigms may be used in the outer control loop [224]. Time varying latency in today's internet network represents further technological challenges that need to be addressed [225].

The results to be achieved could be applied to other fields as well.

Appendix A

REGULATIONS AND STANDARDS ADDRESSING SURGICAL ROBOTICS

A.1 International regulations for CIS

To objectively evaluate the performance of a robot-assisted system, it is crucial to understand and apply consistent measurement methods. However, many other factors determine the success of a surgical robot beyond spatial precision. The accuracy of treatment delivery remains the baseline for applicability, but after all, adequate safety measures, a medical robotic system should still address the questions of complexity, cost and ergonomics. Different systems should be measured and assessed through the same validated experiments. The existing industrial standards and medical robotic drafts should be extended to all major areas of CIS systems.

Surgical robot systems typically have an application accuracy between 1–2 mm. This is less precise than robotic setups in industrial applications, as the accumulation of different errors in IGS prevents sub-millimeter accuracy as claimed in the case of many systems. (This is addressed in details in Chapter 4.) A robot must be intuitive and require minimal maintenance and engineering skills to operate [50]. The user acceptance of a system will eventually determine the value of the device, therefore one of the major directives of development is to minimize the change to the existing clinical workflow.

This is also represented in the medical device regulations. The procedures both in Europe and in the United States are focusing on the safety and transparency of systems [164]. Most prototype development and testing begins with the official approval of the *Institutional Review Board (IRB)*, legally taking responsibility for the primer operations.

In the *European Union (EU)*, the *CE mark (Conformité Européenne – European Conformity)* must be obtained, certifying that the product complies with the essential requirements of the relevant EU health, safety and environmental protection legislation. The approval procedure is managed by independent *Notified Bodies (NB)*. There are approximately 100 international, non-governmental NB for medical devices. *International Organization for Standardization's ISO 9000 Quality Standards* family is applied to verify the production management of a company (www.iso.org/iso/iso_catalogue.htm). ISO

9001:2000 combines three previous standards (9001, 9002 and 9003) addressing design and development procedures under the title “Quality management systems—Requirements”. For CIS systems the ISO 13485:2003 (“Medical devices—Quality management systems—Requirements for regulatory purposes”) is in effect. It is possible for ISO 9001 complied companies to self-certify (CE mark) their products within certain limitations, and the NB would periodically audits their system. Since 2010, the 2007/47/EC (*European Council*) regulation extended the existing 1993/42/EEC *Medical Device Directive* (MDD), requiring specific clinical data for new devices and companies are expected to do to ensure safety and demonstrate the performance of their product. The directive also requires the sustained and coordinated clinical post market surveillance of the products. In addition, software developed for diagnostic or therapeutic purposes has become classified as a medical device in the EU.

In the U.S. only the federal *Food and Drug Administration* (FDA) can clear medical systems (www.fda.gov/MedicalDevices/ProductsandMedicalProcedures/default.htm). This can be done either in the form of a *Pre-Market Approval* (PMA) procedure, which is for new devices, requiring extensive clinical trials, and huge amount of documentation. On the other hand, *510(k)* procedure is for devices that can be proved to be “substantially equivalent” to an existing device, already approved by FDA. The validation may still include clinical trials, but less than for PMA. All systems must comply with *FDA Quality System Regulations/Medical Device Good Manufacturing Practices* (Code of Federal Regulations Title 21, Part 820) [226].

Interestingly, all the FDA-cleared surgical robots (e.g., da Vinci, NeuroMate, CyberKnife, ROBODOC, MAKO Arm, SpineAssist) went down the 510(k) procedure, proven to be substantially equivalent to existing technologies. The basic idea behind these regulations is to prevent failures and safety issues originating from bad design. The clinical use and patient outcome might not even be verified during the validation. At the most, the system should show the capability to perform a procedure with the same effectiveness as an existing (manual) technique. They can be argued to rely on the selectivity of the market, which should only allow for the existence of well-sustained systems with significant added value to the surgical procedure.

A.2 Accuracy measurement standards relevant to the field

Several standards exist for medical devices in general (*International Electrotechnical Commission* (IEC) 601, ISO 14971, ISO 13485:2003), separately for industrial robotics (ISO 10219) and for safety-related systems (IEC 1508); however, currently none addresses directly surgical robotics. The ISO 10360 standard “Acceptance and reverification tests for coordinate measuring machines (CMM)” from 1994 (current version: 2001) can be applied to surgical robots in many cases (mostly to semi-autonomous systems). It defines the protocol for CMM based on *Volumetric Length Measuring Error* (VLME) and *Volumetric Probing Error* (VPE). To acquire VLME, a set of 5 gauges has to be measured 3 times with one probing at each end, in 7 different directions in space (Fig. A.1a), and all results must be within the specified error. For VPE, a precision sphere has to be measured with 25 equally distributed probing (Fig. A.1b). The probing error is the range of all radii.

Telesurgery require additional regulations. A report from [228] discusses technical and

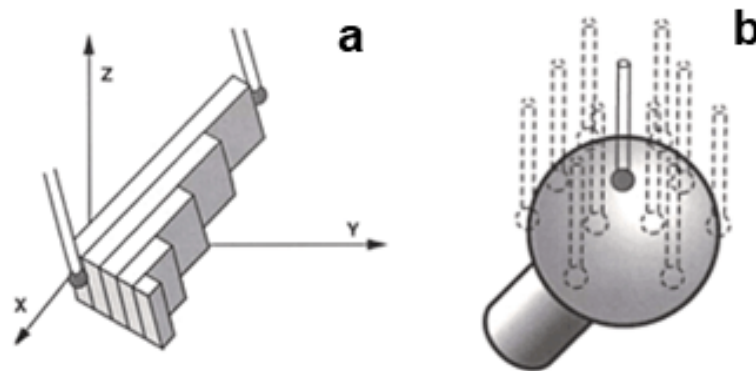


Fig. A.1. ISO 10360-1:2001 standard for coordinate measuring machines. (a) Illustrating Volumetric Length Measuring Error. (b) Illustrating Volumetric Probing Error [227].

human issues along the existing standards according to 1993/42/EEC MDD and the third edition of the IEC 601-1 (2006) for tele-neurology. According to the report, manufacturers of telemedical systems for neurology are required to:

- determine the medical purpose §3.10 of Medical Devices Directive,
- carry out risk classification and risk management (according to DIN EN ISO 14971),
- completely meet the requirements of MDD Annex I.

A.3 Safety standards and methods for CIS

Safety is paramount for any surgical devices, especially where some kind of actuation or automation is involved. This issue has been addressed by many individual researchers, governmental bodies and scientific societies in the past years, pushing for a unified standardization effort to ensure patient and medical staff safety in the OR.

Based on [229], errors in interventional medicine may be categorized as:

- commission (doing the wrong thing),
- omission (not doing the right thing),
- execution (doing the right thing incorrectly).

Errors can be either systematic (a series of errors resulting in an adverse event) or specific (the event itself is a form of error).

Several groups have published methodologies to support safety of design and development of robotic surgical devices. A generic one is the *Hazard Identification and Safety Insurance Control* (HISIC) policy that breaks down the issue into seven principles [230]:

- definitions and requirements,
- hazard identification,
- safety insurance control,
- safety critical limits,

- monitoring and control,
- verification and validation,
- system log and documentation.

The HISIC has been realized for multiple surgical robotic systems so far.

Further, an evolutionary method [231] and a *Unified Modeling Language* (UML) based approach [232] have also been successfully prototyped, relying on safe design, safe execution and risk assessment as cornerstones. Risk management in general is a key component of the entire medical device safety. This includes [232]:

- risk analysis (system definition, hazard identification and risk estimation),
- risk evaluation (determine risk tolerance levels),
- risk control (implementing the right action for maximum safety).

Failure mode analysis and risk assessment methods both for hardware and software in general have been addressed by many standards [50, 233, 231]:

- *International Electrotechnical Commission* (IEC) 60812 International Standard on Fault Mode and Effects Analysis (1985),
- IEC 1508 Functional Safety: Safety-Related Systems (1995),
- *European Norm* (EN) 1441 on risk management (1997),
- *American National Standards Institute* (ANSI) R15.06 standard for industrial robot safety (1999),
- IEC 62304 on Medical Device Software—Software Life Cycle Processes (2006),
- IEC 61025 Fault Tree Analysis (Ed. 2.0, 2006),
- ISO 14971 Application of Risk Management to Medical Devices (2007),
- IEC 60601 international standard on Medical Electrical Equipment (Ed. 3.0, 2010),
- IEC 1508 draft standard on Functional Safety for software developers.

Appendix B

SPACE COMMUNICATION, TELEOPERATION AND TELESURGERY

B.1 Latency in teleoperation and human adaptation

Telecommunication between distant locations involves latency, and even the most advanced channels will show some distortion and latency. Current systems rely more and more on satellite routes to transfer data. Satellite-based internet connections can use a fleet of *Low or Medium Earth Orbit* (LEO/MEO) satellites such as the commercial constellations of Orbcom, Globalstar or Iridium. Typical roundtrip delays are 40 ms, but the bandwidth is only 64 kbps per channel. For the newer O3b Networks satellites (scheduled for deployment in late 2010) would provide 1 Gbps with approximately 125 ms lag time. Geosynchronous satellites provide higher latency due to their 36,000 km altitude above the equator, but round-trip latency is 540–700 ms typically. Understandably, designated military satellites can provide faster communication channel, the minimum latency per satellite hop is expected to be 4.3–7.8 ms one way [234]. Despite the recent improvement in ground line speed, satellite communication has the potential to overcome it primarily in speed, with a reasonable quality of service and availability. In the distant future, quantum communication promises to entirely reshape current paradigms [235].

Communication protocols employed also have huge impact on latency. Presently, the majority of telepresence systems use *Transmission Control Protocol* (TCP) over the *Internet Protocol* (IP) to send data in the form of individual packets. Another common type is the *User Datagram Protocol* (UDP), a connectionless protocol that runs on top of IP networks. UDP/IP provides very few error recovery services, offering instead a direct way to send and receive datagrams. *Asynchronous Transfer Mode* (ATM/AAL1), which encodes data traffic into small fixed sized packets is also frequently used, but similarly, lacks advanced services. In the case of communication breakdown, the recovery time may be critical, therefore redesigned gateway architecture should be added to allow TCP transfers to survive a long duration blockage.

The Zeus and the da Vinci robots were designed to discard each packet that has any sort of internal error; they do not correct *bit-level errors*. If several packets are lost or

there is a breakdown, the robots suspend their operation. To some extent, the da Vinci is capable of handling packet loss due to a proprietary recovery algorithm. To meet the special communication requirements through satellites, the *Space Communications Protocol Specifications* (SCPS) standard was developed and tested by DoD and NASA [236]. SCPS uses similar architecture to TCP/IP, but it is more effective in handling latency created by long distance transmissions and the noise associated with wireless links. The SCPS exists as a full ISO standard and also meets the U.S. Military Standards.

To ensure superior quality visual and tactile feedback, high sampling rate must be used at the patient site (approximately 1 kHz). This has a significant bandwidth demand long with the HD video feedback. Under regular circumstances a 2 Mbps connection is already suitable for teleoperation; however in the case of a HD quality, multi-modal device, a 40 Mbps two-channel link would be required [237]. This would not cause much problem on the International Space Station that was equipped with a 150 Mbps connection in 2005, but in the case of a Mars mission, NASA only plans to develop a 5 Mbps connection as a part of the new space communication architecture relying on the reconfigurable *Space Telecommunications Radio System* (STRS). Further upgrades to 20 Mbps are only scheduled by 2020 [238].

Latencies in a telesurgical system may have various sources, just as in the case of an integrated IGS system discussed in Section 1.6.10. In a series of experiment in Canada [71], the following average values were derived:

- robotic data transport delay: 70 ms,
- commanded robotic motion on the patient side: 85,7 ms,
- CCD and camera controller latency: 20 ms,
- video transport delay: 70 ms,
- video compression/decompression (CODEC): 90 ms,
- video synchronizer delay: 33.6 ms.

Researchers showed that varying latency (jitter) significantly reduces the operators' performance both with robotic telesurgery and Virtual Reality (VR) applications [183]. Most humans are capable of adapting to sensory feedback latency up to 600 ms [38, 71] and some experiments suggest that individuals might be able to perform simple tasks even with a consistent 1000 ms delay [239]. It has been shown that latency above 0.5 s in general disrupts physicians, significantly prolongs execution time and therefore does not allow for effective surgical treatment. It is advisable to use the consistent, maximum latency of system to achieve performance continuity. A general approach to handle latency is to slow down the surgeons' movements, allowing time for the visual feedback to confirm the intended move. However, in extreme cases this prevents the effective work and firm reaction to unexpected events. The on-site medical assistant can also help with imminent moves and minor tasks [240].

Keeping the stereo vision system's two video channels synchronized is crucial for high quality performance. Other modalities might also be useful, if delivered ahead of the video. By reflecting e.g., forces sooner back to the operator (bypassing the time video coding/decoding takes), they can improve their ability to compensate for latency. The compression and decompression of the video stream can be reduced by the use of novel CODECs and state-of-the-art computing hardware, but it still takes 100–700 ms.

Approaching from the control theory point of view, several strategies have been developed to overcome the difficulties at the master side. One solution is to realize communication delays as force reflection for the human operator [241]. It feels as if the remote manipulator was controlled through a virtually coupled spring, applying adequate counter forces. This method can be well used to provide information on the remote manipulator's movement while there is no real feedback due to the latency. Unfortunately, the method is not precise enough (and may alter the surgeons decisions by providing unreal forces) to approve it for surgical applications.

B.2 Operations in weightlessness

Despite the technological challenges, health care in space has great achievements. Up to date, no emergency procedure has been performed in space. One of the primary safety criteria has always been to return all crew members safe without any serious injuries or illnesses. Based on the recorded medical events at NASA, collected from 89 Space Shuttle mission from 1981 to 1998, there have been several dozens of medical events and complaints affecting basically all of the organs, involving the risk of serious consequences. Once in 1982, an astronaut almost had to be evacuated on a Space Shuttle with the symptoms of kidney stones [242]. In the meantime, scheduled long-term exploration missions have higher probability of medical complications.

Surgical experiments (laparotomy and celiotomy on rabbits) were first reported by Russian cosmonauts in 1967. The first survival procedure was performed on STS-90 Neurolab mission on rats in 1998 [243]. The world's first human operation on-board was a cyst removal from a patient's arm on board of the *European Space Agency's* (ESA) Airbus A-300 Zero-G aircraft. The plane performed 25 parabola curves, providing 20-25 s of weightlessness every time [244]. ESA planed to perform teleoperation in 2008 with a robot controlled through satellite connection, but the mission was postponed. NASA had its first zero gravity robotic surgery experiment in 2007 [245]. Suturing tasks were performed with the M7 (Fig. 1.9a) on a DC-9 hyperbolic aircraft. The performance of classical and teleoperated robotic knob tying was measured. Both the master and the slave devices were equipped with acceleration compensators to help task execution. The experiments showed that humans can better adapt to extreme environments; however, advanced robotic solutions performed comparably.

Appendix C

INTERNATIONAL ORGANIZATIONS AND LITERATURE OF CIS

C.1 International organizations and literature of CIS

Surgical robotics and CIS have accumulated vast literature in the past 25 years. The most prominent research articles are published in the *Institute of Electrical and Electronics Engineers* (IEEE) Transactions on Biomedical Engineering, Transactions on Robotics (former Transactions on Robotics and Automation), IEEE/ASME Transactions on Mechatronics, IEEE Robotics and Automation Magazine and in the various thematic journals, such as the Journal of Computer Aided Surgery (Taylor and Francis), International Journal of Medical Robotics and Computer Assisted Surgery (Wiley), International Journal of Computer Assisted Radiology and Surgery (Springer), Journal of Robotic Surgery (Springer), Surgical Endoscopy (Springer) and the Journal of Medical Devices (ASME). These publications are all available online.

The 24th Technical Committee of the IEEE Robotics and Automation Society (RAS) is entirely dedicated to surgical robotics, and many other organizations have CIS related bodies that typically organize annual conferences. The Minimally Invasive Robotic Association (MIRA), the Society for Medical Innovation and Technology (SMIT), the International Society and Conference Series on Medical Image Computing and Computer-Assisted Intervention (MICCAI) and the Computer Assisted Orthopaedic Surgery (CAOS) organize topical conferences every year. The Society of Photographic Instrumentation Engineers (SPIE) has numerous events, out of which the SPIE Medical Imaging conference is most attended by CIS professionals. In addition, the Medicine Meets Virtual Reality (MMVR) conference, the Congress of Computer Assisted Radiology and Surgery (CARS), the Annual International Conference of the IEEE Engineering in Medicine and Biology Society (EMBC), the IEEE International Conference on Robotics and Automation (ICRA), the IEEE/RSJ International Conference on Intelligent Robots and Systems (IROS), the new Conference on Information Processing in Computer-Assisted Interventions (IPCAI), Conference on Applied Bionics and Biomechanics (ICABB) and the biannual IEEE/ RAS–EMBS International Conference on Biomedical Robotics and Biomechanics (BioRob) all welcome original publications from the field.

Several portals and websites are dedicated to information sharing and knowledge dis-

tribution, providing free tutorials, video materials and presentations. Probably the most complete source of clinical information are WebSurg (www.websurg.com) virtual university run by the European Institute of TeleSurgery (EITS, Strasbourg, France), the da Vinci Surgery site (www.davincisurgery.com) and the OR Live (www.orlive.com). An aggregating site is the All About Robotic Surgery (www.allaboutroboticsurgery.com), the MedGadget internet journal (www.medgadget.com), the Hungarian MediQ (mediq.blog.hu) and some relevant blogs (e.g., surgrob.blogspot.com, managed by the author). For specific devices and systems, information brochures and teaching materials are available at the manufacturers' websites.

Appendix D

DETAILED LIST OF NEUROSURGICAL ROBOTS

Neurosurgery was the first field of application for robots in interventional medicine 25 years ago to support physicians in procedures where high precision is required. Since 1985, dozens of research projects have been focusing on brain and spine surgery, differently addressing the challenges of accuracy and effectiveness [32, 30, 46, 246, 247, 248, 249, 250, 251, 252]. Nearly all neurosurgical procedures require some amount of bone cutting—typically a craniotomy or craniectomy—that are all suitable for robotic treatment. While the automated handling of soft tissue is currently beyond our reach, needle based procedures (i.e., biopsy, Deep Brain Stimulation), High-Intensity Focused Ultrasound (HIFU) treatment, bone milling inside the skull, IG tumor or vascular lesion removal (including aneurysms, malformations of the veins and arteries and fistulas). The skull and the brain are the most complex and vulnerable anatomical areas, making it a unique challenge to navigate into while avoiding damage to the cranial nerves, brain tissue and fine blood vessels. Table D.I gives a extensive list of different projects and prototypes in the field.

TABLE D.1
NEUROSURGICAL ROBOTIC PROJECTS AND THEIR MAIN FEATURES. (CA: COMMERCIALY AVAILABLE)

Project [ref.]	Category	Institute/company	Main features
1 Alpha robot [248]	Active, teleoperated	MicroDexterity Systems Inc.; Albuquerque, NM, USA	5 DOF parallel manipulator mounted on the stereotactic frame, CA
2 Amadeus [253]	Active, teleoperated	Titan Medical Inc.; Toronto, Canada	6+ DOF da Vinci-like general purpose MIS robot
3 BWH MRI robot [254]	Active, automated	Brigham and Women's Hospital; Harvard Medical School; Boston, MA, USA	5 DOF MRI guided robot for percutaneous procedures, tool navigation and biopsy
4 CAS-BH5 robot system [255]	Active, teleoperated	Navy General Hospital of PLA; Beijing University; Beijing, China	Facilitates remote planning and transmission of neuro-navigation data, monitoring and manipulating
5 Cranio [256]	Active, automated	RWTH-Aachen / Lehrstuhl für Biomedizinische Technik; Aachen, Germany	Cranioectomy with 6 DOF hexapod robot
6 Craniofacial surgery robot [257]	Active, automated	University of Karlsruhe; Karlsruhe, Germany	Modified 6 DOF Stäubli RX-90 robot for craniofacial bone milling, under optical tracking for safety
7 CyberKnife [258]	Active, automated	Accuray Inc.; Sunnyvale, CA, USA	Image guided radiotherapy, tumor irradiation, CA
8 DAANS and LANS [259]	Active-passive, semi-automated	DIEGM / Università degli Studi di Udine; Italy	1 and 2 DOF actuator for biopsy and photon radiotherapy with the NeuroMate robot as a passive arm
9 da Vinci Surgical System [51]	Active, teleoperated	Intuitive Surgical Inc.; Sunnyvale CA, USA	4-armed multi-manipulator system approved for various procedures, CA
10 Evolution 1 [260]	Semi-active, automated	Universal Robot Systems; Schwerin, Germany	6 DOF hexapod robot for pedicle screw placement and adenoma dissection, CA—discontinued
11 Fraunhofer robot [261]	Active, automated	University of Saarland; Homburg, Germany	Force-controlled Stäubli RX-130 robot for automated temporal skull base drilling
12 Hannover robotic setup [119]	Active, automated	Hannover Medical School; Hannover, Germany	6 DOF KUKA KR3 robot with BrainLAB navigation for cochlea implant surgery
13 IGOR [262]	Passive/active/semi-active	TIMB (Trait. de l'Information et Modélisation en Bio-médecine); Grenoble, France	Prototype robot for general image guided neurosurgery (later became NeuroMate)
14 JHU project w/ NeuroMate [137]	Cooperative control	Johns Hopkins University; Baltimore, MD, USA	Skull base drilling with force control, using Virtual Fixtures
15 KineMedic [263]	Active, teleoperated	DLR / BrainLAB AG; Feldkirchen, Germany	Light-weight, high payload 7DOF robot for MIS neurosurgery, CA soon
16 MARS robot (SmartAssist) [116]	Active, automated	Mazor Surgical Technologies Inc.; Caesarea, Israel	FDA approved, light-weight, head mountable robot for needle insertion, CA soon
17 MITransspenoidal surgical robot [115]	Active, automated /teleoperated	University of Erlangen-Nuremberg; FAU Medical School; Erlangen, Germany	Fully automated sphenoidotomy, with a Mitsubishi RV-1a 6 DOF robot
18 Minerva [264]	Active, automated	Lab. of Microengineering; Swiss Federal Inst. of Technology; Lausanne, Switzerland	Real-time, frameless stereotactic instrument guidance in CT scanner—discontinued
19 MiroSurg [62]	Active, teleoperated	DLR; Oberpfaffenhofen-Wessling, Germany	Complete multi-manipulator system with force sensing for general endoscopic procedures
20 MIS stereotactic robot [265]	Passive, automated	Beijing University of Aeronautics and Astronautics; Beijing, China	PUMA260 robot based system with optical tracking for brain biopsy
21 MKM [266]	Active, automated	Carl Zeiss AG; Oberkochen, Germany	6 DOF manipulator for surgical microscope positioning, CA
22 MM-1 robot [267]	Active, teleoperated	University of Tokyo; Tokyo, Japan	Master-slave system with two 6 DOF arms and a HD stereo vision system for neuro-microsurgery
23 Modular parallel robot [268]	Active, automated	Yuan Ze University; Chung-Li, Taiwan	Light-weight, 6 DOF universal-prismatic-spherical parallel mechanism for skull drilling
24 Motorized HIFU system [269]	Active, automated	Imperial College of Science, Tech. and Medicine; London, UK	High Intensity Focused Ultrasound treatment for destruction of subcortical lesions
25 neuroArm [270]	Active, teleoperated	University of Calgary / IMRIS Inc.; Canada	MRI compatible complete multi-manipulator, in clinical trials
26 NeuRobot [271]	Active, automated	Nanyang Technological University; Singapore	Instrument guidance, skull-base surgery with a 5+6 DOF parallel robot with force sensor
27 NeuroBot [272]	Active, teleoperated	Shinshu University School of Medicine; Matsumoto, Japan	Teleoperated system with three arms and increased micromanipulation capabilities
28 Neurobot [273]	Cooperative control	Imperial College; London, UK	4 DOF serial robot with remote center of motion for general neurosurgery—discontinued
29 NEUROBUD [274]	Active-passive, semi-automated	DIEGM / Università degli Studi di Udine; Italy	1 DOF actuator for biopsy and photon radiotherapy with the NeuroMate robot as a passive arm
30 NeuroMaster [275]	Active, automated	Robotic Institute Beihang University; Beijing, China	6 DOF robot for stereotactic procedures
31 NeuroMate [54]	Passive, automated	IMMI / ISS / Schaefer Mayfield NeuroMate Sarl / Renishaw plc; Nyon, CH	5 DOF cannulae positioning for biopsy, neuroendoscopy, CA
32 NIRS [117]	Active, automated	Prosurge Ltd. (formerly Armstrong health care Ltd.); High Wycombe, UK	Automated pocket milling of the skull base
33 PathFinder [276]	Active, teleoperated	University of Washington; Seattle, WA, USA	6 DOF manipulator for instrument guidance, CA
34 Raven [58]	Active, teleoperated	NASA Jet Propulsion Laboratory; Pasadena, CA, USA	6 DOF robot for general surgery with automated suction
35 RAMS [56]	Active, teleoperated	Johns Hopkins University; Baltimore, MD, USA	7 DOF robot with advanced tremor filtering for MIS needle driving
36 Steady-Hand robot [128]	Cooperative control	Intelligent Surgical Instruments & Systems; Grenoble, France	Teleoperated smart tool for the resection of residual tumors
37 SingiScope [277]	Active, manual/automated	Nagoya University; Nagoya, Japan	Colling mounted robotized tool-holder device for surgical navigation, CA
38 Teleoperated catheter [278]	Active, teleoperated	Dalhousie University; Halifax, NS, Canada	Test bed for skull base drilling with Mitsubishi PA 10 6 DOF robot
39 Tele-robotic bone drill system [279]	Active, automated/teleoperated	IPA and University of Tübingen; Tübingen, Germany	An image-guided robot with multi-modal sensory feedback for skull base surgery
40 Tübingen robot [280]	Active, automated	Chonnam National University; NT Research Co.; Seoul, Korea	13 DOF master-slave system to execute surgery without tool change
41 Tubular micro brain surgery robot [281]	Active, teleoperated	Nagoya University; Nagoya, Japan	Test bed for skull base drilling with Mitsubishi PA-10, 6 DOF robot
42 Tumor resection robot [282]	Active, teleoperated	University of Tokyo; Tokyo, Japan	Two ultrasonic motors and 6 DOF sterilizable manipulator for needle insertion
43 U-Tokyo MRI robot [283]	Active, automated	University of Pennsylvania; Philadelphia, PA, USA	Transoral skull base surgery with the da Vinci robot; first human application
44 UPenn robotic setup [284]	Active, teleoperated		

Appendix E

NEW SURGICAL ROBOT CONCEPTS

Small scale, in-body robots offer great advantages, as they are always remote controlled, facilitating the spatial displacement of the physician from the patient. Researchers at the University of Nebraska (Lincoln, NE) developed a special mobile in-vivo wheeled robot for biopsy [285]. Equipped with a camera, the coin-sized robot can enter the abdominal cavity through one small incision and move around the organs teleoperated. The robot is able to traverse the abdomen without causing any tissue damage, therefore reducing patient trauma. More recently, the group has developed various swallowable robots, controlled with external magnets [286].

The CRIM group at Scuola Superiore Sant'Anna (Pisa, Italy) leads a European Union FP7 funded international research collaboration to develop tethered, partially autonomous robots to perform surgery in the endolumen (*ARAKNES project*) [287, 288]. Another EU project (*Vector*) aims for the creation of effective capsule robots for local surgical procedures all along the gastro-intestinal tract [289].

A remotely-controlled catheter guiding robot was used in Milan in 2006 to automatically perform cardiac ablation, initiated and supervised by a group of professionals from Boston, MA. The robot used high magnetic fields to insert the catheter to the desired location, taking advantage of the pre-operative CT scans of the patient and real-time EM navigation. Initial trials were performed on 40 patients before the telesurgical experiment took place. The novelty of the system was that it could create the surgical plan on its own relying on an anatomical atlas built on 10,000 patients' data [290].

NeuroArm [270] is a recent teleoperated anthropomorphic robot from a University of Calgary led consortium. The MR safe robot (compatible up to 1.5 Tesla magnetic field) is designed for stereotaxis and microsurgery. Beyond motion scaling and high definition visual feedback, the neuroArm is able to provide very accurate 3D information of its two 7 DOF arms. It uses three displays to give complete visual coverage of the operating environment, showing in parallel the 3D stereoscopic view of the operation, the MR image of the patient and the control panel. The system has been used on a few human patients so far, and after further clinical trials, it may hit the market within a few years. A major barrier however is the increased cost of the MR compatible components.

More recently, a Canadian company—Titan Medical Inc. (Toronto, Ontario Canada)—announced its new four-armed manipulator system, the *Amadeus* [253]. It promises better

view of the surgical field, and emphasis is put on the development of intelligent tools that facilitate surgery. The robot is being built in cooperation with Bell Canada's Health division to integrate Internet Protocol based advanced telesurgery capabilities for Amadeus. The clinical trials of the system should begin shortly.

Surgical microscopes have also profited from the development of technology for neurosurgical tools, with applications including a robotized microscope holder for frameless registration. The *Mehrkoordinaten Manipulator* (MKM) (Carl Zeiss AG, Oberkochen, Germany) [266] and the *SurgiScope* (Intelligent Surgical Instruments & Systems, Grenoble, France) [277] systems both use laser beams to determine the location of the focal point of the robotic microscopes. The pre-operative images of the brain are downloaded to the workstation, where the surgeon can determine the target point and the access route to the lesion. The microscopes are able to auto-focus on the chosen markers and assist throughout the procedure. It is also possible to superimpose additional information on the image, such as the contours of the lesion.

Appendix F

SUPPLEMENTARY DVD

A supplementary DVD-ROM is available with the thesis containing the source files, simulation results, videos, pictures and additional materials related to my work. To create the executable files and run the programs, MATLAB environment is required. For the neurosurgical robot application, the entire CISST Software framework must be installed. (It is open source and freely available at <https://trac.lcsr.jhu.edu/cisst>.) The webpage of the research is <http://www.iit.bme.hu/biomed/own/Kutatas/Haidegger.html>, where the supplementary materials are available and continuously updated.

The materials are arranged into the following folders:

- ..\ *Thesis_materials*
 - ..\ *1_Documentation*
 - ..\ *Figures*
 - ..\ *Publications*
 - ..\ *2_Source*
 - ..\ *Thesis_1*
 - ..\ *Thesis_2*
 - ..\ *Thesis_3*
 - ..\ *Neurosurgery_robot_control*
 - ..\ *3_Additional_materials*
 - ..\ *Pictures*
 - ..\ *References*
 - ..\ *Support*
 - ..\ *Adobe_Reader*
 - ..\ *FastStone_viewer*
 - ..\ *VLC_media_player*

The folder *Documentation* contains the thesis in .pdf format, my publications and the figures of the thesis. *Source* incorporate all the work files related to the theses. Under *Additional_materials* the electronically available references can be found and a selection of additional CIS pictures. *Support* contains the necessary programs to read the thesis and papers, to view the pictures and videos.

REFERENCES

- [1] R. H. Taylor, A. Menciassi, G. Fichtinger, and P. Dario, *Medical Robotics in Computer-Integrated Surgery*. Ch. 66 in B. Siciliano and O. Khatib, Eds., *Handbook of Robotics*, 2nd ed. Cambridge, MA, Springer, 2008, pp. 1199–1222.
- [2] D. M. Herron, M. Marohn, and the SAGES–MIRA Robotic Surgery Consensus Group, “A consensus document on robotic surgery,” *Surgical Endoscopy*, vol. 22, no. 2, pp. 313–325, 2007.
- [3] C. E. Scott-Conner, Ed., *The SAGES Manual: Fundamentals of Laparoscopy, Thoracoscopy, and GI Endoscopy*, 2nd ed. Iowa, Springer, 2006.
- [4] J. Sándor, B. Lengyel, T. Haidegger, G. Saftics, G. Papp, A. Nagy, and G. Wéber, “Minimally invasive surgical technologies: Challenges in education and training,” *Asian J. of Endoscopic Surgery*, vol. 3, no. 3, pp. 101–108, 2010.
- [5] K. H. Wong, “Imaging Modalities,” in *Lecture Notes in Computer Science (LNCS), Proc. of the 1st Intl. Conf. on Information Processing in Computer-Assisted Interventions (IPCAI)*, Geneva, 2010, pp. 241–273.
- [6] C. Picard, A. Olivier, and G. Bertrand, “The first human stereotaxic apparatus. The contribution of Aubrey Mussen to the field of stereotaxis.” *J. of Neurosurgery*, vol. 59, no. 4, pp. 673–676, 1983.
- [7] P. J. Kelly, “Stereotactic Surgery: What Is Past Is Prologue,” *Neurosurgery*, vol. 46, no. 1, pp. 16–27, 2000.
- [8] J. Maintz and M. Viergever, “A survey of medical image registration,” *Medical Image Analysis*, vol. 2, no. 1, pp. 1–37, 1998.
- [9] P. Grunert, K. Darabi, J. Espinosa, and R. Filippi, “Computer-aided navigation in neurosurgery,” *Neurosurgical Review*, vol. 26, no. 2, pp. 73–99, 2003.
- [10] P. Markelj, D. Tomaževič, B. Likar, and F. Pernuš, “A review of 3D/2D registration methods for image-guided interventions,” *Medical Image Analysis (in press)*, 2010.
- [11] C. Nafis, V. Jensen, and R. von Jako, “Method for evaluating compatibility of commercial electromagnetic (EM) microsensor tracking systems with surgical and imaging tables,” vol. 6918–20, San Diego, CA, 2008, pp. 1–15.
- [12] R. W. J. Pease, Ed., *Medical Dictionary*. USA, Merriam-Webster, 2003.
- [13] SAGES Group, “Guidelines for the surgical practice of telemedicine,” *Surgical Endoscopy*, vol. 14, no. 10, pp. 975–979, 2000.

- [14] B. Herman, "On the Role of Three Dimensional Visualization for Surgical Applications in Interactive Human Machine Systems," M.Sc. thesis in Computer Science, Johns Hopkins University, 2005.
- [15] R. Thirsk, D. Williams, and M. Anvari, "Neemo 7 undersea mission," *Acta Astronautica*, vol. 60, no. 4–7, pp. 512–517, 2007.
- [16] G. Hager, A. Okamura, P. Kazanzides, L. Whitcomb, G. Fichtinger, and R. Taylor, "Surgical and Interventional Robotics: part III," *IEEE Robotics and Automation Magazine (RAM)*, vol. 15, no. 4, pp. 84–93, 2008.
- [17] C. R. Doarn, A. E. Nicogossian, and R. C. Merrel, "Applications of Telemedicine in the United States Space Program," *Telemedicine Journal*, vol. 4, no. 1, pp. 19–30, 1998.
- [18] J. Rosser, M. Wood, J. Payne, T. Fullum, G. Lisehora, L. E. Rosser, P. J. Barcia, and R. S. Savalgi, "Telementoring: A practical option in surgical training," *Surgical Endoscopy*, vol. 11, no. 8, pp. 852–855, 1997.
- [19] Y. Kwoh, J. Hou, E. Jonckheere, and S. Hayati, "A Robot with Improved Absolute Positioning Accuracy for CT Guided Stereotactic Brain Surgery," *IEEE Trans. Biomedical Engineering*, vol. 35, no. 2, pp. 153–160, 1988.
- [20] J. Bowersox, A. Shah, J. Jensen, J. Hill, P. Cordts, and P. Green, "Vascular applications of telepresence surgery: initial feasibility studies in swine," *J. of Vascular Surgery*, vol. 23, no. 2, pp. 281–287, 1996.
- [21] A. Rovetta, R. Sala, F. Cosmi, X. Wen, S. Milanese, D. Sabbadini, A. Togno, L. Angelini, and A. K. Bejczy, "A New Telerobotic Application: Remote Laparoscopic Surgery Using Satellites and Optical Fiber Networks for Data Exchange," *Intl. J. of Robotics Research*, vol. 15, no. 3, pp. 267–279, 1996.
- [22] R. Satava, "Telesurgery, Virtual Reality and the New World Order of Medicine," *Computer Aided Surgery*, vol. 1, no. 1, pp. 12–16, 1995.
- [23] P. Garcia, J. Rosen, C. Kapoor, M. Noakes, G. Elbert, M. Treat, T. Ganous, M. Hanson, J. Manak, C. Hasser, D. Rohler, and R. Satava, "Trauma pod: a semi-automated telerobotic surgical system," *J. of Medicine*, vol. 5, no. 2, pp. 136–146, 2009.
- [24] A. Alexander, "Impacts of telementation on modern society," in *Proc. of the Annual Meeting of Human Factors and Ergonomics Society*, vol. 17, no. 2, Santa Monica, CA, 1973, pp. 299–304.
- [25] M. P. Ottensmeyer, J. Hu, J. M. Thompson, J. Ren, and T. B. Sheridan, "Investigations into Performance of Minimally Invasive Telesurgery with Feedback Time Delays," *Presence*, vol. 9, no. 4, pp. 369–382, 2000.
- [26] J. C. Rosser, S. M. Young, and J. Klonsky, "Telementoring: an application whose time has come," *Surgical Endoscopy*, vol. 21, no. 8, pp. 1458–1463, 2007.
- [27] T. Haidegger, J. Sándor, and Z. Benyó, "Surgery in space: the future of robotic telesurgery," *Surgical Endoscopy*, vol. 25, no. 3, pp. 681–690, 2011.
- [28] H. I. Christensen et al., "A Roadmap for US Robotics: From Internet to Robotics," pp. 1–94, 2009.

- [29] R. Taylor, "Robots as surgical assistants: Where we are, wither we are tending, and how to get there," *Lecture Notes in Artificial Intelligence in Medicine*, vol. 1211, no. 1, pp. 3–11, 1997.
- [30] C. S. Karas and E. A. Chiocca, "Neurosurgical robotics: a review of brain and spine applications," *J. of Robotic Surgery*, vol. 1, no. 1, pp. 39–43, 2007.
- [31] M. M. Lirici, V. Papaspyropoulos, and L. Angelini, "Telerobotics in medicine and surgery," *Minimally Invasive Therapy and Allied Technologies*, vol. 5, no. 6, pp. 364–378, 1997.
- [32] N. Nathoo, M. C. Cavusoglu, M. A. Vogelbaum, and G. H. Barnett, "In Touch with Robotics: Neurosurgery for the Future," *Neurosurgery*, vol. 56, no. 3, pp. 421–433, 2005.
- [33] M. D. O'Toole, K. Bouazza-Marouf, D. Kerr, M. Gooroochurn, and M. Vloeberghs, "A methodology for design and appraisal of surgical robotic systems," *Robotica*, vol. 28, no. 2, pp. 297–310, 2010.
- [34] P. Gomes, "Surgical robotics: Reviewing the past, analysing the present, imagining the future," *Robotics and Computer-Integrated Manufacturing*, vol. 27, no. 2, pp. 261–266.
- [35] P. Kazanzides, B. Mittelstadt, J. Zuhars, P. Cain, and H. Paul, "Surgical and Industrial Robots: Comparison and Case Study," in *Proc. of the Intl. Robots and Vision Automation Conf.*, Detroit, IL, 1993, pp. 10–19.
- [36] P. Stolka and D. Henrich, "Improving Navigation Precision of Milling Operations in Surgical Robotics," in *Proc. of the IEEE/RSJ Intl. Conf. on Intelligent Robots and Systems (IROS)*, Beijing, 2006, pp. 2351–2357.
- [37] Mass Device, "Intuitive Surgical off the hook in erectile dysfunction lawsuit," online edition, <http://www.massdevice.com/news/intuitive-surgical-hook-erectile-dysfunction-lawsuit>, 2010.
- [38] M. Anvari, "Robot-Assisted Remote Telepresence Surgery," *Surgical Innovation*, vol. 11, no. 2, pp. 123–128, 2004.
- [39] R. Rayman, S. Primak, R. Patel, M. Moallem, R. Morady, M. Tavakoli, V. Subotic, N. Galbraith, A. van Wynsberghe, and K. Croome, "Effects of latency on telesurgery: an experimental study," in *Lecture Notes in Computer Science (LNCS), Proc. of the Annual Conf. of the Medical Image Computing and Computer Assisted Intervention Society (MICCAI)*, vol. 3750. Palm Springs, CA, Springer, 2005, pp. 57–64.
- [40] H. King, B. Hannaford, K. Kwok, G. Yang, P. Griffiths, A. Okamura, I. Farkhatdinov, J. Ryu, G. Sankaranarayanan, V. Arikatla, K. Tadano, K. Kawashima, A. Peer, T. Schau, M. Buss, L. Miller, D. Glozman, J. Rosen, and T. Low, "Plugfest 2009: Global Interoperability in Telerobotics and Telemedicine," in *Proc. of the IEEE Intl. Conf. on Robotics and Automation (ICRA)*, Anchorage, AK, 2010, pp. 1733–1738.
- [41] "Medical Robotic Database: MeRoDa," University of Heidelberg, <http://meroda.uni-hd.de/>, 2010.

- [42] R. H. Taylor, S. Lavallée, G. C. Burdea, and R. Mösges, Eds., *Computer-Integrated Surgery*. Cambridge, MA, MIT Press, 1995.
- [43] P. Dario, B. Hannaford, and A. Menciassi, “Smart Surgical Tools and Augmenting Devices,” *IEEE Trans. on Robotics and Automation*, vol. 19, no. 5, pp. 782–792, 2003.
- [44] G. H. Ballantyne, J. Marescaux, and P. C. Giulianotti, Eds., *The Primer of Robotic and Telerobotic Surgery*. Philadelphia, PA, Lippincott Williams & Wilkins, 2004.
- [45] P. Pott, H.-P. Scharf, and M. Schwarz, “Today’s state of the art in surgical robotics,” *Computer Aided Surgery*, vol. 10, no. 2, pp. 101–132, 2005.
- [46] V. Bozovic, Ed., *Medical Robotics*. Vienna, IN-TECH, 2007.
- [47] R. A. Faust, Ed., *Robotics in Surgery: History, Current and Future Applications*. Hauppauge, NY, Nova Science, 2007.
- [48] S. H. Baik, Ed., *Robot Surgery*. Vienna, IN-TECH, 2010.
- [49] R. H. Taylor and D. Stoianovici, “Medical Robotics in Computer-Integrated Surgery,” *IEEE Trans. on Robotics and Automation*, vol. 19, no. 5, pp. 765–781, 2003.
- [50] P. Kazanzides, G. Fichtinger, G. D. Hager, A. M. Okamura, L. L. Whitcomb, and R. H. Taylor, “Surgical and Interventional Robotics: part I,” *IEEE Robotics and Automation Magazine (RAM)*, vol. 15, no. 2, pp. 122–130, 2008.
- [51] G. S. Guthart and J. K. Salisbury, “The Intuitive Telesurgery System: Overview and Application,” in *Proc. of the IEEE Intl. Conf. on Robotics and Automation (ICRA)*, San Francisco, CA, 2000, pp. 618–621.
- [52] T. Haidegger, “The advancement of robotic surgery—successes, failures, challenges,” *Orvosi Hetilap (in Hungarian)*, vol. 151, no. 41, pp. 1688–1694, 2010.
- [53] A. Benabid, P. Cinquin, S. Lavalle, J. Le Bas, J. Demongeot, and J. De Rougemont, “Computer-driven robot for stereotactic surgery connected to CT scan and magnetic resonance imaging. Technological design and preliminary results,” *Applied Neurophysiology*, vol. 50, no. 1–6, pp. 153–154, 1987.
- [54] Q. H. Li, L. Zamorano, A. Pandya, R. Perez, J. Gong, and F. Diaz, “The application accuracy of the NeuroMate robot—A quantitative comparison with frameless and frame-based surgical localization systems.” *Computer Aided Surgery*, vol. 7, no. 2, pp. 90–98, 2002.
- [55] T. Varma and P. Eldridge, “Use of the NeuroMate stereotactic robot in a frameless mode for functional neurosurgery,” *Intl. J. of Medical Robotics and Computer Assisted Surgery*, vol. 2, no. 2, pp. 107–113, 2006.
- [56] H. Das, T. I. M. Ohm, C. Boswell, R. O. B. Steele, and G. Rodriguez, “Robot-Assisted Microsurgery Development at JPL,” *Rehabilitation*, vol. 2, no. 1, pp. 85–99, 2001.
- [57] J. Rosen and B. Hannaford, “Doc at a distance,” *IEEE Spectrum*, vol. 43, no. 10, pp. 34–39, 2006.

- [58] M. J. H. Lum, D. C. W. Friedman, G. Sankaranarayanan, H. King, K. Fodero, R. Leuschke, B. Hannaford, J. Rosen, and M. N. Sinanan, "The RAVEN: Design and Validation of a Telesurgery System," *Intl. J. of Robotics Research*, vol. 28, no. 9, pp. 1183–1197, 2009.
- [59] H. King, T. Low, K. Hufford, and T. Broderick, "Acceleration compensation for vehicle based telesurgery on earth or in space," in *Proc. of the IEEE/RSJ Intl. Conf. on Intelligent Robots and Systems (IROS)*, Nice, 2008, pp. 1459–1464.
- [60] D. Reintsema, C. Preusche, T. Ortmaier, and G. Hirzinger, "Toward High-Fidelity Telepresence in Space and Surgery Robotics," *Presence*, vol. 13, no. 1, pp. 77–98, 2004.
- [61] U. Hagn, M. Nickl, S. Jörg, G. Passig, T. Bahls, A. Nothhelfer, F. Hacker, L. Le-Tien, A. Albu-Schäffer, R. Konietschke, M. Grebenstein, R. Warpup, R. Haslinger, M. Frommberger, and G. Hirzinger, "The DLR MIRO: a versatile lightweight robot for surgical applications," *Industrial Robot: an Intl. Journal*, vol. 35, no. 4, pp. 324–336, 2008.
- [62] U. Hagn, R. Tobergte, A. Konietschke, M. Jörg, S. Nickl, G. Gröger, M. Passig, F. Seibold, F. U. A. Hacker, F. Nothhelfer, M. Grebenstein, and G. Hirzinger, "DLR MiroSurge: a versatile system for research in endoscopic telesurgery," *Intl. J. of Computer Assisted Radiology and Surgery*, vol. 5, no. 2, pp. 183–193, 2010.
- [63] S. Butner and M. Ghodoussi, "Transforming a surgical robot for human telesurgery," *IEEE Trans. on Robotics and Automation*, vol. 19, no. 5, pp. 818–824, 2003.
- [64] R. S. Kumar and J. Marescaux, Eds., *Telesurgery*. Berlin, Springer, 2008.
- [65] J. Marescaux and F. Rubino, "Transcontinental Robot-Assisted Remote Telesurgery, Feasibility and Potential Applications," *Teleophthalmology*, vol. 235, pp. 261–265, 2002.
- [66] M. Fabrizio, B. Lee, D. Stoianovici, T. Jarett, C. Yang, and L. Kavoussi, "Effect of time delay on surgical performance during telesurgical manipulation," *J. of Endourology*, vol. 14, no. 2, pp. 133–138, 2000.
- [67] M. Anvari, T. Broderick, H. Stein, T. Chapman, M. Ghodoussi, D. W. Birch, C. McKinley, P. Trudeau, S. Dutta, and C. H. Goldsmith, "The impact of latency on surgical precision and task completion during robotic-assisted remote telepresence surgery," *Computer Aided Surgery*, vol. 10, no. 2, pp. 93–99, 2005.
- [68] M. Perez, F. Quiaios, P. Andrivon, D. Husson, M. Dufaut, and J. Felblinger, "Paradigms and experimental set-up for the determination of the acceptable delay in telesurgery," in *Proc. of the Annual Intl. Conf. of the IEEE Engineering in Medicine and Biology Society (EMBC)*, Lyon, 2007, pp. 453–456.
- [69] E. Flynn, "Telesurgery in the United States," *Homeland Defense Journal*, pp. 24–28, June 2005.

- [70] J. R. Sterbis, E. J. Hanly, B. C. Herman, M. R. Marohn, T. J. Broderick, S. P. Shih, B. Harnett, C. Doarn, and N. S. Schenkman, "Transcontinental telesurgical nephrectomy using the da Vinci robot in a porcine model." *Urology*, vol. 71, no. 5, pp. 971–973, 2008.
- [71] C. Nguan, B. Miller, R. Patel, P. P. Luke, and C. M. Schlachta, "Pre-clinical remote telesurgery trial of a da Vinci telesurgery prototype," *Intl. J. of Medical Robotics Computer Assisted Surgery*, vol. 4, no. 4, pp. 304–309, 2008.
- [72] M. Lum, D. C. Friedman, G. Sankaranarayanan, H. King, A. Wright, M. Sinanan, T. Lendvay, J. Rosen, and B. Hannaford, "Objective assessment of telesurgical robot systems: Telerobotic FLS," in *Proc. of the Medicine Meets Virtual Reality (MMVR15)*, Long Beach, CA, 2008, pp. 263–265.
- [73] C. R. Doarn, M. Anvari, T. Low, and T. J. Broderick, "Evaluation of teleoperated surgical robots in an enclosed undersea environment." *Telemedicine Journal: the official journal of the American Telemedicine Association*, vol. 15, no. 4, pp. 325–335, 2009.
- [74] J. Peters, G. Fried, L. Swanstrom, N. Soper, and L. Sillin, "Development and validation of a comprehensive program of education and assessment of the basic fundamentals of laparoscopic surgery," *Surgery*, vol. 135, no. 1, pp. 21–27, 2004.
- [75] B. Lantos, *Theory and design of control systems I-II. (in Hungarian)* Budapest, Akademia Press, 2001.
- [76] D. A. Simon, M. Blackwell, F. Morgan, A. M. Digioia, and T. Kanade, "Accuracy Validation in Image-Guided Orthopaedic Surgery." Wiley, 1995, pp. 185–192.
- [77] T. Haidegger, P. Kazanzides, I. Rudas, B. Benyó, and Z. Benyó, "The Importance of Accuracy Measurement Standards for Computer-Integrated Interventional Systems," in *Proc. of the EURON GEM Sig Workshop on The Role of Experiments in Robotics Research at IEEE ICRA*, Anchorage, AK, 2010, pp. 19–24.
- [78] S. Y. Nof, Ed., *Handbook of Industrial Robotics*, 2nd ed. Wiley, 1999.
- [79] J. B. Stiehl, J. Bach, and D. A. Heck, *Validation and Metrology in CAOS*. Ch. 9 in J. B. Stiehl, W. H. Konermann, R. G. Haaker, Eds., *Navigation and MIS in Orthopedic Surgery, Germany*, Springer, 2007, pp. 68–78.
- [80] NDI Inc., "Accuracy Assessment Kit for the Polaris family of products," *brochure*, pp. 1–2, 2006.
- [81] D. D. Frantz, S. R. Kirsch, and A. D. Wiles, "Specifying 3D Tracking System Accuracy," technical Report, NDI Inc., pp. 1–5, 2004.
- [82] G. Kronreif, "Medical Robotics—General Aspects and Applications," in *Proc. of the 12th Summer School in Image Processing (SSIP2004)*, Graz, 2004.
- [83] D. Y. Hsu, *Spatial Error Analysis*. New York, NY, Wiley–IEEE, 1998.
- [84] C. R. Maurer, J. M. Fitzpatrick, M. Y. Wang, R. L. Galloway, R. J. Maciunas, and G. S. Allen, "Registration of head volume images using implantable fiducial markers," *IEEE Trans. on Medical Imaging*, vol. 16, no. 4, pp. 447–462, 1997.

- [85] J. M. Fitzpatrick, J. B. West, and C. R. Maurer, "Predicting Error in Rigid-Body Point-Based Registration," *IEEE Trans. on Medical Imaging*, vol. 17, no. 5, pp. 694–702, 1998.
- [86] J. M. Fitzpatrick, "Fiducial registration error and target registration error are uncorrelated," in *Proc. of SPIE Medical Imaging*, vol. 7261, Orlando, FL, 2009, pp. 1–12.
- [87] A. Danilchenko and J. M. Fitzpatrick, "General approach to error prediction in point registration," in *Proc. of SPIE Medical Imaging*, vol. 7625–0F, San Diego, CA, 2010, pp. 1–14.
- [88] M. Hofer, G. Straus, K. Koulechov, and A. Dietz, "Definition of accuracy and precision—evaluating CAS-systems," in *Intl. Congress Series, Proc. of the 19th Intl. Congress and Exhibition on Computer Assisted Radiology and Surgery (CARS)*, vol. 1281, Berlin, 2005, pp. 548–552.
- [89] T. Sielhorst, M. Bauer, O. Wensch, G. Klinker, and N. Navab, "Online Estimation of the Target Registration Error for n-Ocular Optical Tracking Systems," in *Lecture Notes in Computer Science (LNCS), Proc. of the Annual Conf. of the Medical Image Computing and Computer Assisted Intervention Society (MICCAI)*, vol. 4792, Brisbane, 2007, pp. 652–659.
- [90] G. Widmann, R. Stoffner, M. Sieb, and R. Bale, "Target registration and target positioning errors in computer-assisted neurosurgery," *Intl. J. of Medical Robotics and Computer Assisted Surgery*, vol. 5, no. 4, pp. 355–365, 2009.
- [91] J. M. Fitzpatrick, "The role of registration in accurate surgical guidance," *Proc. of the Institution of Mechanical Engineers, Part H: J. of Engineering in Medicine*, vol. 224, no. 5, pp. 607–622, 2010.
- [92] J. M. Phillips, "Survey of Absolute Orientation Techniques," pp. 7–8, 2004.
- [93] R. Balachandran and J. M. Fitzpatrick, "Iterative solution for rigid-body point-based registration with anisotropic weighting," in *Proc. of SPIE Medical Imaging*, vol. 7261–3D, Orlando, FL, 2009, pp. 1–10.
- [94] M. H. Moghari, B. Ma, and P. Abolmaesumi, "A theoretical comparison of different target registration error estimators," in *Lecture Notes in Computer Science (LNCS), Proc. of the Annual Conf. of the Medical Image Computing and Computer Assisted Intervention Society (MICCAI)*, vol. 5424, New York, NY, 2008, pp. 1032–1040.
- [95] A. D. Wiles and T. M. Peters, "Real-time estimation of FLE statistics for 3-D tracking with point-based registration," *IEEE Trans. on Medical Imaging*, vol. 28, no. 9, pp. 1384–1398, 2009.
- [96] A. Barrera, J. Bach, P. Kazanzides, and H. Haider, "Validation of an ASTM standard proposed to assess localizer functionality of CAOS systems: a joint effort by three laboratories," in *Proc. of the 20th Annual Congress of Intl. Society for Technology in Arthroplasty (ISTA)*, Paris, 2007, pp. 81–81.

- [97] N. Dagalakis, Y. Kim, D. Sawyer, and C. Shakarji, "Development of tools for measuring the performance of computer assisted orthopaedic hip surgery systems," in *Proc. of the ACM Workshop on Performance Metrics for Intelligent Systems (PerMIS)*, Gaithersburg, 2007, pp. 180–187.
- [98] P. Kazanzides, "Surgical Robots and Phantom (Artifact) Devices," in *Proc. of the ASTM Workshop on Medical Devices Metrology and Standards Needs*. ASTM, NIST, NCI, FDA and U.T. Arlington, Atlanta, 2006.
- [99] J. Chiao, J. Goldman, D. Heck, P. Kazanzides, W. Peine, J. Stiehl, D. Yen, and N. Dagalakis, "Metrology and Standards Needs for Some Categories of Medical Devices," *J. of Research of the NIST*, vol. 113, no. 2, pp. 121–129, 2008.
- [100] H. Paul, B. Mittlestadt, W. Bargar, B. Musits, R. H. Taylor, P. Kazanzides, J. Zuhars, B. Williamson, and W. Hanson, "A surgical robot for total hip replacement surgery," in *Proc. of the IEEE Intl. Conf. on Robotics and Automation (ICRA)*, Nice, 1992, pp. 606–611.
- [101] R. H. Taylor, "Robotic Joint Replacement Surgery," Course materials, the Johns Hopkins University, Baltimore, pp. 1–37, 2001.
- [102] S. Nishihara, N. Sugano, T. Nishii, H. Miki, N. Nakamura, and H. Yoshikawa, "Comparison between hand rasping and robotic milling for stem implantation in cementless total hip arthroplasty." *J. of Arthroplasty*, vol. 21, no. 7, pp. 957–966, 2006.
- [103] T. Haidegger, T. Xia, and P. Kazanzides, "Accuracy improvement of a neurosurgical robot system," in *Proc. of the 2nd IEEE RAS/EMBS Intl. Conf. on Biomedical Robotics and Biomechatronics (BioRob)*, Scottsdale, AZ, 2008, pp. 836–841.
- [104] D. M. Kwartowitz, S. D. Herrell, and R. L. Galloway, "Toward image-guided robotic surgery: determining intrinsic accuracy of the da Vinci robot," *Intl. J. of Computer Assisted Radiology and Surgery*, vol. 1, no. 3, pp. 157–165, 2006.
- [105] —, "Update: Toward image-guided robotic surgery: determining the intrinsic accuracy of the daVinci-S robot," *Intl. J. of Computer Assisted Radiology and Surgery*, vol. 1, no. 5, pp. 301–304, 2007.
- [106] S. Dieterich, J. Tang, J. Rodgers, and K. Cleary, "Skin respiratory motion tracking for stereotactic radiosurgery using the CyberKnife," in *Intl. Congress Series, Proc. of the 17th Intl. Congress and Exhibition on Computer Assisted Radiology and Surgery (CARS)*, vol. 1256. London, Elsevier, 2003, pp. 130–136.
- [107] J. Jang, Y. Kang, B. Choi, I. Choi, M. Kim, D. Shin, D. Shin, K. Cho, C. Min, and S. Kwon, "Evaluation of the Accuracy of the CyberKnife," in *Proc. of the World Congress on Medical Physics and Biomedical Engineering*. Seoul, Springer, 2006, pp. 2024–2027.
- [108] K. Cleary, A. Melzer, V. Watson, G. Kronreif, and D. Stoianovici, "Interventional robotic systems: Applications and technology state-of-the-art," *Minimally Invasive Therapy*, vol. 15, no. 2, pp. 101–113, 2008.

- [109] I. H. Lieberman, D. Togawa, M. M. Kayanja, M. K. Reinhardt, A. Friedlander, N. Knoller, and E. C. Benzel, "Bone-mounted miniature robotic guidance for pedicle screw and translaminar facet screw placement: Part I—Technical development and a test case result," *Neurosurgery*, vol. 59, no. 3, pp. 641–650, 2006.
- [110] M. Matinfar, C. Baird, A. Batouli, R. Clatterbuck, and P. Kazanzides, "Robot-assisted skull base surgery," in *Proc. of the IEEE/RSJ Intl. Conf. on Intelligent Robots and Systems (IROS)*, San Diego, CA, 2007, pp. 865–870.
- [111] M. Li and R. H. Taylor, "Spatial Motion Constraints in Medical Robot Using Virtual Fixtures Generated by Anatomy," in *Proc. of the IEEE Intl. Conf. on Robotics and Automation (ICRA)*, New Orleans, LA, 2004, pp. 1270–1275.
- [112] M. Jakopec, F. R. Y. Baena, S. J. Harris, P. Gomes, J. Cobb, and B. L. Davies, "The hands-on orthopaedic robot "Acrobot": Early clinical trials of total knee replacement surgery," *IEEE Trans. on Robotics and Automation*, vol. 19, no. 5, pp. 902–911, 2003.
- [113] B. Plinkert and P. Plinkert, in *Intl. Congress Series, Proc. of the 15th Intl. Congress and Exhibition on Computer Assisted Radiology and Surgery (CARS)*. Berlin, Elsevier, pp. 138–142.
- [114] M. Engelhardt, P. Bast, W. Lauer, V. Rohde, K. Schmieder, and K. Radermacher, "Manual vs. robotic milling parameters for development of a new robotic system in cranial surgery," *Intl. Congress Series, Proc. of the 18th Intl. Congress and Exhibition on Computer Assisted Radiology and Surgery (CARS)*, vol. 1268, pp. 533–538, 2004.
- [115] K. Bumm, J. Wurm, J. Rachinger, T. Dannenmann, C. Bohr, R. Fahlbusch, H. Iro, and C. Nimsky, "An automated robotic approach with redundant navigation for minimal invasive extended transsphenoidal skull base surgery," *Minimally Invasive Neurosurgery*, vol. 48, no. 3, pp. 159–164, 2005.
- [116] R. Shamir, M. Freiman, L. Joskowicz, M. Shoham, E. Zehavi, and Y. Shoshan, "Robot-assisted image-guided targeting for minimally invasive neurosurgery: planning, registration, and in-vitro experiment," in *Lecture Notes in Computer Science (LNCS), Proc. of the Annual Conf. of the Medical Image Computing and Computer Assisted Intervention Society (MICCAI)*. Palm Springs, CA, Springer, 2005, pp. 131–138.
- [117] F. Chan, I. Kassim, C. Lo, C. L. Ho, D. Low, B. T. Ang, and I. Ng, "Image-guided robotic neurosurgery—an in vitro and in vivo point accuracy evaluation experimental study," *Surgical Neurology*, vol. 71, no. 6, pp. 640–648, 2009.
- [118] T. Klenzner, C. C. Ngan, F. B. Knapp, H. Knoop, J. Kromeier, A. Aschendorff, E. Papastathopoulos, J. Raczowsky, H. Wrn, and J. Schipper, "New strategies for high precision surgery of the temporal bone using a robotic approach for cochlear implantation," *European Archives of Oto-Rhino-Laryngology*, vol. 266, pp. 955–960, 2009.

- [119] O. Majdani, T. S. Rau, S. Baron, H. Eilers, C. Baier, B. Heimann, T. Ortmaier, S. Bartling, T. Lenarz, and M. Leinung, "A robot-guided minimally invasive approach for cochlear implant surgery: preliminary results of a temporal bone study." *Intl. J. of Computer Assisted Radiology and Surgery*, vol. 4, no. 5, pp. 475–86, 2009.
- [120] S. Baron, H. Eilers, B. Munske, J. L. Toennies, R. Balachandran, R. F. Labadie, T. Ortmaier, and R. J. Webster, "Percutaneous inner-ear access via an image-guided industrial robot system," in *Proc. of the Institution of Mechanical Engineers, Part H: J. of Engineering in Medicine*, vol. 224, no. 5, 2010, pp. 633–649.
- [121] Medtronic Inc., "StealthLink Manual, draft," pp. 1–18, 2005.
- [122] S. Pieper, M. Halle, and R. Kikinis, "3D Slicer," in *IEEE Intl. Symp. on Biomedical Imaging*, Arlington, VA, 2004, pp. 632–635.
- [123] L. Dozio and P. Mantegazza, "Real-time distributed control systems using RTAI," in *Proc. of the 6th IEEE Intl. Symp. on Object-Oriented Real-Time Distributed Computing*, Hakodate, 2003, pp. 11–18.
- [124] A. Kapoor, A. Deguet, and P. Kazanzides, "Software components and frameworks for medical robot control," in *Proc. of the IEEE Conf. Robotics and Automation (ICRA)*, Orlando, FL, 2006, pp. 3813–3818.
- [125] T. Xia, T. Haidegger, K. Hayes, N. Hata, and P. Kazanzides, "Integration of Open Source and Commercial Software for a Neurosurgical Robot System," *Workshop on Systems & Architecture for Computer Assisted Intervention at MICCAI*, 2008.
- [126] T. Xia, C. Baird, G. Jallo, K. Hayes, N. Nakajima, N. Hata, and P. Kazanzides, "An integrated system for planning, navigation and robotic assistance for skull base surgery," *Intl. J. of Medical Robotics and Computer Assisted Surgery*, vol. 4, no. 4, pp. 321–330, 2008.
- [127] L. Rosenberg, "Virtual fixtures: Perceptual tools for telerobotic manipulation," in *Proc. of the Annual IEEE Intl. Symp. on Virtual Reality*, Seattle, WA, 1993, pp. 76–82.
- [128] R. H. Taylor, P. Jensen, L. Whitcomb, A. Barnes, and R. Kumar, "A steady-hand robotic system for microsurgical augmentation," *Medical Image Computing*, vol. 18, no. 12, pp. 1201–1210, 1999.
- [129] M. Li, A. Kapoor, and R. H. Taylor, "Telerobotic Control by Virtual Fixtures for Surgical Applications," *Springer Tracts in Advanced Robotics*, vol. 31, pp. 381–401, 2007.
- [130] P. Kazanzides, "Virtual Fixture applications for skull base drilling (*unpublished notes*), the Johns Hopkins University," Baltimore, 2008.
- [131] G. Welch and G. Bishop, "An introduction to the Kalman filter," *technical notes*, University of North Carolina, Chapel Hill, NC, 1995, pp. 1–16.
- [132] M. H. Moghari and P. Abolmaesumi, "Point-based rigid-body registration using an unscented Kalman filter," *IEEE Trans. on Medical Imaging*, vol. 26, no. 12, pp. 1708–1728, 2007.

- [133] T. Haidegger, "Improving the Accuracy and Safety of a Robotic System for Neurosurgery," M.Sc. thesis in Biomedical Engineering, Budapest University of Technology and Economics, 2008.
- [134] A. Tobergte, M. Pomarlan, and G. Hirzinger, "Robust multi sensor pose estimation for medical applications," in *Proc. of the IEEE/RSJ Intl. Conf. on Intelligent Robots and Systems (IROS)*, 2009, pp. 492–497.
- [135] A. Tobergte, F. A. Fröhlich, M. Pomarlan, and G. Hirzinger, "Towards Accurate Motion Compensation in Surgical Robotics," in *Proc. of the IEEE Intl. Conf. on Robotics and Automation (ICRA)*, Anchorage, AK, 2010, pp. 4566–4572.
- [136] M. Kaus, R. Steinmeier, T. Sporer, and O. Ganslandt, "Technical accuracy of a neuronavigation system measured with a high-precision Mechanical Micromanipulator," *Neurosurgery*, vol. 41, no. 6, pp. 1431–1437, 1997.
- [137] P. Kazanzides, T. Xia, C. Baird, G. Jallo, K. Hayes, N. Nakajima, and N. Hata, "A Cooperatively-Controlled Image Guided Robot System for Skull Base Surgery," *Studies in Health Technology and Informatics*, vol. 132, no. 1, pp. 198–203, 2008.
- [138] M. T. Stechison, "A Digitized Biopsy Needle for Frameless Stereotactic Biopsies with the StealthStation," *Neurosurgery*, vol. 46, no. 1, pp. 239–242, 2000.
- [139] B. Widrow and I. Kollár, *Quantization Noise: Roundoff Error in Digital Computation, Signal Processing, Control, and Communications*. Cambridge, UK, Cambridge University Press, 2008.
- [140] T. Haidegger and Z. Benyó, "Surgical robotics in neurosurgery," *Orvosi Hetilap (in Hungarian)*, vol. 150, no. 39, pp. 1701–1711, 2009.
- [141] S. Misra, K. T. Ramesh, and A. M. Okamura, "Modeling of Tool-Tissue Interactions for Computer-Based Surgical Simulation: A Literature Review," *Presence (Cambridge)*, vol. 17, no. 5, pp. 463–491, 2008.
- [142] R. Ginhoux, J. Gangloff, M. D. Mathelin, L. Soler, M. M. A. Sanchez, and J. Marescaux, "Active Filtering of Physiological Motion in Robotized Surgery Using Predictive Control," *IEEE Trans. on Robotics*, vol. 21, no. 1, pp. 67–79, 2005.
- [143] P. Jannin and X. Morandi, "Surgical models for computer-assisted neurosurgery." *NeuroImage*, vol. 37, no. 3, pp. 783–791, 2007.
- [144] U. Lahiri, R. F. Labadie, C. Liu, R. Balachandran, O. Majdani, and N. Sarkar, "A step toward identification of surgical actions in mastoidectomy." *IEEE Trans. on Biomedical Engineering*, vol. 57, no. 2, pp. 479–487, 2010.
- [145] M. Hayashibe, N. Suzuki, M. Hashizume, Y. Kakeji, K. Konishi, S. Suzuki, and A. Hattori, "Preoperative planning system for surgical robotics setup with kinematics and haptics," *Intl. J. of Medical Robotics and Computer Assisted Surgery*, vol. 1, no. 2, pp. 76–85, 2005.
- [146] M. Hayashibe, N. Suzuki, M. Hashizume, K. Konishi, and A. Hattori, "Robotic surgery setup simulation with the integration of inverse-kinematics computation and medical imaging." *Computer methods and programs in biomedicine*, vol. 83, no. 1, pp. 63–72, 2006.

- [147] C. Plaskos, P. Cinquin, S. Lavallée, and A. J. Hodgson, “Praxiteles: a miniature bone-mounted robot for minimal access total knee arthroplasty,” *Intl. J. of Medical Robotics and Computer Assisted Surgery*, vol. 1, no. 4, pp. 67–79, 2005.
- [148] A. Wolf, B. Jaramaz, B. Lisien, and A. M. DiGioia, “MBARS: mini bone-attached robotic system for joint arthroplasty,” *Intl. J. of Medical Robotics and Computer Assisted Surgery*, vol. 1, no. 2, pp. 101–121, 2005.
- [149] P. Kazanzides, “Robot assisted surgery: the ROBODOC experience,” in *Proc. of the 30th Intl. Symp. on Robotics (ISR)*, Tokyo, 1999, pp. 281–286.
- [150] K. Saito, M. Fujii, K. Kajiwara, and M. Suzuki, “Introducing sitetrack: continuous patient motion monitoring during stereotactic radiotherapy for the head,” *Neurosurgery*, vol. 64, no. 2S, pp. 110–122, 2009.
- [151] G. Boschettim, G. Rosati, and A. Rossi, “A Haptic System for Robotic Assisted Spine Surgery,” in *Proc. of the IEEE Conf. on Control Applications*, Toronto, 2005, pp. 19–24.
- [152] H. Kenngott, J. Neuhaus, B. P. Muller-Stich, I. Wolf, M. Vetter, H.-P. Meinzer, J. Koninger, M. W. Buchler, and C. N. Gutt, “Development of a navigation system for minimally invasive esophagectomy,” *Surgical Endoscopy*, vol. 22, no. 8, pp. 1858–1865, 2008.
- [153] R. Fulton, S. Meikle, S. Eberl, J. Pfeiffer, C. Constable, and M. Fulham, “Correction for head movements in positron emission tomography using an optical motion-tracking system,” *IEEE Trans. on Nuclear Science*, vol. 49, no. 4, pp. 116–123, 2002.
- [154] P. Bruyant, M. Gennert, G. Speckert, R. Beach, J. Morgenstern, N. Kumar, S. Nadella, and M. King, “A robust visual tracking system for patient motion detection in SPECT: Hardware solutions,” *IEEE Trans. on Nuclear Science*, vol. 52, no. 5I, pp. 1288–1294, 2005.
- [155] A. Rahmim, O. Rousset, and H. Zaidi, “Strategies for motion tracking and correction in PET,” *PET Clinics*, vol. 2, no. 2, pp. 251–266, 2007.
- [156] T. Haidegger, Z. Benyó, and P. Kazanzides, “Patient motion tracking in the presence of measurement errors,” in *Proc. of the Annual Intl. Conf. of the IEEE Engineering in Medicine and Biology Society (EMBC)*, Minneapolis, MN, 2009, pp. 5563–5567.
- [157] T. Haidegger, P. Kazanzides, B. Benyó, L. Kovács, and Z. Benyó, “Surgical case identification for an image-guided interventional system,” in *Proc. of the IEEE/RSJ Intl. Conf. on Intelligent Robots and Systems (IROS)*, Taipei, 2010.
- [158] T. Haidegger, P. Kazanzides, J. Sándor, and Z. Benyó, “Technological challenges of image-guided robotic surgery—abrupt changes in the operating room,” in *Proc. of the 4th Scientific Meeting of the Japan-Hungary Surgical Society (JHSS)*, Yokohama.
- [159] S. Umeyama, “Least squares estimation of transformation parameters between two point patterns,” *IEEE Trans. on Pattern Analysis and Machine Intelligence*, vol. 13, no. 4, pp. 376–380, 1991.

- [160] Y. S. Shiu and S. Ahmad, "Calibration of Wrist-Mounted Robotic Sensors by Solving Homogeneous Transform Equations the Form $AX = XB$," *IEEE Trans. on Robotics and Automation*, vol. 5, no. 1, pp. 16–29, 1989.
- [161] B. Westermann and R. Hauser, "Online head motion tracking applied to the patient registration problem," *J. of Image Guided Surgery*, vol. 5, no. 3, pp. 137–147, 2000.
- [162] M. J. Ryan, R. K. Erickson, D. N. Levin, C. A. Pelizzari, R. L. MacDonald, and G. J. Dohrmann, "Frameless stereotaxy with real-time tracking of patient head movement and retrospective patient–image registration," *J. of Neurosurgery*, vol. 85, no. 2, pp. 287–292, 1996.
- [163] M. Kuhn, M. Jablonowski, P. Gieles, M. Fuchs, and H.-A. Wischmann, "A Unifying Framework for Accuracy Analysis in Image-Guided Surgery," in *Proc. of the Annual Intl. Conf. of the IEEE Engineering in Medicine and Biology Society (EMBC)*, Amsterdam, 1996, pp. 238–240.
- [164] R. H. Taylor and P. Kazanzides, "Medical Robotics and Computer-Integrated Interventional Medicine," *Advances in Computers: Emerging Technologies*, vol. 73, pp. 219–258, 2008.
- [165] K. O. Arras, "An Introduction To Error Propagation: Derivation, Meaning and Examples of Equation $C_Y = F_X C_X F_X^T$," Lausanne, pp. 1–14, 1998.
- [166] M. H. Moghari and P. Abolmaesumi, "A high-order solution for the distribution of target registration error in rigid-body point-based registration." in *Lecture Notes in Computer Science (LNCS), Proc. of the Annual Conf. of the Medical Image Computing and Computer Assisted Intervention Society (MICCAI)*, vol. 9, no. 2, Kobenhavn, 2006, pp. 603–611.
- [167] W. Zylka, J. Sabczynski, and G. Schmitz, "A Gaussian approach for the calculation of the accuracy of stereotactic frame systems," *J. Medical Physics*, vol. 26, no. 3, pp. 381–392, 1999.
- [168] A. D. Wiles, D. G. Thompsona, and D. D. Frantz, "Accuracy assessment and interpretation for optical tracking systems," in *Proc. of SPIE Medical Imaging*, vol. 5367, San Diego, CA, 2004, pp. 421–432.
- [169] R. Khadem, C. C. Yeh, M. Sadeghi-tehrani, M. R. Bax, J. A. Johnson, J. N. Welch, E. P. Wilkinson, and R. Shahidi, "Comparative tracking error analysis of five different optical tracking systems," *Computer Aided Surgery*, vol. 5, no. 2, pp. 98–107, 2000.
- [170] B. Allen and G. Welch, "A general method for comparing the expected performance of tracking and motion capture systems," in *Proc. of the ACM Symp. on VR Software and Technology*, Monterey, CA, 2005, pp. 210–220.
- [171] W. Hoff and T. Vincent, "Analysis of Head Pose Accuracy in Augmented Reality," *IEEE Trans. on Visualization and Computer Graphics*, vol. 6, no. 4, pp. 319–334, 2000.

- [172] M. Bauer, M. Schlegel, D. Pustka, N. Navab, and G. Klinker, "Predicting and estimating the accuracy of n-ocular optical tracking systems," in *Proc. of the 5th IEEE/ACM Intl. Symp. on Mixed and Augmented Reality (ISMAR)*, Santa Barbara, 2006, pp. 43–51.
- [173] A. Danilchenko, A. Wiles, R. Balachandran, and J. M. Fitzpatrick, "Improved Method for Point-Based Tracking," in *Lecture Notes in Computer Science (LNCS), Proc. of the Annual Conf. of the Medical Image Computing and Computer Assisted Intervention Society (MICCAI)*, Beijing, 2010.
- [174] S. Mishra, "Application of telemedicine in surgery," in *INTELEMED*, Bangalore, 2005, pp. 83–90.
- [175] L. H. Eadie, A. M. Seifalian, and B. R. Davidson, "Telemedicine in Surgery," *British J. of Surgery*, vol. 90, no. 6, pp. 647–58, 2003.
- [176] N. F. Güler and E. D. Ubeyli, "Theory and applications of telemedicine." *J. of Medical Systems*, vol. 26, no. 3, pp. 199–220, 2002.
- [177] C. Benedetti, M. Franchini, and P. Fiorini, "Stable tracking in variable time-delay teleoperation," in *Proc. of the IEEE/RSJ Intl. Conf. on Intelligent Robots and Systems (IROS)*, Lausanne, 2002, pp. 2252–2257.
- [178] J. Cui, S. Tosunoglu, R. Roberts, C. Moore, and D. Repperger, "A review of teleoperation system control," in *Proc. of the Florida Conf. on Recent Advances in Robotics (FCRAR)*, Dania Beach, 2003, pp. 1–12.
- [179] K. Kawashima, K. Tadano, G. Sankaranarayanan, and B. Hannaford, "Bilateral teleoperation with time delay using modified wave variable based controller," in *Proc. of the IEEE Intl. Conf. on Robotics and Automation (ICRA)*, Kobe, 2009, pp. 4326–4331.
- [180] T. Haidegger and Z. Benyó, "Extreme telemedicine: feasibility of telesurgery and telementoring in space (*electronic full version*)," *J. of Telemedicine and e-Health, Proc. of the 13th Annual Intl. Meeting and Exposition of the American Telemedicine Association*, vol. 14, no. S1, pp. 75–75, 2008.
- [181] T. Haidegger and Z. Benyó, "Surgical robotic support for long duration space missions," *Acta Astronautica*, vol. 63, no. 7-10, pp. 996–1005, 2008.
- [182] N. Chopra, "Control of Robotic Manipulators under Time-Varying Sensing-Control Delays," in *Proc. of the IEEE Intl. Conf. on Robotics and Automation (ICRA)*, Anchorage, AK, 2010, pp. 1768–1773.
- [183] J. M. Thompson, M. P. Ottensmeyer, and T. B. Sheridan, "Human factors in telesurgery: effects of time delay and asynchrony in video and control feedback with local manipulative assistance." *Telemedicine Journal: the official journal of the American Telemedicine Association*, vol. 5, no. 2, pp. 129–37, 1999.
- [184] R. Rayman, K. Croome, N. Galbraith, R. McClure, R. Morady, S. Peterson, S. Smith, V. Subotic, A. V. Wynsberghe, and S. Primak, "Long-distance robotic telesurgery: a feasibility study for care in remote environments," *Intl. J. of Medical Robotics and Computer Assisted Surgery*, vol. 2, no. 3, pp. 216–224, 2006.

- [185] T. Haidegger, "In-space surgery: impact of robotic technology on future exploration missions," in *Proc. of the 9th Intl. Symp. on Artificial Intelligence, Robotics and Automation in Space (i-SAIRAS08)*. Los Angeles, NASA, 2008, pp. 135–141.
- [186] R. M. Satava, "The Scientific Method is Dead-Long Live the (New) Scientific Method," *Surgical Innovation*, vol. 12, no. 2, pp. 173–176, 2005.
- [187] D. McRuer, D. Graham, E. Krendel, and W. Reisener Jr, "Human pilot dynamics in compensatory systems," technical report, AFFDL-TR-65-15, Wright-Patterson Air Force Base, Greene/Montgomery, OH, 1965.
- [188] S. Baron, "Application of the Optimal Control Model for the Human Operator to Reliability Assessment," *IEEE Trans. on Reliability*, vol. R-22, no. 3, pp. 157–164, 1973.
- [189] M. Kawato, "Adaptation and learning in control of voluntary movement by the central nervous system," *Advanced Robotics*, vol. 3, no. 3, pp. 229–249, 1989.
- [190] P. Prokopiou, S. Tzafestas, and W. Harwin, "A novel scheme for human-friendly and time-delays robust neuropredictive teleoperation," *J. of Intelligent and Robotic Systems*, vol. 25, no. 4, pp. 311–340, 1999.
- [191] T. B. Sheridan, "Space teleoperation through time delay: review and prognosis," *IEEE Trans. on Robotics and Automation*, vol. 9, no. 5, pp. 592–606, 1993.
- [192] D. Kleinman, S. Baron, and W. Levison, "An optimal control model of human response. I—Theory and validation," *Automatica*, vol. 6, no. 3, pp. 357–369, 1970.
- [193] D. McRuer and H. Jex, "A Review of Quasi-Linear Pilot Models," *IEEE Trans. on Human Factors in Electronics*, vol. 8, no. 3, pp. 231–249, 1967.
- [194] D. McRuer, "Pilot-induced oscillations and human dynamic behavior," Ph.D. thesis, NASA, 1995.
- [195] Hildo, Bijl, "Human–Machine Systems, Summary," course materials, TU Delft, available: www.aerostudents.com, pp. 1–19, 2006.
- [196] P. M. Fitts, "The information capacity of the human motor system in controlling the amplitude of movement. 1954." *J. of Experimental Psychology: General*, vol. 121, no. 3, pp. 262–269, 1992.
- [197] J. H. Chien, M. M. Tiwari, I. H. Suh, D. Oleynikov, and K.-C. Siu, "Accuracy and speed trade-off in robot-assisted surgery," *Intl. J. of Medical Robotics Computer Assisted Surgery*, vol. 6, no. 5, pp. 324–329, 2010.
- [198] S. D. Eppinger and W. P. Seering, "Introduction to Dynamic Models for Robot Force Control," *IEEE Control Systems Magazine*, vol. 7, no. 2, pp. 48–52, 1987.
- [199] K. Kawashima, K. Tadano, G. Sankaranarayanan, and B. Hannaford, "Model-based passivity control for bilateral teleoperation of a surgical robot with time delay," *IEEE/RSJ Intl. Conf. on Intelligent Robots and Systems (IROS)*, pp. 1427–1432, 2008.
- [200] Y. Fung, *Biomechanics: Motion, Flow, Stress, and Growth*. New York, NY, Springer-Verlag, 1990.

- [201] I. Brouwer, J. Ustin, L. Bentley, A. Sherman, N. Dhruv, and F. Tendick, in *Proc. of the Medicine Meets Virtual Reality (MMVR8)*, Long Beach, CA, 2001, pp. 69–74.
- [202] G. Hirzinger, J. Heindl, and K. Landzettel, “Predictive and knowledge-based telerobotic control concepts,” in *Proc. of the IEEE Intl. Conf. on Robotics and Automation (ICRA)*, Scottsdale, AZ, 1989, pp. 1768–1777.
- [203] T. Haidegger, L. Kovács, S. Preitl, R.-E. Precup, A. Kovács, B. Benyó, and Z. Benyó, “Modeling and Control Aspects of Long Distance Telesurgical Applications,” in *Proc. of the IEEE Intl. Joint Conf. on Computational Cybernetics and Technical Informatics (ICCC–CONTI)*, Timisoara, 2010, pp. 197–202.
- [204] A. Voda and I. Landau, “A method for the auto-calibration of PID controllers,” *Automatica*, vol. 31, no. 1, pp. 41–53, 1995.
- [205] C. Kessler, “Das Symmetrische Optimum,” *Regelungstechnik*, vol. 6, pp. 395–400, 432–436, 1958.
- [206] S. Preitl, R.-E. Precup, L. Kovács, and Z. Preitl, “Control Solutions for Electrical Driving Systems. Tuning Methodologies for PI and PID Controllers,” in *Proc. of the Kandó Conf.; 60 years in Electrical Training*. Budapest, BMF, 2002.
- [207] K. Astrom and T. Hagglund, *PID controllers: theory, design, and tuning*, 2nd ed. USA, Instrument Society of America, 1995.
- [208] S. Preitl and R.-E. Precup, “An extension of tuning relations after symmetrical optimum method for PI and PID controllers,” *Automatica*, vol. 35, no. 10, pp. 1731–1736, 1999.
- [209] D. Vrancic, S. Strmcnik, and J. Juricich, “A magnitude optimum multiple integration tuning method for filtered PID controller,” *Automatica*, vol. 37, no. 9, pp. 1473–1479, 2001.
- [210] S. Preitl and R.-E. Precup, “Points of View in Controller Design by Means of Extended Symmetrical Optimum Method,” in *Proc. of the IFAC Control Systems Design (CSD)*, Brastislava, 2003, pp. 95–100.
- [211] ———, “Extended Symmetrical Optimum (ESO) Method: A New Tuning Strategy for PI/PID Controllers,” in *Proc. of the IFAC Workshop on Digital Control: Past, Present and Future of PID Control*, 2000, pp. 421–426.
- [212] T. Haidegger, L. Kovács, S. Preitl, R.-E. Precup, A. Kovács, B. Benyó, and Z. Benyó, “Cascade Control for Telehealth Applications,” *Scientific Bulletin “Politehnica” University of Timisoara, Romania, Transactions on Automatic Control and Computer Science*, vol. 55(69), no. 4, pp. 99–108.
- [213] P. Arcara and C. Melchiorri, “Control schemes for teleoperation with time delay: A comparative study,” *Robotics and Autonomous Systems*, vol. 38, no. 1, pp. 49–64, 2002.
- [214] A. Alvarez-Aguirre, *Predictor Based Control Strategy for Wheeled Mobile Robots Subject to Transport Delay*. Ch. 3 in N. Mollet, Ed., *Remote and Telerobotics*, Vienna, IN-TECH, 2010, pp. 33–59.

- [215] W. Kim and A. Bejczy, "Demonstration of a high-fidelity predictive/preview display technique for telerobotic servicing in space," *IEEE Trans. on Robotics and Automation*, vol. 9, no. 5, pp. 698–702, 1993.
- [216] R. Hess, *Human-in-the-loop Control*. Ch. 12 in W. S. Levine, Ed., *Control System Application*, College Park, CRC Press, 1996.
- [217] A. Phatak, H. Weinert, I. Segall, and C. N. Day, "Identification of a modified optimal control model for the human operator," *Automatica*, vol. 12, no. 1, pp. 31–41, 1976.
- [218] J. Ziegler and N. Nichols, "Optimum settings for automatic controllers," *Trans. of the ASME*, vol. 64, pp. 759–768, 1942.
- [219] T. Ando, J. Okamoto, M. Takahashi, and M. G. Fujie, "EMG based Design and Evaluation of Micro Macro Neural Network for Rollover Support Trunk Orthosis," in *Proc. of the IEEE Intl. Conf. on Robotics and Automation (ICRA)*, Anchorage, AK, 2010, pp. 2916–2921.
- [220] P. Hokayem and M. Spong, "Bilateral teleoperation: A historical survey," *Automatica*, vol. 42, no. 12, pp. 2035–2057, 2006.
- [221] N. Iiyama, K. Natori, R. Kubo, K. Ohnishi, H. Furukawa, K. Miura, and M. Takahata, "A Bilateral Controller Design Method Using Delay Compensators," in *Proc. of IEEE Intl. Conf. on Industrial Technology*, Mumbai, 2006, pp. 836–841.
- [222] M. Franken, S. Stramigioli, R. Reilink, C. Secchi, and A. Macchelli, "Bridging the gap between passivity and transparency," in *Proc. of the Robotics: Science and Systems Conf. (RSS)*, Seattle, WA, 2009, pp. 36–41.
- [223] K. Ohnishi, T. Shimono, and K. Natori, "Haptics for medical applications," *J. of Artificial Life and Robotics*, vol. 13, no. 2, pp. 383–389, 2009.
- [224] R.-E. Precup and S. Preitl, "PI-Fuzzy controllers for integral plants to ensure robust stability," *Information Sciences*, vol. 177, no. 20, pp. 4410–4429, 2007.
- [225] G. Sankaranarayanan, L. Potter, and B. Hannaford, "Measurement and Emulation of Time Varying Packet Delay with Applications to Networked Haptic Virtual Environments," in *ACM Proc. Series, 1st Intl. Conf. on Robot Communication and Coordination (ROBOCOMM)*, vol. 318, Athens, 2007.
- [226] A. Lowery, J. Strojny, and J. Puleo, "Medical Device Quality Systems Manual. A Small Entity Compliance Guide," HHS Publication, FDA 97-4179, 1996.
- [227] "ISO 10360-1:2000 standard," http://www.iso.org/iso/catalogue_detail.htm?csnumber=37694, 2000.
- [228] A. Gärtner, "Teleneurology and requirements of the Medical Devices Directive (MDD)," *Baaske Medical GmbH & Co., Lübbecke*, pp. 1–22, 2008.
- [229] R. M. Satava, "The nature of surgical error: a cautionary tale and a call to reason," *Surgical Endoscopy*, vol. 19, no. 8, pp. 1014–1016, 2005.
- [230] B. Fei, "The safety issues of medical robotics," *Reliability Engineering & System Safety*, vol. 73, no. 2, pp. 183–192, 2001.

- [231] P. Varley, "Techniques for development of safety-related software for surgical robots." *IEEE Trans. on Information Technology in Biomedicine*, vol. 3, no. 4, pp. 261–267, 1999.
- [232] J. Guiochet and A. Vilchis, "Safety analysis of a medical robot for tele-echography," in *Proc. of the 2nd IARP IEEE/RAS joint workshop on Technical Challenge for Dependable Robots in Human Environments*, Toulouse, 2002, pp. 217–227.
- [233] P. Kazanzides, "Safety design for medical robots." in *Proc. of the Annual Intl. Conf. of the IEEE Engineering in Medicine and Biology Society (EMBC)*, Minneapolis, MN, 2009, pp. 7208–7211.
- [234] G. Berlocher, "Minimizing Latency in Satellite Networks," *Via Satellite*, online edition, www.viasatellite.com, September 2009.
- [235] L. Bacsardi and S. Imre, *Quantum Based Information Transfer in Satellite Communication*. Ch. 2 in *Satellite Communications*, Vienna, Sciyo, 2010, pp. 1199–1222.
- [236] R. Wang and S. Horan, "Protocol Testing of SCPS-TP over NASA's ACTS Asymmetric Links," *IEEE Trans. on Aerospace and Electronic Systems*, vol. 45, no. 2, pp. 790–798, 2009.
- [237] R. Spearing and M. Regan, "4.0 Communication and Navigation Capability Roadmap," *NASA Executive Summary*, pp. 1–19, 2005.
- [238] R. C. Reinhart and S. K. Johnson, "SDR/STRS Flight Experiment and the Role of SDR-Based Communication and Navigation Systems," in *Proc. of the 6th Annual IDGA Software Radio Summit*, Vienna, VA, 2008.
- [239] M. J. H. Lum, J. Rosen, T. S. Lendvay, A. S. Wright, M. N. Sinanan, and B. Hanaford, "TeleRobotic fundamentals of laparoscopic surgery (FLS): effects of time delay–pilot study." in *Proc. of the Annual Intl. Conf. of the IEEE Engineering in Medicine and Biology Society (EMBC)*, Nice, 2008, pp. 5597–6000.
- [240] E. Hanly and T. Broderick, "Telerobotic Surgery," *Operative Techniques in General Surgery*, vol. 7, no. 4, pp. 170–181, 2005.
- [241] M. Nohmi, "Space Teleoperation Using Force Reflection of Communication Time Delay," in *Proc. of the IEEE/RSJ Intl. Conf. on Intelligent Robots and Systems (IROS)*, Las Vegas, NV, 2003, pp. 2809–2814.
- [242] C. S. Allen, R. Burnett, J. Charles, F. Cucinotta, R. Fullerton, R. Goodman, A. D. Griffith, J. J. Kosmo, M. Perchonok, J. Railsback, S. Rajulu, D. Stilwell, G. Thomas, T. Tri, J. Joshi, R. Wheeler, M. Rudisill, J. Wilson, A. Mueller, and A. Simmons, "Guidelines and Capabilities for Designing Human Missions," technical report TM-2003-210785, NASA, pp. 1–102, 2003.
- [243] M. R. Campbell, A. W. Kirkpatrick, R. D. Billica, S. L. Johnston, R. Jennings, D. Short, D. Hamilton, and S. A. Dulchavsky, "Endoscopic surgery in weightlessness: the investigation of basic principles for surgery in space." *Surgical Endoscopy*, vol. 15, no. 12, pp. 1413–1418, 2001.
- [244] New Scientist, "Doctors remove tumor in first zero-g surgery," *New Scientist*, online edition, www.newscientist.com, September 2006.

- [245] K. Kamler, "How I Survived a Zero-G Robot Operating Room: Extreme Surgeon," *Popular Mechanics*, online edition, www.popularmechanics.com, November 2007.
- [246] N. Nathoo, T. Pesek, and G. H. Barnett, "Robotics and neurosurgery," *Surgical Clinics Of North America*, vol. 83, pp. 1339–1350, 2003.
- [247] D. F. Louw, T. Fielding, P. B. McBeth, D. Gregoris, P. Newhook, and G. R. Sutherland, "Surgical Robotics: A Review and Neurosurgical Prototype," *Neurosurgery*, vol. 54, no. 3, pp. 525–537, 2004.
- [248] P. McBeth, D. Louw, P. Rizun, and G. Sutherland, "Robotics in neurosurgery," *American J. of Surgery*, vol. 188, no. 4(1), pp. 68–75, 2004.
- [249] L. Zamorano, Q. Li, S. Jain, and G. Kaur, "Robotics in neurosurgery: state of the art and future technological challenges," *Intl. J. of Medical Robotics and Computer Assisted Surgery*, vol. 1, no. 1, pp. 7–22, 2005.
- [250] E. Seigneuret and S. Chabardes, "Robotics in neurosurgery: which tools for what?" *Acta Neurochirurgica*, vol. 98, pp. 43–50, 2006.
- [251] T. Haidegger, L. Kovács, G. Fördös, Z. Benyó, and P. Kazantzides, "Future Trends in Robotic Neurosurgery," in *Proc. of the 14th Nordic-Baltic Conf. on Biomedical Engineering and Medical Physics (NBC)*, Riga, 2008, pp. 229–233.
- [252] M. Alric, F. Chapelle, J.-J. Lemaire, and G. Gogu, "Potential applications of medical and non-medical robots for neurosurgical applications." *Minimally Invasive Therapy & Allied Technologies: the official J. of the Society for Minimally Invasive Therapy*, vol. 18, no. 4, pp. 193–216, 2009.
- [253] R. Rayman, "Is surgery a remote possibility? Robotic surgical system under development has telesurgery capabilities," *Health Technology Trends*, vol. 21, no. 7, pp. 5–7, 2009.
- [254] K. Chinzei and K. Miller, "An MRI Guided Surgical Robot," in *Proc. of the Australian Conf. on Robotics and Automation (ACRA)*, Sydney, 2001, pp. 50–56.
- [255] Z. Tian, W. Lu, T. Wang, B. Ma, Q. Zhao, and G. Zhang, "Application of a robotic telemanipulation system in stereotactic surgery," *Stereotactic and Functional Neurosurgery*, vol. 86, no. 1, pp. 54–61, 2008.
- [256] A. Popovic, M. Engelhardt, T. Wu, F. Portheine, K. Schmieder, and K. Radermacher, "CRANIO—computer-assisted planning for navigated and robot-assisted surgery on the skull," *Cranio: the J. of Craniomandibular Practice*, vol. 1256, pp. 1269 – 1275, 2003.
- [257] D. Engel, J. Raczkowski, and H. Wörn, "A safe robot system for craniofacial surgery," in *Proc. of the IEEE Intl. Conf. on Robotics and Automation (ICRA)*, Seoul, 2001, pp. 2020–2024.
- [258] A. Muacevic and B. Wowra, "Cyberknife Radiosurgery—A New Treatment Method for Image-guided, Robotic, High-precision Radiosurgery," *European Neurological Disease*, no. 7, pp. 32–33, 2007.
- [259] A. Gasparetto and V. Zanutto, "Toward an optimal performance index for neurosurgical robot's design," *Robotica*, vol. 28, no. 2, pp. 279–296, 2010.

- [260] M. Zimmermann, R. Krishnan, A. Raabe, and V. Seifert, "Robot-assisted navigated neuroendoscopy," *Neurosurgery*, vol. 51, no. 6, pp. 1446–1452, 2002.
- [261] P. Federspil, U. Geisthoff, D. Henrich, and P. Plinkert, "Development of the first force-controlled robot for otoneurosurgery," *Laryngoscope*, vol. 113, no. 3, pp. 465–471, 2003.
- [262] S. Lavallee and P. Cinquin, "IGOR: image guided operating robot," in *Proc. of the 5th Intl. Conf. on Advanced Robotics (ICAR)*, Pisa, 1991, pp. 876–881.
- [263] T. Ortmaier, H. Weiss, U. Hagn, M. Grebenstein, M. Nickl, A. Albu-Schaffer, C. Ott, S. Jorg, R. Konietzschke, and G. Hirzinger, "A hands-on-robot for accurate placement of pedicle screws," in *Proc. of the IEEE Intl. Conf. on Robotics and Automation (ICRA)*, Orlando, FL, 2006, pp. 4179–4186.
- [264] N. Villotte, D. Glauser, P. Flury, and C. Burckhardt, "Conception of stereotactic instruments for the neurosurgical robot Minerva," in *Proc. of the 14th Annual Intl. Conf. of the IEEE Engineering in Medicine and Biology Society (EMBC)*, Paris, 1992, pp. 1089–1090.
- [265] M. Chen, T. Wang, Q. Zhang, Y. Zhang, and Z. Tian, "A Robotics System for Stereotactic Neurosurgery and its Clinical Application," in *Proc. of the IEEE Intl. Conf. on Robotics and Automation (ICRA)*, Leuven, 1998, pp. 995–1000.
- [266] M. Nakamura, N. Tamaki, S. Tamura, H. Yamashita, and Y. Hara, "Image-guided microsurgery with the Mehrkoordinaten Manipulator system for cerebral arteriovenous malformations," *J. of Clinical Neuroscience*, vol. 7, no. S1, pp. 10–13, 2000.
- [267] T. Kirino, "Microsurgical robotic system for the deep surgical field: development of a prototype and feasibility studies in animal and cadaveric models," *Neurosurgery*, vol. 103, no. 2, pp. 320–327, 2005.
- [268] T.-C. Tsai and Y. Hsu, "Development of a parallel surgical robot with automatic bone drilling carriage for stereotactic neurosurgery," in *Proc. of the IEEE Intl. Conf. on Systems, Man and Cybernetics*, Hague, 2004, pp. 2156–2161.
- [269] B. Davies, S. Chauhan, and M. Lowe, "A robotic approach to HIFU based neurosurgery," in *Lecture Notes in Computer Science (LNCS), Proc. of the Annual Conf. of the Medical Image Computing and Computer Assisted Intervention Society (MICCAI)*, Cambridge, MA, 1998, pp. 386–396.
- [270] G. R. Sutherland, I. Latour, A. D. Greer, T. Fielding, G. Feil, and P. Newhook, "An image-guided magnetic resonance-compatible surgical robot," *Neurosurgery*, vol. 62, no. 2, pp. 286–293, 2008.
- [271] D. Handini, T. Yeong, and L. Hong, "System integration of NeuroBot: a skull-base surgical robotic system," in *Proc. of the IEEE Conf. on Robotics, Automation and Mechatronics (RAM)*, San Diego, CA, 2004, pp. 43–48.
- [272] K. Hongo, S. Kobayashi, Y. Kakizawa, J. Koyama, T. Goto, H. Okudera, K. Kan, M. Fujie, H. Iseki, and K. Takakura, "NeuRobot: telecontrolled micromanipulator system for minimally invasive microneurosurgery-preliminary results," *Neurosurgery*, vol. 51, no. 4, pp. 985–988, 2002.

- [273] B. Davies, S. Starkie, S. Harris, E. Agterhuis, V. Paul, and L. Auer, "Neurobot: A special-purpose robot for neurosurgery," in *Proc. of the IEEE Intl. Conf. on Automation and Robotics (ICRA)*, San Francisco, CA, 2000, pp. 4103–4108.
- [274] A. Gasparetto, R. Vidoni, and V. Zanotto, "NEUROBUD: a Novel Robot for Neurosurgery," in *Proc. of the 16th Intl. Workshop in Alpe-Adria Danube Region (RAAD)*, Ljubljana, 2007.
- [275] J. Liu, Y. Zhang, and Z. Li, "Improving the positioning accuracy of a neurosurgical robot system," *IEEE/ASME Trans. on Mechatronics*, vol. 12, no. 5, pp. 527–533, 2007.
- [276] M. Eljamel, "Validation of the PathFinder Neurosurgical Robot Using a Phantom," *Intl. J. of Medical Robotics and Computer Assisted Surgery*, vol. 3, no. 4, pp. 372–377, 2007.
- [277] D. V. Amin and L. D. Lunsford, "Volumetric resection using the SurgiScope: a quantitative accuracy analysis of robot-assisted resection," *Stereotactic and Functional Neurosurgery*, vol. 82, no. 5–6, pp. 250–253, 2004.
- [278] M. Tanimoto, F. Arai, T. Fukuda, K. Itoigawa, and M., "Telesurgery system for intravascular neurosurgery," in *Lecture Notes in Computer Science (LNCS), Proc. of the Annual Conf. of the Medical Image Computing and Computer Assisted Intervention Society (MICCAI)*, vol. 1935, Pittsburgh, PA, 2000, pp. 29–39.
- [279] W. Shen, J. Gu, and Y. Shen, "Using Tele-robotic Skull Drill for Neurosurgical Applications," in *Proc. of the IEEE Intl. Conf. on Mechatronics and Automation (ICMA)*, Luoyang, 2006, pp. 334–338.
- [280] D. Malthan, J. Stallkamp, F. Dammann, E. Schwaderer, and M. M. Maassen, "Improvement of Computer and Robot-Assisted Surgery at the Lateral Skull Base by Sensory Feedback," in *Medical Robotics, Navigation and Visualization (MRNV)*, Remagen, 2004, pp. 54–54.
- [281] B. Kang, S. Seung, W. Kim, S. Park, J. Park, and K. Kim, "Development of a Master-Slave system for Tubular Micro Brain surgery," in *Intl. Congress Series, Proc. of the 24th Intl. Congress and Exhibition Computer Assisted Radiology and Surgery (CARS)*, Geneva, 2010, pp. 256–257.
- [282] J. Arata, Y. Tada, H. Kozuka, T. Wada, Y. Saito, N. Ikedo, Y. Hayashi, M. Fujii, Y. Kajita, M. Mizuno, T. Wakabayashi, J. Yoshida, and H. Fujimoto, "Neurosurgical robotic system for brain tumor removal." *Intl. J. of Computer Assisted Radiology and Surgery*, vol. 6, no. 3, pp. 375–385, 2010.
- [283] K. Masamune, E. Kobayashi, Y. Masutani, M. Suzuki, T. Dohi, H. Iseki, and K. Takakura, "Development of an MRI-compatible needle insertion manipulator for stereotactic neurosurgery," *J. of Image Guided Surgery*, vol. 1, no. 4, pp. 242–248, 1995.
- [284] B. W. O'Malley and G. S. Weinstein, "Robotic skull base surgery: preclinical investigations to human clinical application." *Archives of Otolaryngology—Head & Neck Surgery*, vol. 133, no. 12, pp. 1215–1219, 2007.

- [285] M. Rentschler, J. Dumpert, S. Platt, D. Oleynikov, S. Farritor, and K. Iagnemma, "Mobile in vivo biopsy robot," in *Proc. of the IEEE Intl. Conf. on Robotics and Automation (ICRA)*, Orlando, FL, 2006, pp. 4155–4160.
- [286] A. C. Lehman, J. Dumpert, N. a. Wood, L. Redden, A. Q. Visty, S. Farritor, B. Varnell, and D. Oleynikov, "Natural orifice cholecystectomy using a miniature robot." *Surgical Endoscopy*, vol. 23, no. 2, pp. 260–266, 2009.
- [287] A. Menciassi and P. Dario, "Miniaturized robotic devices for endoluminal diagnosis and surgery: A single-module and a multiple-module approach." in *Proc. of the Annual Intl. Conf. of the IEEE Engineering in Medicine and Biology Society (EMBC)*, Minneapolis, MN, 2009, pp. 6842–6845.
- [288] K. Harada, D. Oetomo, E. Susilo, A. Menciassi, D. Daney, J.-P. Merlet, and P. Dario, "A reconfigurable modular robotic endoluminal surgical system: vision and preliminary results," *Robotica*, vol. 28, no. 2, pp. 171–183, 2009.
- [289] L. Eirik, B. Johansen, T. Gjelsvik, and T. Langø, "Ultrasound based localisation of wireless microrobotic endoscopic capsule for the GI tract," in *Proc. of the 21st Conf. of the Society for Medical Innovation and Technology (SMIT)*, Sinaia, 2009, pp. 77–77.
- [290] C. Pappone, G. Vicedomini, F. Manguso, F. Gugliotta, P. Mazzone, S. Gulletta, N. Sora, S. Sala, A. Marzi, G. Augello, L. Livolsi, A. Santagostino, and V. Santinelli, "Robotic magnetic navigation for atrial fibrillation ablation." *J. of the American College of Cardiology*, vol. 47, no. 7, pp. 1390–1400, 2006.

PUBLICATIONS RELATED TO THE THESIS

- [HT-1] T. Haidegger, T. Xia and P. Kazanzides, “Accuracy improvement of a neurosurgical robot system,” in *Proc. of the 2nd IEEE RAS/EMBS Intl. Conf. on Biomedical Robotics and Biomechatronics (BioRob)*, Scottsdale, 2008, pp. 836–841.
- [HT-2] T. Haidegger, L. Kovács, G. Fördős, Z. Benyó and P. Kazanzides, “Future Trends in Robotic Neurosurgery,” in *Proc. of the 14th Nordic-Baltic Conf. on Biomedical Engineering and Medical Physics*, Riga, 2008, pp. 229–233.
- [HT-3] T. Haidegger, P. Kazanzides and Z. Benyó, “Integrated robotic system to assist skull base surgery (*in Hungarian*),” in *Proc. of the Conf. for Biomedical and Clinical Engineers (BUDAMED08)*, Budapest, 2008, pp. 45–49.
- [HT-4] T. Xia, T. Haidegger, K. Hayes, N. Hata and P. Kazanzides, “Integration of Open Source and Commercial Software for a Neurosurgical Robot System,” *Workshop on Systems & Architecture for Computer Assisted Intervention at MICCAI (electronic full version)*, 2008.
- [HT-5] T. Haidegger, L. Kovács, B. Benyó and Z. Benyó, “Spatial Accuracy of Surgical Robots,” in *Proc. of the 5th Intl. Symp. on Applied Computational Intelligence and Informatics (SACI)*, Timisoara, 2009, pp. 133–138.
- [HT-6] T. Haidegger, Z. Benyó and P. Kazanzides, “Sensor fusion for patient motion compensation,” in *Proc. of the Workshop on Advanced Sensing and Sensor Integration in Medical Robotics at IEEE ICRA*, Kobe, 2009, pp. 19–24.
- [HT-7] T. Haidegger and Z. Benyó, “Surgical robotics in neurosurgery (*in Hungarian*),” *Orvosi Hetilap*, vol. 150, no. 39, pp. 1701–1711, 2009.
- [HT-8] T. Haidegger, Z. Benyó and P. Kazanzides, “Patient motion tracking in the presence of measurement errors,” in *Proc. of the Annual Intl. Conf. of the IEEE Engineering in Medicine and Biology Society (EMBC)*, Minneapolis, 2009, pp. 5563–5567.
- [HT-9] T. Haidegger, Z. Benyó and P. Kazanzides, “Manufacturing the Human Body—the Era of Surgical Robots,” *J. of Machine Manufacturing*, vol. XLIX, no. E2, pp. 18–24, 2009.
- [HT-10] T. Haidegger, B. Benyó, L. Kovács and Z. Benyó, “Force Sensing and Force Control for Surgical Robots,” in *Proc. of the 7th IFAC Symp. on Modelling and Control in Biomedical Systems*, Aalborg, 2009, pp. 413–418.

- [HT-11] T. Haidegger, P. Kazanzides, B. Benyó, L. Kovács and Z. Benyó, “Surgical case identification for an image-guided interventional system,” in *Proc. of the IEEE/RSJ Intl. Conf. on Intelligent Robots and Systems (IROS)*, Taipei, 2010.
- [HT-12] T. Haidegger, P. Kazanzides, J. Sándor, and Z. Benyó, “Technological challenges of image-guided robotic surgery—abrupt changes in the operating room,” in *Proc. of the 4th Scientific Meeting of the Japan-Hungary Surgical Society (JHSS)*, Yokohama, 2010.
- [HT-13] T. Haidegger, Z. Benyó and P. Kazanzides, “Machines for Humans—the dawn of robot surgery (*in Hungarian*),” *Gépgyártás (in press)*, 2010.
- [HT-14] T. Haidegger and Z. Benyó, “Accuracy of CIS systems (*in Hungarian*),” in *Proc. of the BME–MATE CIS Mini-Symp. II.*, Budapest, 2009, pp. 33–34.
- [HT-15] T. Haidegger, P. Kazanzides, I. Rudas, B. Benyó and Z. Benyó, “The Importance of Accuracy Measurement Standards for Computer-Integrated Interventional Systems,” in *Proc. of the EURON GEM Sig Workshop on The Role of Experiments in Robotics Research at IEEE ICRA*, Anchorage, 2010, pp. 19–24.
- [HT-16] T. Haidegger, S. Győri, B. Benyó and Z. Benyó, “Stochastic approach to error estimation for image-guided robotic systems,” in *Proc. of the Annual Intl. Conf. of the IEEE Engineering in Medicine and Biology Society (EMBC)*, Buenos Aires, 2010, pp. 984–987.
- [HT-17] T. Haidegger and Z. Benyó, “Surgical robotic support for long duration space missions (*electronic full version*),” in *Proc. of the 16th IAA Humans in Space Symp.*, Beijing, 2007, pp. 234–234.
- [HT-18] T. Haidegger, “Surgical Robots in Space: Long Distance Telesurgery,” *3rd SEU on Surgical Robotics (electronic version)*, Montpellier, pp. 1–15, 2007.
- [HT-19] T. Haidegger and Z. Benyó, “Future of Surgical Robots in Space,” in *Proc. of the 58th Intl. Astronautical Congress (IAC)*, Hyderabad, 2007, pp. 1461–1471.
- [HT-20] T. Haidegger and Z. Benyó, “Surgical robotic support for long duration space missions,” *Acta Astronautica*, vol. 63, no. 7-10, pp. 996–1005, IF: 0.374, 2008.
- [HT-21] T. Haidegger and Z. Benyó, “Extreme telemedicine: feasibility of telesurgery and telementoring in space (*electronic full version*),” *J. of Telemedicine and e-Health, Proc. of the 13th Annual Intl. Meeting and Exposition of the American Telemedicine Association*, IF: 0.97, vol. 14, no. S1, pp. 75–75, 2008.
- [HT-22] T. Haidegger, “In-space surgery: impact of robotic technology on future exploration missions,” in *Proc. of the 9th Intl. Symp. on Artificial Intelligence, Robotics and Automation in Space (i-SAIRAS08)*, Los Angeles, NASA, 2008, pp. 135–141.
- [HT-23] T. Haidegger, L. Kovács, S. Preitl, R.-E. Precup, A. Kovács, B. Benyó and Z. Benyó, “Modeling and Control Aspects of Long Distance Telesurgical Applications,” in *Proc. of the IEEE Intl. Joint Conf. on Computational Cybernetics and Technical Informatics (ICCC–CONTI)*, Timisoara, 2010, pp. 197–202.
- [HT-24] T. Haidegger, J. Sándor and Z. Benyó, “Surgery in space: the future of robotic telesurgery,” *Surgical Endoscopy*, vol. 25, issue: 3, p.681-690, IF: 3.304, 2011.

- [HT-25] T. Haidegger and Z. Benyó, *Extreme Telesurgery*, ch. 2. in S. H. Baik, Ed. *Robot Surgery*, IN-TECH, Vienna, 2010, pp. 25–44.
- [HT-26] T. Haidegger, L. Kovács, S. Preitl, R.-E. Precup, A. Kovács, B. Benyó and Z. Benyó, “Cascade Control for Telehealth Applications,” *Scientific Bulletin “Politehnica” University of Timisoara, Romania, Transactions on Automatic Control and Computer Science*, vol. 55(69), no. 4, 2010, pp. 99–108.
- [HT-27] T. Haidegger, L. Kovács, S. Preitl, R.-E. Precup, A. Kovács, B. Benyó and Z. Benyó, “Controller Design Solutions for Long Distance Telesurgical Applications,” *Intl. J. of Artificial Intelligence (IJAI)*, vol. 6, no. S11, 2011
- [HT-28] T. Haidegger, L. Kovács, S. Preitl, R.-E. Precup, B. Benyó and Z. Benyó, “Cascade Control for Telerobotic Systems Serving Space Medicine,” 18th *IFAC World Congress*, *accepted*, 2011